Development of an Eco-friendly Composite Material for Engineering Applications

By

Marwa Aly

B. Sc., M. Sc.

A Thesis Submitted in Fulfilment of the Requirements for the Degree of Doctor of Philosophy (PhD)

School of Mechanical and Manufacturing Engineering

Supervisors

Prof. Saleem Hashmi, Dr. Abdul-Ghani Olabi

& Prof. Medhat El-Messeiry

February, 2012

Declaration

I hereby certify that this material, which I now submit for assessment on the programme of study leading to the award of PhD in Engineering is entirely my own work, that I have exercised reasonable care to ensure that the work is original, and does not to the best of my knowledge breach any law of copyright, and has not been taken from the work of others save and to the extent that such work has been cited and acknowledged within the text of my work.

Signed: _____ ID: _____

Date: _____

Acknowledgements

First, I am very grateful to my gracious Allah for granting me the patience and perseverance to get through the entire journey of my PhD and also for allowing me to meet and work with some of the finest people I have known in my entire life.

I am also thankful to my supervisors Prof. Hashmi, Dr. Olabi and Prof. El-Messiery for their invaluable suggestions and inspirations. I would like to express my sincere thanks to Prof. Ehab Abadir, Cairo University Egypt, for his constant encouragement and valuable suggestions. Special thanks and appreciation is devoted to Prof. Ahmed Hussain, National Research Centre Egypt, for his continuous guidance and support for me. I would like to thank Dr. Khaled Benyounis for his help and suggestions. I would also like to thank the School of Mechanical Engineering technicians who provided the technical assistance for my research, especially Mr. Christopher Crouch and Mr. Michael May.

I gratefully acknowledge EKA Chemicals AB, Sweden for their supply of the colloidal silica sol (Cembinder 50^{TM}) and also Southern Clay Products Inc, USA for their supply of nano clay particles.

I would like to convey my sincere thanks to the School of Mechanical Engineering Secretary Suzanne Dockery, who was always ready to help me with a smile. I am also grateful to Dr. Haymen for his constant encouragement, which helped inspire me to complete this research work.

I would never have been able to accomplish any of my goals without the support of my mother and sisters. They were always there when I needed them. Very special thanks to my husband, Mohamed. I will never be able to express all of my appreciation. You had faith in me and what I was doing even when I had lost it. Thank you for all of your support and sacrifices.

Abstract

In response to increases in worldwide environmental awareness, there is increasing and encouraging scientific research being done on the development of eco-friendly and more sustainable construction materials. The use of recycled materials and agriculture waste in construction is among the most attractive options because of the increasing need of the construction industry for these materials, their relatively low quality requirements and the industry's use of widespread construction sites.

The primary objective of this thesis is to assess the performance of flax fibre/waste glass cement composites. Flax fibres are used to reinforce two systems. The first system contains Ordinary Portland Cement (OPC) only as a binder while in the second system a part of OPC is replaced by finely ground waste glass powder. The fibre parameters were selected by applying a Central Composite Design to plan the experiments, develop mathematical models and optimise the fibre parameters. In order to improve the durability and long term performance of these composites, nano clay particles and colloidal nano silica was added in the production of both systems. In order to remove the surface impurities from the fibre surface, to enhance the adhesion between the matrix and the fibres and to improve long term stability of the composites, alkali treatment of the fibres was carried out in the production of both systems. Alkali treatment conditions were selected by applying a Box-Behnken method to design the experiments, develop mathematical models and optimise the treatment conditions.

Several fibre and composite characterisation techniques were utilized in this research. The characterisation was designed to obtain information on surface morphology, fibre crystallinity, mineralogical composition, thermal stability and the mechanical properties of alkali treated flax fibre and its composites. Hence, the following techniques, X-ray diffraction (XRD), thermogravimetry (TGA/TDA), scanning electron microscopy (SEM), tensile, flexure, toughness, fracture energy, impact and compressive properties testing were employed to analyse the results.

The results obtained in this study provide ample evidence that waste glass powder (up to 20% by cement weight) and nano-silica (3% by cement weight) or nano-clay (2.5% by cement weight) can be used together in concrete without any adverse impact. The presence of nanoparticles improves the mechanical and physical properties of waste glass cement systems, enabling the development of high performance cement composites. Moreover, the use of nanoparticles and waste glass powder reduces the CO_2 footprint of the cement composites which are produced and is also economically attractive. In brief, the proposed new composite offers superior performance, lower costs and provides better ecological and environmental benefits.

Table of Contents

Declaration I

Acknowledgements II

Abstract III

Table of Contents IV

List of Figures X

List of Tables XVII

List of Acronyms and Symbols XIX

Chapter 1 : Introduction 1

1.1 Introduction 1

1.2 Aim of the thesis 6

1.3 Thesis Objectives 6

1.4 Thesis Structure 8

Chapter 2 : Literature Review 10

2.1 Introduction 10

2.2 Pozzolanic Materials 11

2.2.1 Waste Glass Powder as a Pozzolanic Material 13

2.3 Nanotechnology in Concrete 16

2.3.1 Incorporation of Nano-Silica (NS) in Cement Matrix 18

2.3.2 Nano Minerals Clay 20

2.3.3 Incorporation of Nano Clay Particle in Cement Matrix 23

2.4 Natural Fibre Classification and Properties 24

2.4.1 Flax Fibre 26

2.4.1.1 Flax Fibre Constituents 27

2.4.1.1.1 Cellulose 29

2.4.1.1.2 Hemicelluloses 31

2.4.1.1.3 Lignin 32

2.4.1.1.4 Pectin 32

2.5 Issues Regarding the Use of Natural Fibres in Cement Composites 33

2.5.1 Moisture Absorption Characteristics 33
2.5.2 Interfaces and Bond 34
2.5.2.1 Chemical Bonding 34
2.5.2.2 Mechanical Bonding (interlocking) 35
2.5.3 Long-term Performance of Cellulose Fibres 35
2.5.4 Natural Cellulose Fibres Treatments 37
2.5.4.1 Biological treatments 37
2.5.4.2 Chemical Modifications of Natural Fibres 39
2.5.4.2.1 Alkali Treatments 39
2.6 Natural Fibres for Low Cost Cementitious Composites 41
2.6.1 Factors Govern the Properties of Short Fibre Reinforced Composites 42
2.6.1.1 Fibre Length 42
2.6.1.2 Fibre Aspect Ratio 42
2.6.1.3 Fibre Volume Fraction 43
2.6.2 Mechanical and Physical and Properties of Natural Fibre Cement Composites 44
2.6.2.1 Post-cracking Performance 44
2.6.2.2 The Flexure, Impact and Toughness Properties 44
2.6.2.3 Compressive Strength 46
2.6.3 Durability of Natural Fibre Cement Composites (NFC) 46
2.6.3.1 Modification of Cement Matrix 49
2.6.3.2 Modification of Fibres 49
Chapter 3 : Materials and Methods 51
3.1 Experimental Overview 51
3.2 Materials 51
3.3 Methods 55
3.3.1 Surface Treatment of Flax Fibre 55
3.3.2 Production of Flax Fibre Composites 56
3.3.2.1 Normal Flax Fibre Composites 56

3.3.2.2 Nano-Clay Flax Fibre Composites 57
3.3.2.3 Nano-Silica Flax Fibre Composites 57
3.4 Characterisation Techniques 58
3.4.1 Differential Thermal Analysis/Thermogravimetric Analysis (DTA/TGA) 58
3.4.1.1 Application of DTA/TGA Analysis to Cement Hydration 58
3.4.1.1.1 Measurement 59
3.4.1.2 Application of DTA/TGA Analysis to Cellulose Fibres 60
3.4.1.2.1 Measurement 60
3.4.2 X-ray Diffraction (XRD) 61
3.4.2.1 Application of X-ray diffraction technique to Cellulose Fibres 62
3.4.2.1.1 Measurement 65
3.4.2.2 Application of XRD to Concrete Chemistry 65
3.4.2.2.1 Measurement 66
3.4.3 Scanning Electron Microscope (SEM) and Energy Dispersive X-ray Analyses (EDX) 66
3.4.3.1 Measurement 68
3.4.4 Single Fibre Tensile Testing 69
3.4.5 Thermal Expansion 70
3.4.6 Flexure strength 71
3.4.7 Compressive Strength 72
3.4.8 Impact Strength 72
3.4.9 Flexural Toughness Measurements 73
3.4.9.1 ASTM C 1018 74
3.4.9.2 Fracture Energy (G_F) 75
3.4.10 Evaluation of composite durability 75
3.4.11 Lime-Glass Test 76
3.4.12 Alkali Silica Reaction (ASR) 77
3.4.13 Porosity 77
Chapter 4 : Design of Experiments 78

4.1 Design of Experiments (DOE) 78
4.2 Response Surface Methodology (RSM) 80
4.2.1 Central Composite Design (CCD) 80
4.2.2 Box-Behnken Design (BBD) 82
4.3 General Steps in RSM 83
4.3.1 Planning Experiments 84
4.3.2 Designing and Running Experiments 84
4.3.3 Development of the mathematical model 85
4.3.4 Estimation of the coefficients in the model 85
4.3.5 Testing the adequacy of the models developed 85
4.3.6 Model Reduction 86
4.3.7 Development of final reduced model 87
4.4 Optimisation 87
4.4.1 Desirability approach 87
4.4.2 Optimisation by Means of Design-Expert Software 90
Chapter 5 : Results and Discussions 91
5.1 Introduction 91
5.2 Alkali Treatment of Flax Fibre 92
5.2.1 Selection of the Levels of Treatment Factors 92
5.2.2 Development of Mathematical Models 95
5.2.3 Effect of Processing Parameters on Single Fibre Tensile Strength (TS) 98
5.2.4 Effect of Process Parameters on Young's Modulus (YM) 100
5.2.5 The Effects of Fibre Diameter on Fibre Tensile Strength (TS) 101
5.2.6 Optimisation method 102
5.2.7 Validation of the developed models 103
5.2.8 Surface Morphology by Scanning Electron Microscopy 105
5.2.9 X-ray Diffraction (XRD) 106
5.2.10 Thermal Gravimetric Analyses (TGA/DTA) 107

5.3 Effect of Alkaline Treatment on Thermal and Mechanical Properties of Cement Composites 110
5.3.1 Thermal Expansion 110
5.3.2 Mechanical behaviour analysis of flax fibre cement composites 112
5.4 Effect of Fibre parameters on the Mechanical Properties of Cement Composites 116
5.4.1 Development of Mathematical Models 118
5.4.2 Effect of process parameters on the properties of cement composites 124
5.4.2.1 Flexure strength 124
5.4.2.2 Impact strength 125
5.4.2.3 Compressive strength 127
5.4.2.4 Fracture energy 129
5.4.2.5 Toughness Indices 130
5.4.2.6 Porosity of the Cement Composites 134
5.4.3 Optimisation 135
5.4.4 Validation of the Models 136
5.5 Effect of Nano-clay and Waste Glass Content on the Behaviour of Flax Fibre Cement Composites 140
5.5.1 Effect of Nano-clay Content 140
5.5.1.1 Mechanical Properties 141
5.5.1.2 Microstructural Characterisation 147
5.5.1.3 Porosity 149
5.5.2 Hybrid Effect of Nano-clay and Waste Glass Powder 150
5.5.2.1 Mechanical Properties 151
5.5.2.2 Porosity 157
5.5.2.3 Alkali Silica Reaction 159
5.6 Effect of Nano-silica and Waste Glass content on the Behaviour of Flax Fibre Cement Composites 160
5.6.1 Effect of Nano-silica Content 160
5.6.1.1 Mechanical Properties 161
5.6.1.2 Porosity 166

5.6.2 Hybrid Effect of Nano-silica and Waste Glass Powder 168
5.6.2.1 Mechanical Properties 169
5.6.2.2 Porosity 174
5.6.2.3 Alkali Silica Reaction 175
5.7 Multimodal and Mono- modal Flax Fibre Composites 177
5.7.1 Post Cracking Behaviour 177
5.7.2 TGA and DTA 179
5.7.3 XRD 182
5.7.4 Scanning Electron Microscopy (SEM) 183
5.8 Durability of Mono-modal and Multimodal composites 195
5.8.1 Mechanical Behaviour of the Composites after Ageing 195
5.8.2 Analysis of the SEM Images 202
5.8.3 Changes in the Mineral Composition of the Composites 204
Chapter 6 : Conclusions 207
6.1 Overview 207
6.2 Conclusions 207
6.2.1 Treatment of flax fibres 207
6.2.2 Flax Fibre Cement Composites 208
6.2.3 Partial Replacement of Ordinary Portland Cement by Glass Powder and Nanoparticles 209
6.2.4 Durability of Flax Fibre Cement Composites 211
6.3 Recommendations for Future Work 212
References 213
Appendix I 225
Appendix II 226

List of Figures

Figure 2.1: Setup of the ‘‘top-down” and ‘‘bottom-up” approaches in nanotechnology [49].....17
Figure 2.2: Structure of 2:1 clay minerals [66].....21
Figure 2.3: Schematic of morphologies of nano-clay composites: (a) conventional miscible, (b) intercalated and dispersed, and (c) fully exfoliated and dispersed [66]. 22
Figure 2.4: Schematic plot of a flax stem down to a micro fibre [81].....27
Figure 2.5: Principles of the flax fibre structure, a) the structure of a flax fibre cell, b) S2—layers in a 3D view, (c) S2—layers projected into a 2D view [80,82].....27
Figure 2.6: SEM micrographs showing (a) cross-section of flax stem x100 showing thickness of fibre walls and lumen and (b) cross-section of flax stem x 40 showing distinct fibre bundles [1].....28
Figure 2.7: The break area of a flax fibre after a tensile test. The secondary wall shows the structure of a unidirectional composite, microfibrils are directed according to the axis of the fibre [82].....28
Figure 2.8: The molecular structure and arrangement of cellulose [74].....30
Figure 2.9: Schematic representation of the crystallite structure of cellulose [74]....30
Figure 2.10: Microfibril surface [86].....31
Figure 2.11: Schematic of mechanical interlocking [74].....35
Figure 2.12: Schematic description of the degradation of sisal fibres in concrete [76]. 36
Figure 2.13: Typical structure of (a) untreated and (b) alkalized cellulosic fibre [83]. 39
Figure 3.1: Photography of helium gas Pycnometer.....52
Figure 3.2: SEM micrograph of Closite® 30B.....53
Figure 3.3: SEM photograph of ground green waste glass powder.....54
Figure 3.4: Particle size distributions of waste glass powder and Portland cement. .55
Figure 3.5: Compressive strength of lime-WG mixture.....55
Figure 3.6: Photograph of DTA/ TGA analyser.....60
Figure 3.7: Geometric construction of the Bragg Law [159].....62
Figure 3.8: X-ray diffraction profile of cellulose polymorphs [160].....63

Figure 3.9: Intercepts of a lattice plane (hkl) on the unit cell's vectors a, b, c. ON= d_{hkl} = inter-plannar spacing [159].....64
Figure 3.10: Families of planes making rational intercepts with the unit cell edges are identified by a set of three integers, h k l, known as Miller indices [159].....64
Figure 3.11: Photograph of the XRD machine.....65
Figure 3.12: Different interactions of an electron beam (PE) with a solid target, BSE: backscattered electron, SE: secondary electron, X: x-ray, AE: auger electron [28]..67
Figure 3.13: Photograph of the SEM/EDX machine. 69
Figure 3.14: Photograph of the Edwards sputter coater.....69
Figure 3.15: The set up for the single fibre tensile strength test.....70
Figure 3.16: Photograph of the optical microscope. 70
Figure 3.17: Photograph of the Netzsch Model 402 E Dilatometer.....71
Figure 3.18: Photograph of the Zwick machine used for flexural strength test.....72
Figure 3.19: Photograph of the Charpy impact pendulum.....73
Figure 3.20: Fracture toughness and Indices according to ASTM C1018 [170]. 75
Figure 4.1: Generation of CCD for two factors [178].....82
Figure 4.2: A schematic diagram for BBD with three factors [187].....82
Figure 4.3: Optimisation steps [178].....90
Figure 5.1: Effect of Concentration of NaOH on TS (at 100℃ and 60 min).....92
Figure 5.2: Effect of soaking time on TS (at 100℃ and 5% NaOH). 93
Figure 5.3: Effect of soaking temperature on TS (at 60 min and 5% NaOH).....94
Figure 5.4: Perturbation plot showing the effect of all factors on TS.....99
Figure 5.5: Contour plot showing the effect of NaOH concentration and soaking time on TS at 55°C soaking temperature. 99
Figure 5.6: Perturbation plot showing the effect of all factors on YM. 100
Figure 5.7: Contour plot showing the effect of NaOH concentration and soaking temperature on YM at a soaking time of 10 min. 101
Figure 5.8: The relation between average fibre diameter and average fibre TS. 102
Figure 5.9: Overlay plot showing the region of optimal treatment condition.....103
Figure 5.10: Scatter diagram of (a) single fibre tensile strength (TS) and (b) Young's Modulus (YM). 104
Figure 5.11: SEM photographs of; (a) untreated flax fibre, (b) 5% treated flax fibre (run# 1), (c) 7.5% treated flax fibre (run# 9) and (d) 10% treated flax fibre (run# 2). 106

Figure 5.12: XRD pattern of untreated and alkali treated fibres. 107
Figure 5.13: DTA curves of alkali treated and untreated flax fibres. 108
Figure 5.14: TGA curves of alkali treated and untreated flax fibres. 109
Figure 5.15: Thermal strain (ε) of plain mortar and treated/untreated flax fibre composites. 111
Figure 5.16: SEM micrographs showing (a) untreated flax fibre composites and (b) treated flax fibre composite. 112
Figure 5.17: Flexural strength–deflection curves for plain mortar, treated and untreated flax fibre composites (n = 3). 114
Figure 5.18: Propagation of the crack in the composite during the three point bending test. 114
Figure 5.19: SEM micrographs of the composite after three point bending test showing (a) pull-out fibres and (b) pull-out sites. 115
Figure 5.20: Chronology of loading and associated mechanical behaviour of the composite. 115
Figure 5.21: SEM micrograph of fracture surface of flax cement composite after three point bending test. 116
Figure 5.22: Contour plot showing the effect of fibre parameters on flexural strength. 125
Figure 5.23: Perturbation plot showing the effect of all factors on the flexure strength. 125
Figure 5.24: Contour plot showing the effect of fibre parameters on impact strength. 126
Figure 5.25: Perturbation plot showing the effect of all factors on the impact strength. 127
Figure 5.26: Contour plot showing the effect of fibre parameters on compressive strength. 128
Figure 5.27: Perturbation plot showing the effect of all factors on the compressive strength. 129
Figure 5.28: Contour plot showing the effect of fibre parameters on fracture energy (N.mm). 130
Figure 5.29: Perturbation plot showing the effect of all factors on the fracture energy. 130
Figure 5.30: Contour plot showing the effect of fibre parameters on I_5. 132

Figure 5.31: Contour plot showing the effect of fibre parameters on I_{10}. 132
Figure 5.32: Contour plot showing the effect of fibre parameters on I_{20}. 132
Figure 5.33: Perturbation plot showing the effect of all factors on I_5. 133
Figure 5.34: Perturbation plot showing the effect of all factors on I_{10}. 133
Figure 5.35:Perturbation plot showing the effect of all factors on I_{20}. 133
Figure 5.36: Contour plot showing the effect of fibre parameters on the porosity. . 134
Figure 5.37: Perturbation plot showing the effect of all factors on the porosity. 135
Figure 5.38: Overlay plot shows the region of the optimal fibre parameters condition. 136
Figure 5.39: Scatter diagram of flexural strength. 137
Figure 5.40: Scatter diagram of impact strength. 137
Figure 5.41: Scatter diagram of compressive strength. 138
Figure 5.42: Scatter diagram of fracture energy. 138
Figure 5.43: Scatter diagram of toughness index I_5. 138
Figure 5.44: Scatter diagram of toughness index I_{10}. 139
Figure 5.45: Scatter diagram of toughness index I_{20}. 139
Figure 5.46: Scatter diagram of porosity. 139
Figure 5.47: Effect of NC content on the compressive strength of cement composites (n = 3). 143
Figure 5.48: Effect of NC content on the flexural strength of cement composites (n = 3). 144
Figure 5.49: Effect of NC content on the impact strength of cement composites (n = 3). 144
Figure 5.50: Effect of NC content on the fracture energy of cement composites (n = 3). 145
Figure 5.51: Effect of NC content on the toughness index I_5 of cement composites (n = 3). 145
Figure 5.52: Effect of NC content on the toughness index I_{10} of cement composites (n = 3). 146
Figure 5.53: Effect of NC content on the toughness index I_{20} of cement composites (n = 3). 146
Figure 5.54: SEM micrographs of cement composites reinforced with (a) 0%, (b) 2.5 % and (c) 5 % NC. 148
Figure 5.55: A typical EDX result of the NC around capillary pores. 149

Figure 5.56: Effect of NC content on the porosity of cement composites (n = 3). ..150
Figure 5.57: Variation of the compressive strengths of cement composites with different contents of WG when NC dosage is 2.5% (n = 3). 154
Figure 5.58: Variation of the flexural strengths of cement composites with different contents of WG when NC dosage is 2.5% (n = 3). 154
Figure 5.59: Variation of the impact strengths of cement composites with different contents of WG when NC dosage is 2.5% (n = 3). 155
Figure 5.60: Variations of the fracture energy of cement composites with different contents of WG when NC dosage is 2.5% (n = 3). 155
Figure 5.61: Variations of the toughness index I_5 of cement composites with different contents of WG when NC dosage is 2.5% (n = 3). 156
Figure 5.62: Variations of the toughness index I_{10} of cement composites with different contents of WG when NC dosage is 2.5% (n = 3). 156
Figure 5.63: Variations of the toughness index I_{20} of cement composites with different contents of WG when NC dosage is 2.5% (n = 3). 157
Figure 5.64: Variation of the porosity of cement composites with different contents of WG when NC dosage is 2.5% (n = 3). 158
Figure 5.65: ASR test results of cement composites at 2.5 % NC and different contents of WG (n = 3). 160
Figure 5.66: Effect of NS content on the compressive strength of cement composites (n = 3).....163
Figure 5.67: Effect of NS content on the flexural strength of cement composites (n = 3).....163
Figure 5.68: Effect of NS content on the impact strength of cement composites (n = 3).....164
Figure 5.69: Effect of NS content on the fracture energy of cement composites (n = 3).....164
Figure 5.70: Effect of NS content on the toughness index I_5 of cement composites (n = 3).....165
Figure 5.71: Effect of NS content on the toughness index I_{10} of cement composites (n = 3).....165
Figure 5.72: Effect of NS content on the toughness index I_{20} of cement composites (n = 3).....166
Figure 5.73: Effect of NS content on the porosity of cement composites (n = 3). ..168

Figure 5.74: Variation of compressive strength of cement composites with different contents of WG when NS dosage is 3% (n = 3).....171
Figure 5.75: Variation of flexural strength of cement composites with different contents of WG when NS dosage is 3% (n = 3).....171
Figure 5.76: Variation of impact strength of cement composites with different contents of WG when NS dosage is 3% (n = 3).....172
Figure 5.77: Variation of fracture energy of cement composites with different contents of WG when NS dosage is 3% (n = 3).....172
Figure 5.78: Variation of toughness index I_5 of cement composites with different contents of WG when NS dosage is 3% (n = 3).....173
Figure 5.79: Variation of toughness index I_{10} of cement composites with different contents of WG when NS dosage is 3% (n = 3).....173
Figure 5.80: Variation of toughness index I_{20} of cement composites with different contents of WG when NS dosage is 3% (n = 3).....174
Figure 5.81: Variation of porosity of cement composites with different contents of WG when NS dosage is 3% (n = 3). 175
Figure 5.82: ASR test results of cement composites at 3 % NS and different contents of WG (n = 3).....176
Figure 5.83: Load-deflection curves of (a) mono-modal and (b) multimodal composites (n = 3).....178
Figure 5.84: DTA/TGA profiles for cement composites after 28 days of hydration. 181
Figure 5.85: CH content for cement composites as measured by TGA and DTA methods. 182
Figure 5.86: XRD pattern for cement composites. 183
Figure 5.87: Microstructure of control specimen.....186
Figure 5.88: Microstructure of NCPC2.5 specimen. 187
Figure 5.89: Microstructure of NSPC3 specimen. 188
Figure 5.90: Microstructure of WG specimen. 189
Figure 5.91: Microstructure of NCWG20specimen.....190
Figure 5.92: SEM micrograph showing the showing the hydration of glass grains in NSWG20. 191
Figure 5.93: SEM micrograph showing the hydration of glass grains in NCWG20. 192

Figure 5.94: SEM micrograph showing the reactions of glass grains in NCWG20.193
Figure 5.95: SEM micrograph showing the reactions of glass grains in NSWG20. 194
Figure 5.96: Load-deflection curves of control specimens after ageing (n = 3). 199
Figure 5.97: Load-deflection curves of WG specimens after ageing (n = 3).....199
Figure 5.98: Load-deflection curves of NCPC2.5 specimens after ageing (n = 3)..199
Figure 5.99: Load-deflection curves of NSPC3 specimens after ageing (n = 3). 200
Figure 5.100: Load-deflection curves of NCWG20 specimens after ageing (n = 3). 200
Figure 5.101: Load-deflection curves of NSWG20 specimens after ageing (n = 3). 200
Figure 5.102: SEM micrographs of flax fibre surfaces (a) Before ageing, (b-g) fibre extracted from specimens after ageing (b) control, (c) WG20, (d) NCPC2.5, (e) NSPC3, (f) NCWG20 and (g) NSWG20. 203
Figure 5.103: XRD patterns of control specimens after ageing.....204
Figure 5.104: XRD patterns of WG specimens after ageing. 205
Figure 5.105: XRD patterns of NCPC2.5 specimens after ageing.....205
Figure 5.106: XRD patterns of NSPC3 specimens after ageing. 205
Figure 5.107: XRD patterns of NCWG20specimens after ageing.....206
Figure 5.108: XRD patterns of NSWG20 specimens after ageing. 206

List of Tables

Table 1.1: Properties of glass and natural fibres [1] 3
Table 2.1: Chemical composition of waste glass powder and other pozzolans 16
Table 2.2: Relative prices for commonly used fibres [8,74,75] 25
Table 2.3: Chemical composition of plant fibres by percentage mass (%) [80,82] ... 29
Table 3.1: Physical and chemical properties of Closite® 30B as provided by the manufacture 53
Table 3.2: Chemical composition of green waste glass powder used in this work 54
Table 3.3: Mixture proportions for lime test (by weight percent) 77
Table 4.1: Comparison between the Central Composite (CCD) and Box-Behnken designs (BBD) [191] 83
Table 5.1: Experimental parameters for the selection of levels of concentration of NaOH 92
Table 5.2: Experimental parameters for the selection of levels of soaking time 93
Table 5.3: Experimental parameters for the selection of levels of soaking temperature 93
Table 5.4: Experimental data and results for treated and untreated flax fibres ($n \geq 30$) 95
Table 5.5: ANOVA analysis for single fibre tensile strength model 97
Table 5.6: ANOVA analysis for Young's Modulus model 97
Table 5.7: Optimisation criteria used for treatment conditions 102
Table 5.8: Optimal solution as obtained by Design-Expert 103
Table 5.9: Validation test results 105
Table 5.10: Crystallinity indices, I_{cr} of control untreated and alkali treated flax fibres. 107
Table 5.11: The peaks, peak onsets, peak finishing temperatures and nature of peaks for the treated and untreated fibres obtained from the DTA thermograms 109
Table 5.12: Process variables and experimental design levels used 117
Table 5.13: Design matrix in actual values 117
Table 5.14: Experimental data and results for treated flax fibre cement composites 117
Table 5.15: ANOVA analysis for the flexural strength model 120
Table 5.16: ANOVA analysis for the compressive strength model 120

Table 5.17: ANOVA analysis for the impact strength model 121
Table 5.18: ANOVA analysis for the fraction energy model 121
Table 5.19: ANOVA analysis for the toughness index I_5 model 122
Table 5.20: ANOVA analysis for the toughness index I_{10} model 122
Table 5.21: ANOVA analysis for the toughness index I_{20} model 123
Table 5.22: ANOVA analysis for the porosity model 123
Table 5.23: Optimisation criteria used for fibre parameters 135
Table 5.24: Optimal solution as obtained with design-expert software 136
Table 5.25: Confirmation experiments for fibre parameters 140
Table 5.26: Mixture proportions used to study the effect of NC on the behaviour of the flax fibre cement composites 141
Table 5.27: Mechanical properties and porosity of flax fibre cement composites reinforced with various doses of NC 143
Table 5.28: Mixture proportions used to study the effect of NC/WG on the behaviour of the flax fibre cement composites 151
Table 5.29: Mechanical properties and porosity of flax fibre cement composites reinforced with various contents of WG at 2.5% NC (n = 3). 153
Table 5.30: Mixture proportions used to study the effect of NS on the behaviour of flax fibre cement composites 161
Table 5.31: Mechanical properties and porosity of flax fibre cement composites reinforced with various doses of NS (n = 3) 162
Table 5.32: Mixture proportions used to study the effect of NS/WG on the behaviour of flax fibre cement composites 169
Table 5.33: Mechanical properties and porosity of flax fibre cement composites reinforced with various contents of WG at 3% NS (n = 3) 170
Table 5.34: Toughness properties of cement composites after ageing (n = 3) 201

List of Acronyms and Symbols

Acronyms

FRC	Fibre reinforced cement composite
ASR	Alkali silica reaction
OPC	Ordinary Portland cement
AFt	Ettringite
AF_m	Monosulfate
XRD	X-ray diffraction
SEM	Scanning electron microscopy
ASTM	American Society for Testing and Materials
ANOVA	Analysis of variances
C-S-H	Calcium silicate hydrates
CH	Calcium hydroxide (Portlandite)
NS	Nano-silica particles
NC	Nano-clay particles
WG	Waste glass powder
DOE	Design of Experiments
OVAT	One-variable-at-a-time
RSM	Responses surface methodology
CCD	Central composite design
BBD	Box-Behnken design
DTA	Differential Thermal Analysis
TGA	Thermogravimetric Analysis
SCMs	Supplementary cementitious materials
MMT	Montmorillonite
OMMT	Organo-modified montmorillonite
NFC	Natural fibre cement composites
EDX	Energy Dispersive X-ray
rpm	Revolutions per minute
NIST	National Institute of Standards and Technology
BSE	backscattered electrons
WD	wavelength dispersive
PE	primary electrons
AE	auger electron
PC	Personal computer
JSCE	Japan Society of Civil Engineers
RILEM	International Union of Laboratories and Experts in Construction Materials, Systems, and Structures

Symbols

TS	Tensile strength
YM	Young's modulus
I_{cr}	crystallinity index
ε	thermal strain
V	Fibre volume fraction
L	Fibre length
I_5, I_{10} and I_{20}	Toughness indices
G_F	fracture energy
P	Porosity
F_{st}	first crack strength
F_{max}	peak strength
F_{flex}	flexural strength
F_{imp}	impact strength
F_{com}	compressive strength
A	peak area taken from the DTA profile
R	calibration constant (8.11×10−4))
CO_2	Carbon dioxide
C_3S	tri-calcium silicate (alite)
β-C_2S	di-calcium silicate (belite)
C_3A	tri-calcium aluminates
C_4AF	tetra calcium alumina ferrite (celite)
SiO_2	silicon dioxide
Ca	Calcium
CaO	Calcium oxide
Na	Sodium
K	Potassium
NaOH	Sodium Hydroxide
OH	Hydroxyl
TiO_2	Titanium dioxide
Al_2O_3	Aluminium oxide
Fe_2O_3	ferric oxide
$C_6H_{11}O_5$	glucan polymer
C	Carbon
CH_2OH	iso-saccharin acid
Mo	Molybdenum
Cu	Copper
Si-Li	Silicon-Lithium

Chapter 1 : Introduction

1.1 Introduction

Next to food shortages, housing shortages is one of the most important issues on our planet, particularly in developing countries. To improve this situation and make it possible to build more houses, especially for low-income families, it is necessary to consider all locally available materials which can be used in the construction sector. Material sciences have always been a leading driver in construction innovation. This is still true today with new technologies producing new materials and improving the performance and application of old materials. However, many problems have to be addressed and resolved before such materials are broadly accepted in the marketplace. Issues such as sustainability, eco-friendliness, durability, long-term performance, design methods to allow their integration in construction, and new or modified standards to facilitate these new construction materials acceptance in the marketplace are often mentioned.

Globally, large amounts of agriculture wastes are generated every year. For example, flax is an oilseed crop where the seed is processed for its high oil content, while the biomass left behind tends to be a problem because it has strong fibres which breakdown very slowly under natural conditions. Traditionally, flax straw has been discarded or burned as a waste material by farmers. On the other hand, the re-use of this waste material to reinforce cement matrixes and as a substitute for synthetic fibres, particularly glass fibres, provides a more environmentally responsible use for flax straw [1,2].

The use of natural fibres to strengthen brittle materials, which are much weaker in tension than they are in compression, can be traced back to the beginning of human civilization. The ancient history of using natural fibres goes back to Egypt some 3500 years ago; clay was reinforced with straw and hair from animals to build walls used in housing. Around the same time period, sun-baked bricks reinforced with straw were used to build the 57 m high hill of Aqar Quf (near present-day Baghdad). Afterwards, the use of natural fibre in construction declined, due to the

introduction of more durable fibres such as steel and glass fibres. The history of modern manufactured fibre cement composites began around 1900 with the invention of Hatschek process. Asbestos–cement was the first fibre reinforced cement composite (FRC) in modern history, and was widely used as a cladding material, for roofs and walls. However, this composite is of little interest today due to its attendant health hazards. Following the success of asbestos fibres, the pace of FRC development accelerated through the use of a wide variety of conventional fibres such as steel and glass as well as new fibres such as carbon, Kevlar, polypropylene and nylon [3].

Although synthetic fibres are strong and stiff, recently, due to increasing environmental awareness, depletion of petroleum resources, disposal problems, and the introduction of new rules and regulations by legislative authorities, the production and use of traditional cement composite materials made with synthetic fibres like glass, has been criticised [4,5]. As a consequence, natural fibres such as flax, hemp, sisal, jute, ramie, coir and cotton have attracted attention as a replacement for synthetic fibres due to and increased emphasis on sustainability. These natural fibres offer many advantages which make them attractive for cement reinforcement. For example; natural fibres are abundant, relatively cheap, low in density, environmentally friendly, nonabrasive and their specific properties are comparable with the most commonly used reinforcing glass fibres [5,6,7]. The leading driver for replacing glass fibres with natural fibres is their low cost. While the cost of glass fibre is about US $1.5-3.2 per kg and it has a density of 2.5 g/cc. , the price of natural fibre is about US $ 0.1-1 per kg and its density is 1.2-1.5 g/cc [8]. Table 1.1 [1], clearly shows that although the tensile strength (TS) of natural fibre is lower than that of glass fibre, the specific modulus of natural fibres (Young's Modulus (YM) per unit specific gravity) show values that are comparable to or even better than values for glass fibres.

Table 1.1: Properties of glass and natural fibres [1]

Properties	Fibre							
	E-glass	Flax	Hemp	Jute	Ramie	Coir	Sisal	Cotton
Density (gm/cc)	2.55	1.4	1.48	1.46	1.5	1.25	1.33	1.51
TS (Mpa)	2400	800-1500	550-900	400-800	500	220	600-700	400
YM (GPa)	73	60-80	70	10-30	44	6	38	12
Specific modulus (YM/density)	29	26-46	47	7-21	29	5	29	8
Elongation at failure (%)	3	1.2-1.6	1.6	1.8	2	15-25	2-3	3-10
Moisture absorption (%)	-	7	8	12	12	10	11	8-25

Despite all of the aforementioned advantages, the industrial production of natural cement composites has been hindered by its weakness in terms of durability and long term performance. The alkalinity of the cement matrix and the volumetric instability of the fibres are the main causes of the loss of resistance of natural fibre-reinforced cement mortar composites. As a result, the scientific community has made substantial efforts in the last decade to improve the durability and long term performance of natural fibre-reinforced cement composites to address these weaknesses [7,9].

The decomposition of natural fibres in cement-based composites occurs due to the fact that the alkaline pore water dissolves the lignin and hemicelluloses existing in the middle lamellae of the fibres, thus weakening the link between the individual fibre cells. Furthermore, the alkaline hydrolysis mechanism of cellulose molecules causes degradation of molecular chains, thereby leading to a reduction in the degree of polymerisation and the lower tensile strength of the fibres [7,10]. Currently, two approaches have been explored for the reduction of alkaline attack on fibres in natural fibre-reinforced composites. One involves the modification of the cement matrix by using pozzolanic materials or polymers to reduce or remove the alkaline compounds. This can also be achieved by the modification of the surface of the fibres with chemical or physical treatments in order to increase their stability in the cementitious matrix [7]. The reduction of cement matrix alkalinity by using pozzolanic materials, such as silica fume [11], fine powdered metakaolin and

calcined waste crushed clay brick [12] is one of the most successful techniques for improving the durability of natural fibre cement composites [9].

The use of recycled materials in construction is among the most attractive options because of the huge need of this industry for these materials, relatively low quality requirements and widespread construction sites [13]. Although glass is a highly recyclable material, recycling of coloured bottle glass causes major problems due to the high cost of cleaning and colour sorting. It is also widely believed that the storage of coloured bottles is cheaper than recycling them. Therefore, most coloured bottle glass is regarded as a low-value product and it is usually dispatched to landfills as waste material. Since glass is not biodegradable, landfills also do not offer an ecological solution. However a potential answer that would provide a sustainable, ecological and economic solution for mixed-colour bottle storage would be to re-use coloured waste glass in the cement and concrete industries.

As reported by Shao et al. [14], a typical pozzolanic material should satisfy three characteristics: it should have a high silica content, be amorphous in nature and have a large surface area. When compared to silica fume, glass contains relatively large quantities of silica (54-81% by weight) and is amorphous in nature. Therefore, in theory, glass is pozzolanic or even cementitious in nature and thus it might satisfy the basic requirements for a pozzolan if it was also finely ground in order to mitigate the alkali silica reaction (ASR) and to activate pozzolanic behaviour [15,16]. Hence, it could be used as a cement replacement in natural fibre cement composites. The use of finely ground glass as a pozzolanic material is a relatively recent development, and it has also been encouraged due to the environmental issues associated with the continual accumulation of waste glass [17]. Furthermore, according to the requirements of ASTM C618 [18], glass has the potential to be functionally acceptable as a cement replacement.

However, one of the limiting factors in the use of finely ground waste glass powder in concrete is the lower reactivity of glass powder when compared to cement powder. This limitation requires the use of practical methods for increasing the reactivity of waste glass powder [19].

Recent advances in nano materials science show that nano-sized particles, such as nano silica and nano clay particles, have a high surface area to volume ratio that have the potential for tremendous chemical reactivity [20]. Furthermore, adding a small amount of these materials (< 3% by cement weight) to the cement matrix could accelerate pozzolanic activity, improve workability, control ASR, and increase the strength and durability of concrete [20,21,22,23,24,25,26]. Therefore, using nano particles to increase the pozzolanic activity of waste glass powder would be a promising approach in improving the performance of this material.

Besides the properties of fibre and matrix, the interface between these two constituents also plays a significant role in composite materials. The interface has to be sufficiently strong so that mechanical loading is transferred from the matrix to the reinforcing fibres, thus improving toughening mechanisms like debonding and pull-out. Fibre-matrix adhesion should also be treated to improve fibre surface properties [3,27].

Accordingly, the incorporation of flax fibre, waste glass powder and nano particles into the cement matrix, provides substantial benefits. Material cost savings and high mechanical performance, coupled with the advantage of being ecologically acceptable, make flax fibre, waste glass, cement nano composites a promising alternative construction material. Furthermore, re-using waste glass in construction can reduce the CO_2 emissions associated with cement production. The social and environmental benefits of this composite are realized through the use of a natural renewable fibre and a green cement matrix.

Therefore, the use of these new cement composites addresses several different sustainable construction issues: first: the environmental impact of building materials, secondly: the re-use of huge amounts of waste glass, third: the effective utilisation of a high-growth raw material (flax), and finally; the increasing demand for housing growing populations particularly in developing countries.

While technical solutions for construction material concerns have long been provided by engineers, this thesis intends to address to the primary goal of civil engineering; using technical excellence and creativity to improve the quality of life

by addressing the underlying concerns of environmental protection, social considerations, economic viability, sustainability and public safety.

1.2 Aim of the thesis

While the reduction of negative environmental impacts is one of the primary goals, the need for durable and high-quality building materials, which can be economically produced using simple production processes and tools, is the underlying concern.

The aim of this work is to produce high quality flax fibre waste glass cement composites for potential use in construction applications.

In this work, flax fibres will be used to reinforce two systems; the first system contains only Ordinary Portland cement (OPC) as a binder, while in the second system; a portion of OPC will be replaced by finely ground waste glass powder. In order to improve the durability and long term performance of these composites, nano-clay particles and colloidal nano-silica will be added during the production of both systems. An alkali treatment of the fibres will be carried out during the production of both systems in order to; remove the surface impurities from the fibre surface, enhance the adhesion between matrix and fibre, and improve long term stability of the composites.

1.3 Thesis Objectives

The primary objective of this thesis is to assess the performance of flax fibre cement composites. Based on a critical review of the literature, this study has been broken down into the following components:

- Gain an understanding of natural fibre reinforced cement composites, the application of waste glass and nano materials in concrete industries, and an insight into work previously done by other researchers in this particular area.
- Treatment of flax fibres with alkali and the development of mathematical models using factorial design with the aid of Design-Expert version-7 statistical software in order to predict the tensile strength and Young's modulus of treated fibres. Also determine the optimal treatment conditions,

based on the developed models and numerical optimisation, required to achieve the desired criteria.

- Characterisation of the alkali treated fibres through the use of X-ray diffraction (XRD), scanning electron microscopy (SEM) and thermogravimetric analysis (TGA) and differential thermal analysis (DTA).
- Investigate the influence of alkali fibre treatment on the mechanical and thermal properties of natural fibre cement composites.
- Determine the optimal amount of fibre content and fibre length by using factorial design. Also develop mathematical models in order to predict and optimize the following process responses:
    1. Flexure strength
    2. Fracture energy
    3. Impact strength
    4. Compressive strength
    5. Toughness indices
    6. Porosity
- Present the developed models graphically in order to illustrate the effect of each mix parameter on the above mentioned responses.
- Apply the analysis of variances (ANOVA) to test the adequacy of the developed models and examine each term in the developed models using statistical significance tools.
- Determine the optimal combinations of mix parameters, using the developed models with numerical optimisation and graphical optimisation, required to achieve the desired criteria for the responses listed above.
- Improve the performance of the optimised flax fibre composites through the incorporation of waste glass powder, nano-clay particles and colloidal nano-silica.
- Characterisations of the flax fibre cement composites through the use of X-ray diffraction (XRD), ASR test, scanning electron microscopy (SEM), thermal expansion and thermogravimetric analyses (TGA/DTA).
- Study the durability and long term performance of cement composites, which were subjected to the following three (different) ageing conditions:
    1. Immersion in water at 20 ℃ $\pm$ 2 for 360 days,

2. 50 controlled wetting and drying cycles.
3. Dublin open air weathering which started in September 2009 and ended in September 2010.

1.4 Thesis Structure

This thesis is divided into two major sections and consists of six chapters. The first section consists of Chapters 1, 2, 3 and 4, which represent the introduction, literature review, materials and characterisation techniques as well as the optimisation methods used in this work.

Chapter 1 provides a general introduction to the thesis with a brief history on the development of natural fibre cement composites. It also includes the thesis aim, thesis objectives and the structure of the thesis.

Chapter 2 contains background information and a comprehensive literature review related to the present work.

Chapter 3 contains details of relevant test methods, materials, experimental procedures and the equipment used for testing.

Chapter 4 explains the design of experiments and some details on the Box-Behnken and central composite designs, as well as the steps followed to establish the design matrix and mathematical model.

The second section includes chapters 5 and 6 which contain the results, discussion and conclusions drawn from the results.

Chapter 5 deals with the chemical modification of fibres, optimisation of the alkali treatment conditions of flax fibres and fibre characterisation. It also shows the influence of fibre treatment on the mechanical and thermal properties of flax fibre cement composites. Additionally, it covers the optimisation of fibre parameters (i.e. length and volume fraction) and the content of waste glass powder, nano-clay and nano-silica particles. Moreover, it addresses the influence adding different types of additives such as waste glass powder, nano-clay and nano-silica have on the mechanical properties, thermal behaviour, microstructure, alkali silica reaction and durability of flax fibre composites.

Chapter 6 provides the conclusions drawn from the results, some recommendations and suggestions for future work based on the current study.

Chapter 2 : Literature Review

2.1 Introduction

According to ASTM C-150, ordinary Portland cement (OPC) is hydraulic cement produced by pulverizing clinker, which consists of hydraulic calcium silicates, usually containing one or more types of calcium sulphate, as an interground addition. OPC is a mixture of silica, aluminium oxide, calcium oxide and ferric oxide. The primary source of lime is limestone or chalk and the main source for silica and aluminium oxide are shales, clays or salts. The major phases of OPC are tri-calcium silicate C_3S (alite), di-calcium silicate β-C_2S (belite), tri-calcium aluminates (C_3A) and the ferrite phase of tetra calcium alumina ferrite, C_4AF (celite). Alite and belite together make up 75-80% of OPC. In the presence of a limited amount of water, the reaction of alite is characterised by a rapid rate of hydration within a few hours and rapid strength development, while the reaction of belite is characterised by a slow rate of hydration within days and slow strength development within weeks. Although celite makes up about 4-11% of OPC, it significantly influences the early reactions. Celite is characterised by a very rapid rate of hydration within a few minutes and very rapid strength development within the first 24 hours [28].

Generally, the hydration process is a chemical reaction between the cement clinker and water. Calcium silicate reacts with water in two phases. In the first phase, calcium silicate hydrates (C-S-H) produce particles of colloidal sizes with poor crystallinity that develops a high surface area. The second phase uses calcium hydroxide (Portlandite) for hexagonal crystallinity. The hydration process is explained as follows. As soon as the alite comes into contact with water, it releases calcium and hydroxyl ions exothermally with rapid heat generation until a certain critical concentration of crystallisation of both Portlandite (CH) and C-S-H is reached. Finally, within about 12-24 hours, a slow formation of the product is reached. The hydration of celite proceeds in similar way to that of alite, but is slower. The hydration of belite also proceeds in a similar way to that of alite, but at much slower rate and with a lower heat release when compared to alite. The hydration of

tricalcium aluminate is controlled by the addition of gypsum in order to regulate setting time. It reacts with gypsum and water to form ettringite within a few minutes. Ettringite has prism-shaped hexagonal crystals (needle-like) which are longer than CH crystals. After all of the gypsum is converted to ettringite, the excess tricalcium aluminate reacts with ettringite to form a monosulpho-aluminate hydrate. This takes, on average, 12-36 hours depending on the sulphate ion contents of the gypsum. Generally, the rate of hydration in order of decreasing rates are as follows; aluminate > alite> celite> belite [28].

The ettringite phase (abbreviated as AF_t) in cement paste, develops during the first few hours leaving a small amount in cement past after a few days of hydration. The ettringite appears as stumpy rods in SEM analysis with an average length of a few micrometres. The monosulpho-aluminate phase (AF_m) forms after the aft disappears and comprises around 10% of the solid phase in the mature cement phase. The monosulpho-aluminate has a hexagonal morphology resembling that of CH. C-S-H is the principal product of the OPC hydration process, which governs the mechanical and physical properties of hardened cement paste. The morphology of C-S-H is subdivided into three types; Type (I) C-S-H, occurs at an early age and appears as elongated or fibrous particles a few micrometres in length. Type (II) C-S-H forms in conjunction with type (I), and appears as a reticular or honeycombed structure, while type (III), which is a late hydration product, appears as a compacted and dimpled structure [28,29,30]. Calcium hydroxide (CH) is a soluble compound, which means it moves throughout the pore system in the presence of water. This movement increases the past's porosity and its susceptibility to sulphate attack. Supplementary cementitious materials (SCMs) such as silica fume and blast furnace slag are used as partial cement replacements in concrete in order to improve durability, ultimate strength, workability, hydration heat and permeability. These improvements develop during the pozzolanic reaction between amorphous silica in the SCMs and Portlandite (CH) and the formation of insoluble C-S-H [19].

2.2 Pozzolanic Materials

A pozzolan is a siliceous or aluminous material, which in itself posses little or no cementitious property, but it the presence of moisture chemically reacts with calcium hydroxide at room temperature to form compounds that possess cementing properties.

The concept of using of pozzolans in building materials can be traced back to the very beginning of civilization. Lime- natural pozzolan composites were used as

the primary cementitious material for the construction of ancient structures in Egypt, Greece, Rome and India. In Egyptian and Indian civilizations the source of pozzolans was calcined clay from crushed bricks, tile and pottery, while, in Greece and Rome the source was volcanic ash. In fact, the term pozzolan was first used in Italy to describe the volcanic ash mined at Pozzuoli, a village near Naples [31].

Later on, lime- natural pozzolans lost favour, due to the discovery and use of hydraulic lime (impure lime that contained a substantial amount of calcined clay) during the 18^{th} century, which was the forerunner for the invention of Portland cement in 1824. Due to the superior setting and hardening characterises of OPC, it rapidly became the most favoured cementing material instead of lime- natural pozzolans. However, due to the technological, economical and environmental considerations (described below), large quantities of pozzolans are in use today by concrete industries in the form of mineral admixture and supplementary cementitious materials (SCMs) such as silica fume and blast furnace slag [31]. The benefits of using pozzolans in the cement and concrete industries can be divided into the following three categories:

Engineering benefits: The incorporation of finely divided particles into a concrete mixture tends to improve workability, increase ultimate strength, enhance durability, reduce porosity, improve resistance to thermal cracking due to the lower heat of hydration, and increase tensile strain capacity.

Economic benefits: Whenever a pozzolanic and/or cementitious by-product can be used as a partial replacement for OPC in concrete, it provides substantial energy and cost savings. OPC is a highly energy intensive material and increases in energy costs have been reflected in correspondingly higher cement costs. Therefore, OPC also represents the most expensive component of a concrete mixture. On the other hand, most of the pozzolanic and cementitious materials are industry by-products that require low or even no expenditure of energy for their use in concrete industries.

Ecological benefits: the total volume of pozzolanic and cementitious by-products exceeds 500 million tons per year. Many of these by-products are hazardous to human health, ground water and soil if they are not disposed of safely. The concrete industries provide an excellent way to dispose these hazardous by-products, where

the most harmful components can be safely incorporated into the hydration of cement. Furthermore, incorporation of these by-products into the cement matrix can greatly mitigate the emissions of CO_2 and other air pollutants emitted from the manufacturer cement clinker, where every ton of OPC production is accompanied by a similar amount of CO_2 emissions into the environment [19,31].

2.2.1 Waste Glass Powder as a Pozzolanic Material

The concept of using waste glass in concrete is not new; early efforts were conducted in the 1960s to use crushed waste glass as an aggregate replacement [15]. However, these attempts were not satisfactory due to the strong reaction between the alkalinity of the cement and the reactive silica in glass, also known as alkali silica reaction (ASR) [14,15]. In addition to ASR, using waste bottle glass limits the size and shape of coarse aggregate because crushed bottles will tend to form flat and elongated shapes, which may negatively affect workability and reduce compressive strength. Also, most mixed colour bottles are of different chemical compositions and may be contaminated due to paper or plastic labels, caps and sugars that remain from the original contents of the bottles [19,32]. Furthermore, using waste glass as an aggregate could decrease slump, air content, fresh unit weight, tensile and flexure strengths [33].

In the last decade, the re-use of waste glass in the cement and concrete industries has again attracted many researchers [13,14,34] due to the high disposal costs for glass and environmental regulations. Currently, several efforts have been made to overcome the limitations of ASR, which focused on reducing the particle size of the waste glass through prolonged grinding. The results of this work showed that very fine glass powder greatly decreased ASR expansion. Furthermore, the results revealed an improvement in compressive strength, resistance to sulphate attack and chloride ion penetration with the use of very fine glass powder (less than 100 μm).

Shao et al. [14] used 30% waste glass, namely fluorescent lamps, as cement a replacement, and their results showed that waste glass finer than 38μm recorded a significant reduction in ASR expansion when compared to control mortar.

Shi et al. [13] also found that finely ground glass powders exhibited very high pozzolanic activity. Their results showed that the pozzolanic activity of glass powder greatly increased by decreasing the glass particle size, which in turn greatly deceased the tendency for ASR and improved the compressive strength of concrete.

However, using up to 50% waste glass as a cement replacement, Chen et al. [34] found that a particle size less than 75μm possesses cementitious capability and improves compressive strength, resistance to sulphate attack and chloride ion penetration.

Whereas, The works of Shi et al. [13], and Schwarz et al. [35] , indicated that below 100 μm, glass can have a pozzolanic reactivity greater than that of fly ash as a low cement replacement (10 to 20%) after 90 days of curing.

Corinaldesi et al. [36] used sodium-calcium glasses with particle sizes ranging from 36 μm to 100 μm, to study the effect of glass particle size on ASR. Their results did not detect any deleterious effect at a macroscopic level due to the reaction between cement paste and ground waste glass with particle sizes up to 100 μm. Also, their results showed a strong improvement in the compressive and flexure strength of the mortar, due to the positive contribution of the waste glass to the micro-structural properties.

Work by Karamberi and Moutsatsou [37] indicated that finely ground colour glass cullet up to 90 μm was found to increase pozzolanic activity, improve compressive strength and caused negligible ASR expansion.

Idir et al. [16] showed that pozzolanic activity increases with glass fineness and that equivalent or superior compressive strength can be attained using up to 40% mixed colour glass (less than 40μm) when compared to their reference specimen without glass.

Some researchers [38, 39] also investigated the effect of glass colour on the mechanical properties of concrete. Park et al. [38] and Sobolev et al. [39] showed that there was no significant difference in the performance of coloured glasses.

The incorporation of glass into concrete as a SCM will depend on its performance, namely its strength, durability and volumetric stability over time. Controlling of the beneficial pozzolanic reactions and damaging ASR, which depends on several factors involving calcium content, particle size, and alkalinity, the dissolved silica will depolymerise into expansive gel, hydrate into C-S-H or a combination of both. Buchwald el al. [40] and Urhan [41] proposed that at any time in a cement matrix containing either reactive aggregate or pozzolanic material, ASR gel and C-S-H, as well as a range of intermediate products, can be found. The availability of calcium ions in combination with a relatively high rate of C-S-H formation will lead to a pozzolanic reaction, and over time, any ASR product will take on the texture of C-S-H. AS glass powder reacting like a pozzolan will follow Eq. (1), and the product will be a type of C-S-H [19].

$$SiO_2\,(s) + Ca^{2+}(aq) + 2OH^-\,(aq) \rightarrow n_1 CaO.SiO_2.n_2H_2O\,(s) \qquad (1)$$

When the reaction of glass results in ASR gel, sodium or potassium ions may be substituted for calcium as shown in Eq.(2) [19].

$$SiO_2 + 2Na^{2+}(K^+) + 2OH^- \rightarrow Na_2(K_2).SiO_3.H_2O \qquad (2)$$

This system may be lead to variability in the swelling properties of ASR products.

Wang and Gillott [42] proposed that the mechanism which differentiates between pozzolanic and ASR products is the degree of aggregation or the particle size of the silica source. They demonstrated that the two reactions compete with each other and that the ease with which calcium ions can reach the pozzolanic reaction results in a more stable and less expansive product. The re-use of glass in concrete industries is accompanied by two antagonistic behaviours, depending on the size of the glass particles. First; ASR involves the production of a swelling product and secondly; beneficial pozzolanic reaction improves the strength and durability of concrete.

Previous works show that the use of waste glass as a SCM produces controversial and mixed results over a range of levels of replacement and particle sizes. As regards the requirements of ASTM C 618 [18], glass has the potential to function at acceptable level as an SCM, as shown in Table 2.1.

However, proper methods must be developed to control the ASR/pozzolanic reaction and increase glass powder reactivity. Recent studies have shown that nano sized particles such as nano clay and nano silica have a high surface area to volume ratio that provides the potential for tremendous chemical reactivity [20, 48, 49]. Also, they accelerate pozzolanic activity, improve workability, control ASR, and increase the strength and durability of concrete.

Table 2.1: Chemical composition of waste glass powder and other pozzolans

Compound	Glass [43,44]	OPC [45]	Slag [19,46]	Silica fume [47]
SiO_2	63.0-80.5	21.78	11.8-35	92
Al_2O_3	0.8-6.2	6.56	2.0-12	0.7
Fe_2O_3	0.0-3.0	4.13	0.3-22.6	1.2
CaO	0.3-12.76	60.12	39.6-47.5	0.3
MgO	0.0-8.7	2.08	0.0-7.5	0.2
K_2O	0.4-6.0	0.42	0.0-0.4	1.8
Na_2O	1.9-22.0	0.36	0.2-0.3	1.5
SO_3	0.0-3.50	2.16	0.2-9.0	0.3
others	0.05-3.5	2.39	-	2

2.3 Nanotechnology in Concrete

Nanotechnology is commonly defined as the creation of materials with fundamentally new properties and functions by controlling matter at the levels of atoms, molecules and super molecular (i.e., less than 100 nm) to create materials. Although nanotechnology science is new, nano-sized materials have been on earth for as long as life. The superior mechanical performance of biomaterials, such as bone, tooth, lobster and crab exoskeletons, oyster shells, coral, ivory, pearls, sea urchin spines, cuttlefish bone, is due to the presence of nano-crystals of calcium compounds [48,49]. Although nano-products are costly, research in nano-technology is gaining momentum with the motivation of immediate novel properties.

Since nanotechnology was introduced by Richard Feynman on December, 29, 1959, during his famous lecture ‘‘There’s Plenty of Room at the Bottom,” there have been many revolutionary breakthroughs in physics, chemistry, and biology that have employed Feynman’s ideas of manipulating matter at an extremely small scale,

i.e., the nano-scale [49]. As shown in Figure 2.1 nano materials can be created by two main approaches:

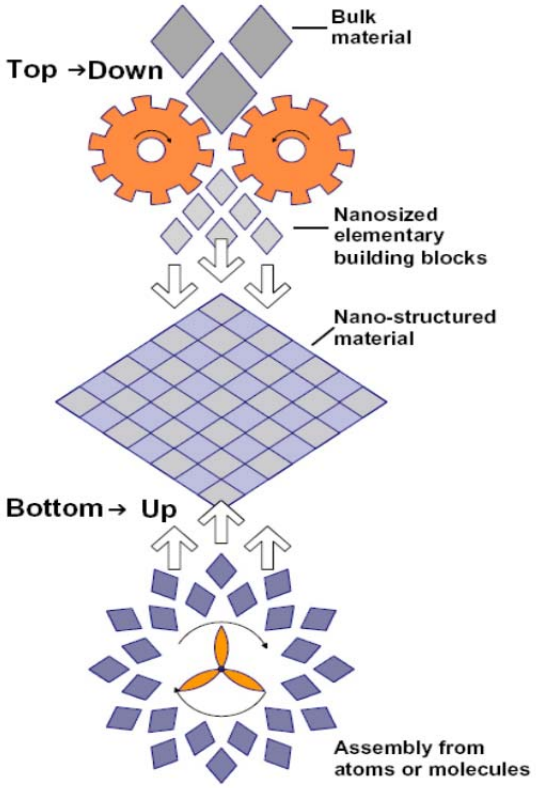

Figure 2.1: Setup of the ‘‘top-down” and ‘‘bottom-up” approaches in nanotechnology [49].

1- The ‘‘top-down” approach, in which bulk materials are broken down into nano-particles by mechanical attrition and etching techniques at nano-scale, while maintaining their original properties without atomic-level control (e.g., miniaturisation in the domain of electronics) or deconstructed from larger structures into their smaller composite parts [49].

2- The ‘‘bottom-up” approach defined by Drexler et al. [50], in which materials are constructed from atoms or molecular components through a process of assembly or self-assembly.

Successfully mimicking nature's bottom-up construction processes; is one of the most promising directions in contemporary nanotechnology. Although, nano applications in the construction and building materials fields; are mostly at laboratory stage, construction industry will be one of the major potential consumers

of nano-structured materials. Nanotechnology has the potential to enhance the desirable properties of concrete and overcome the common problems in concrete such as brittleness, dimensional instability, moisture fluctuation and insufficient resistance to chemical attacks. The majority of recent nanotechnology research in construction has been in the nano-science of cementitious materials that focuses on the structure of cement-based materials and their fracture mechanisms [20,49]. New advances in equipment for observation and measurement at the nano-scale; are providing a wealth of new and unprecedented information about concrete. This makes it possible to observe the structure at its atomic level. It provides further insight into the mechanism of cementisation at the nano-scale (e.g., structure and mechanical properties of the main hydrate phases, origins of cement cohesion, cement hydration, interfaces in concrete, and mechanisms of degradation) [20,49]. To date, nanotechnology applications in the building materials ranked eighth out of ten of most major developing areas of research. The most important areas of nano-engineering and nano-modifications of cementitious composites involve [20]:

- Incorporation of nano-scale spherical materials (e.g., nano-SiO2, TiO2, Al2O3, Fe2O3 etc.) and nano-tubes or fibres and nano-clay into cementitious materials during mixing , which improve mechanical and thermal behaviour as well as add novel properties,
- improve interfacial transition zone in concrete by adding nano-porous thin film on aggregate surfaces before concrete mixing,
- Enhance the workability of self-consolidated concrete.

2.3.1 Incorporation of Nano-Silica (NS) in Cement Matrix

Incorporation of nano-particles into the cement matrix to improve mechanical properties emerged as a promising research field of nano-composite. Most of the recent research [24, 51, 52, 53] is conducted with nano-silica particles (NS) and a few studies on incorporation of nano-clay particles (NC). Nano-scale particles are characterized by a high surface area to volume ratio providing potential for tremendous chemical reactivity. Nano-particles can act as nuclei for different cement phases, promoting cement hydration owing to their high reactivity. Furthermore, nano-reinforcement and as filler, densify the microstructure and the transition zone. Thus, leading to a reduced porosity and permeability. On the other

hand; the most significant issue for all nano-particles is that of effective dispersion especially at high loadings, even low loadings experiences problems with self-aggregation. This reduces the benefits of their small size and forms un-reacted pockets leading to increase concentration of stresses in the material [20,49].

Li et al. [51] showed that the compressive and flexural strengths of cement mortars containing NS (3%, 5% and 10% by weight of binder) were higher than those of plain cement. Also, their results showed that the compressive strengths of mortars with NS were all higher than those of mortars containing silica fume at 7 and 28 days period.

Even small amount of NS (i.e., 0.25%) Sobolev et al. [52] recorded 10% increase in compressive strength and 25% increase of flexure strength at 28 days. Björnström et al. [24] noticed that the addition of colloidal nano silica resulted in the acceleration of C_3S dissolution and rapid formation of C-S-H phase in cement paste.

Nano-silica decreases the permeability and hinders the leaching of calcium. Ji [53], as well as, Zhang and Li [54] demonstrated that the NS concrete has better water permeability resistant behaviour than the normal concrete. Li [55] noted that addition of small amount of NS (2wt %) leads to decrease in permeability of high fly concrete. In similar work, Lin et al. [25] shown that the relative permeability and pores sizes in sludge ash mortar decrease with NS addition (1wt %). Mandal et al. [56] showed that the volume fraction of the high-stiffness C-S-H gel increased significantly with addition of nano-silica, which provides an evidence of pozzolanic reaction. Also, their results revealed that NS did not change the average values of the hardness and modulus of any of the phases of C-S-H gel. On the other hand, it modifies the relative proportions of the two C-S-H phases, promotes the formation of the high-stiffness phase over the low stiffness. This has definitely positive significance on durability of concrete. In similar work, Gaitero et al. [57] reported that high stiffness C-S-H is more resistant to calcium leaching. They found that cement paste with NS showed increases in the average chain length of C-S-H gel, which hinders the leaching of calcium and improves durability.

Several authors [24,55,58] have studied the effect of NS particles on the microstructure of concrete and mortars by using SEM technique. They revealed that

when a small quantity (up to 3wt. %) of NS is uniformly dispersed in the cement paste, the microstructure of the NS concrete is more uniform, dense and compact than for normal concrete. Also, the microstructural studies by Nuclear Magnetic Resonance and Mercury Intrusion Porosimerty demonstrated that NS cement composite produce more solid, dense, and stable bonding framework [59].

A combined effect of the above mentioned mechanisms; produces a uniform dense microstructure with improvement not only in the mechanical properties of cement matrix but also in the physical properties. Good dispersion of NS is the key to achieve the full benefits of adding nano-particles in cement matrix. Self-aggregation especially at high amount of nano-particles is a common concern, which sometimes leads to in-homogeneous microstructure development and poor mechanical properties. The use of superplasticizer and high speed mixing were found to be effective in proper dispersion of nano-silica particles [20]. Also, Gaitero et al. [60], as well as, Björnström et al. [24] noticed that the colloidal nano silica being more effective in cement matrix than the powder.

2.3.2 Nano Minerals Clay

From the beginning of human civilisation, the use of clay is known in architecture, industry, and agriculture. Still, the production of sun-dried or fired bricks for building construction follow the same ancient procedures. Clay-based products, involving tiles for wall and floor, ceramics, earthenware, and pipes for drainage, were all used for several ages. An attractive behaviour of clay is its capability to swell and to mould in water, and to retain the shape of the container after drying. This characteristic performance had been used in the creation of several traditional clay products [61].

Although clay belongs to a wider group of minerals, in chemistry, all clay minerals may simply be described as hydrous silicates. These involve the kaolinite group, the montmorillonite/smectite group and the illite group [61,62]. The smectite and particularly montmorillonite are the clay minerals most used as fillers in nano composites. Montmorillonite is a flat structured smectite and it is classified as a magnesium aluminium silicate, which is the most abundantly available type of smectite. Thus, montmorillonite has an economical benefit over the other clay and,

therefore, it is commonly used for producing nano-composites [63]. Basically, it consists of a three layered structure of aluminium sandwiched between two layers of silicon. Montmorillonite is an active and major ingredient in a volcanic ash called bentonite, which has the ability to swell when it absorbs water. Thus, it is often mixed with water to give water higher viscosity and used as the drilling mud in removing drill debris of foundation excavation of civil constructions. In 1987, the techniques of cation exchange and intercalated polymerization were originally developed by Usuki and his colleagues in (Toyota central lab.) [65]. They produced for the first time to make a sheet-like nano montmorillonite with 1-nm thick individual layers and 100–1000 nm wide in platey dimensions and dispersed in nylon 6 matrix. Since then, the practical application of nano-montmorillonite has been improved from the traditional stabilizing drilling mud to some advanced utilizations like nano-composites [64,65]. As shown in Figure 2.2 montmorillonite clay is a sheet-like structure composed of tetrahedral SiO_4 and octahedral AlO_6 at a 2:1 ratio.

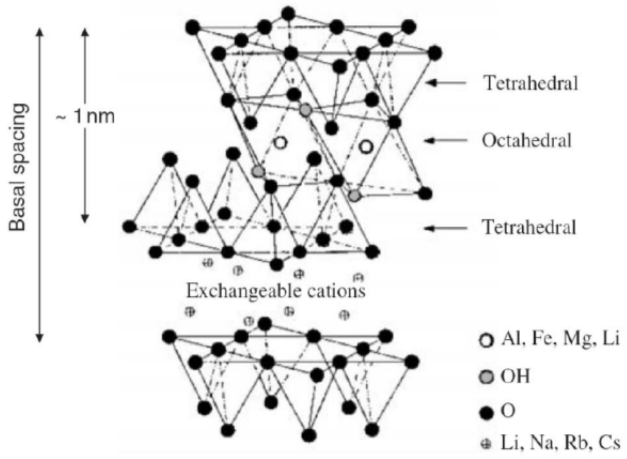

Figure 2.2: Structure of 2:1 clay minerals [66].

The stacking of silicate layers leads to a regular van der Waals gap between the layers called the interlayer or gallery. Each of these layers sustains a charge on their surface and edges. Montmorillonite clay is characterized by their ion exchange properties that lead to a high affinity to water, which makes the clay incompatible for use in cement matrix in their raw form. The advantage of the sheet-like configuration over other small particles is that the multi-layer silicate structure can be penetrated between layers by small molecules, forcing the silicate platelets apart. This process is

called intercalation. If the penetrating molecules reactive enough, this process may result in complete separation of the silicate layers (i.e. exfoliation), as presented in Figure 2.2 [20,66,67,68].

The morphology of nano-clay composites can be divided into three categories: conventional miscible composites, intercalated nano-composites, and exfoliated nano-composites, as shown in Figure 2.3.

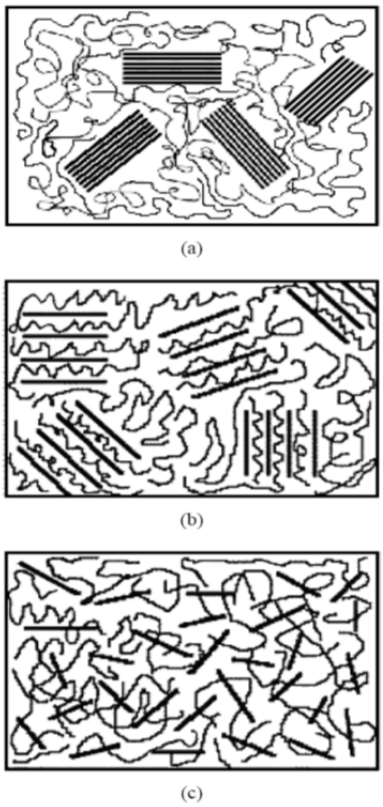

Figure 2.3: Schematic of morphologies of nano-clay composites: (a) conventional miscible, (b) intercalated and dispersed, and (c) fully exfoliated and dispersed [66].

In the miscible state, the clay particles maintain their crystal structure and the particle size at micro-scale. In the intercalated state, few composite molecules are inserted into the silicate galleries with fixed interlayer spacing. In the exfoliated state, the most popular one, a small mass of montmorillonite clay results in numerous small, thin (e.g. 20-nm) platelets, fully separated and with very large surface area. These nano-size silicate platelets may be used directly as a high reactive pozzolans in concrete, as a result, the nano-composites exhibits vastly improved properties. Therefore, the most advantageous morphological state for the clay nano-composites is exfoliation [20,66,67,68].

2.3.3 Incorporation of Nano Clay Particle in Cement Matrix

Nano-clay particles (NC) have shown promising results in improving the compressive and flexure properties, the resistance to chloride penetration, and the self-compacting properties. It also leads to reducing porosity, permeability and shrinkage [26,64,69,70]. As it stated earlier, the hydrophilic montmorillonite (MMT) micro-particles cannot be directly used as reinforcements in cement and concrete because;

- Water absorbed in the interlayer regions between silicate sheets causes damaging swelling and
- The interlayer alkali cations of MMT micro-particles are harmful to the durability of cement mortar and concrete.

The organo-modified montmorillonite (OMMT) micro-particles modified by a cationic exchange reaction become hydrophobic and thus can be employed to greatly enhance the strength and permeability of cement matrix [20,26].

Kuo et al. [26] found that for an optimal dosage (less than 1%) of OMMT micro-particles, the compressive and flexural strengths of cement mortars can be increased up to 40% and 10%, respectively and the coefficients of permeability of cement mortars could be 100 times lower .

They reported that the OMMT micro-particles around capillary pores can obstruct the diffusion of pore solution and aggressive chemicals and thus reduce the permeability of cement mortar and concrete. In addition, SEM micrographs revealed clusters of OMMT micro-particles for the dosage of OMMT micro-particles that exceeds 1%.

Chang et al. [64] shown that addition of nano-montmorillonite in cement paste (0.4 and 0.6 wt. %) causes increase of compressive strength (~ 13.24%) and a decrease of the permeability coefficient (~ 49.95%) with more dense solid materials and a stable bonding framework in the microstructure. Additionally, non-modified, nano-sized smectite clays were observed to act as nucleation agents for C–S–H and modified the structure of C–S–H [71].

The economic and environmental benefits can also be considered to be among the reasons for the large research interest in smectite clays. Clays are not costly and available in all countries. Even after the required treatments, their price is still within an acceptable range in view of the superior properties that nano-composites [72]. Because the structure of cement nano-composites is usually determined during their preparation, it becomes the most crucial step to achieve good properties in nano-composites. Using high speed shear mixers to mix nano-clay particles and water were found to be effective in the proper dispersion of nano-particles into a cement matrix according to Kuo et al. [26].

Although the incorporation of nano particles greatly improves the strength and permeability of cement matrix, however, the nano cement composite is still relatively brittle under normal stress and impact loads. The incorporation of short fibres (either natural or synthetic) in concrete, mortar and cement paste can improve many of the engineering properties of the basic materials, such as their fracture toughness, flexural strength, impact resistance and thermal shock [73]. Recently, due to government regulations and a growing environmental awareness throughout the world, the development and utilisation of natural fibre cement composites has been encouraged. Natural fibres have become the most acceptable alternatives to synthetic fibre, especially glass fibre, and have the potential to be used in cheaper, more sustainable and more environmentally friendly cement composite materials.

2.4 Natural Fibre Classification and Properties

Depending on the source of natural fibres, they can be classified into plant, animal and mineral fibres. All plant fibres are composed of cellulose, while the fibres of animals basically consist of proteins. Compared to animal fibres, natural cellulose fibres tend to be strong and stiff, and they are, therefore, widely used to reinforce cement matrix. Depending on the morphology of plant fibre, they can be classified into one of four categories [3,74]:

- ***Stem or bast fibres***: These fibres are derived from the stalks of plants, and are freed from the substances surrounding them by a process known as retting, which involves the combined action of bacteria and moisture. Common examples of this type of fibre are flax, hemp and kenaf.

- ***Leaf fibres***: These fibres are extracted from the leaves of monocotyledonous plants by a process in which the leaf is crushed and scraped to remove the fibres, followed by a drying process. Common examples of fibres in this category are sisal, henequen and abaca.
- ***Surface fibres***: These fibres are found as single cell fibres on the surface of stems, fruits and the seeds of plants. The most common examples of this category of fibres are cotton, coconut and coir.
- ***Wood (cellulose) fibres***: These fibres are relatively short and inflexible and are found in the xylem of angiosperm (hardwood) and gymnosperm (softwood). Common examples are bamboo, pine, maple and spruce. There are several factors that govern the selection of suitable cellulose fibres for use in composites. Chemical composition, structure defects, strength, durability stiffness and costs are the most important factors in selecting cellulose fibres for use in cement composites.

Table 2.2 presents a comparison of the relative costs for commonly used fibres, which depend on a number of factors such as supply, quality, demand and exchange rates [8,74,75].

Table 2.2: Relative prices for commonly used fibres [8,74,75]

Fibre	Price [US $/kg]	Fibre	Price [US $/kg]
Jute	0.3 - 0.7	Wood	0.2 - 0.4
Hemp	0.5 - 1.5	Glass	1.5 - 3.2
Flax	0.4 - 0.8	Carbon	100- 200
Sisal	0.1 - 1	-	-

As it is clear from Table 2.2, the prices of cellulose fibres are considerably lower than those for glass and carbon, however; cellulose fibres require further treatment to get them ready for use in composites. Despite this, cellulose fibres are still cheaper than synthetic fibres [74]. Wood is the most abundantly used cellulose

fibre because it is widely used in the paper and pulp industries. On the other hand, cellulose bast fibres like flax, hemp and jute are becoming more important in composite production because of their superior strength and stiffness. As it can be seen from Table 1.1, the strongest cellulose fibres are flax, hemp and jute. Flax fibres are more widely accessible and somewhat cheaper than hemp because of their widespread use in the textiles industry. They have considerably high value for Young's modulus of elasticity and have a high aspect ratio (length/diameter), which makes them an ideal candidate for use as an effective fibre reinforcement in cement matrix. Furthermore, Gram [76] noticed that flax fibres appear to be more resistant in concrete than sisal and jute fibres.

2.4.1 Flax Fibre

Flax has grown and its fibres spun and woven into linen textile for millennia. Still, flax is an agronomically important plant throughout the world and has been given the Latin appellation "linum usitatissimum", which means the extremely useful flax plant. It is an existing product source for many high-value markets in textile, oil, feedstock, cosmetics, medicine, paint, composites and paper/pulp [77].

The flax plant, Linum Usitatissimum is a member of family Linaceae which is distributed geographically in subtropical areas of the world. Its plant seed, linseed, is used for the production of linseed oil. Flax plants grow to a height of about 90-120 cm and about 0.15- 0.3 cm in diameter. Flax fibres are extracted from the plant by retting method. The number of fibre bundles in the stem is around 15 to 40 and each bundle includes from 12 to 40 elementary fibres [78]. These bundles are assembled and maintained together by pectin, which is removed during the retting process to enable the separation of the bundles [79]. The elementary fibres have a length of between 8mm and 30 mm and each fibre has highly crystalline cellulose fibrils spirally connected in a complete layer by amorphous lignin and hemicelluloses [80]. The principles for different levels of fibres in plants are described in Figure 2.4.

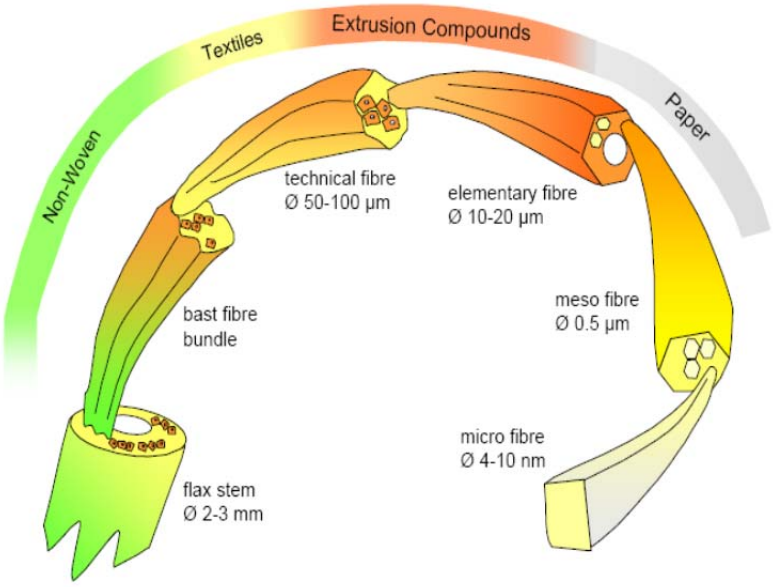

Figure 2.4: Schematic plot of a flax stem down to a micro fibre [81].

2.4.1.1 Flax Fibre Constituents

Cellulose, hemicelluloses and lignin are the basic components of cellulose natural fibres and govern the physical and mechanical properties of natural fibres. Table 2.3 [1], shows the chemical composition of some natural cellulose fibres. To better understand the behaviour of flax fibre-reinforced cement composites, it is important to know the physical and chemical properties of flax fibres. A single flax fibre consists of several cells arranged as concentric cylinders with a small channel in the middle called the lumen that contributes to water uptake as shown in Figure 2.5.

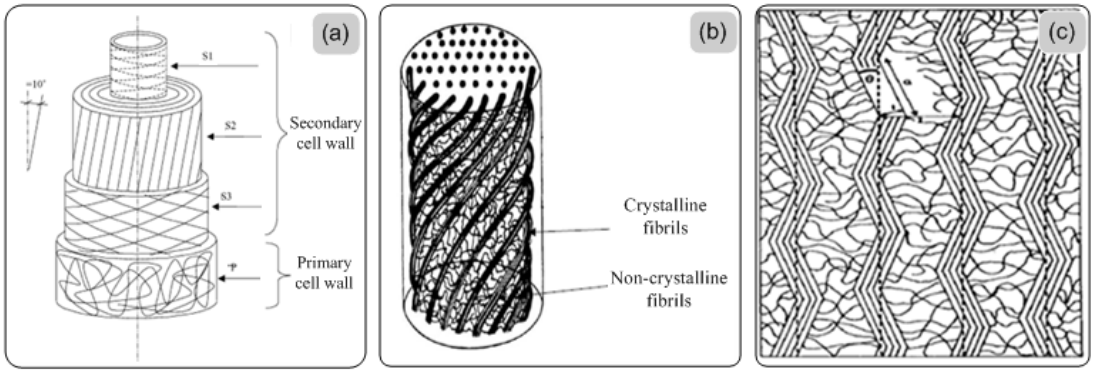

Figure 2.5: Principles of the flax fibre structure, a) the structure of a flax fibre cell, b) S2—layers in a 3D view, (c) S2—layers projected into a 2D view [80,82].

These cells consist of crystalline microfibrils based on cellulose that are connected to a complete layer by lignin and hemicelluloses. They are oriented at a tilt angle of 10º with the axis of the fibre and, therefore, display a unidirectional structure, as shown in Figures 2.6 and 2.7.

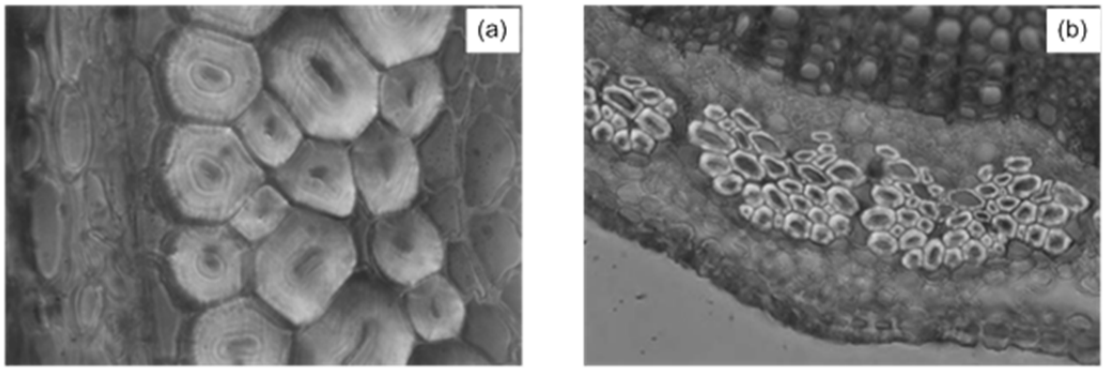

Figure 2.6: SEM micrographs showing (a) cross-section of flax stem x100 showing thickness of fibre walls and lumen and (b) cross-section of flax stem x 40 showing distinct fibre bundles [1].

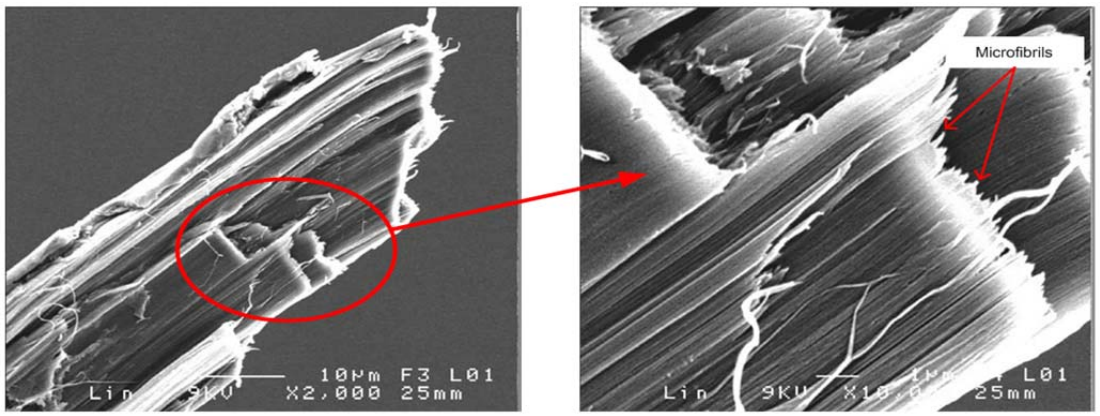

Figure 2.7: The break area of a flax fibre after a tensile test. The secondary wall shows the structure of a unidirectional composite, microfibrils are directed according to the axis of the fibre [82].

As summarised in Table 2.3, the main components of fully developed flax fibre cell walls are cellulose, hemicelluloses, lignin, pectin, waxes and water soluble substances. Climatic conditions, soil quality, the level of plant maturity and the quality of the retting process influence not only the structure of the fibres but also the chemical composition [80,82].

Table 2.3: Chemical composition of plant fibres by percentage mass (%) [80,82]

Fibre	Cellulose	Hemicellulose	Pectin	Lignin	Water soluble substances	Waxes
Flax	56.6-72	15.4-16.7	1.8-3.1	2-4.1	3.9-10.5	1.3-2.2
Coir	32.9-43.4	0.15-0.25	2.7-3	40.5-45.8	5.2-16	-
Jute	61-72.4	12-13.3	0.2	11.8-14.2	1.2	0.1-0.6
Sisal	65.8-70	13.3	0.9	9.9-12	1.3	0.3
Hemp	60-72	Nov-19	0.2-2	2.3-4.7	-	14
Ramie	68.9-83	13.1-14.5	1.9-2.1	0.6-0.7	6.1	0.2

2.4.1.1.1 Cellulose

The long thin crystalline microfibrils in the secondary cell wall are essentially made of cellulose, which are responsible for providing the fibres with high tensile strength. Over 150 years ago the French chemist, Anselme Payenfirst, discovered and isolated cellulose from green plants, and in 1842 he reported its elemental composition. Cellulose is glucan polymer ($C_6H_{11}O_5$) repeating units joined by 1, 4-β-D-glycosidic linkages at the C_1 and C_4 positions. Each repeating unit contains three hydroxyl groups, which form hydrogen bonds inside the macromolecule itself and also among other cellulose macromolecules, as well as with hydroxyl groups from the air (Figure 2.8) [74].

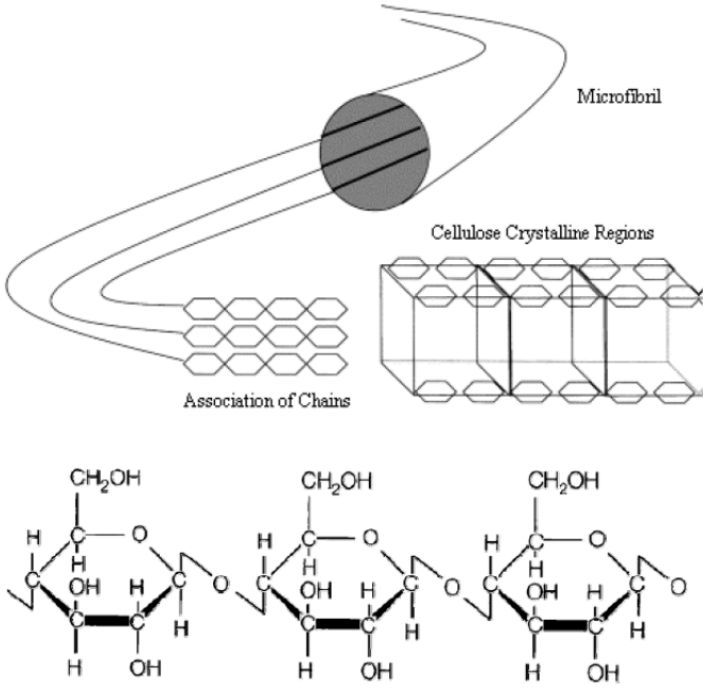

Figure 2.8: The molecular structure and arrangement of cellulose [74].

Therefore, all of the natural fibres are hydrophilic in nature [83,84,85]. Cellulose may either be crystalline or non-crystalline (amorphous), and most native cellulose is composed of crystalline segments (around 80%) alternating with regions of amorphous cellulose, as presented in Figure 2.9 [74].

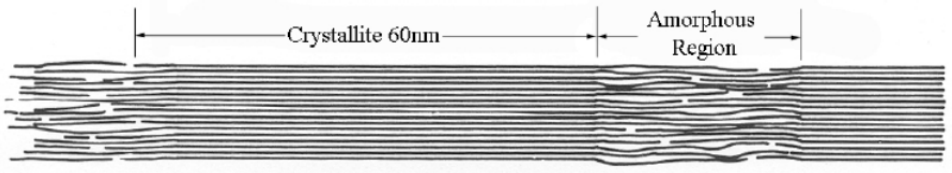

Figure 2.9: Schematic representation of the crystallite structure of cellulose [74].

The rigidity and mechanical strength of cellulose based materials is a result of hydrogen bonding, both between chains and within chains. The amorphous cellulose regions have fewer inter-chain hydrogen bonds, thus revealing reactive inter-chain hydroxyl groups (OH) used for bonding with water molecules. On the other hand, crystalline cellulose is closely packed, and very few accessible inter-chain OH groups are accessible for bonding with water. Therefore, crystalline cellulose is far less hydrophilic than amorphous cellulose. Crystalline microfibrils consist of tightly packed cellulose chains with available hydroxyl groups present on

the surface of the structure, as shown in Figure 2.10. Only the very strongest acids and alkalis such as sodium hydroxide can penetrate and modify the crystalline lattice of cellulose [74,80].

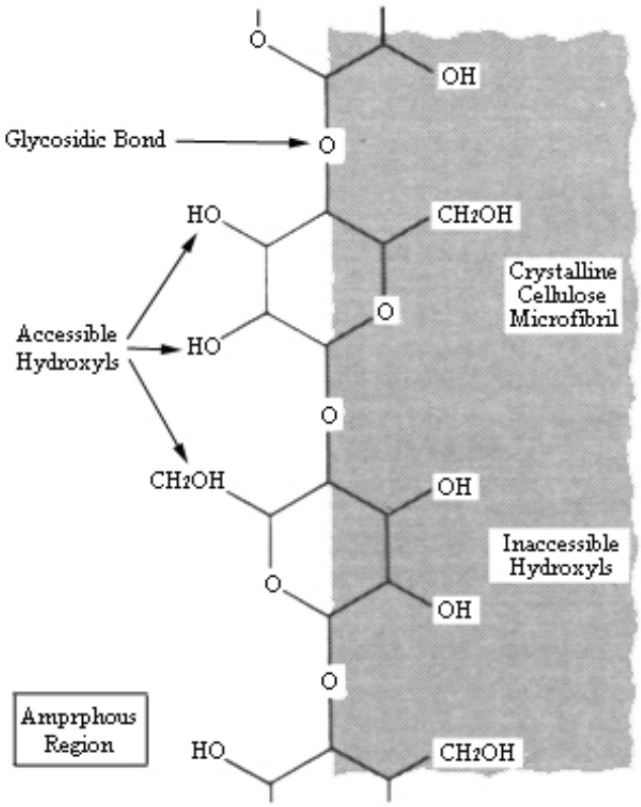

Figure 2.10: Microfibril surface [86].

2.4.1.1.2 Hemicelluloses

Hemicelluloses are not a form of cellulose but instead consist of a group of polysaccharide polymers containing mainly the sugars D-xylopyranose, D-glocopyranose, Dgalactopyranose, L-arabinofuranose, D-mannopyranose, and Dglucopyranosyluronic acid along with small quantities of other sugars [74,80]. The hemicelluloses differ from cellulose in three important features. First, hemicelluloses contain several different sugar units whereas cellulose contains only 1,4-β -D-glucopyranose units. Secondly they show a considerable degree of chain branching, whereas cellulose is a linear polymer. Third, the degree of polymerization of native cellulose is ten to one hundred times higher than that of hemicelluloses [80]. Hemicelluloses appear to form a link between cellulose and lignin, which leads to an effective transfer of shear stresses between the cellulose microfibrils and the lignin

[86]. Unlike cellulose, the hemicelluloses polymer chains are rarely crystalline and are mostly responsible for water absorption in the fibre wall. Also, they are heavily branched and have short side chains, while cellulose is a long unbranched polymer. It is suspected that no chemical bonding arises between cellulose and hemicelluloses, but sufficient mutual adhesion is achieved through hydrogen bonds and van der Waals forces [87]. Hemicelluloses have greater solubility in solvents when compared to cellulose, and can be thermally degraded at lower temperatures (150-180°C) than cellulose (200-230°C) [88].

2.4.1.1.3 Lignin

Together with cellulose, lignin is the most abundant and important polymeric organic material in the plant world. Lignin enhances the compression strength of slender microfibrils, and prevents them from buckling by gluing the fibres together to form a stiff structure, making it possible for trees of 100 meters to remain upright [89]. Lignin is a poorly understood hydrocarbon polymer with a highly complex structure comprising aliphatic and aromatic constituents that form a matrix sheath around the cellulose microfibrils and fibres [90]. No regular structure for lignin has ever been verified, and it is totally amorphous as opposed to the ordered structure of crystalline cellulose. Lignin is distributed throughout the primary and secondary cell walls, with the highest concentration being found in the middle lamella. The dissolution of lignin using chemicals, as is commonly done in the pulp and paper industries aids fibre separation. [91]. Lignin is thermally stable but is also highly susceptible to ultraviolet light, which is why lignin is responsible for the ultraviolet degradation of the fibre [27].

2.4.1.1.4 Pectin

Pectin is found in the primary cell walls of most non-wood plant fibres, and it consists of a complex branched structure of acidic structural polysaccharides, found in fruits and bast fibres. The majority of the structure consists of homopolymeric partially methylated poly-α-(1-4)-D-galacturonic acid residues, but there are substantial 'hairy' non-gelling areas of alternating α-(1-2)-L-rhamnosyl-α-(1-4) Dgalacturonosyl sections containing branch-points with mostly neutral side chains (1-20 residues) of mainly L-arabinose and D-galactose (rhamnogalacturonan I).

Pectin is the most hydrophilic compound in plant fibres due to its carboxylic acid groups and is easily degraded by de-fibration with fungi [90,92]. Pectin, along with lignin and hemicelluloses, are used to connect the elementary fibres together and can easily be hydrolysed at elevated temperatures. Pectin is the most hydrophilic compound in plant fibres due to the presence of carboxylic acid groups and is easily degraded by de-fibration with fungi [74,92].

2.5 Issues Regarding the Use of Natural Fibres in Cement Composites

Natural fibres offer many advantages which make them attractive for low cost cement reinforcement. Yet, despite their fibre advantages, untreated cellulose fibre composites have performed well below their potential capacities, and have therefore not been widely used in the concrete industry. The main reasons for their limited use are as follows:

- The high moisture absorption of natural fibres
- Poor interfacial bonding between natural fibres and the cement matrix
- The long-term performance of Cellulose fibres

2.5.1 Moisture Absorption Characteristics

Natural fibres are hygroscopic in nature; therefore they are very sensitive to changes in moisture content which affects both the mechanical properties of the fibre and its dimensions. Hence, one of the limitations of using natural fibres in durable composite applications is their high moisture absorption and poor dimensional stability. The swelling and shrinking of the fibres during wetting and drying may lead to micro-cracking of the composite and the degradation of its mechanical properties. As a result, the overall properties of the composite are more sensitive to moisture content than other fibre reinforced cementitious systems in which the fibres are not hygroscopic [2].

Another problem associated with fibre swelling is the week adhesion between the cellulose fibres and the cement matrix, resulting in a reduction in the mechanical properties of the composite. The interaction between the fibre and matrix may begin in the development of osmotic pressure pockets at the surface of the fibre

which lead to leaching of water soluble substances from the fibre surface [93,94]. This problem can be overcome by treating these fibres with suitable chemicals such as sodium hydroxide in order to decrease the hydroxyl group in the fibres. The strong intermolecular fibre-matrix bonding results in a decreasing rate of moisture absorption in natural fibre composites. Also, to increase the interface adhesion between the fibre and matrix, the fibre surface must be cleaned, bleached, chemically modified and its surface roughness must be increased [95].

2.5.2 Interfaces and Bond

Interfacial bonding is mainly dependent on the adhesion between the reinforcement and the matrix. The matrix/fibre interface plays a dual role of transmitting the stress between the two phases and of increasing the fracture energy of the composite by deflecting cracks and delocalising stress at the crack tip [96]. Poor surface adhesion due to surface impurities is the main reason for the formation of a weak or ineffective interface between the fibre and the matrix. Hence, these surface impurities prevent the hydroxyl groups from reacting with polar matrices, and form mechanical interlocking adhesion with non-polar matrices [97]. The interfacial bond itself can be mechanical or chemical in nature, or a combination of both [96].

2.5.2.1 Chemical Bonding

The chemical bonding occurs when a reaction takes place between reactive chemical groups on the fibre surface and compatible groups within the matrix. The strength of the structure mainly depends on the type of bond and the number of bonds per unit area. The most common chemical bonds and their approximate bond strengths are as follows [86]:

- Covalent Bond: 200 – 800 kJ mol^{-1}
- Hydrogen Bond: 10 – 40 kJ mol^{-1}
- Van der Waals: 1 – 10 kJ mol^{-1}

Cement is strongly alkaline (pH > 12) and presents metal hydroxy groups at its surface, such as -Ca-OH, -Si- OH, -Al-OH and -Fe-OH (due to hydration and the

hydrolysis of silicates, aluminates and to a lesser extent ferrites of calcium that are present in the cement matrix). Cellulose fibres include covalent hydroxyl groups, -C-OH, either phenolic (from residual lignin) or alcoholic (from the cellulose component) and carboxylic groups due to the oxidation of end groups. Hydrogen bonding and /or hydroxide bridges may play a significant role in the bonding of natural fibre cement composites [96].

2.5.2.2 Mechanical Bonding (interlocking)

Mechanical interlocking on the fibre/matrix interface occurs when the fibre surface is rough and jagged, as shown in Figure 2.11.

Figure 2.11: Schematic of mechanical interlocking [74].

This mechanical interlocking increases the interfacial shear strength, and reduces the possibility of fibre pullout [74]. Alkali treatments were found to improve the fibre surface adhesive characteristics by removing natural and artificial impurities, hence producing a rough surface topography. These changes in the morphology and in the chemical composition of the fibres results in improvements to the interfacial bonding by giving rise to additional sites of mechanical interlocking, which leads to an improvement of the mechanical properties [27].

2.5.3 Long-term Performance of Cellulose Fibres

Cellulose fibres degrade easily when exposed to natural weathering which may lead to changes in mechanical properties that are deleterious such as reductions in strength and toughness. Some of degradation processes involved are biological, thermal, aqueous, photochemical, chemical and mechanical degradation processes. These processes are independent but lead to undesirable results such as an increased sensitivity to cracking. However, with accurately designed components and adequately formulated and treated composites, these effects may be minimised or even prevented [3,74]. The key mechanism to be considered, with regard to the ageing of cellulose fibre in cement matrix, is the degradation of fibres due to alkaline

attack. The degradation of cellulose fibres in an alkaline environment can occur in conjunction with the following two mechanisms [3,76]:

- The peeling-off mechanism that occurs at the end of the molecular chain, which reacts with OH− ions and forms iso-saccharin acid (CH_2OH) that is unhooked from the molecular chain. The peeling-off effect is fairly harmless, since its rate at temperatures below 75 ℃ is low, and its effect on the long cellulose molecule (with a degree of polymerization of 25,000) is thus relatively small.
- The alkaline hydrolysis mechanism, which causes degradation of molecular chains, thus leading to a reduction in the degree of polymerization and lower tensile strength. Hemicelluloses and lignin are particularly susceptible to this particular degradation mechanism.

Gram [76] was the first to study the durability of sisal and coir fibre reinforced cement composites. Gram [76] suggested that in cellulose fibres the major mechanism of alkaline attack is associated with the dissolution and decomposition of the hemicelluloses and lignin in the middle lamella. As a result, the link between the individual fibre cells breaks down, as shown in Figure 2.12.

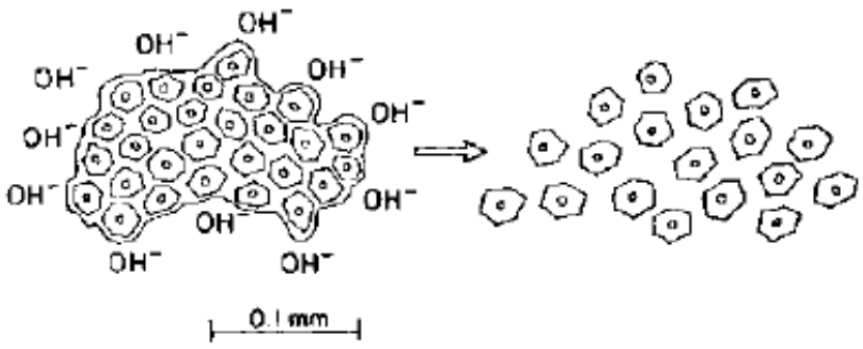

Figure 2.12: Schematic description of the degradation of sisal fibres in concrete [76].

The breakdown of the long fibre into small unit cells results in the loss of its reinforcing efficiency. It should be noted that Gram [76] found that the degree of alkaline attack was greater in a calcium hydroxide solution than in a sodium hydroxide solution, even though the latter has a higher pH. This effect could also contribute to the presence of Ca++ ions that result in some additional degradation.

Ramakrishna and Sundararajan [98,99] found similar mechanisms when they studied the effect of alkaline mediums (calcium hydroxide and sodium hydroxide) and fresh water on the durability of coir, sisal, jute and hibiscus cannabinus. They noticed that there was a substantial reduction in the salient chemical composition of all four of these natural fibres (i.e. 20–85% of celluloses and 30–70% of lignin) due to their exposure to all three mediums and two types of immersion. It was observed that lignin was leaching out and that the fibre gradually broke down and fibrillized. In similar work, Filho et al. [100] observed similar effects in a SEM backscattered images of short sisal or coconut fibres extracted from a cement matrix after six months of outdoor ageing or when the cement matrix was submitted to wetting and drying cycles. They also observed that the embrittlement was mainly associated with the mineralisation of the fibres due to the migration of hydration products, especially calcium hydroxide, to the fibre lumen, walls and voids.

2.5.4 Natural Cellulose Fibres Treatments

Cellulose fibre-reinforced composites could offer specific properties comparable to those of conventional fibre composites, however, low interfacial properties between the fibre and cement matrix often reduce the potential of natural fibres as reinforcement [101,102]. Interfaces play an essential role in the physical and mechanical behaviour of composites [94]. In order to enhance cellulose fibre-matrix adhesion, the fibre should be modified to better match fibre surface properties. Cellulose Fibres may be subject to biological, physical or chemical treatments in order to achieve one or more of the following objectives [74]:

- Removal of surface impurities and undesirable fibre constituents
- Roughening of the fibre surface
- Separation of individual fibres from their fibre bundles
- Chemical modification of the cellulose fibre surface
- Reducing the hydrophilicity of the fibres

2.5.4.1 Biological treatments

Biological treatments include the use of naturally occurring microorganisms such as bacteria and fungi. These types of treatments occur in aqueous environments

and are somewhat cheap to perform, however they also tend to be time consuming and water polluting. The two biological fibre treatments that are usually used are retting and fungal treatment.

Retting process

The retting process is the controlled decomposition of plant stems in order to free the bast fibres from their fibre bundles and separate them from the woody core and epidermis. During this process, bacteria (predominantly from the Clostridia species) and fungi liberate enzymes in order to degrade pectin and hemicelluloses in the middle lamella between the individual fibre cells. This leads to the separation of the bast fibres from the woody core, and leaves the fibres soft and clean [1,103]. The retting process produces high quality fibre, however it is highly dependent on weather conditions and the skill and judgment of the farmer [104,105].

Fungal treatment

Fungal infestations of wood, particularly by sapstain and white-rot fungi, cause serious wood quality problems such as decay and discolouration. On the other hand, these disadvantages can be used in a positive manner to assist in the selective removal of plant fibre components (i.e. cellulose, hemicelluloses, and lignin), and in physically modifying the fibre wall for improved fibre/matrix interfacial bonding.

Sapstain fungi (Ophiostoma) obtain their nourishment from the plant cell contents and can spread rapidly throughout a suitable growing medium. Sapstain fungi are harmful because their hyphae can break into the plant fibres and make fine holes as they pass through the cell wall. This results in an increase in the permeability of the fibre, thus making it more susceptible to water absorption [74]. But sapstain activity has many advantages for fibre treatment, as the holes in the cell wall created by the fungal hyphae increase the fibre surface area and expose additional reactive hydroxyl (OH) groups for bonding with the matrix. These holes enhance the surface roughness of the cell wall, which may result in improvements in mechanical interlocking with the matrix [106].

2.5.4.2 Chemical Modifications of Natural Fibres

Chemical modifications of cellulose fibres play an important role in improving the reinforcing capabilities of cellulose fibres. These chemical treatments could be classified as fibre pre-treatments, coupling agents or as dispersing agents. Pre-treatments include the use of chemicals that remove surface impurities and non-strength contributing fibre constituents such as lignin, pectin and hemicelluloses. Dispersing agents are applied in order to enhance the dispersion of fibres in the matrix. Coupling agents are mainly responsible for improving the adhesion between natural fibres and the matrix material, but can also decrease the water uptake of the fibres and assist with fibre dispersion. At present, the most popular treatments include the use of alkalis and acid hydrolysis [107].

2.5.4.2.1 Alkali Treatments

Alkaline treatment or mercerization is one of the most effective methods to produce high quality fibres [108]. The addition of aqueous sodium hydroxide (NaOH) to the natural fibre, promotes the ionization of the hydroxyl group to the alkoxide [101] Furthermore, alkaline treatment causes changes in crystallinity, which leads to better backing of cellulose chains [80]. The alkaline treatment causes disruption of the hydrogen bonding in the network structure, thereby increasing surface roughness which results in better mechanical interlocking. Moreover, it removes certain amounts of lignin, wax and oil on the surface of the fibre cell wall as shown in Figure 2.13.

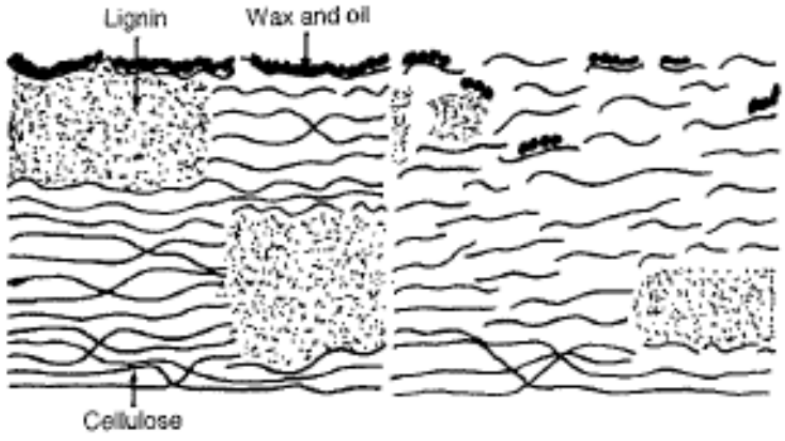

Figure 2.13: Typical structure of (a) untreated and (b) alkalized cellulosic fibre [83].

These changes in the physical and mechanical properties of natural fibres are considerably dependent on the concentration of the alkali solution and the soaking time and temperature [85]. Alkali treatments performed at elevated temperatures can lead to the selective degradation of lignin, pectin and hemicelluloses in the fibre wall while having little effect on the cellulose components. The removal of these cementing materials thus leads to stronger natural fibre reinforced composites [74].

The use of NaOH to modify cellulose fibres for use in composites has been extensively reported [75,109,110,111]. NaOH plays a critical role in removing lignin by means of alkaline cleavage of ether linkages in the lignin, which may be accomplished through condensation reactions [112]. Pectin can be completely attacked and removed without any residue being left in the cellulose fibres after NaOH treatment. However the rate of lignin removal is also dependent on the NaOH concentration [8,112].

Jähn et al. [113] noticed that the cellulosic fine structure of flax fibres was directly influenced by mercerization treatment. Furthermore, they found that the alkali treatment influenced the chemical composition of the flax fibres, the degree of polymerization and the molecular orientation of the cellulose crystallites. This was attributed to the removal of cementing substances like lignin and hemicelluloses during the mercerization process. Le Troedec et al. [114] found that treatment with 6% NaOH cleaned fibres by removing amorphous compounds, and increased the crystallinity index of hemp fibre bundles. Many studies were conducted on the alkali treatment of natural cellulose fibres [115,116]. They reported that alkali treatment of cellulose fibres leads to an increase in the amount of amorphous cellulose at the cost of crystalline cellulose and the removal of hydrogen bonding in the network structure. Saha et al. [117] also studied the effect of alkali steam treatment on the tensile strength of jute fibre. They found that alkali-steam treatment leads to an increase in the tensile strength of up to 65%. This increase in tensile strength was due to the removal of non-cellulosic materials like lignin, pectin and hemicelluloses which, in turn, resulted in increased crystallinity. In a similar study, Sawpan et al. [118] recorded an increase in the tensile strength of hemp fibres after soaking them in a 5 wt.% sodium hydroxide solution at ambient temperature. Sedan et al. [27] examined the effect of alkali treatment on hemp fibres, (soaked in a 6 wt.% NaOH

aqueous solution in a water bath at 20 ± 2 ℃ for 48 h) on the flexure strength of cement composites. They recorded a 39% increase in flexural strength when untreated hemp fibres are replaced by alkali treated fibres.

Sodium hydroxide (NaOH) is the most commonly used chemical for bleaching and/or cleaning the surface of plant fibres. This treatment was chosen for this work in order to change the mechanical properties, like tensile modulus and tensile strength, of the fibres and their surface morphology [27,107,119,120,121].

2.6 Natural Fibres for Low Cost Cementitious Composites

Much of the research on the use of natural fibre cement composites has been motivated by the availability of such fibres as tropical plants and agricultural wastes which currently have limited economic value. The production processes for making cementitious composites of various shapes are, also, much simpler compared to the most common synthetic reinforcing fibres, so they are very suitable for low cost housing applications. In these applications the fibre is short, randomly distributed and its content is usually less than 5%, although it could be greater when using hand lay up of long fibre roving technologies [3,107].

The cement matrix is acknowledged to be a relatively brittle material when subjected to normal stresses and impact loads, where tensile strength is only around one tenth of its compressive strength. As a result, unreinforced concrete members could not support the loads and stresses which commonly take place in most concrete beams and slabs. Historically, concrete members reinforced with continuous reinforcing bars to bear tensile stresses and improve ductility and strength. However, steel reinforcement is adopted to overcome potentially high tensile stresses and shear stresses at critical locations in a concrete member, and it increases the tensile strength of concrete. To produce concrete with homogenous tensile properties, the development of microcracks must be restrained. The incorporation of short fibres, which are a new form of binder could combine OPC in the bonding with cement matrices, was brought in as a solution for concrete to improve its ductility, flexural and tensile strength. Most fibres are generally short and randomly distributed throughout the cement matrices [3].

A wide range of fibres with different mechanical, physical and chemical properties, such as polymeric fibres, mineral fibres and vegetable fibres, have been used for the reinforcement of cement matrices. Fibres can be introduced into cement based matrices as primary or secondary reinforcement. Fibres act as primary reinforcement in thin products such as cladding where conventional reinforcing bars cannot be used. In these applications, the fibres work to improve both the strength and the toughness of the composite. In components such as slabs and pavements, fibres are introduced in order to control cracking so in these applications they act as secondary reinforcement [3,73].

2.6.1 Factors Govern the Properties of Short Fibre Reinforced Composites

2.6.1.1 Fibre Length

A critical fibre length, L_c, is the minimum fibre length required for the build-up of a stress (or load) in the fibre which is equal to its strength (or failure load). It can also be defined as twice the length of the fibre embedment which will cause fibre failure during pull-out. The fibre critical fracture length, L_c, can be calculated from equation (2.3), assuming that fibre strength(δ_f), fibre diameter (D) and the shear stress (δ_S) developed at the interface are all uniform [3,96].

$$L_c = \frac{\delta_f D}{2\delta_S} \qquad (2.3)$$

In order to achieve approximately 90% strength efficiency, the fibre must be 5–10 times longer than its critical length. This can be achieved by controlling the geometry of the fibre (higher aspect ratio) or by enhancing the fibre–matrix interaction [3].

2.6.1.2 Fibre Aspect Ratio

The fibre aspect ratio or the fibre length to diameter ratio ($\frac{L}{D}$) is a critical factor in a composite material. For each short-fibre composite system, there is a critical fibre aspect ratio that may be defined as the minimum fibre aspect ratio in which the maximum allowable fibre stress can be attained for a given load [74]. The

critical fibre aspect ratio of a composite can be derived from equation (2.4) as follows:

$$\frac{L_c}{D} = \frac{\delta_f}{2\delta_S} \qquad (2.4)$$

Along with the fibre and matrix properties, the critical fibre aspect ratio also depends on the quality of the fibre/matrix interface. In order to achieve maximum reinforcement, the fibre aspect ratio of any composite system should be above its critical value in order to ensure maximum stress transfer to the fibres before the composite fails. It should be noted that if the fibre aspect ratio is lower than its critical value, insufficient stress will be transferred and reinforcement of the fibre will be insufficient (i.e. the fibres are not loaded to their maximum stress values). Conversely, if the fibre aspect ratio is too high, the fibres may get entangled during mixing resulting in poor fibre dispersion [8].

2.6.1.3 Fibre Volume Fraction

Fibre volume fraction, V, plays a significant part in determining the composite mechanical properties. The mechanical properties of composites are highly influenced by the fibre content. At low fibre volume fractions, a decrease in tensile strength is usually detected. This is due to the introduction of flaws formed by the fibre ends, which act as stress risers and cause the bonds between the fibre and matrix to break. At higher volume fractions, the matrix is sufficiently restrained and the stress is more uniformly distributed which leads to a reinforcing effect that outweighs the effects of stress concentrations [122]. As the fibre volume fraction is further increased, the tensile properties gradually increase until they exceed those of the matrix. The corresponding fibre volume fraction at which the strength properties of the composite cease to decline and start to increase is known as the critical fibre volume fraction. At high fibre volume fractions, the tensile strength of the composite starts to decline due to insufficient filling of the matrix material [123].

2.6.2 Mechanical and Physical and Properties of Natural Fibre Cement Composites

2.6.2.1 Post-cracking Performance

In fibre reinforced cement based composites the two major roles played by the fibres, (i.e. improving toughness and the post-cracking performance), occur in the post cracking zone in which the fibres cross the crack matrix. In a well-designed composite the fibres can serve two functions in the post-cracking zone [3,73]:

- To increase the strength of the composite over that of the matrix by providing a means of transferring stresses and loads across the cracks.
- To increase the toughness of the composite by providing energy absorbing mechanisms associated with the debonding and pull-out processes of the fibres bridging the cracks.

Boghossian et al. [124] found that the addition of low volume fractions (0.05% to 0.3%) of short flax fibres (10 to 38 mm) to OPC mortar specimens reduced the cracking which results from restrained plastic shrinkage under conditions that produce high evaporation rates. Tests showed that flax fibres were found to be slightly more effective in controlling restrained plastic shrinkage cracking than commercially available polypropylene and glass fibres for the mortar mixture studied. They also found that at a flax fibre volume fraction of 0.3%, total crack areas were decreased by at least 99.5% relative to plain mortar specimens, and that maximum crack widths were reduced by at least 98.5% to less than 0.022 mm. In similar work Filho et al. [125] found that the use of a 0.2% volume fraction of 25 mm sisal fibres leads to free plastic shrinkage reduction. They also noticed that the combined use of coconut and sisal short fibres seemed to delay restrained plastic shrinkage, thus controlling crack development at early ages.

2.6.2.2 The Flexure, Impact and Toughness Properties

Short fibres are often found to have a much greater effect on the toughness, flexure and impact properties of natural fibre cement composites (NFC) than on either the compressive or tensile strengths of NFC, with increases of more than

100% been reported. These increases are particularly sensitive, not only to the fibre volume, but also to the aspect ratio of the fibres, with higher aspect ratios leading to larger strength and toughness increases. Thus, the above properties are often related to the term WL/D, where L/D is the aspect ratio and W is the weight percentage of fibres. On the other hand, it should be noted that for WL/D>600, the mix characteristics tend to become unsatisfactory due to inadequate workability or non-uniform fibre distribution (clamping) [3,126].

The flexure, impact and toughness properties of NFC have been widely reported by many authors [125,127,128,129,130,131]. Al-Oraimi and Seibi [132] found that using a low percentage of palm tree leaves improved the flexure properties and the impact resistance of concrete and had similar performance when it was compared to glass fibre concrete. Li et al. [133] showed that hemp fibre reinforced concrete results in an increase of flexural toughness by 144%, and an increase in the flexural toughness index by 214%. They also showed that flexural toughness and the flexural toughness index of coir fibre reinforced cement composites was increased by more than 10 times.

Sedan et al. [27] observed a strong increase in flexure strength of hemp fibre cement composites compared to plain mortar. In similar work Kriker et al. [134] recorded improvements in the post-crack flexural strength and the toughness coefficients of date palm fibre reinforced concrete. The results obtained by Ramakrishna and Sundararajan [98] have shown that the addition of coir, sisal, jute or hibiscus cannebinus fibres with fibre contents (0.5%, 1.0%, 1.5% and 2.5%—by weight of cement) and three fibre lengths (20mm, 30mm and 40mm) increased the impact resistance by 3–18 times more than that of the reference (i.e. plain mortar slab). Razak and Ferdiansyah [135] found that the use of small volumes (0.6–0.8%) of Arenga pinata fibres showed their capacity to increase the toughness of cement based composites.

Elsaid et al. [136] used kenaf fibres with fibre volume contents of 1.2% and 2.4% to reinforce cement composites. The results of their flexural tests indicate that kenaf cement composites exhibit a ductile failure mode comparable to conventional concrete with an average measured toughness approximately three times that of similar plain concrete control specimens. Furthermore, they observed an

improvement of cracking behaviour which enhances the durability of concrete at a relatively low cost when compared to other types of fibres.

2.6.2.3 Compressive Strength

Members that include conventional reinforcement in conjunction with the short fibres do little to enhance the compressive strength of cement matrix, with increases in strength ranging from essentially nil to perhaps 25% for the normal range of fibre contents (<2%). At a fibre volume fraction of 2% to 3% the compressive strength can be reduced by about 25% to 30%. On the other hand, the fibres do substantially increase the post-cracking ductility or energy absorption of this material. Increasing the aspect ratio of the fibres also increases the compressive toughness, but again this has only a limited effect on compressive strength [3,73].

Kriker et al. [134] found that compressive strength decreases with increasing fibre content and the length of date palm fibre reinforced concrete. Li et al. [126] showed that the addition of hemp fibres into a cementitious matrix reduced the compressive strength of the composite, regardless of the mixing method. The increased porosity of the composite material as a result of fibre addition is the main factor responsible for the reduction in compressive strength. Elsaid et al. [136] showed that the addition of kenaf fibres into the concrete mixture reduced the average measured compressive strength of the concrete. Their results indicated that the compressive strength decreased with an increase in fibre volume content from 0% to 2.5%.

2.6.3 Durability of Natural Fibre Cement Composites (NFC)

The durability of NFC is related to its ability to resist both external (temperature and humidity variations, sulphate or chloride attack, etc.) and internal damage (compatibility between fibres and cement matrix, volumetric changes, etc.) [76]. The natural fibre in the porous alkaline matrix is slowly damaged and the reinforcing effects of the fibre decreases. This is attributed to the fact that the alkaline cement attacks the lignin in the natural fibres. As a result, significant degradation in composite strength is observed [137].

Many studies have noted the presence of calcium hydroxide in the cementitious matrix with the degradation of the vegetable fibres, and thus the loss of durability of the NFC [6]. Gram [76] was the first researcher to study the durability of sisal, coir, jute and flax fibre reinforced concrete. Fibre embrittlement was evaluated by exposing the fibres to alkaline solutions and then measuring the variations in their tensile strength. In addition, the durability of reinforced cement composites stored in water at a temperature of 20℃ or 50℃ for up to 2 years, stored in open air weathering for 2 years and then subjected to alterative wetting and drying cycles have also been investigated. Gram [76] found a deleterious effect for Ca^{2+} elements on fibre embrittlement. Gram also found that fibres were able to preserve their flexibility and strength in areas with carbonated concrete that had a pH of 9 or less. Furthermore, Gram noticed that flax and coir fibres appear to be more resistant within concrete than sisal and jute fibres.

In similar work, Filho et al. [127] investigated the durability of sisal and coconut fibres when they are immersed in alkaline solutions (i.e. calcium and sodium hydroxide). In addition, the durability of cement composites reinforced with these fibres when they are aged under tap water, exposed to controlled cycles of wetting and drying, as well as being exposed to the open air weathering have also been studied. Sisal and coconut fibres aged in a sodium hydroxide solution retained 72.7% and 60.9% respectively of their initial strength after 420 days. As for the immersion of the fibres in a calcium hydroxide solution, it was noticed that their original strength was completely lost after 300 days due to the higher attack by CH which can be related to a crystallization of lime in the fibres' pores. Furthermore, the sisal or coconut short fibre cement composites showed a significant reduction in toughness after six months of exposure to open air weathering or after being subjected to cycles of wetting and drying. The reduction in toughness was due to the migration of hydration products, especially calcium hydroxide, to the fibre lumen, walls and voids, thus leading to degradation of the fibres.

Ramakrishna and Sundararajan [99] also noticed the degradation of coir, sisal, jute and Hibiscus cannabinus fibres when they are subjected to alternate wetting and drying and continuous immersion for 60 days in three mediums (water, saturated lime and sodium hydroxide). Kriker et al. [134] also investigated the

durability of date palm reinforced concrete and reported low durability performance which was related to fibre degradation when immersed in alkaline solutions. Roma et al. [138] found that vegetable fibre–cement based roofing tiles showed a reduction in toughness of between 53% and 68% after 4 months of external weathering. The hygroscopic nature of plant fibres is another way to decrease the durability of fibre reinforced concrete because the swelling and shrinking of the fibres leads to volume changes that can induce concrete micro-cracks [139,140].

Claramunt et al. [141] and Ardanuy et al. [142] used X-ray diffraction techniques and Thermogravimetric Analysis to explain the migration of hydration compounds in cement to bamboo fibres, kraft pulp and cotton linters. Their explanation is as follows:

- In the first dry cycle, the transversal section of the selected fibres is reduced due to the loss of water, which causes the loss of adherence with the matrix and the appearance of void spaces at the fibre– matrix interface.
- In the succeeding wet cycle, water dissolves the hydration compounds of the cement (calcium hydroxide) and as a consequence the fibres absorb this dissolution of calcium hydroxide and swell.
- In the second dry cycle, water is lost through evaporation and the calcium hydroxide precipitates on the surface and in the lumen of the fibres. During the subsequent wet–dry cycles there is a ‘‘pump-like’’ mechanism that results in the densification of the surface and lumen of the fibres with high alkalinity products.

Basically there are two approaches which could be used to improve the durability of natural fibre reinforced cement composites. The first one is to modify the cement matrix in order to reduce or remove the alkaline compounds. This technique includes; using low alkali cement, using cement based polymers and sealing the matrix pore with asphalt [143], using colophon, tannin or montan wax [144] and through partial replacement of OPC by pozzolanic materials, such as silica fume [100], fine powdered metakaolin and calcined waste crushed clay brick [145].

The second approach to improve the durability of the NFC is to modify the surface of the natural fibres. This approach involves the use of chemical or thermal treatments [107,137], hornification of cellulose fibres [7], or modifying the fibres by

coating or impregnating the fibres with formine and stearic acid, potassium nitrate and stearic acid, sodium chromate and fluorine– carbon–hydrogen– stearate, and borax and chromium stearate [100].

2.6.3.1 Modification of Cement Matrix

Gram [76] reported that sealing the matrix pores, admixing small beads of wax or zinc stearate powder in the fresh mortar, or impregnating the hardened product with sulphur also showed promising results. Canovas [144] showed that pore sealing with colophony, tannin or montan wax reduced the water absorption and relative porosity of sisal fibre–mortar composites, slowing, but not halting, the embrittlement process. Filho et al. [100] showed that early curing of composites in a CO_2-rich environment and the partial replacement of OPC with undensified silica fume were also efficient approaches for producing composites with improved durability. In addition, they found that the use of slag as a partial cement replacement had no effect on reducing the embrittlement of composites.

Reduction of cement matrix alkalinity through the use of pozzolanic materials to consume CH has also shown promising results [76,100,146]. Filho et al. [145] replaced 50% of OPC with calcined clay (metakaolin and calcined waste crushed clay brick) in order to produce a matrix totally free of CH. Their results showed that the CH-free matrix avoided the fibre embrittlement process and still retained its toughness after 100 wet/dry cycles. In a similar study, Silva et al. [9] replaced OPC with 30% metakaolin and 20% calcined waste crushed clay brick in order to increase the durability of sisal fibre cement composites. Their results showed that the addition of metakaolin and calcined waste crushed clay brick successfully sustained the energy absorption capacity of the CH free composite, increased its first crack strength and maintained its ultimate strength through accelerated aging, thus proving this to be a good solution for the durability issues of natural fibre as a reinforcement in cement composites.

2.6.3.2 Modification of Fibres

Treatments of natural fibres with blocking agents such as sodium silicate, sodium sulphite, magnesium sulphate, iron or copper compounds and barium and

sulphite salts were studied by Gram [76] but none of them improved the durability of the fibre in a cement matrix. Impregnation of sisal fibres with organic compounds obtained from timber, such as tannins, colophony and vegetable oils, were studied by Canovas [144]. The results indicated that there was a slight slowdown in the embrittlement process, but it was not completely avoided. Filho et al. [100] found that immersion of natural fibres in a silica fume slurry before their addition to cement-based composites was an effective means of reducing embrittlement of the natural fibre cement composite. Asprone et al. [147] found that the latex coating of hemp fibres not only improved the durability of the fibres in the pozzolanic mortar environment, but that it also improved the bond behaviour between the fibres and the pozzolanic mortar. Claramunt et al. [7] found that the prior hornification of kraft pulp fibres and cotton linters improved the durability of cement mortar composites, although it did not prevent a partial loss of their mechanical reinforcement. Their results showed that the prior hornification of the above fibres improved the mechanical performance of their composites, with around 8% (kraft) and 16% (cotton linters) higher values in flexural tests and around 7% (kraft) and 10% (linter) higher values in compressive tests when compared with untreated fibres. The prior hornification of the kraft pulp fibres and cotton linters also improved the mechanical performance of their aged composites, with around 13% (kraft) and 21% (cotton linters) higher values for flexural strength and around 20% (kraft) and 10% (linter) higher values for compressive strength with compared to untreated fibres.

Chapter 3 : Materials and Methods

3.1 Experimental Overview

The purpose of this research was to improve the mechanical properties and long term performance of flax fibre cement composites as compared to the characteristics of flax fibre cement composites described in the literature. Improvements to these properties was achieved by optimising various cement composite parameters, such as fibre treatment conditions, fibre strength, fibre volume fraction and waste glass, as well as nano-clay and nano-silica content.

In order to realise this objective, flax fibres were chemically treated to improve fibre strength, improve fibre separation and to modify the fibre surface. Composites were produced by incorporating chopped fibres into two systems; the first system contained only ordinary Portland cement (OPC) as a binder, while in the second system; a portion of OPC was replaced with finely ground waste glass powder. Furthermore, nano clay particles (NC) and colloidal nano silica (NS) were also added during the construction of both systems.

Several characterisation techniques were employed during this research. These characterisation techniques were designed to obtain information about the surface morphology, crystalline structure, thermal stability and mechanical properties of modified fibres and cement composites containing the modified fibres. Hence, the following characterisation techniques using, X-ray diffraction (XRD), thermogravimetric/differential thermal analysis (TGA/DTA), scanning electron microscopy and Energy Dispersive X-ray Analyses (SEM/EDX) were employed to test tensile, toughness, compressive and impact properties.

3.2 Materials

The ordinary Portland cement (OPC) used in this study was supplied by Irish Cement Ltd. The cement was a grade 42.5 with a specific gravity of 3.15 g/cm^3. Sand with particles up to a size of 1.18 mm and a specific gravity of 2.65 g/ cm^3 was obtained from a local supplier in Ireland. The superplasticizer was obtained from Sika Ireland Ltd.

The raw flax fibres used in this research were obtained from Egypt and came in straight long fibre bundles. The fibre density was measured by a helium gas Pycnometer (Figure 3.1) and was 1.54 gm/cc. The specimen for this test was chopped fibres, and 3 samples were tested to obtain an average value. The test method was similar to the Archimedes method, but was applied using a gas medium rather than a liquid one. Helium gas was used to test the fibre volume using the helium gas Pycnometer (Figure 3.1). A known volume of helium gas was contained in the Pycnometer's reference cell. During a test, the gas was released slowly from the reference cell into the sample cell where the fibres were located. The pressure of the helium gas that remained in the reference container was used to determine the volume of the fibre sample. The mass of the sample was measured on a digital balance (Figure 3.1), and the density of the fibre was determined by dividing the mass by the volume [148], and 98% NaOH pellets were purchased from the Aldrich Company for use in fibre treatment.

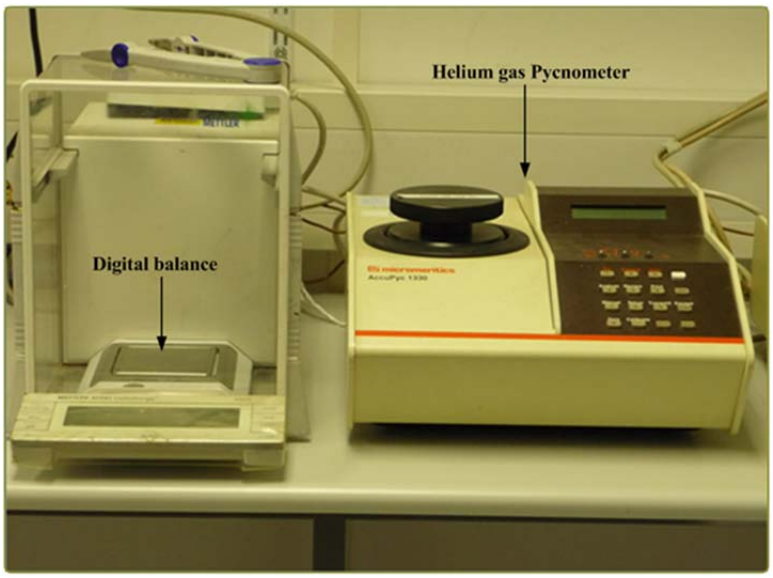

Figure 3.1: Photography of helium gas Pycnometer.

The clay used in this study, Closite® 30B, is commercially available from Southern Clay Products Inc, USA. Closite® 30B is an organically modified montmorillonite with quaternary ammonium salt which has an initial d-space of 18.5 Å. The physical and chemical properties of Closite® 30B provided by the manufacturer are listed in Table 3.1. A SEM micrograph of Closite® 30B particles is shown in Figure 3.2. It shows that the particles consist mainly of fine ball-milled

particles with an irregular and layered microstructure and an average particle size of 6 μm.

Table 3.1: Physical and chemical properties of Closite® 30B as provided by the manufacture

Physical properties and chemical properties	
Density	1.98 g/cc
Moisture content	<2 %
Average size	6 μm
Basal spacing, d_{001}	18.5 Å
Colour	Off-white
Modifier concentration	90 meq*/100 g clay

* milli-equivalents per 100 grams.

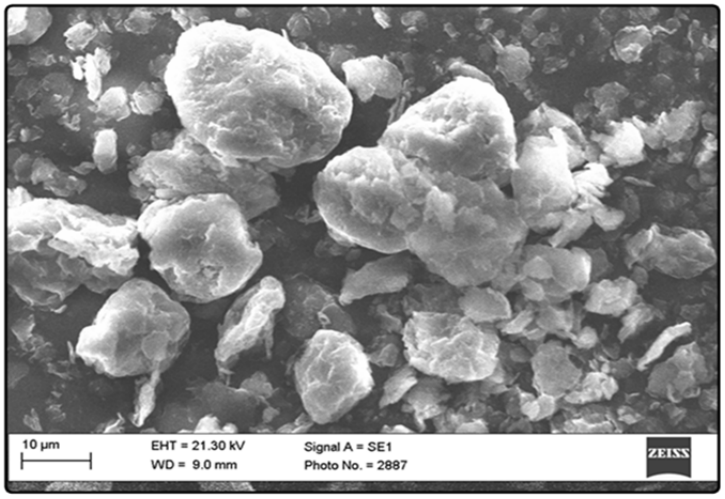

Figure 3.2: SEM micrograph of Closite® 30B.

The colloidal nano-silica sol that was used (Cembinder 50™) contained 15 wt% of solid material. The particle size was 5 nm with a 500 m^2/g specific surface area, and was supplied by EKA Chemicals AB, Bohus, Sweden.

The waste glass used in this study was obtained from recycled green alcohol bottles. In order to satisfy the physical requirement for fineness, glass has to be ground fine enough to pass through a 75 μm sieve. This was accomplished by

crushing and grinding the glass using a ball mill in the laboratory and then sieving the ground glass to the desired particle size. Table 3.2 shows the chemical composition of the green waste glass powder used in this study. The SEM examination indicates that the ground waste glass powder consists mainly of fine angular particles with a narrow particle size range, as shown in Figure 3.3. The particle size analysis of the waste glass powder (WG) was carried out using a Malvern Mastersizer S (Malvern Ltd., UK). Figure 3.4 compares the particle size distribution of the OPC with WG obtained from the grinding process. This characterisation technique shows that 45% of WG particles are smaller than 10 μm, while 50% of PC particles are smaller than 10 μm. Figure 3.5 exhibits, the compressive strength of the lime-glass (as explained in section 3.4.11). It is clear from this figure that WG mixture satisfied the minimum strength requirement test at 7 days (4.1 MPa) and attained an increase in strength after an additional 21 days of curing in water.

Table 3.2: Chemical composition of green waste glass powder used in this work

Na	Al	Si	K	S
10.7	6.65	75.06	4.49	3.1

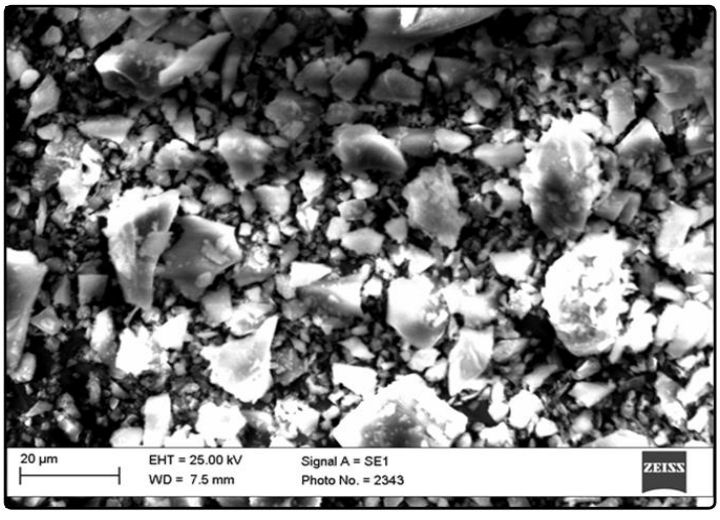

Figure 3.3: SEM photograph of ground green waste glass powder.

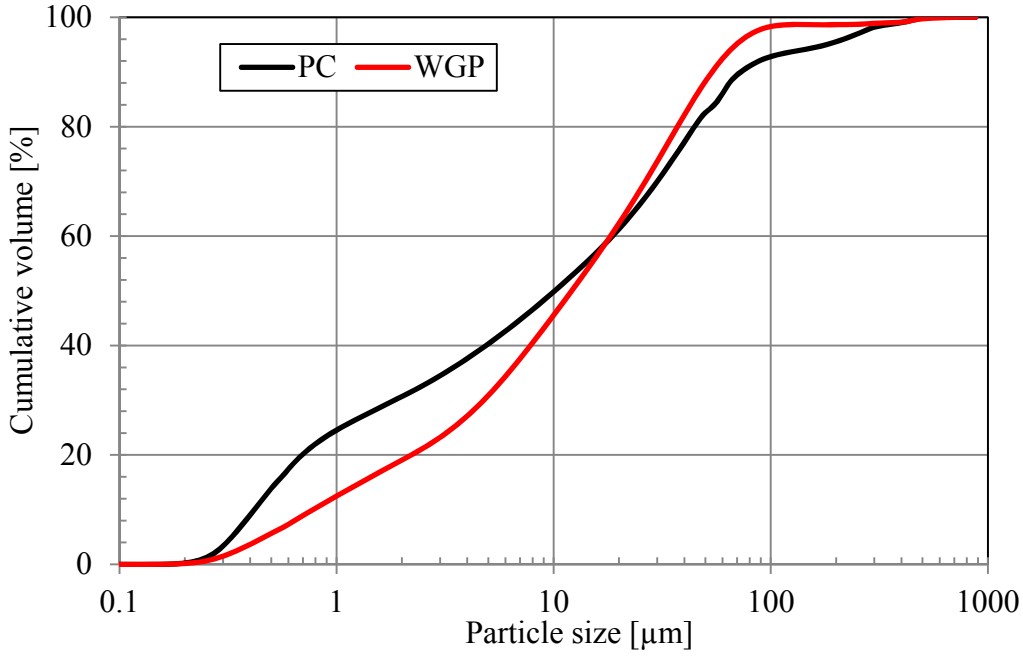

Figure 3.4: Particle size distributions of waste glass powder and Portland cement.

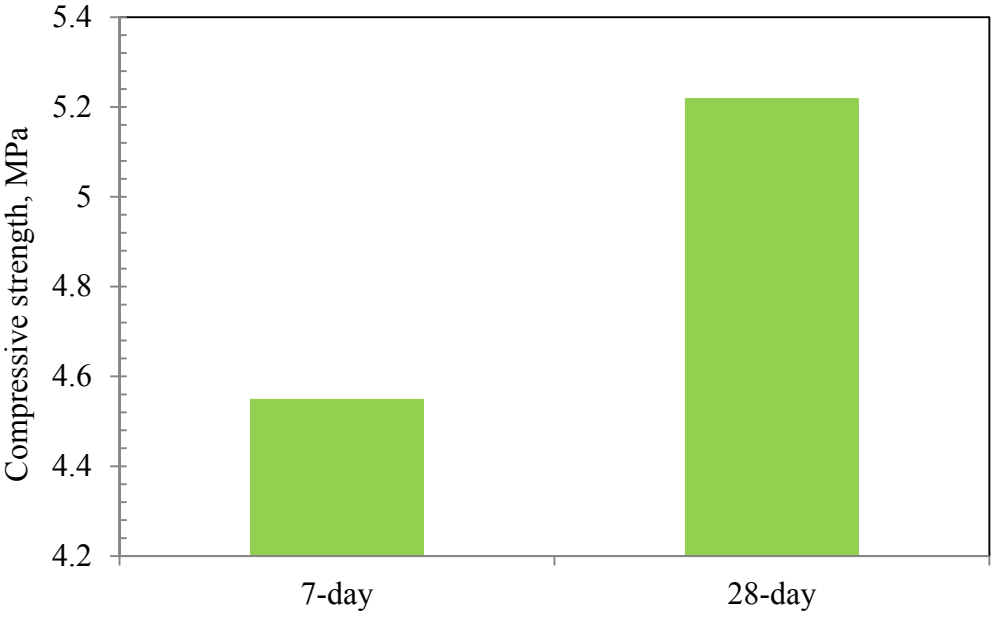

Figure 3.5: Compressive strength of lime-WG mixture.

3.3 Methods

3.3.1 Surface Treatment of Flax Fibre

Prior to Alkali treatment the fibres were placed in a controlled hot water bath for 10 minutes at 100-110ºC (hot water treatment). Then the fibres were removed

from the bath after being cooled to room temperature and after that the fibres were placed in an air oven for 12 hours at 80ºC. After applying the hot water treatment, the fibres were placed in 2L capacity flasks. Pre-weighed sodium hydroxide (NaOH) solutions were developed using pellets of (NaOH) in distilled water. After that the NaOH solutions were poured into the flasks. The flasks were then placed in a controlled water bath at the required soaking temperature and time for an alkali treatment of fibres. The treated fibres were rinsed with distilled water until all of the alkali was removed from their surfaces and a fibre pH of 7 was obtained. The fibres were then air dried for 7days followed by oven drying for 3 hours at 70ºC. Finally, the fibres were characterized and used to fabricate composites.

3.3.2 Production of Flax Fibre Composites

Prior to the preparation of the composites, the treated flax fibres or untreated flax fibres (if applicable) were chopped to the desired length (10, 30 and 50 mm) and manually separated. For all of the cement composites the cement to sand ratio was 1:1, the water/binder ratios were tested to reach a flow of 110 ± 5 in order to permit a medium workability that could be used for mixing the specimens, and the super-plasticizer dosage was 0.1 wt.%.

3.3.2.1 Normal Flax Fibre Composites

The ordinary Portland cement (OPC) and waste glass powder (if applicable), the sand and 50 % of the flax fibres were stirred at medium speed (70 rpm) for about 3 minutes. Afterwards, 50% of the total water required was added to the mixture and stirred for another 1 minute. In order to avoid clumping of the fibres and to keep the mix wet enough, the remaining fibres and water were then slowly added to the mixture and stirred for another 2 minutes in order to enhance fibre dispersion. Next, the superplasticizer was added and stirred again at medium speed (70 rpm) for 2 minutes. Then, the well mixed composite was poured into moulds. After moulding, the specimens were covered with a wet cloth and a polyethylene sheet and were allowed to cure in the moulds for the first 24 hr. Then the specimens were allowed to cure in water for 20 days. Finally the specimens were kept in laboratory conditions of 19 ± 2 ºC and 50% ± 5% relative humidity for an additional 7 days.

3.3.2.2 Nano-Clay Flax Fibre Composites

Organically modified montmorillonite particles have a relatively high surface area per unit volume and are difficult to mix at the same time with water, cement and sand. Hence, the microstructure and mechanical properties of cement mortars reinforced with modified montmorillonite particles are significantly influenced by the mixing procedure of their constituent materials. Kuo et al. [26] have successfully used the high-shear mixing technique to incorporate organo-modified montmorillonite into the cement matrix. Therefore, this technique was chosen to prepare the nano-clay composites. Accordingly, the mixing was performed as follows. The modified montmorillonite particles were mixed with all of the mixing water and stirred vigorously by a high speed shear mixer (1500 rpm) for 24 hours at room temperature in order to form a well dispersed suspension solution. To prepare this group of composites, the OPC, WG (if applicable), 50% of the flax fibres and sand were stirred at medium speed for about 3 minutes. Afterwards, 50% of the total suspension solution was added to the mixture and stirred at medium speed for 3 minutes. In order to avoid clumping of the fibres and to keep the mix wet enough, the remaining fibres and suspension solution were then slowly added to the mixture and stirred for another 3 minutes in order to enhance fibre/suspension solution dispersion. Next, the superplasticizer was added and stirred again at medium speed for 2 minutes. Then, the well mixed composite was poured into moulds. After moulding, the specimens were covered with a wet cloth and a polyethylene sheet, allowed to cure in moulds for the first 24 hr. Then the specimens were allowed to cure in water for 20 days. Finally the specimens were kept in laboratory conditions at 19 ± 2 ºC and 50% ± 5% relative humidity for an additional 7 days. For all of the specimens the fibre content was 1% by volume fraction and the fibre length of 30 mm.

3.3.2.3 Nano-Silica Flax Fibre Composites

To prepare this group of composites, colloidal nano silica was stirred with mixing water at a high speed (150 rpm) for 2 min. After that the OPC and waste glass powder (if applicable) and 50% of the flax fibres were added and stirred at medium speed (70 rpm) for about 1 minute. Afterwards, the sand and the remaining fibres were added to the mixture and stirred at medium speed (70 rpm) for 2 minutes.

After that, superplasticizer was added and stirred at medium speed for 2 min. Then, the well mixed composite was poured into moulds. The specimens were covered with a wet cloth and a polyethylene sheet and allowed to cure in the moulds for the first 24 hr. Then the specimens were allowed to cure in water for 20 days. Finally the specimens were kept in laboratory conditions at 19 ± 2 ºC and 50% ± 5% relative humidity for an additional 7 days. For all of the specimens the fibre content was 1% by volume fraction and the fibre length of 30 mm.

3.4 Characterisation Techniques

3.4.1 Differential Thermal Analysis/Thermogravimetric Analysis (DTA/TGA)

The Differential Thermal Analysis (DTA) and to some extent, the Thermogravimetric Analysis (TGA) methods; are the most widely used thermal analysis techniques. They are more adjustable, easier to use, and yield results in a short span of time. These methods measure the heat changes associated with physical or chemical transformations that occur during the gradual heating of a material. Thermal changes, such as dehydration, crystalline transition, lattice destruction, oxidation and decomposition, are generally accompanied by an appreciable rise or fall in temperature and are thus amenable to DTA investigation [28].

3.4.1.1 Application of DTA/TGA Analysis to Cement Hydration

Le Chatelier, who applied thermal analysis to study clay mineralogy, proposed the DTA method in 1887. However he did not employ this method in cement characterisation [149]. Kalousek et al.[150] were probably the first to introduce this technique for cement chemistry. Since then several papers have been published dealing with the DTA of cementitious materials.

In DTA the temperature difference that develops between a sample and an inert reference material is recorded with both materials subjected to identical temperature regimes, in an environment that is heated at a controlled rate. Changes in the sample leading to either the absorption or evolution of heat can be detected relative to the inert reference. TGA indicates a number of stages of thermal breakdown and the weight loss in the material, in each stage, as a function of

temperature. Both DTA and TGA can be employed to study the thermal behaviour of natural fibre and its composites [8,28].

DTA/TGA is considered to be one of the most powerful tools in the investigation of the hydration of cement pastes. DTA/TGA has yielded important results for cement hydrated for various lengths of time under different conditions [28]. DTA/TGA can be used to determine the amount of pozzolanic reaction and hydration of blended cement pastes by estimating the CH and CHS content. This technique is also more suitable for studying hydration at later stages [151]. Vedalakshmi et al.[152] as well as Esteves [153] employed TGA/DTA to study the pozzolanic activity of mineral additions such as silica fume, fly ash and slag. Furthermore, the hydration of pozzolanic materials such as silica fume, metakaoline, fly ash or slag has also been investigated in Refs.[154,155,156,157].

In the present study, CH exhibits a peak at about 425-495°C. The area of this peak was used to determine the amount of CH by using the method applied by Esteves [153]. Accordingly, in order to calculate the CH content, a separate test was performed with pure CH to check the enthalpy of this compound. Thus, the amount of CH in the system was derived using Eq. (3.1):

$$CH\ [wt.\ \%] = R \cdot A \qquad (3.1)$$

Where CH is the wt. % of calcium hydroxide in the sample, R is the calibration constant obtained from the measurement of pure CH ($R= 8.11\times10^{-4}$) and A is the peak area taken from the DTA profile in μV.

When using the TGA technique to estimate the content of CH, this method does not require any calibration procedure. Thus, the CH content was estimated directly from the weight loss measured in the TGA curve between the initial and final temperature of the corresponding TGA peak [151,152,153].

3.4.1.1.1 Measurement

The thermal behaviour of the composites was analysed using the thermal gravimetric analyses model of Stanton Redcroft DTA/TGA, UK (Figure 3.6). The weight of the specimens used in the analysis ranged from 22 to 30 mg. These

specimens were analysed in a platinum pan in which the analyser heated the furnace from room temperature to 1000ºC at 10ºC/min. Dry Nitrogen gas was circulated within the test cell at a flow rate of 60 cc/min.

Figure 3.6: Photograph of DTA/ TGA analyser.

3.4.1.2 Application of DTA/TGA Analysis to Cellulose Fibres

Both DTA and TGA can be employed to study the thermal behaviour of natural fibre and its composites [93,158]. Many researchers [8,74,117] have studied the influence of chemical treatment of cellulose fibres on their thermal degradation by using DTA/TGA. Sahaet et al. [117] carried out a TGA analysis to study the weight loss and chemical composition of alkali treated and steam alkali treated jute fibres and to compare them with control samples. They found that both alkali and steam alkali jute fibre had better thermal stability than the control samples. In similar work, Islam [8] used TGA/TDA analysis to study the thermal behaviour of alkali treated hemp fibres and found that alkali treated hemp fibres had better thermal stability than untreated fibres.

3.4.1.2.1 Measurement

The thermal behaviour of treated/untreated fibres was measured using the same thermal gravimetric analysis model described in section 3.4.1.1.1. The weight of the fibres used in this analysis ranged from 19 to 24 mg. These fibres were

analysed in a Platinum pan in which the analyser heated the furnace from room temperature to 600ºC at 5ºC/min. Dry Nitrogen gas was circulated within the test cell at a flow rate of 60 cc/min.

3.4.2 X-ray Diffraction (XRD)

X-ray diffraction (XRD) is a non-destructive approach that reveals detailed information about the chemical composition and crystallographic structure of solid materials. Many solid materials are crystalline in nature, and include a regular three-dimensional distribution of their atoms in space. These atoms are organised so that they form a series of parallel planes separated from one another by a distance *d* (or *d*-spacing) that differs according to the nature of the material. Every plane of atoms in a crystalline material can act as a reflecting surface. When X-rays are directed at a crystalline material, they hit each plane of atoms in sequence, diffracting first off the surface layer, and then off the layers below it. Since the wavelengths of X-rays are about equal to the distance between the planes of atoms in crystalline solids, reinforced diffraction peaks of radiation of varying intensities can be produced when a beam of X-rays strikes a crystalline solid [74].

If the crystalline planes are parallel and are at an angle with the incoming X-ray beam so that the diffracted X-rays are in-phase, the diffracted X-rays will reinforce one another resulting in a strong diffracted signal. The fundamental relationship governing the X-ray diffraction process is the Bragg law[28]as follows:

$$n\lambda = 2d\sin\theta \tag{3.2}$$

Where *d* is the distance between the crystallographic planes, λ is the wave length of the X-ray radiation used, n (=1, 2…) is the order of reflection and 2 θ is the diffraction angle, as presented in Figure 3.7.

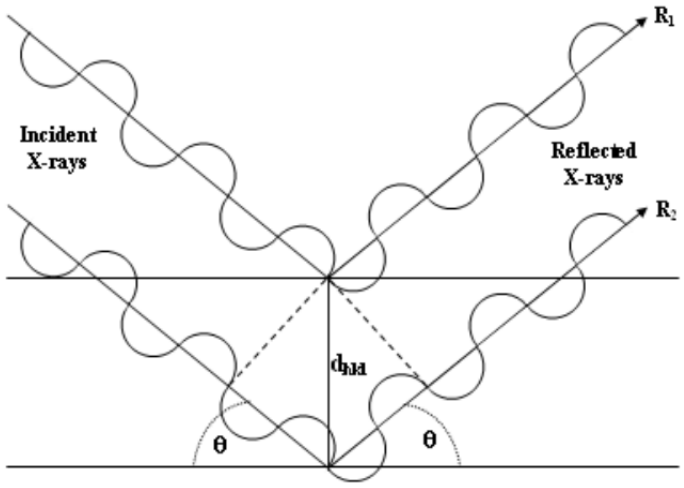

Figure 3.7: Geometric construction of the Bragg Law [159].

Modern powder X-ray diffractometers consist of an X-ray source, a movable sample platform, an X-ray detector, and connected computer-controlled electronics. A powdered sample is used to provide a random distribution of crystal orientations, so that some of the particles will be correctly oriented in the X-ray beam in order to permit diffraction to occur. The sample is packed in a shallow cup-shaped holder, and the sample holder spins slowly during the experiment in order to decrease sample heating. Usually, the X-ray source is Mo or Cu. The X-ray beam is fixed and the specimen platform rotates with respect to the beam by an angle theta (θ), while the detector rotates at an angle of (2θ) with respect to the incoming X-ray beam [28].

3.4.2.1 Application of X-ray diffraction technique to Cellulose Fibres

The X-ray diffraction technique (XRD) is a well-established technique for determining the crystallinity of partially crystalline materials[8]. XRD has been extensively used to investigate the crystallinity of cellulose fibres. Mwaikambo and Ansell [97] measured the crystallinity index of hemp, kapok, sisal, and flax fibres by using the XRD method. They found that the increase in crystallinity index obtained by using XRD was, in fact, an increase in the order of the crystalline packing rather than an increase in the intrinsic crystallinity. Sawpan et al.[118], as well as Troedec et al.[114], used the XRD method to study the crystallinity index of alkali treated hemp fibres. They recorded an improvement in the crystallinity index of alkali

treated fibres as compared to untreated fibres due to the removal of non-cellulosic materials, thus enabling better packing of cellulose chains. Troedec et al.[114].

Different crystalline structures in cellulose fibres can be detected and indicated by the XRD method. The one-dimension patterns of various cellulose structures are shown in Figure 3.8. Usually, the change of cellulose structure affected by treatment and modification can therefore be followed.

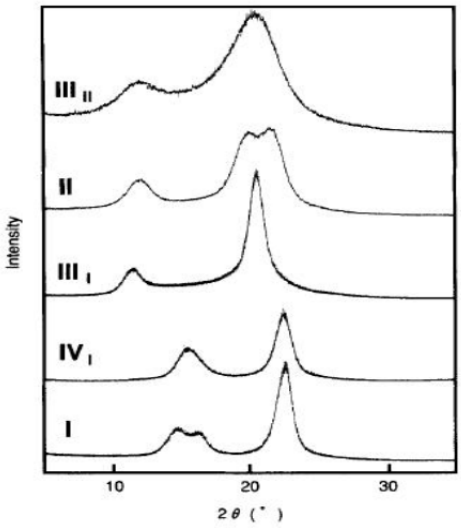

Figure 3.8: X-ray diffraction profile of cellulose polymorphs [160].

The indexing of crystalline planes is the main key for understanding the crystalline structure of cellulose. The general indexing for lattice planes is (hkl), i.e. the first plane in the family from the origin makes intercepts at a/h, b/k, and c/l on the axes as presented in Figures 3.19 and 3.10. When a crystal plane lies parallel to an axis its intercept on that axis is infinity, the reciprocal of which is zero. For example, the 'front' face of a crystal, i.e. the face which intersects the x-axis only and is parallel to the y and z-axes, has Miller index (100); the 'top' face, which intersects the z-axis is (001) and so on. It is useful to remember that a zero Miller index means that the plane (or face) is parallel to the corresponding unit cell's axis [159].

The percentage of crystallinity index (I_{Cr}) was determined using the Segal empirical method according to the following equation:

$$I_{Cr} = \frac{I_{002} - I_{am}}{I_{002}} \times 100 \qquad (3.3)$$

Where,$I_{002}$is the maximum intensity of the 002 lattice reflection (the highest peak for native cellulose) of the cellulose crystallographic form at 2θ = 22.5^{o} and $I_{am}$is the intensity of diffraction of the amorphous material at 2θ =18.5^{o}[97].

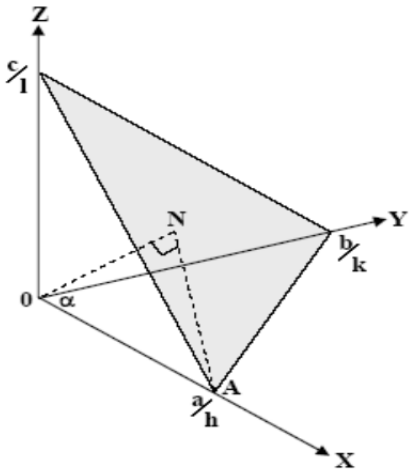

Figure 3.9: Intercepts of a lattice plane (hkl) on the unit cell's vectors a, b, c. ON= d_{hkl} = inter-plannar spacing [159].

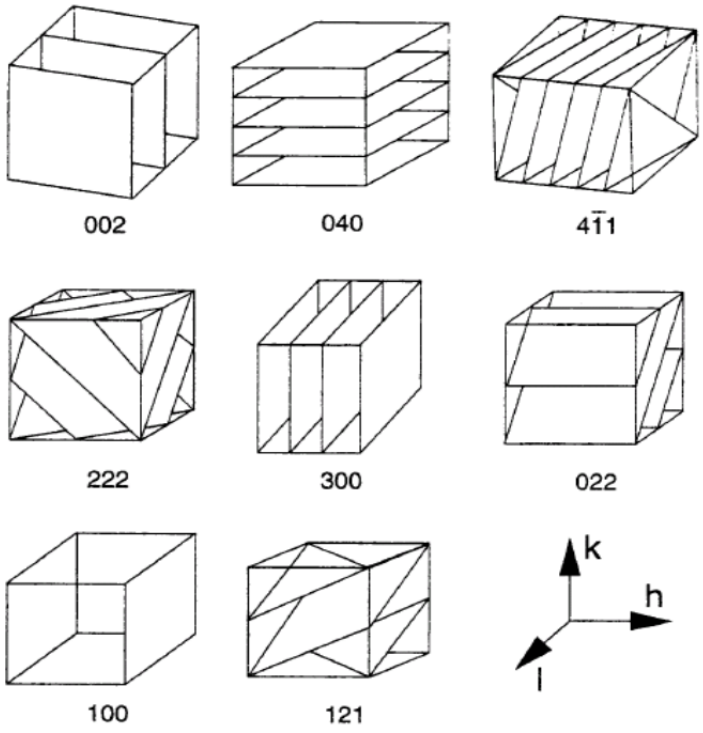

Figure 3.10: Families of planes making rational intercepts with the unit cell edges are identified by a set of three integers, h k l, known as Miller indices [159].

3.4.2.1.1 Measurement

A 0.5 g of fibre was compressed into a tablet by using a hydraulic press at 20 MPa pressure. X-Ray diffraction model Bruker AXS D8 Advance, USA (Figure 3.11) analysis with Cu-Kα radiation and a graphite monochromator with a current of 40 mA and a voltage of 40 mV was used with a diffraction intensity in the range of 6 to 60 ^{o} (2θ-angle range).

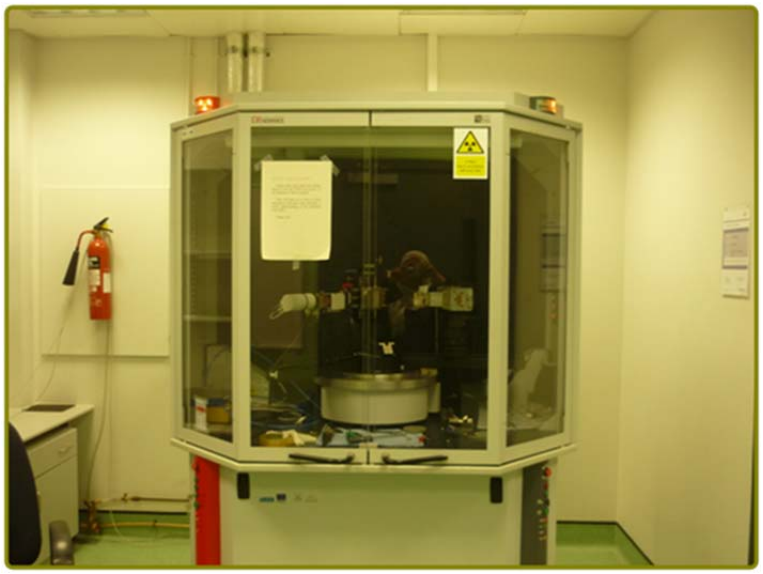

Figure 3.11: Photograph of the XRD machine.

3.4.2.2 Application of XRD to Concrete Chemistry

The application of XRD to quantitative phase abundance analysis goes back to the mid-1920s with the Portland Association Fellowship at the National Bureau of Standards (now National Institute of Standards and Technology, NIST). The late 1950s through the 1980s witnessed an increased use of XRD in the analysis of cements and the first international round robins on quantitative powder diffraction analysis [161].

In the hydration of cement, the chemical reactions that occur between anhydrous cement and water are generally complex in nature because of their multiphase nature and the simultaneous effects of many variables. XRD is employed to identify the polycrystalline phases of cement and hardened cement paste through the recognition of the X-ray patterns that are unique for each of the crystalline phases. Accordingly, this method allows the detection of ettringite (AF_t),

monosulfate (AF_m) and portlandite (CH) and the consumption of the anhydrousphases of the cement (i.e., gypsum, C_3S, C_2S, C_3A andC_4AF), as well as the formation of amorphous C-S-H, which is indicated by an upward shift of the diffractogram [28,162].

3.4.2.2.1 Measurement

For the XRD analyses, the specimens were ground into an agate mortar and immersed in acetone for 45 s, rinsed twice in ethanol and then maintained in the same equipment, with the objective of preventing further hydration, by removing the evaporable water. Just before each analysis, the specimens were dried in an oven at 50 ºC [162]. The mineralogical phases of the mortars were determined by means of X-ray diffraction (XRD) using the same XRD machine shown in Figure 3.11, according to the diffraction powder method, with sweeps from 10 to 60° 2θ.

3.4.3 Scanning Electron Microscope (SEM) and Energy Dispersive X-ray Analyses (EDX)

Scanning electron microscopy (SEM) and its adjunct micro analytical unit, commonly known as the energy dispersive X-ray analyser (EDX), are widely used in microstructure and micro-analytical inspections of cement composites. One of the first applications of SEM in cement hydration was by Gupta, Chatterji, and Jeffery [163], in the early 1970s [28]. Following the development of EDX, Diamond [164] demonstrated the advantages of this SEM attachment in the micro-analysis of concrete. Since then several researchers have practiced, and even improved the technique of concrete evaluation using SEM/EDX [28].

The principle of SEM is explained in the following paragraph. When a beam of primary electrons strikes a bulk solid, the electrons are either reflected (scattered) or absorbed, producing various signals, Figure 3.12. The incident electrons disperse into a “pear shaped” volume in the solid. Besides secondary electrons, backscattered electrons (BSE), X-rays, Auger electrons, and other responses, are also produced. Different modes of observation and/or microanalysis can thus be used with the object under examination. The most frequent modes in SEM involve the capture of secondary and backscattered electrons, while the most commonly used micro-

analytical techniques, based on the detection of X-rays, are energy dispersive X-ray analysis and wavelength dispersive (WD) analysis. Modern SEMs are usually equipped with the EDX detector while the WD analyser unit remains an option for more expensive models [28].

The intensity of the reflected electrons is proportional to the atomic number of the substances in the object and the density of the material. The energy level of primary electrons (PE) is up to about 50 eV as are the scattered electrons. One distinctive feature of the BSE is its relatively high energy. It is important to note that all these responses are produced in a shallow zone of the target [28].

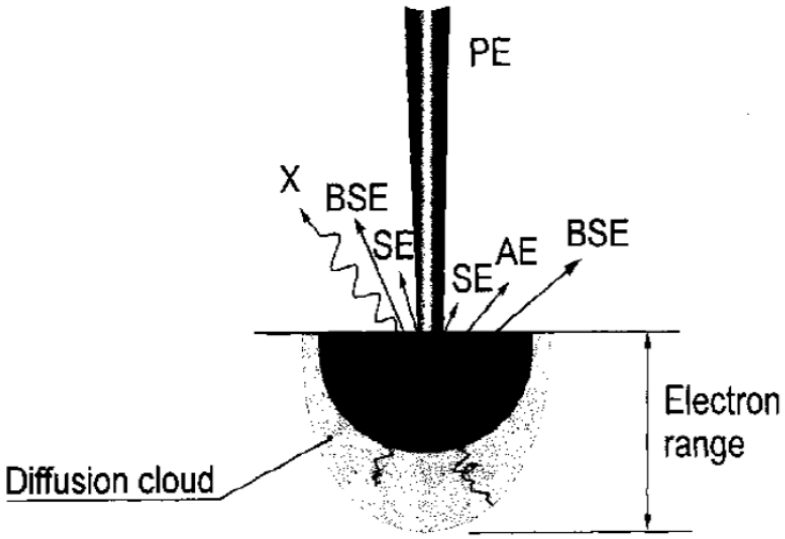

Figure 3.12: Different interactions of an electron beam (PE) with a solid target, BSE: backscattered electron, SE: secondary electron, X: x-ray, AE: auger electron [28].

The method using a scanning electron microscope and an energy dispersive x-ray analyser to simultaneously study the morphology of an object and analyse its elemental composition is called SEM/EDX. SEM/EDX can be done using the following four methods:[28]

- The spot mode, i.e., used for analysing a small spot in a constituent for its elemental composition;
- The area mode, used to analyse the bulk composition of an area;

- The dot mapping mode, used to scan a specific area of interest for elemental mapping in order to study the distribution density of different elements in a particular phase or region;

- The linear traverse mode, used to determine the variation in concentration of one or several elements along a line.

EDX is based on the detection of X-rays emitted by the specimen being examined and the fact that every element has a characteristic emission. The X-ray photons that originate from the specimen are collected by the Si-Li detector. After undergoing a conversion to a voltage pulse output, it is then transformed into counts/channel. These counts are displayed on a cathode ray tube screen. Since each element has its characteristic energy position, different elements can be readily identified by means of a cursor. For example, aluminium Kα is at 1.5 keV, silicon Kα at 1.74 keV, sulphur Kα at 2.34 keV, and calcium Kα is at 3.7 keV [28].

3.4.3.1 Measurement

Scanning electron microscopy (SEM) and energy-dispersive X-ray (EDX) analytical systems were used to characterise the microstructure of composites fracture surfaces using a (SEM/EDS) machine model Hitachi S-3000N VP (Figure 3.13) in the secondary electron (SE) mode operated at around 10 and 30 kV. The samples used for SEM imaging and EDX analysis were slices taken from the same specimens used for the flexure test. The fibres used for SEM imaging were either non-aged treated/untreated fibres or were aged fibres carefully extracted from the composites fracture surfaces, mounted on SEM stubs, and then coated with a gold layer using an Edwards sputter coater, model Pirani 50 I (Figure 3.14).

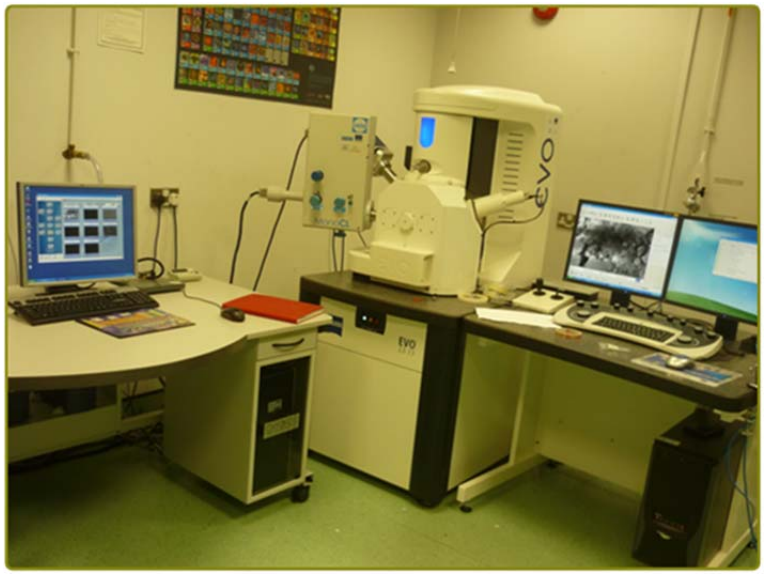

Figure 3.13: Photograph of the SEM/EDX machine.

Figure 3.14: Photograph of the Edwards sputter coater.

3.4.4 Single Fibre Tensile Testing

Treated/untreated single flax fibres were tensile tested using the ASTM D3379 standard test method for tensile strength (TS) and Young's Modulus (YM) for high-modulus single filament materials [165]. Fibres were carefully separated by hand and attached to rectangular pieces of glass with 10 mm marks in their centres in order to provide a gauge length of 10 mm. The fibres were then placed under an optical microscope (Figure 3.15) in order to determine the average diameter of each fibre. After that the fibres were placed in the grips of a Zwick machine model Z5 kN

– BTI – FR005TN (Figure 3.16) with a gauge length of 10 mm and at a crosshead speed of 0.5 mm/min. This machine was equipped with a 5kN load cell and was attached to a PC with TestXpert V11.02 software for data acquisition.

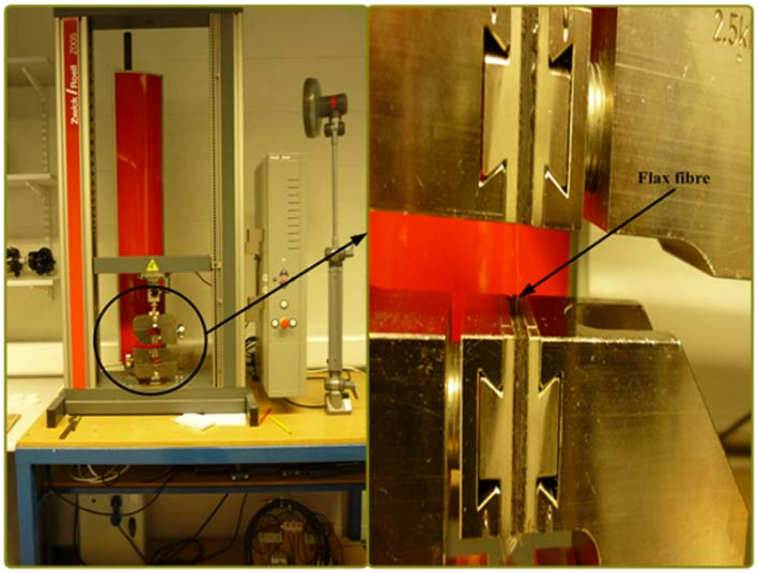

Figure 3.15: The set up for the single fibre tensile strength test.

Figure 3.16: Photograph of the optical microscope.

3.4.5 Thermal Expansion

The thermal strains of the specimens were determined by using the DIL 402 E Netzsch Ltd. Dilatometer, Germany (Figure 3.17). The linear change in the length of each specimen was measured by the dilatometer under temperatures ranging from 20ºC to 1000ºC at a heating rate of 5ºC/min. The data acquisition from the digital

dial indicators was performed with a PC using specially developed software. The average of two specimens was used for defining the thermal strain values. After measurements of each specimen's change in length were taken, the thermal strain values were determined by using Eqs. (3.4), given as follows:

$$\varepsilon = {}^{\Delta L}/_{L_0} \qquad (3.4)$$

Where ε is the thermal strain, ΔL is the unit length change (mm), ΔT is the temperature difference (ºC) and L_o is the initial length (mm) of the specimen at 20ºC.

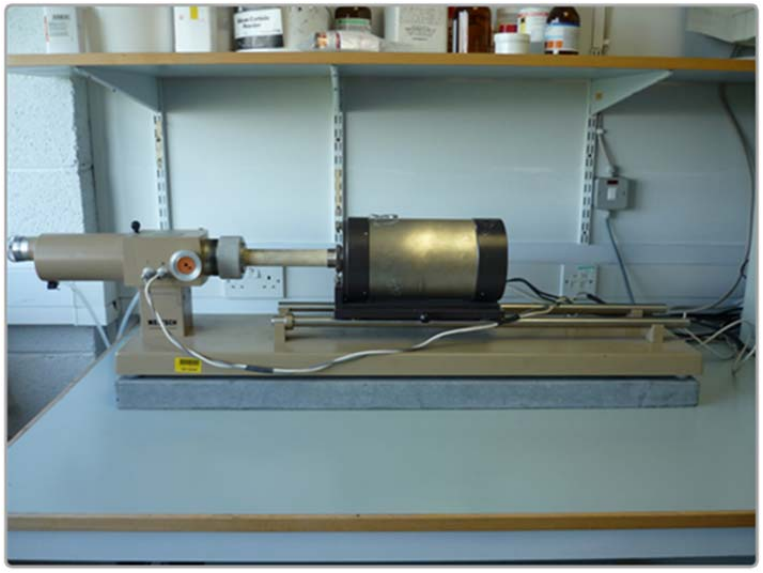

Figure 3.17: Photograph of the Netzsch Model 402 E Dilatometer.

3.4.6 Flexure strength

For the three point flexure test, specimens of 40 x 40 x 160 mm size were prepared in accordance with ASTM C348 [166]. Flexure strength was obtained by using the Zwick machine. This machine is equipped with a 50 kN load cell and attached to a PC interface with TestXpert 2 version 2.1 software for data acquisition, as shown in Figure 3.18. All specimens were tested at room temperature with a cross head speed of 1 mm/min. Flexure strength values were obtained by averaging the measurements of at least three samples.

Figure 3.18: Photograph of the Zwick machine used for flexural strength test.

3.4.7 Compressive Strength

For the compressive tests, specimens of 50 x 50 x 50 mm in size were prepared in accordance with ASTM C 109 [167]. Compressive strength was obtained by using the same Zwick machine used in section 3.4.6. Specimens were tested at room temperature with a cross head speed of 0.5 mm/min. Compressive strength values were obtained by averaging the measurements of at least three samples.

3.4.8 Impact Strength

The Charpy impact strengths of the specimens 20 x 20 x 55 mm were measured using a MAT21 universal pendulum impact tester at a room temperature of 20ºC (Figure 3.19). The impact strength was reported in J/m^2, and the results were the average obtained from four specimens.

Figure 3.19: Photograph of the Charpy impact pendulum.

3.4.9 Flexural Toughness Measurements

The addition of fibres (either natural or synthetic) significantly enhances many of the engineering properties of a cement matrix, especially impact strength and toughness. This enhanced performance in a fibre reinforced cement matrix compared to an unreinforced matrix comes from its greater capacity to absorb energy during fracture. The chief contribution of fibres to the cement matrix can be observed primarily after matrix cracking. While an unreinforced matrix fails with a quasi-brittle behaviour after cracking, the randomly distributed, short fibres in the reinforced matrix arrest microcracks, bridge these cracks, undergo a pullout process and limit crack propagation in the reinforced matrix. Hence, debonding and pulling out the fibres requires more energy, which leads to a significant improvement in toughness, and a resistance to cyclic and dynamic loading occurs, which helps maintain structural integrity and cohesion in the matrix [168,169].

The most common method used to measure toughness is the load-deflection curve obtained by using a simply supported beam loaded at the third points. ASTM C 1018 [170] discusses the evolution of toughness indices (I_5, I_{10} and I_{20}), which refers to the area under the load-deflection curve calculated according to three different specified deflections. Whilst in the Japan Society of Civil Engineers (JSCE) standard SF-4 method, the area under the load deflection curve up to a specified deflection (L/150) is measured and referred to as the toughness [171]. However, the practical uses of these toughness parameters are not sufficient to define the tensile strain-softening law, which simulates the behaviour of the damaged region ahead of a continuous crack. This is referred to as the fracture process zone. To define this softening behaviour, Hillerborg et al. introduced the concept of fracture energy (G_F)[172]. The standard test for the evaluation of this behavioural property was established by the RILEM 50-FMC Technical Committee [173]. In this study, two methods were used to describe composite toughness. In the first method, toughness indices (I_5, I_{10}, I_{20} and I_{30}) were obtained based on ASTM C 1018 [170]. In the second method three point bending tests were performed to evaluate G_F based on the RILEM 50-FMC Technical Committee's standard test [173].

3.4.9.1 ASTM C 1018

In ASTM C l0l8 [170], toughness (or energy absorption introduced as the area under the load deflection curve) is calculated at four specified deflections($\sigma, 3\sigma, 5.5\sigma, and\ 10.5\sigma$) as shown in Figure 3.20. The toughness is calculated at the deflection σ which is considered the elastic or pre-peak toughness (first-crack toughness), while the other deflections ($3\sigma, 5.5\sigma\ and\ 10.5\sigma$) are considered the post-peak toughness. In addition, the terms of the toughness indices (I_5, I_{10} and I_{20}) are also calculated, as follows:

$$I_5 = Area\ OACD/Area\ OAB$$

$$I_{10} = Area\ OAEF/Area\ OAB$$

$$I_{20} = Area\ OAGH/Area\ OAB$$

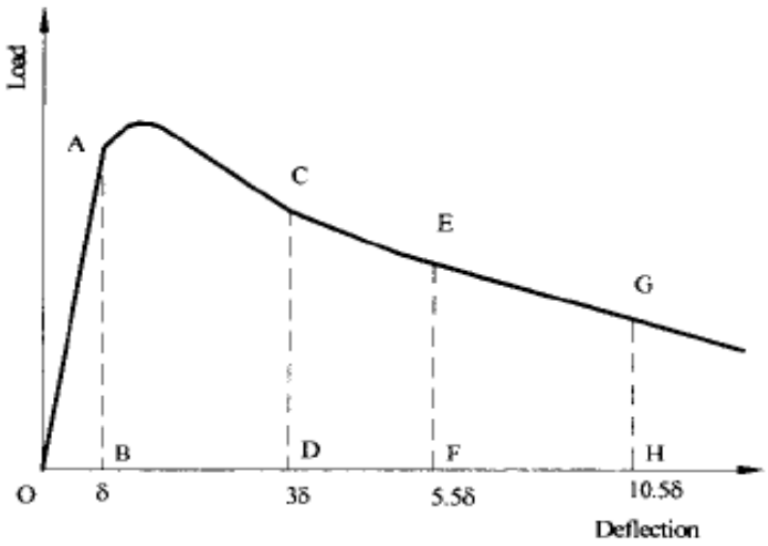

Figure 3.20: Fracture toughness and Indices according to ASTM C1018 [170].

3.4.9.2 Fracture Energy (G_F)

One of the major roles of fibre in cement matrix is to provide an increase in the energy required for fracture by the resultant crack arresting process. Fracture energy (G_F) is the energy required to develop one crack completely. In this study, for a notched beam in three-point bending, the procedures recommended by the RILEM TC 50-FMC Technical Committee [173] were applied to measure G_F. The load–deflection curves were utilised for evaluating the G_F. The area under the load versus deflection at the mid span curve was described as a measure of the fracture energy of the material. The results obtained here are based on the area under the complete load–deflection curve up to a specified deflection (i.e. 6 mm).

3.4.10 Evaluation of composite durability

The durability of the flax fibre cement composites was evaluated on the basis of the flexural strength, toughness indices and fracture energy of the composites before and after exposure to various environments. From the load deflection curves, three parameters were calculated in order to evaluate the reinforcing effect of the fibre and consequently its durability or embrittlement over time:

- Flexural strength of the composite was determined from the maximum post-peak load,

- Toughness indices (I_5, I_{10} and I_{20}) as explained in section 3.4.9.1,
- The fracture energy of the composite as described in section 3.4.9.2.

In order to study the durability of flax fibre cement composites, the specimens were subjected to the following three different ageing conditions:

- 360 days soaking in water at a temperature of about 20 ±2 ºC,
- 50 controlled wetting and drying cycles,
- 1 year (from 21st September 2009 to 20th September 2010) under natural weathering conditions in Dublin-Ireland (latitude 53° 19′ 59′′ N, longitude 6° 14′ 56′′ W). During the period under consideration the maximum and minimum temperatures were 24˚C and -4˚C, respectively, the mean wind speed was 12 m/h, rainfall was around 70 mm/month, the maximum and minimum relative humidity was 86% and 70%, respectively, and solar radiation was around 921 J/cm^2/ day. During the same period (1 year) some of the specimens were kept under laboratory conditions of 19ºC ± 2ºC and 50% ± 5% relative humidity and used as reference specimens.

To determine the period of saturation and drying of the specimens, the percent of mass change versus time curve was developed. In order to develop this curve, a flax fibre cement specimen was completely saturated in water at 20 ±2 ºC and left to dry in an oven at 60±5 ºC. Readings of gain and loss of mass were also recorded during this period. The mass stabilized when the mass changed less than 1% over a period of 3 hours, and then the specimen was assumed to be either dry or wet, depending on the exposure. As a result, it was found that a 48 hour cycle period was suitable for wet and dry conditions in flax fibre cement composites.

3.4.11 Lime-Glass Test

In order to study the pozzolanic activity of WG, a Lime-glass test was conducted following ASTM C593 [174]. The mixture proportions are given in Table 3.3. The mixture was cast in 50 mm cube moulds, wrapped in wet burlap, sealed in a plastic bag, and cured at 54°C in an oven. Compressive strength was obtained using the same Zwick machine noted in section 3.4.6. Specimens were tested at room temperature with a cross head speed of 0.5 mm/min. Compressive strength tests were carried out after 7 days of curing at 54°C and after an additional 21 days curing at 23°C in water in order to monitor the long-term strength gain. As recommended

by ASTM C593 [174], a satisfactory pozzolanic material should have a minimum compressive strength of 4.1 MPa when mixed with lime after 7 days of curing at 54°C and after an additional 21 days of curing in water at 23°C.

Table 3.3: Mixture proportions for lime test (by weight percent)

Lime	WGP	NC	Sand	Water/lime +WG
9	18	0	73	85

3.4.12 Alkali Silica Reaction (ASR)

A study of the alkali silica reaction (ASR) was performed in accordance with ASTM C1260 [175]. Mortar bars 25 x 25 x 100 mm in size were cast. Then, the moulds were covered carefully with plastic sheets and placed in the lab at 22 ºC for 24 hours. After that, the bars were placed in water at 80°C for another 24 hours to gain a reference length. They were then transferred to a solution of 1N of NaOH at 80°C. Readings were then taken every day for 14 days.

3.4.13 Porosity

The porosity of composites is measured with the methanol displacement method [176]. In this method small cubes of 20x20x20 mm were dried until a constant weight W_0 was reached. The dried specimen was dipped into methanol for 24 h and the weight of the specimen hung in the methanol was recorded (W_1). Then, the specimen was taken out of the methanol and was surface dried immediately. The weight of the methanol-saturated specimen with a dry surface was recorded as W_2. The porosity (P) of the specimen was calculated as:

$$P = \frac{W_2 - W_0}{W_2 - W_1} \qquad (3.5)$$

Where: W_0 is dried weight, W_1 is weight of the hung in the methanol and W_2 is the weight of the methanol-saturated specimen with a dry surface.

Chapter 4 : Design of Experiments

4.1 Design of Experiments (DOE)

In the engineering field, experiments are typically carried out to explore and understand the data collected from the experiment, to estimate and determine the effect of process variables on output performance characteristics, and or to confirm and verify the predicted results obtained from an experiment [177]. One of the most common approaches employed by many engineers is one-variable-at-a-time (OVAT), where the engineer varies one variable at a time, while keeping all of the other variables involved in the experiment fixed. However, this approach always carries the risk that the experimenter may find that one input variable has a significant effect on the response (output), but will fail to notice that a change in another variable has also altered the effect of the first variable (i.e. due to these variables dependency or interaction). OVAT also requires the use of large amounts of resources in order to obtain a limited amount of information about the process. As a consequence, OVAT experiments are often unreliable and time consuming. Furthermore, they may not determine the optimal conditions and also do not address the interaction effect between the process variables [177,178,179].

Statistical methods play an important role in planning, conducting, analysing and interpreting data from engineering experiments. DOE is a systematic technique used in the investigation of a system or process. With this technique, a series of structured tests involving planned changes are made to the input variables of a process or system. Then the effects of these changes on a pre-defined output are assessed. DOE is essential as a formal way of maximizing the amount of information gained while minimizing the amount of resources required. It has more to offer than the OVAT approach, because it allows a judgment on the significance of input variables acting alone on the output, as well the effect of input variables acting in combination with one another.

Sir R. Fisher introduced DOE in the early 1920s, at the Rothamsted Agricultural Field Research Station in London, England, in order to determine the

effect of various fertilizers on a range of land plots. Since then, DOE has been applied in many other disciplines such as biology, pharmaceuticals, engineering etc. [177]. In the concrete industry a number of studies have been conducted on the optimisation of cement composites that use a statistical design of experiments and modelling. In one study, Sanjuán and Moragues [180] used a factorial design of experiments to study the effect of mix proportions (i.e. water/cement ratio, sand/cement ratio, and fibre content) on the tensile shrinkage stresses of polypropylene-fibre-reinforced mortars. They used this technique to optimise the mortar mix in order to minimise the plastic shrinkage process. In a similar study, Filho and Sanjuán [10] utilized a prediction model for the free plastic shrinkage of natural sisal fibre reinforced mortars based on a factorial design of experiments at two levels, with three factors (water/cement, sand/cement, and percentage of fibre) and two replications. In order to assess the durability of silica fume and blast furnace slag concretes, Türkmen et al. [181] used the Taguchi method to determine the optimum working conditions (e.g. curing time and water/binder ratio) needed to obtain the physical properties (e.g. capillary and porosity) that would yield the most durable mixtures. Correia et al. [182] used a full factorial design to model the physical and mechanical properties of fresh and hardened concretes that contain recycled aggregate which was reclaimed as a replacement for natural fine aggregate. In another attempt to replace natural aggregates with waste vulcanised rubber scrap (WRS), Correia et al. [183] used a 3^2 full factorial design of experiments to optimise the amount of WRS. They studied the effect of WRS content and water/cement weight ratio (factors) on the fresh mortar's consistency index and compressive strength (responses).

Although natural fibres such as sisal, hemp, bamboo and jute have already been used to reinforce cement matrix in many countries like Brazil [184], India [185] and Australia [186], very little has been reported in the literature on the optimisation of the fracture parameters of natural fibre cement composites. In one study, Li et al. [126] used responses surface methodology (RSM) to model the mechanical properties (i.e. compressive and flexure strength, flexure toughness and toughness indices) of hemp fibre reinforced concrete composite. They used composite methods to analyse the reinforced concrete composite under the conditions of fibre content $0.1 <$ fibre volume fraction $< 1\%$ and with an aspect ratio larger than 400.

The responses surface methodology (RSM) concept was introduced in the early 50's by Box and Wilson and is the best known type of DOE technique [178]. Among the RSM methods, the two most popular types of experimental designs that exist for developing second-order models are the central composite design (CCD) and the Box-Behnken design (BBD) [178,187]. Since these particular methods are the ones being used in this study, some details about them will be presented in the following sections.

4.2 Response Surface Methodology (RSM)

RSM is a collection of mathematical and statistical techniques that are useful for modelling and predicting how the response of interest is influenced by several input variables with the goal of optimizing this response [187]. RSM combines statistical and mathematical methods of experiment design, regression analysis and optimisation in order to deliver useful techniques for problem development, improvement, or optimisation. It provides a comprehensive, statistically based technique for planning, executing, and evaluating batches [168]. If all independent variables are measurable and can then be repeated with negligible errors, the response surface can be expressed as follows [188]:

$$y = f\ (x_1, x_2, \dots\dots\dots\dots\dots x_k) \tag{4.1}$$

Where: k is the number of independent variables

In order to optimize the response "y", it is necessary to find an appropriate estimate for the true functional relationship between the independent variables and the response surface. Typically a second order polynomial Eq.4.2 is used in RSM.

$$\mathrm{y} = b_o + \sum b_i \chi_i + \sum b_{ij} \chi_i \chi_j + \sum b_{ii} \chi_{ii}^2 + \varepsilon \tag{4.2}$$

4.2.1 Central Composite Design (CCD)

The CCD is a very efficient design for fitting the second order model, which was originally developed by Box and Wilson and improved upon by Box and Hunter. The CCD gives almost as much information as a multilevel factorial, but requires much fewer experiments than a full factorial and has also been shown to be

adequate to describe the mechanical properties responses [189,190]. The CCD consists of: (a) factorial or fractional factorial design points, (b) axial points or star points and (c) centre points. The CCD is designed to estimate the coefficients of a quadratic model. All point descriptions will be made in terms of the coded values of the factors [178,187].

Factorial points

The factorial portion of the CCD design is used to fit all linear and interaction terms. The two-level factorial part of the design includes all possible combinations of the +1 and -1 levels of the factors. For the two factors case there are four design points: (-1, -1) (+1, -1) (-1, +1) (+1, +1). Generally, the CCD consists of 2^k factorial points [178,190].

Star or axial points

The star points provide additional levels of the factor for purposes of estimation of the quadratic terms. The star points consist of all of the factors set to 0, the midpoint, except one factor, which has the value +/-α (the distance α of the axial runs from the design centre and the number of centre points). In the case of two factors, the star points are: ($-\alpha$, 0) (α, 0) (0, $-\alpha$) (0, α). The choice of α depends upon the design's region of interest. In this work, a face centred design was selected. In this design the star or axial points are located at the centre of each face of the factorial space, so $\alpha = \pm 1$. This particular variety requires 3 levels of each factor [177,178,190].

Centre points

Centre points (mid points) are points with all levels set to the coded level (0) the midpoint of each factor range: (0, 0). Centre points are typically repeated 4-6 times in order to get a good estimate of experimental error (pure error). These points are shown in Figure 4.1 for the two factors design [178,190].

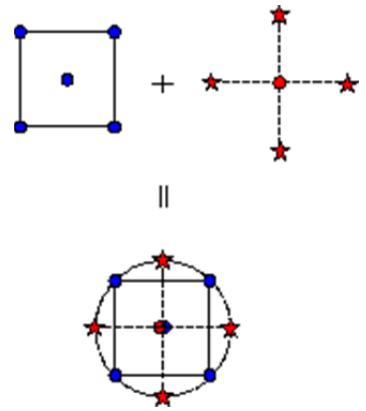

Figure 4.1: Generation of CCD for two factors [178].

4.2.2 Box-Behnken Design (BBD)

BBD was developed by Box and Behnken in 1960 and is based on three levels of each factor. They are constructed by first combining 2^k factorial designs with incomplete block designs and then adding a specified number of centre points. The designs that are developed are usually very efficient in terms of the number of required runs [187]. In the case of three factors, the total number of points is equal to 12 design points and 5 centre points for a total of 17 points. Although the 12 unique combinations represent less than one-half of all possible combinations for three factors with the same number of levels, they provide enough information to fit the coefficients of the polynomial shown in Eq. 4.2 [178]. Figure 4.2 shows a schematic diagram for BBD with three factors. Table 4.1 presents a comparison between the Central Composite and Box-Behnken designs.

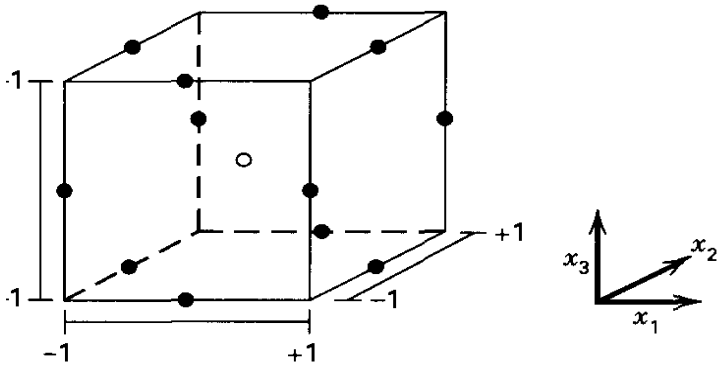

Figure 4.2: A schematic diagram for BBD with three factors [187].

Table 4.1: Comparison between the Central Composite (CCD) and Box-Behnken designs (BBD) [191]

CCD	BBD
Created from a 2-level factorial design, improved with centre points and axial points.	Has specific positioning of design points.
Normally has 5 levels for each factor, this can be modified to a face-centred CCD by choosing a = 1.0. The face-centred design has only three levels for each factor.	This design has 3 levels for each factor.
Created for estimating a quadratic model.	
Tend to be sensitive to missing data, making them more susceptible to problems.	Provides strong coefficient estimates near the centre of the design space, but weaker at the corners of the cube due to the absence of design points.
Replicated centre points provide excellent prediction capability near the centre of the design space.	Sensitive to missing data and a bad run.
Region of operability must be greater than the region of interest in order to accommodate axial runs.	Region of interest and region of operability are nearly the same.

4.3 General Steps in RSM

Well-designed experiments are often carried out in four phases: planning, process characterisation, optimisation, and verification. The following steps are performed in order to develop and optimise a mathematical model for this work:

4.3.1 Planning Experiments

Careful planning helps to avoid problems that can occur during the execution of the experimental plan such as, personnel, equipment availability, or funding, and the mechanical aspects of the system may affect the ability to complete the experiment. Planning is the first step in any application. The planning session should involve individuals with first-hand knowledge of the project and this step is usually covered by the literature review. The critical factors can be defined through the literature review or by conducting a preliminary study (i.e. screening study) based on a factorial design or a partial factorial design. In this study the vital process factors were determined through the literature review and are summarised as follows:

- The process input factors for flax fibre treatment conditions are alkali (NaOH) concentration, soaking time and soaking temperature.
- The selected fibre variables are fibre length and fibre volume fraction.

The limits of each factor (or variable) were determined through a pilot experiment which was carried out by changing one factor at time. Once the limits of each factor were determined, Design-Expert 7 software was used to divide them into levels determined by the selected design.

4.3.2 Designing and Running Experiments

Using the factors and levels determined in the previous step, the experiments now can be designed and the process carrying them out can be established. The matrix depends on the type of RSM design chosen. For three factors, the experimental runs for BBD are 17, while for two factors; the experimental runs for CCD are 13. These experimental runs are sufficient for the estimation of the coefficients in Eq. 4.2. After this step, the experiments were carried out according to the design matrix and in a random order in order to avoid any systematic error in the experiment.

The mechanical properties (or responses), mentioned earlier in this study, were tested and measured in sequential order following the standard procedures available for each response. An average of at least thirty recorded measurements was calculated and considered for further analysis in the case of single fibre tensile

strength, and an average of at least three recorded measurements was calculated in the case of flax fibre cement composites.

4.3.3 Development of the mathematical model

Design expert software develops and displays the possible modules which can fit the input data and suggest the model that best fits the experiment data.

4.3.4 Estimation of the coefficients in the model

Regression analysis is carried out in order to evaluate the values of the coefficients in Eq. 4.2. The computer software was used to estimate the coefficients for all of the responses of each experiment.

4.3.5 Testing the adequacy of the models developed

The adequacy of the models developed was tested by using the analysis of variance (ANOVA). ANOVA is a general technique for studying sampled-data relationships. This technique enables the difference between two or more sample means to be analysed and is obtained by subdividing the total sum of the squares. One way ANOVA is the simplest case. The purpose of ANOVA is to test for significant differences between class means, and this is done by analysing the variances. The statistical significance of the models that were developed and each term in the regression equation were examined using the sequential F-test, lack-of-fit test and other adequacy measures such as R^2, Adj- R^2, Pred. R^2 and Adeq. Precision ratio by using the same computer software to obtain the best fit [187,191].

Fv value: Check for comparing model variance with residual (error) variance. When the variances are close to each other, the ratio will be close to one and it is less likely that any of the variables (or factors) have a significant effect on the response. Model Fv- Value and related probability value (Prob. > Fv) are used to confirm model significance. Fv value is computed by dividing the term mean square by the residual mean square.

The p-value (or Prob.>F) of the model and of each term in the model can be calculated by means of ANOVA. If the p-value of the model and of each term in the

model does not exceed the level of significance (say α= 0.05) then the model can be considered adequate within the confidence interval of (1- α). For the lack-of-fit test, the lack of fit would be considered insignificant if the p-value of the lack of fit exceeds the level of significance.

Precision of a parameter estimate is based on the number of independent samples of information which can be determined by the degree of freedom (df), which is equal to the number of experiments minus the number of additional parameters estimated for that calculation.

The Adequate Precision compares the range of the predicted value at the design points to the average predicted error. An adequate precision ratio above 4 indicates adequate model discrimination. In this study, the values of adequate precision are significantly greater than 4.

4.3.6 Model Reduction

Model reduction includes eliminating those terms that are not desired or which are statistically insignificant (terms that have p-value greater that the level of significance α). The elimination process can be done manually or automatically by using three procedures to evaluate all possible regression equations [178,187,191]. In this study the elimination process was done automatically with computer software. With the automatic model regression, those terms which are forced into the model regardless of their entry/exit α values could be controlled. Basically, there are three types of automatic model regression:

Forward selection technique: This technique starts with only the constant term, and the first variable added is the one with the highest simple correlation with y. If the regression coefficient of this variable is significant it will continue in the equation. After y has been adjusted for the effect of the first variable, a new search for the second variable with the highest correlation with y is started. The significance of the regression coefficient of the second variable is then checked. If the regression coefficient is significant, a search for a third variable is done in the same way. The procedure is complete when the last variable entered into the equation has an insignificant regression coefficient or when all of the variables are involved.

***Backward elimination procedure*:** In this method, the full equation is fitted and the variables are sequentially eliminated at each step. In the backward procedure, the variable with the smallest contribution to the reduction of error is eliminated first, or the variable with the smallest t ratio (i.e. the ratio of the regression coefficient to its standard error) and so on. In the case of more than one variable having an insignificant t ratio, the technique works by dropping the variable with the smallest insignificant t ratio and the equation with the remaining variables is then fitted and the ratios for the new regression coefficient are tested.

***Stepwise regression method*:** this method is a combination of the forward and backward regressions, where the calculations used for the inclusion and deletion of variables are the same as they are for the forward and backward procedures. However, the possibility of eliminating a variable that might be added in at an earlier stage, as in the backward technique, is also considered. This method has the advantage of assuming different or similar levels of significance for inclusion or the deletion of variables from the regression equation.

4.3.7 Development of final reduced model

At this stage of development, the program automatically defaults to the "Suggested" polynomial model which best fits the criteria discussed in the Fit Summary section. This model includes only the significant terms and the terms that are essential in order to maintain hierarchy. When the final model has been tested and checked and found to be adequate, the responses can be predicted at any midpoint using the adequate model. In addition, some important plots, such as contours, 3D surface, and perturbation plots are produced in order to show the factors effect and how they contribute to the response. Also, it is now possible to use the developed model to find the setting at which the process can be optimized.

4.4 Optimisation

4.4.1 Desirability approach

The desirability approach is one of the most commonly used techniques in the industry for the optimisation of multiple response processes. This approach is based on the idea that the "quality" of a product or process that has multiple quality

characteristics, with one of them outside of some "desired" limits, is completely unacceptable. The desirability method is widely used due to its simplicity, availability in the software and because it also provides flexibility in weighting and giving importance to individual responses. Solving such multiple response optimisation problems using this approach involves using a technique for combining multiple responses into a dimensionless measure of performance called the overall desirability function. The desirability technique includes the transformation of each estimated response, Y_i, into a dimensionless utility bounded by $0 < d_i < 1$, where a higher d_i value indicates that the response value Y_i is more desirable and if $d_i = 0$ this means a completely undesired response or vice versa, when $d_i = 1$ [192]. In this study, the individual desirability for each response d_i was calculated using Eqs. 4.3-4.7. It is possible to change the shape of the desirability function for each goal by the weight field 'wt_i'. Weights are used to give added emphasis to the upper/lower bounds or to emphasize the target value. Weights can be ranged between 0.1 and 10; weights greater than one provides more emphasis on the goal, while weights less than one provides less emphasis on the goal. In the desirability objective function (D), each response can be given an importance (r), relative to the other responses. Importance varies from the least important value of 1(+), to the most important value of 5 (+++++). If varying degrees of importance are assigned to different responses, the overall objective function is presented below in Eq. 4.7. Where n is the number of responses in the measure and T_i is the target value of i^{th} response [191].

- For a goal of maximum, the desirability will be defined by:

$$d_i = \begin{cases} 0 & , \quad Y_i \le Low_i \\ \left(\dfrac{Y_i - Low_i}{High_i - Low_i} \right)^{wt_i} & , \quad Low_i \langle Y_i \langle High_i \\ 1 & , \quad Y_i \ge High_i \end{cases} \tag{4.3}$$

- *For a goal of minimum, the desirability will be defined by:*

$$d_i = \begin{cases} 1 & , \quad Y_i \le Low_i \\ \left(\dfrac{High_i - Y_i}{High_i - Low_i} \right)^{wt_i} & , \quad Low_i \langle Y_i \langle High_i \\ 0 & , \quad Y_i \ge High_i \end{cases} \tag{4.4}$$

- *For a goal as a target, the desirability will be defined by:*

$$d_i = \begin{cases} \left(\dfrac{Y_i - Low_i}{T_i - Low_i} \right)^{wt_{1i}} & , \quad Low_i \langle Y_i \langle T_i \\ \left(\dfrac{Y_i - High_i}{T_i - High_i} \right)^{wt_{2i}} & , \quad T_i \langle Y_i \langle High_i \\ 0 & , \quad Otherwise \end{cases} \tag{4.5}$$

- *For a goal within range, the desirability will be defined by:*

$$d_i = \begin{cases} 1 & , \quad Low_i \langle Y_i \langle High_i \\ 0 & , \quad Otherwise \end{cases} \tag{4.6}$$

$$D = \left(\prod_{i=1}^{n} d_i^{r_i} \right)^{\frac{1}{\sum r_i}} \tag{4.7}$$

4.4.2 Optimisation by Means of Design-Expert Software

The optimisation part of Design-expert software V7 searches for a combination of factor levels that simultaneously satisfy the requirements placed on each one of the responses and the process variables. In this study, numerical and graphical optimisation methods were used by choosing the desired goals for each factor and response. As stated earlier, the numerical optimisation process includes combining the goals into an overall desirability function (D). The numerical optimisation feature in the design expert software package finds a point or more in the factors domain that would maximise this objective function. In a graphical optimisation with multiple responses, the software introduces regions where requirements simultaneously meet the proposed criteria by superimposing or overlaying critical response contours on a contour plot. After that, a visual search for the best compromise becomes possible. In the case of dealing with multiple responses, it is recommended that the user perform numerical optimisation first; otherwise it might be impossible to uncover a feasible region. The graphical optimisation shows the area of feasible response values in the factor space [191]. Figure 4.3 presents a flow chart of the optimisation steps in the design-expert software.

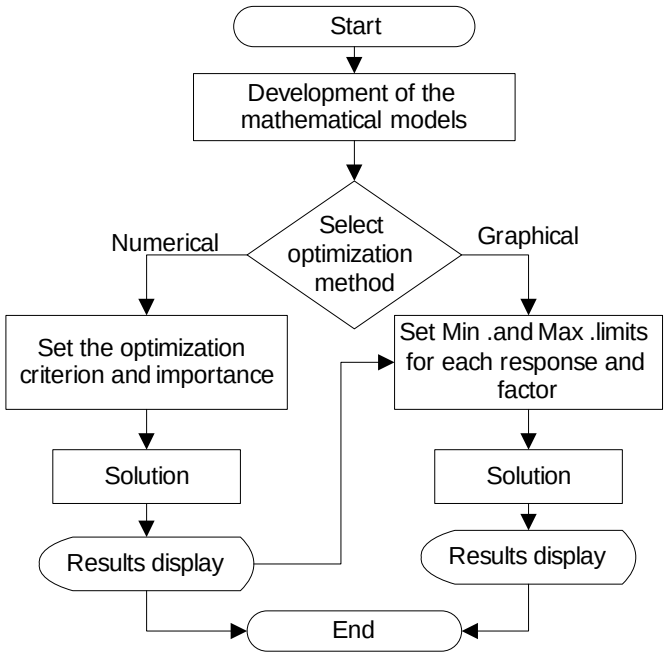

Figure 4.3: Optimisation steps [178].

Chapter 5 : Results and Discussions

5.1 Introduction

This chapter describes the results of the studies that were carried out to make eco-friendly cement composites by using alkali treated flax fibre, waste glass powder (WG), nano-clay particles (NC) and colloidal nano-silica (NS). Following is a summary of the studies that were completed during this research project:

- Treatment of flax fibres with alkali to obtain an optimum alkali treatment method and the development of an empirical model for the tensile strengths of various alkali treated fibres using a Box-Behnken design.

- Comparisons of untreated and alkali treated flax fibres using single fibre tensile testing as well as SEM, DTA/TGA, and XRD.

- The effect of alkali treatments on flax fibre diameter, tensile strength (TS) and Young's modulus (YM).

- Comparisons of the mechanical and thermal behaviour of untreated and optimised treated flax fibre composites.

- Optimisation of fibre parameters (i.e. volume fraction and fibre length) in terms of the compressive, impact, porosity, flexural and toughness properties of cement composites a central composite design.

- The effect of WG, NC and nano-silica (NS) content on the alkali silica reaction (ASR), porosity, compressive, impact, flexural and toughness properties of cement composites.

- Further characterisation of optimised WG, NC and NS composites in terms of post cracking behaviour, TGA/DTA, SEM, XRD and thermal strain.

- Durability and long term performance of optimised flax fibre composites. The durability of the optimised composites was assessed in terms of flexural, fracture energy and toughness well as SEM and XRD analysis.

5.2 Alkali Treatment of Flax Fibre

5.2.1 Selection of the Levels of Treatment Factors

In order to select the level of NaOH concentration, soaking time and temperature pilot experiments were conducted under the following conditions that are explained in Tables 5.1 to 5.3, and the effects of the concentration of NaOH, soaking time, and temperature on the TS of the fibres are shown in Figures 5.1, 5.2, and 5.3, respectively.

Table 5.1: Experimental parameters for the selection of levels of concentration of NaOH

NaOH (wt. %)	Soaking time (min)	Temperature (℃)
3	60	90
5	60	90
7	60	90
10	60	90
15	60	90
20	60	90

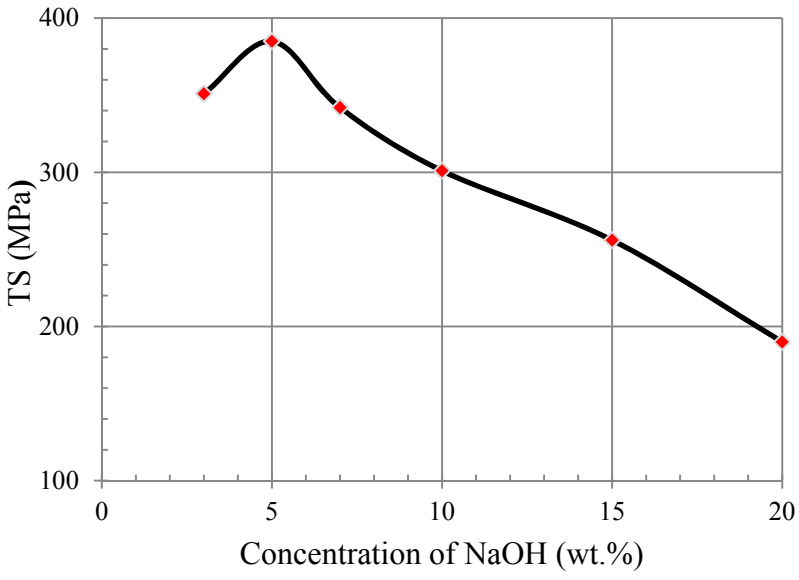

Figure 5.1: Effect of Concentration of NaOH on TS (at 100℃ and 60 min).

Table 5.2: Experimental parameters for the selection of levels of soaking time

NaOH (wt. %)	Soaking time (min)	Temperature (℃)
5	10	90
5	30	90
5	60	90
5	180	90
5	240	90
5	300	90

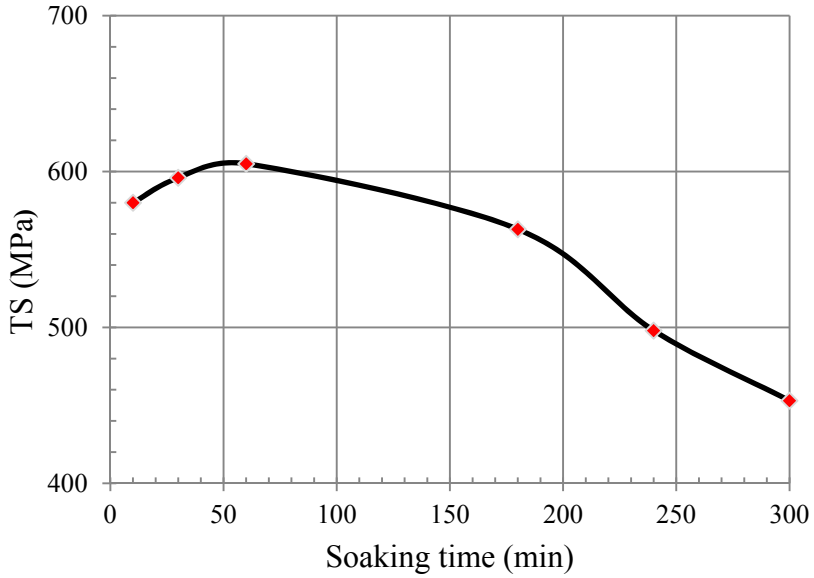

Figure 5.2: Effect of soaking time on TS (at 100℃ and 5% NaOH).

Table 5.3: Experimental parameters for the selection of levels of soaking temperature

NaOH (wt. %)	Soaking time (min)	Temperature (℃)
5	60	20
5	60	50
5	60	100
5	60	150
5	60	200

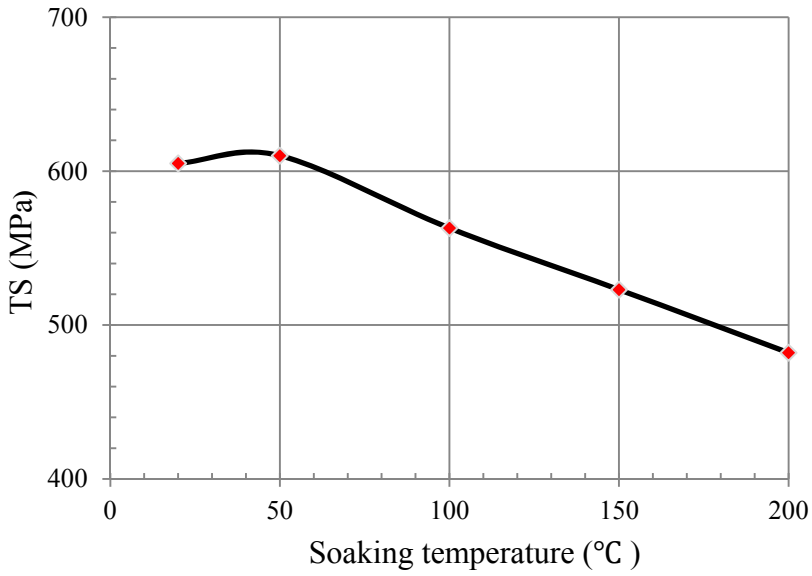

Figure 5.3: Effect of soaking temperature on TS (at 60 min and 5% NaOH).

As can be seen in Figures 5.1 to 5.3, if the levels are too close, the change in fibre strengths are so small that they might remain masked within range of experimental errors. However, the linear approximation of the TS over the whole range of NaOH concentration, soaking time and digestion temperature under study would result in large inaccuracies. Therefore, in order to make linear approximations, it is reasonable to select neither a very small range nor a very large one. This leads to the selection of the following levels of treatment:

$$5\% \leq NaOH\ concentration\ (x_1) \leq 10\%$$

$$10\ min \leq soaking\ time\ (x_2) \leq 180\ \text{min}$$

$$20\ ℃ \leq temperature\ (x_3) \leq 90℃$$

Table 5.4 shows the treatment input variables and experiment design levels. In this study, the test was designed based on a three factors, three levels Box-Behnken design, as presented in Table 5.4. Each of the results presented in Table 5.4 is an average of at least thirty readings.

Table 5.4: Experimental data and results for treated and untreated flax fibres ($n \geq 30$)

Run	Concentration of NaOH (wt. %)	Soaking time (min)	Temperature (Celsius)	TS (MPa)	YM (GPa)	Diameter (μm)
Untreated fibre	0	0	0	611	37.2	39.04
1	5	10	55	627	36.2	27.5
2	10	10	55	483.75	34.4	28.43
3	5	180	55	397.5	29.3	29.05
4	10	180	55	398.25	26.3	29.53
5	5	95	20	436	30.6	28.62
6	10	95	20	312	31.9	31.65
7	5	95	90	352.5	30.2	30.2
8	10	95	90	229.5	24.1	30.41
9	7.5	10	20	491.25	33.6	28.35
10	7.5	180	20	395	29.4	30.52
11	7.5	10	90	471	32.4	28.68
12	7.5	180	90	290	25.3	30.1
13	7.5	95	55	400	30.3	29.65
14	7.5	95	55	413.75	30	28.21
15	7.5	95	55	417.25	31.2	28.06
16	7.5	95	55	410.5	32.5	28.68

5.2.2 Development of Mathematical Models

Further investigations of alkali treatment parameters were carried out, using ANOVA, in order to identify which parameters significantly affect fibre strength. Applying design-expert software to the outcomes, the result suggests the highest order polynomial where the additional terms are significant and where the model is not aliased. Selecting the step-wise regression method eliminates the insignificant model terms automatically. The sequential F-test for the significance of both the regression model and the individual models' terms along with the lack of fit test were carried out using Design-Expert V7 software. The ANOVA for the reduced quadratic models summarise the analysis of tensile strength and show the significant model terms. Tables (5.5 to 5.6) show the ANOVA results for the tensile strength and Young's Modulus. The same tables also show the other adequacy measures R^2, adjusted R^2 and predicted R^2. All of the adequacy measures are in logical agreement and indicate significant relationships. The adequate precision ratios in all cases are

greater than 4 which indicate adequate model discrimination. The analysis of the variance results for the tensile strength model and Young's Modulus model show that, according to the results obtained, the developed models are statistically accurate and can be used for further analysis. The final models in terms of the actual factors are shown below in Equations 5.1 and 5.2.

For the tensile strength model, the Analysis of Variance indicates that the main effects are NaOH concentration (x_1), soaking time (x_2), the soaking temperature (x_3), the two level interaction between concentration and soaking time (x_1x_2) and the second order effect of soaking time and temperature (x_2^2) and (x_3^2) . In the case of the Young's Modulus model, the main effect of NaOH concentration (x_1), soaking time (x_2), the soaking temperature (x_3), the two level interactions between concentration and soaking time (x_1x_2) and the second order effect of soaking temperature (x_3^2) are significant model terms.

$$\text{TS} = 692.95 - 35.56x_1 - 3.68x_2 + 5.97x_3 + 0.17x_1x_2 + 0.01x_2^2 - 0.06x_3^2 \quad (5.1)$$

$$\text{YM} = 28.72 + 0.68x_1 - 0.4x_2 - 0.24x_3 - 0.02x_1x_3 - 0.0012\,x_3^2 \quad (5.2)$$

where:

TS is single fibre tensile strength (MPa)
YM is Young's Modulus (GPa)
x_1 is NaOH concentration (wt. %)
x_2 is soaking time (min)
x_3 is soaking temperature (Celsius)

Table 5.5: ANOVA analysis for single fibre tensile strength model

Source	Sum of Squares	df	Mean Square	F Value	p-value	
Model	121954.3	7	17422.04	73.69	< 0.0001	significant
x_1	18963.78	1	18963.78	80.22	< 0.0001	
x_2	43845	1	43845	185.47	< 0.0001	
x_3	10603.32	1	10603.32	44.85	< 0.0001	
x_1x_2	5184	1	5184	21.929	0.0011	
x_2x_3	1795.64	1	1795.64	7.59	0.0223	
$(x_2)^2$	22811.54	1	22811.54	96.49	< 0.0001	
$(x_3)^2$	21058.02	1	21058.02	89.08	< 0.0001	
Residual	2127.54	9	236.39			
Lack of Fit	1879.22	5	375.84	6.05	0.0528	not significant
Pure Error	248.32	4	62.08			
Cor Total	124081.9	16				
R^2=0.982			adj. R^2= 0.969			
Pred. R^2=0.892			Adeq. Precision= 36.87			

Table 5.6: ANOVA analysis for Young's Modulus model

Source	Sum of Squares	df	Mean Square	F Value	p-value	
Model	143.71	5	28.74	25.58	< 0.0001	significant
x_1	11.52	1	11.52	10.25	0.0084	
x_2	86.46	1	86.46	76.97	< 0.0001	
x_3	22.78	1	22.78	20.28	0.0009	
x_1x_3	13.69	1	13.69	12.18	0.005	
$(x_3)^2$	9.26	1	9.26	8.24	0.0152	
Residual	12.35	11	1.12			
Lack of Fit	8.18	7	1.16	1.12	0.484	not significant
Pure Error	4.17	4	1.04			
Cor Total	156.07	16				
R^2=0.920			adj. R^2= 0.884			
Pred. R^2=0.794			Adeq. Precision= 17.37			

5.2.3 Effect of Processing Parameters on Single Fibre Tensile Strength (TS)

The effect of alkali treatment on the tensile strength of flax fibres is summarised in Table 5.4. Figures 5.4 and 5.5 then show the effects of NaOH concentration, soaking time and treatment temperature on the average fibre's TS. Figures 5.4 presents a perturbation plot which illustrates the effect of the treatment condition on TS and Figure 5.5 is a contours graph that shows the effect of treatment parameters on fibre TS. From these results, it can be seen that the alkali treatment which resulted in the strongest fibre was treatment (1), followed by (9) and then (2). Compared to the TS of untreated fibre (control), it can be seen that alkali treatment resulted in a similar fibre TS from treatment (1), and decreased fibre TSs from treatments (9) and (2). As Equation clearly shows (5.1), the process variable that most notably affected fibre strength was NaOH concentration followed by soaking temperature and then soaking time. For 5% NaOH treatment at 95 min, a 19% reduction in TS was recorded when the temperature was increased from 20 to 90℃. The reduction in strength was even more pronounced with a 10% NaOH, hence the fibre TS was reduced by 26% when the temperature was increased from 20 to 90℃. As Figure 5.4 clearly shows, the increase in NaOH concentration and soaking time has a negative effect on single fibre tensile strength. A very high concentration of NaOH would certainly damage the fibre and consequently reduce the tensile strength of the fibre [83,193]. However, the reduction in TS due to the increase in soaking time might be caused by a softening of the inter-fibrils matrix which adversely affects the stress transfer between the fibrils as well as the overall stress development in the fibre undergoing tensile deformation [80,194]. On the other hand, the increase in the temperature has a slightly positive effect on TS up to 55ºC, but after that it seems that TS decreases with the increases in temperature.

As can be seen from the above results, the alkali treatment (1) resulted in a similar fibre TS to the TS of untreated fibre. This could be caused by the removal of non-strength contributing fibre surface components which, as a consequence, would have resulted in a reduction in the average fibre cross-sectional area**.** The alkali treatment would also have led to a better packing of the cellulose microfibrils, a reduction in the microfibril spiral angle, and an increase in the molecular orientation

of the cellulose chains [80]; all of which would have acted to not reduce the fibre TS of the fibre for that particular treatment. For alkali treatments (9) and (2), the TS appeared to have been reduced slightly owing to the removal of non-strength contributing components during alkali treatment, and because of a weakening of the cellulose fibres. For other alkali treatments, the TS were found to be reduced and the reductions were proportional to the degree of severity of the alkali treatments. These reductions reveal that the cellulose had been degraded or the fibre structure had been disrupted and that the fibres had been considerably weakened.

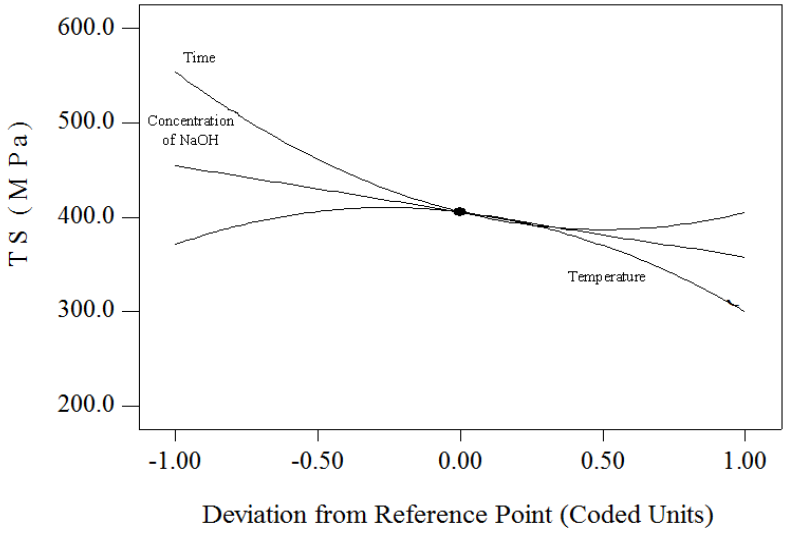

Figure 5.4: Perturbation plot showing the effect of all factors on TS.

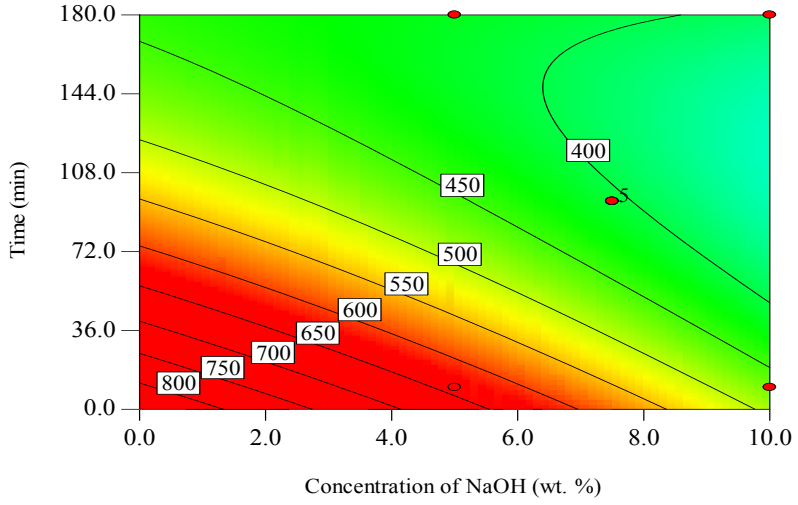

Figure 5.5: Contour plot showing the effect of NaOH concentration and soaking time on TS at 55°C soaking temperature.

5.2.4 Effect of Process Parameters on Young's Modulus (YM)

The Young's modulus of the treated flax fibres are shown in Table 5.4. Figure 5.6 shows a perturbation plot illustrating the effect of the treatment condition on YM while Figure 5.7 displays a contour plot showing the effect of the treatment condition on YM. From these results, one can see that the fibre YM of treatments (1), (2), and (9) are slightly lower than that of the untreated control sample. For other alkali treatments, the reduction of YM was notable when compared to the untreated control fibre and it appears to decrease with the increase of the severity of the alkali treatment conditions. From the results, it can be seen that YM decreases with an increasing concentration of NaOH, soaking time and fibre treatment temperature. Generally, it can be said that the fibre YM decreases with the increase of the removal of surface components such as hemicelluloses, lignin, and pectin. In fact, lignin, hemicelluloses, and pectin are generally highly cross-linked, branched structures that keep the fibres in their proper orientation and locations, and thus provide good structural integrity and rigidity in the cellulose fibres. Therefore, the removal of these surface components from a fibre surface would lead to a decrease in fibre YM. These results are in substantial agreement with the results obtained by Islam [8].

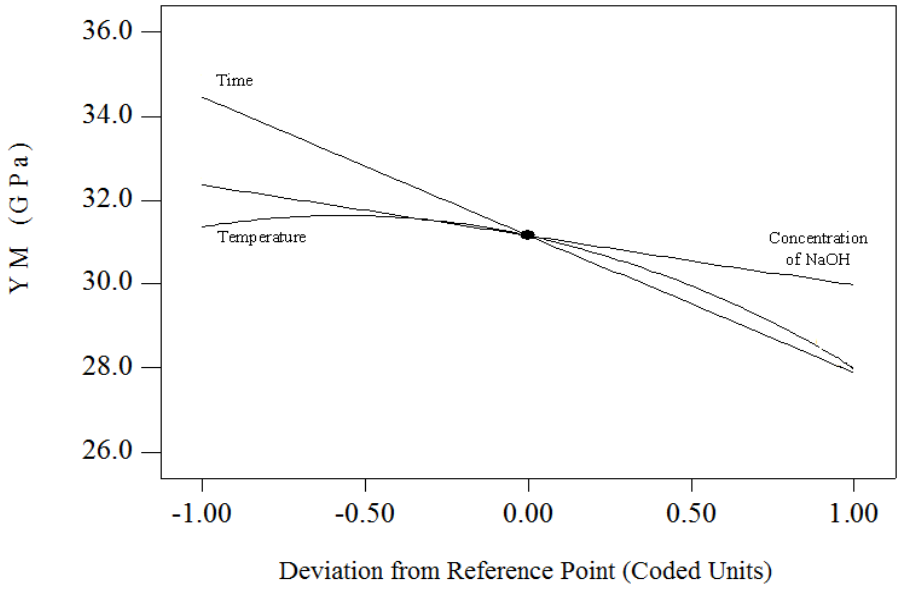

Figure 5.6: Perturbation plot showing the effect of all factors on YM.

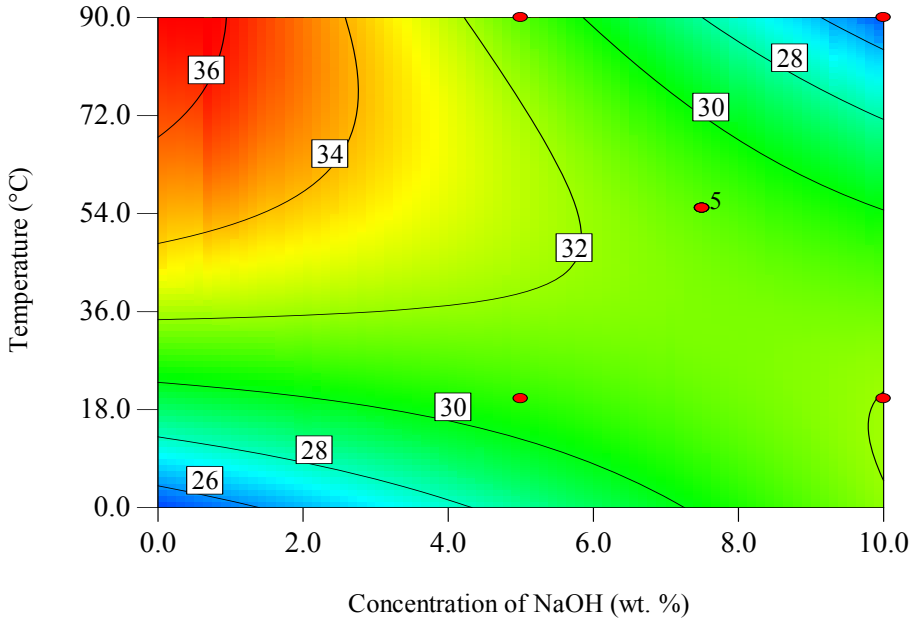

Figure 5.7: Contour plot showing the effect of NaOH concentration and soaking temperature on YM at a soaking time of 10 min.

5.2.5 The Effects of Fibre Diameter on Fibre Tensile Strength (TS)

Figure 5.8 and Table 5.4 present the relationship between average fibre diameter and average fibre TS. The results show that there is a general trend for smaller diameter fibres to have higher TSs when compared to the larger diameter fibres. This trend could be due to the presence of larger amounts of flaws and imperfections in the bigger diameter fibres. Hence, the presence of such flaws and imperfections adversely affects the mechanical properties of the fibres [105]. The number of flaws will increase in proportion to the fibre diameter and thus contribute to a decrease in fibre TSs [195]. On the other hand, it is possible that the reduction in TS with increased fibre diameter could be due to the fibre's geometry. Where the larger fibres were slightly distorted and had elliptical, rather that circular cross sections. This distortion of the fibres' cross sections from circular to elliptical resulted in an increase in the cross-sectional area for the larger fibre diameters. Since the TSs were calculated based on the assumption that the fibre cross sections were circular, the elliptical fibres would have been calculated as having a larger cross-sectional area than they actually had. The TS was calculated by dividing the tensile load by the fibre cross-sectional area, consequently, fibres with larger than actual cross-sectional areas would then result in lower calculated TSs.

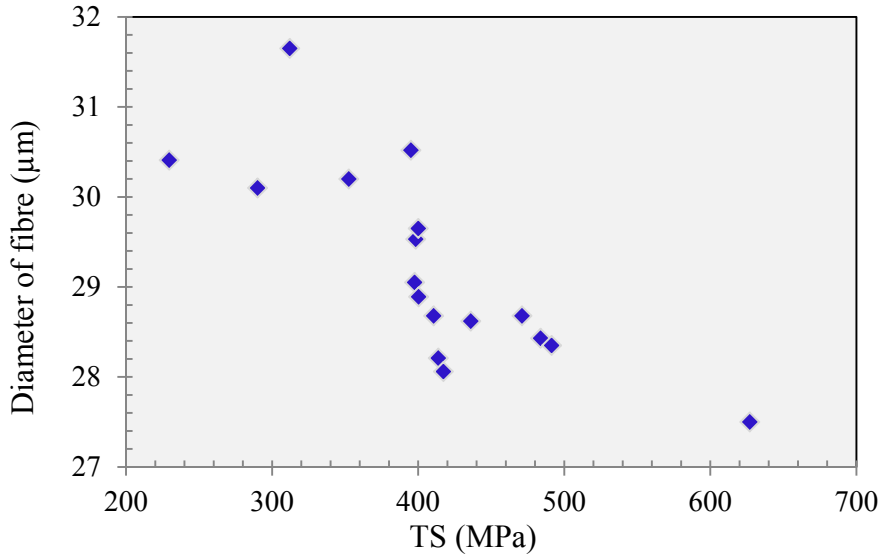

Figure 5.8: The relation between average fibre diameter and average fibre TS.

5.2.6 Optimisation method

Once the models have been developed and checked for adequacy, the optimisation criteria can then be set to find out the optimum dose. In this investigation, the optimisation criteria were implemented to maximise fibre tensile strength (TS) and Young's Modulus (YM). Using these criteria, the goal was to reach the maximum TS and YM at minimum NaOH concentration, soaking time and temperature, as explained in Table 5.7. Table 5.8 summarises the optimal solution obtained by Design-Expert. It is obvious that the graphical optimisation allows for a visual selection of the optimum conditions according to certain criteria. The yellow/shaded area on the overlay plot in Figure 5.9 is the region that meets the proposed criteria.

Table 5.7: Optimisation criteria used for treatment conditions

Criterion	Limits		Importance	Goal
	Lower	Upper		
Concentration of NaOH (%)	5	10	5	minimise
Time (min)	10	180	5	minimise
Temperature (°C)	20	90	5	minimise
TS (MPa)	290	627	5	maximise
YM (GPa)	24.1	36.2	5	maximise

Table 5.8: Optimal solution as obtained by Design-Expert

Number	NaOH concentration (wt. %)	Time (min)	Temperature (°C)	TS (MPa)	YM (GPa)	Desirability
1	5.0	10.00	29.09	610.81	34.72	0.94
5	5.0	10.42	23.35	593.07	34.28	0.94
6	5.0	10.56	26.09	601.06	34.48	0.94
7	5.0	10.39	28.39	607.88	34.66	0.94
8	5.0	10.00	30.59	614.51	34.82	0.94
9	5.0	10.67	26.95	603.20	34.54	0.94
15	5.0	12.77	20.00	575.24	33.90	0.93
16	5.4	10.06	22.33	577.03	34.29	0.92
17	5.0	16.67	30.98	596.83	34.58	0.92

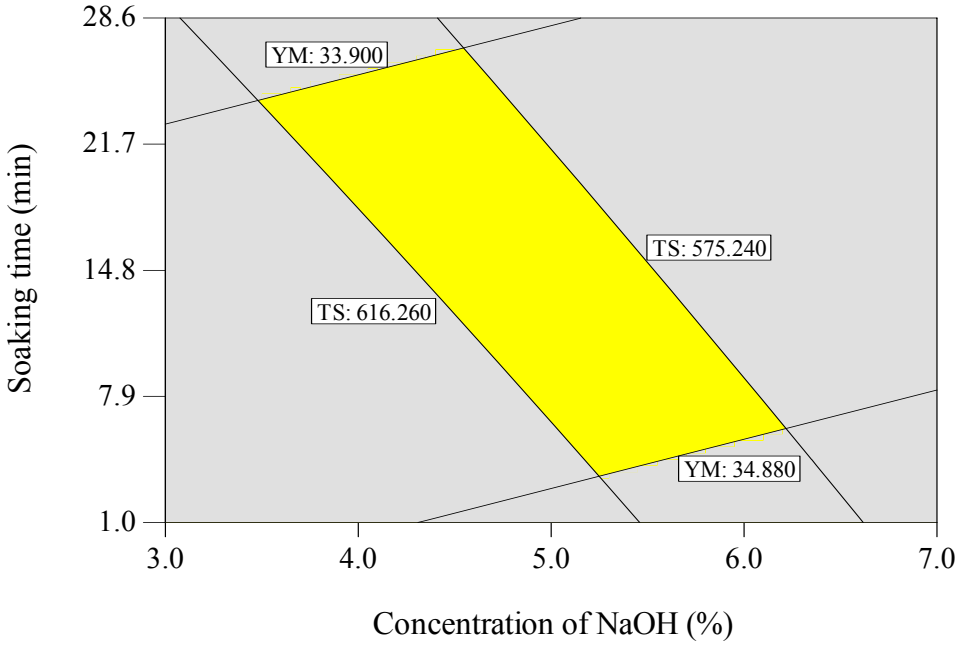

Figure 5.9: Overlay plot showing the region of optimal treatment condition.

5.2.7 Validation of the developed models

Figure 5.10 (a) and (b) shows the relationship between the actual and predicted values of TS and YM respectively. These figures indicate that the developed models are adequate because the residuals in the prediction of each response are minimal, since the residuals tend to be close to the diagonal line. In addition, to validate the developed model, two confirmation experiments were

carried out with conditions chosen randomly from the optimisation results. Table 5.9 summarises the experimental conditions, the average of actual experimental values, the predicted value and the percentage error. It is clear that all the values of the percentage error for tensile strength and Young's Modulus are in reasonable agreement.

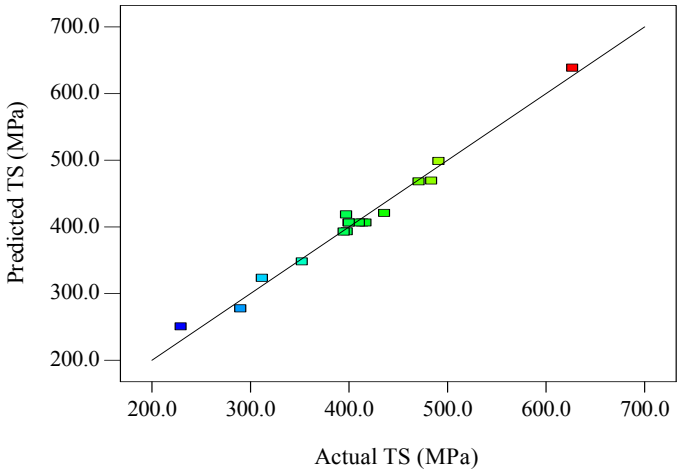

(a)

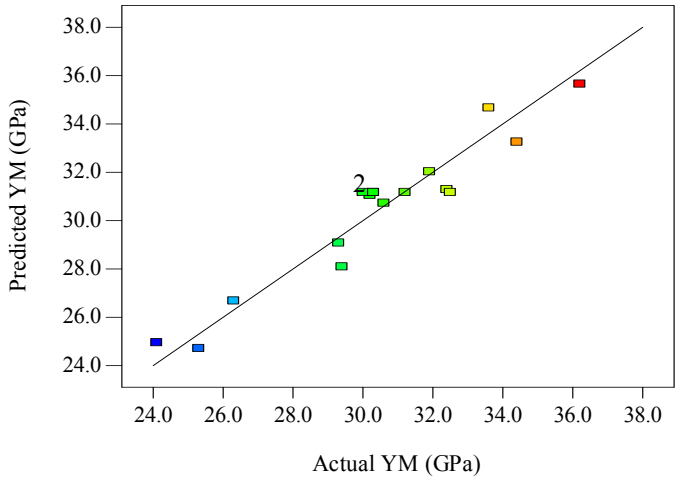

(b)

Figure 5.10: Scatter diagram of (a) single fibre tensile strength (TS) and (b) Young's Modulus (YM).

Table 5.9: Validation test results

Concentration (wt. %)	Time (min)	Temperature (°C)		TS (MPa)	YM (GPa)
5	16.67	30.98	Actual	610.81	34.72
			Predicted	596.83	34.58
			Error %	2.22	0.41
5	12.77	20.00	Actual	627.41	35.66
			Predicted	575.24	33.90
			Error %	8.32	4.91

5.2.8 Surface Morphology by Scanning Electron Microscopy

Scanning electron microscopy (SEM) provides an excellent technique for studying the surface morphology of untreated and treated plant fibres [193]. Significant changes in flax fibre surface morphology, particularly in terms of their level of smoothness and roughness, were observed after alkali treatments. These observations can be attributed to the removal of surface impurities, non-cellulosic materials, inorganic substances and waxes, which result in rougher surfaces and better fibre separation. Figure 5.11 (a to d) shows the SEM micrographs of untreated and alkali treated fibres (1, 2 and 9). Clearly, impurities were observed on the surface of the untreated flax fibre, as shown in Figure 5.11 (a). On the other hand, Figure 5.11 (b –d) presents the SEM micrographs of 5, 7.5 and 10% NaOH treated fibres. Cleary from these figures, all of the impurities have been removed from the flax surfaces. Also, it can be seen that although the 10% NaOH treated fibre has a cleaner and bleached surface, it also looks jagged, rougher and more defibrillated, which confirms the observations obtained by Edeerozey et al. [193] and Jähn et al. [113].

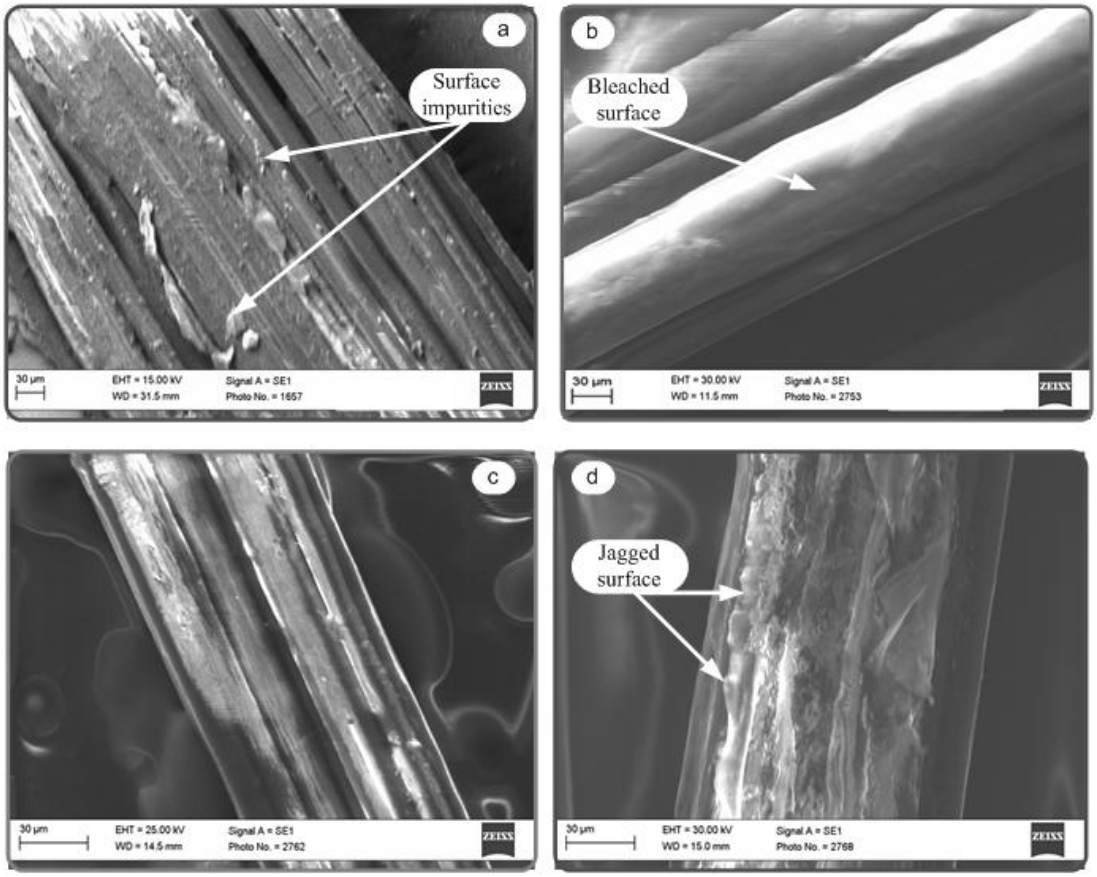

Figure 5.11: SEM photographs of; (a) untreated flax fibre, (b) 5% treated flax fibre (run# 1), (c) 7.5% treated flax fibre (run# 9) and (d) 10% treated flax fibre (run# 2).

5.2.9 X-ray Diffraction (XRD)

Figure 5.12 shows the XRD pattern of the untreated control fibre and alkali treated fibres (1, 2 and 9). As can be seen, the untreated and treated fibres exhibit three main peaks at 2θ-angles of 15, 16.5 and 22.5 that correspond to the $(\bar{1}\ 0\ 1)$, $(\bar{1}\ 1\ 1)$ and $(0\ 0\ 2)$ crystallographic planes of cellulose [8]. For untreated fibre, it appears that the peaks at 2θ of 15 and 16.5 are merged, which could be due to the presence of a large amount of amorphous material such as lignin, hemicelluloses and amorphous cellulose [108,196]. As can be seen in the case of alkali treated fibres, the two peaks at 2θ of 15 and 16.5 are more separate which indicates higher cellulose content. As summarised in Table 5.10, alkali treatment fibres show an increase in their crystallinity index, which suggests an increase in crystalline and amorphous cellulose. This could be due to the removal of non-cellulosic materials such as waxes, lignin and hemicelluloses, as supported by the separation of

$(\bar{1}\ 0\ 1)\ and\ (\bar{1}\ 1\ 1)$ peaks which enabled better packing of cellulose chains [83,97,197].

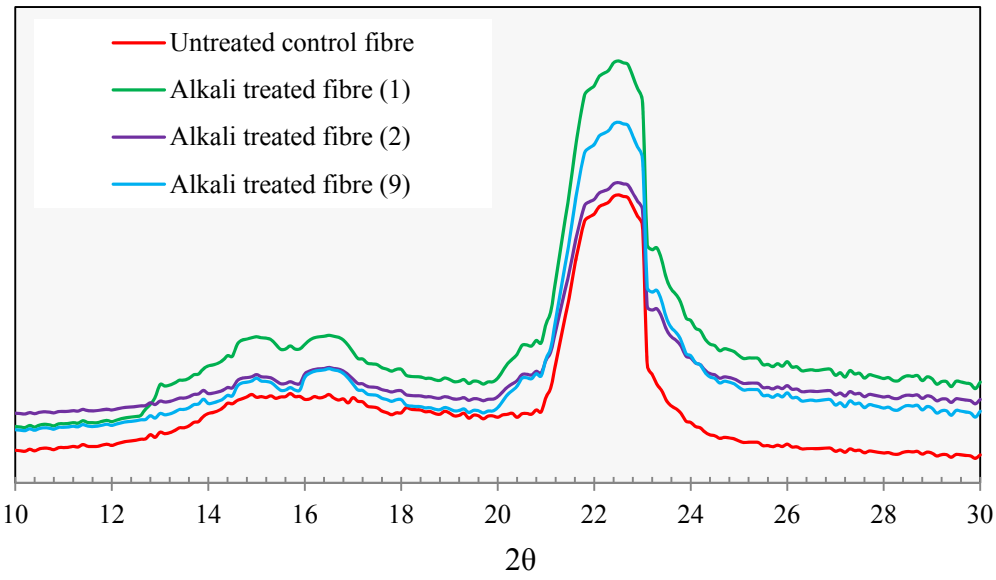

Figure 5.12: XRD pattern of untreated and alkali treated fibres.

Table 5.10: Crystallinity indices, I_{cr} of control untreated and alkali treated flax fibres.

	Untreated fibre	Alkali treated fibre (1)	Alkali treated fibre (2)	Alkali treated fibre (9)
I_{cr} (%)	75.05	84.81	84.35	83.43

5.2.10 Thermal Gravimetric Analyses (TGA/DTA)

The DTA and TGA curves of the untreated control fibre and alkali treated flax fibres (runs # 1, 2 and 9) are shown in Figures 5.13 and 5.14. From the DTA curves an endotherm can be observed for treated/untreated fibres around 60°C and 80°C due to the moisture lost. It can also be seen that there are two exotherms at higher temperatures. The first one has a peak temperature of about 306 - 340°C, and could be caused by the decomposition of cellulose, which leads to the formation of volatile products [8,193]. While the second exotherm for treated/untreated fibres is observed at a peak temperature of about 408 - 432°C, this could be due to the oxidation of volatile and charred products [8,193]. Table 5.11 summarises the peaks, peak onsets, peak finishing temperatures and the nature of the peaks for both treated and untreated flax fibres.

The mass loss of the untreated control fibre and the alkali treated flax fibres are presented in Figure 5.13 The mass loss is shown to be slightly higher for treated flax fibres at the initial stages (≈ 20-370°C) of thermal degradation and slightly lower at the later stages (above 370°C) of thermal degradation when compared to the untreated flax fibre. Furthermore, the residual char left at 600°C increased from 1.4% (untreated) to 4%, 3%, and 2.5 % in the cases of all of the alkali treated fibres (run# 1, 9, 2 respectively). This may be due to the formation of a stable lingo-cellulose complex which helps to shield the fibres from mass loss at higher temperatures, and this was reflected in the increased amount of residual char [8,193]. In light of these results, it is clear that after the alkali treatment, the rate of decomposition of flax fibres decreased. This indicates that alkali treatment leads to an enhancement in the thermal stability of flax fibres, which agrees with the results obtained by Islam [8].

In this investigation it was shown that a 5% NaOH solution for 10 min at 55ºC could be used to bleach, clean and separate flax fibres from their fibre bundles without reducing the fibre tensile strength and Young's modulus. Therefore, this treatment was chosen to fabricate all of the cement composites.

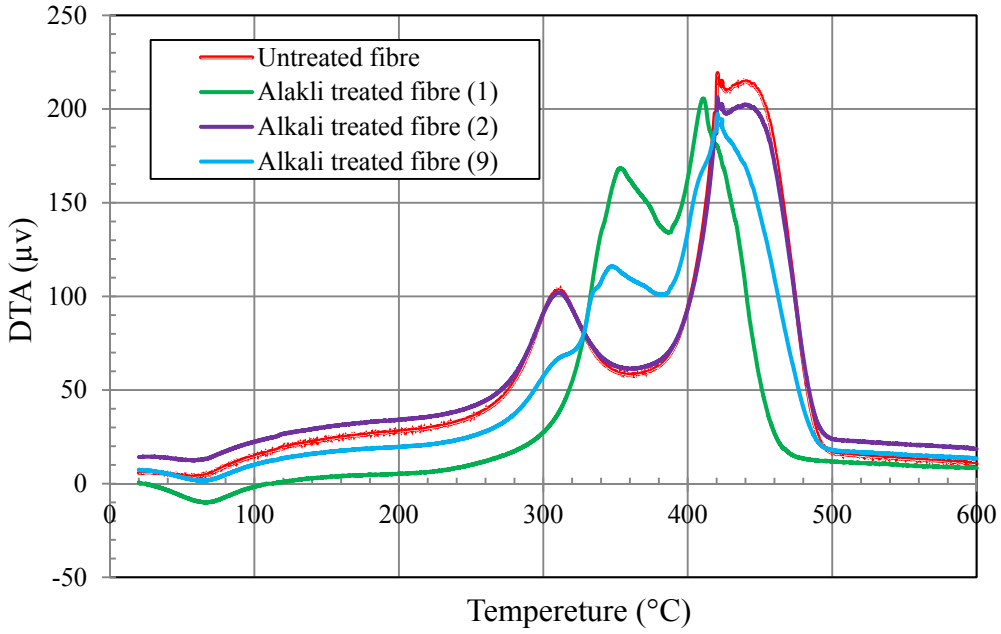

Figure 5.13: DTA curves of alkali treated and untreated flax fibres.

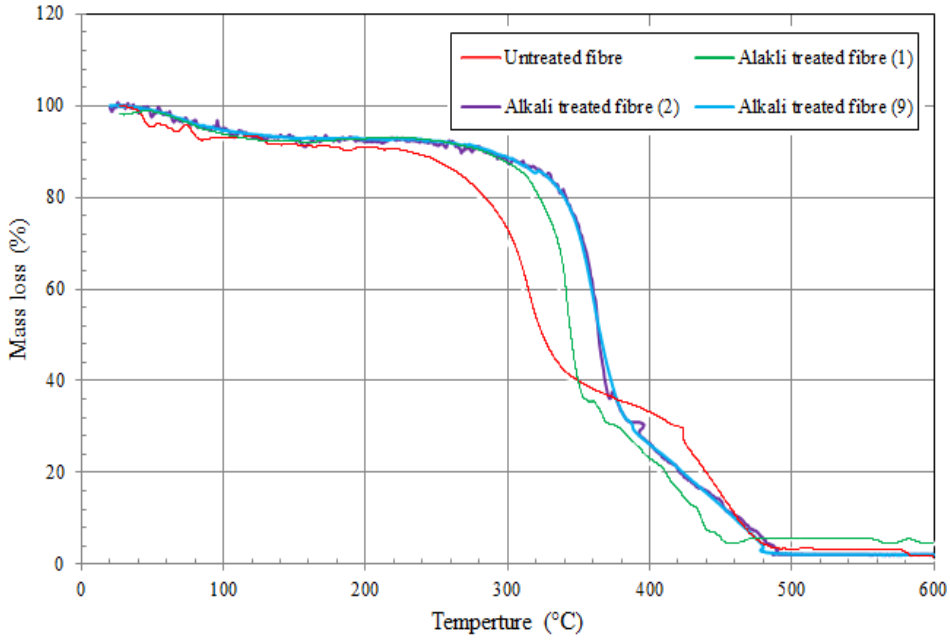

Figure 5.14: TGA curves of alkali treated and untreated flax fibres.

Table 5.11: The peaks, peak onsets, peak finishing temperatures and nature of peaks for the treated and untreated fibres obtained from the DTA thermograms

Type of fibre	Peak onset temperature, ˚C	Peak temperature, ˚C	Peak finishing temperature, ˚C	Nature of peak
Untreated fibre	38	54	78	Endo
	265	306	340	Exo
	380	436	492	Exo
Treated fibre (1)	29	60	100	Endo
	300	358	380	Exo
	383	408	472	Exo
Treated fibre (2)	38	54	65	Endo
	243	305	353	Exo
	388	420	489	Exo
Treated fibre (9)	37	58	99	Endo
	305	353	377	Exo
	378	420	490	Exo

5.3 Effect of Alkaline Treatment on Thermal and Mechanical Properties of Cement Composites

In order to study the effect of the alkali treatment of flax fibres on cement composites, thermal strain measurements and flexural strength were carried out on specimens of plain mortar (unreinforced) and specimens with treated and untreated flax fibres.

5.3.1 Thermal Expansion

Cement reinforced composites are heterogeneous composite materials with multiple components that have different thermal expansion properties. Internal stresses are increased if the matrix is speedily heated or cooled, which causes cracking at the micro- or macro-scale. If the thermal strain of hardened cement pastes is adjusted, the thermal stress caused by the mismatch of the thermal expansion properties of the components can be mitigated [176].

Figure 5.15 shows the thermal strains as a function of the temperature of cement composites. It can be seen that the trend of the thermal strain for each specimen with fibres is the same as that of the plain mortar specimen. Furthermore, the thermal strain steadily increases with the temperature up to 600°C, and then it steeply increases with the temperature up to 830°C. After this it slightly increases with the temperature up to 1000°C.

Up to 200°C the thermal expansion of unreinforced mortar (i.e. plain mortar) is slightly higher than that of fibre reinforced specimens. Beyond 200°C almost all specimens have similar thermal strains. As reported by several authors [198,199,200], at about 573°C siliceous aggregates containing quartz, such as natural sand, may cause distress in the mortar matrix since the allotropic transformation of quartz from the α to β form takes place with a sudden expansion (cracking in siliceous aggregate) of the cement matrix. This transformation causes a significant volume expansion in all specimens at about 600°C.

Also, it is clear from Figure 5.15 that the thermal strain of treated composites is slightly lower than that of untreated composites (up to 200°C). As reported by Islam and Sedan et al. [8,27] and supported in the next section, fibres have excellent

resistance to fracture and tension. Therefore, the incorporation of fibres in the cement matrix can increase the ability of this material to resist the volume changes. Under the same conditions of volume content, length and type of fibre, one factor which results in different restrain effects of expansion is the fibre/matrix interfacial [201]. Under the same conditions of fibre content, the larger the size of the fibres, the less the number of fibres contained in the unit volume of matrix and the less the contact area of fibre/matrix, which results in less restraint of expansion. In this study, flax fibres are subjected to an alkaline treatment which removes lignin, pectin, waxy substances, and natural oils covering the external surface of the fibre cell wall. This reveals the fibrils, shrinks the dimensions, increases the contact area and gives a rough surface topography to the fibre [83,85]. These physical and chemical changes result in better mechanical interlocking, which lowers the thermal strain when compared to an untreated composite. Hence, the elementary fibres in untreated fibres still glue together (Figure 5.16) and the fibre bundles consist of cellulose, pectin, hemicelluloses, and lignin.

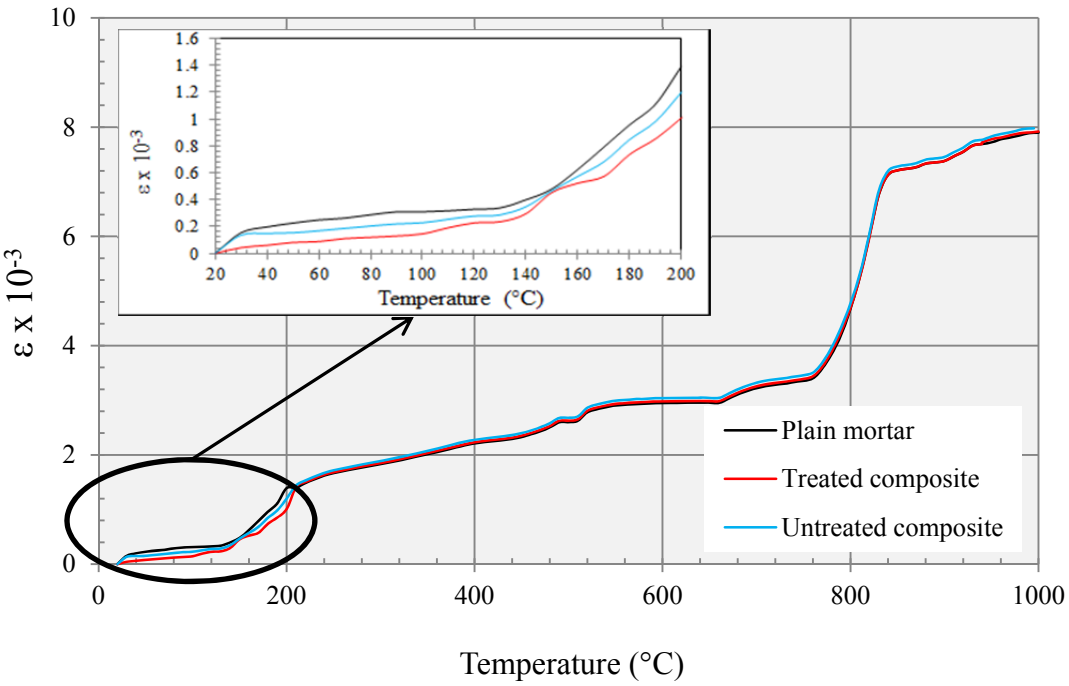

Figure 5.15: Thermal strain (ε) of plain mortar and treated/untreated flax fibre composites.

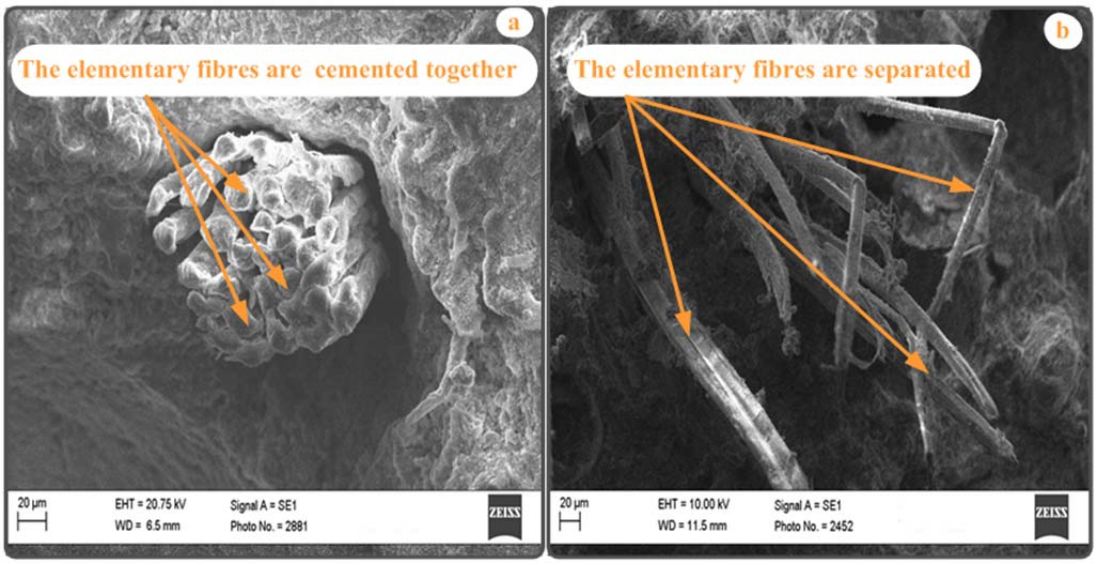

Figure 5.16: SEM micrographs showing (a) untreated flax fibre composites and (b) treated flax fibre composite.

5.3.2 Mechanical behaviour analysis of flax fibre cement composites

Figure 5.17 illustrates the load deflection curves for plain mortar (i.e. unreinforced), untreated and treated flax fibre composites. Here it can be seen that there are two different types of load deflection curves. The first one shows a linear brittle behaviour for plain mortar, while the second curve demonstrates a typical composite behaviour for both treated/untreated flax fibre composites. These curves can be divided into three regions, with each zone separated by a characteristic force value (i.e. F_{st} and F_{max}). The first crack strength (F_{st}) can be considered to be the initial pull-out debonding force and the peak strength (F_{max}) can be regarded as the maximum failure force. Region I shows a typical linear deflection for plain mortar as well as for reinforced composites. In this region, the material exhibits an elastic behaviour and it appears that the matrix is bearing the main applied load. Region II records the onset of the first macroscopic crack which can be easily observed on the specimen in this region, as shown in Figure 5.18. Furthermore, in this region we can also observe that some of the fibres are debonded on the crack's sides and that some of the fibres link the two sides of the crack. This behaviour can be explained as follows: during the bending test of randomly short fibre composites, as bending is increased the direction of the fibres becomes more and more perpendicular to the direction of the load. This leads to a pull-out phenomenon (Figure 5.19) which perturbs the load transfer along the fibre/matrix interface and controls crack

propagation [27]. Beyond the peak strength (Region III), the mechanical behaviour of the plain mortar is completely different than that of both treated and untreated flax fibre composites. The plain mortar exhibits brittle and sudden failure, while both flax fibre composites demonstrate a continuous fall of load and no sudden failures are detected. The behaviour of the flax fibre composites highlights the most important role of the debonding process on the damage of the cement matrix. Figure 5.20 summarises the different stages explained above. Figure 5.21 shows a micrograph of the fracture surfaces of the treated flax fibre composite. There it can be seen that the fibres are entirely covered with nodules that are identified as calcium rich by an EDX analysis. This calcium coating, that is sometimes irregularly distributed, at the fibre/matrix interface can explain the behaviour of the material.

As it is clear from Figure 5.17, the flexural strength values for the untreated and treated composites were higher than the plain mortar's value, which is in agreement with the results obtained by Sedan et al.[27] and Kriker et al.[134]. Furthermore, the flexural strength of treated composites was 17% higher than the flexural strength of untreated composites. These differences in flexural strength could be attributed to the bond considerations. Alkali treatment tends to reveal the fibrils (Figure 5.16), increase the contact area and improve the fibre surface adhesive characteristics by removing natural and artificial impurities, thus producing a rough surface topography. These changes in morphology and in the chemical composition of the fibres result in improvements to the interfacial bonding by giving rise to additional sites of mechanical interlocking, which leads to an improvement of the mechanical properties and toughness.

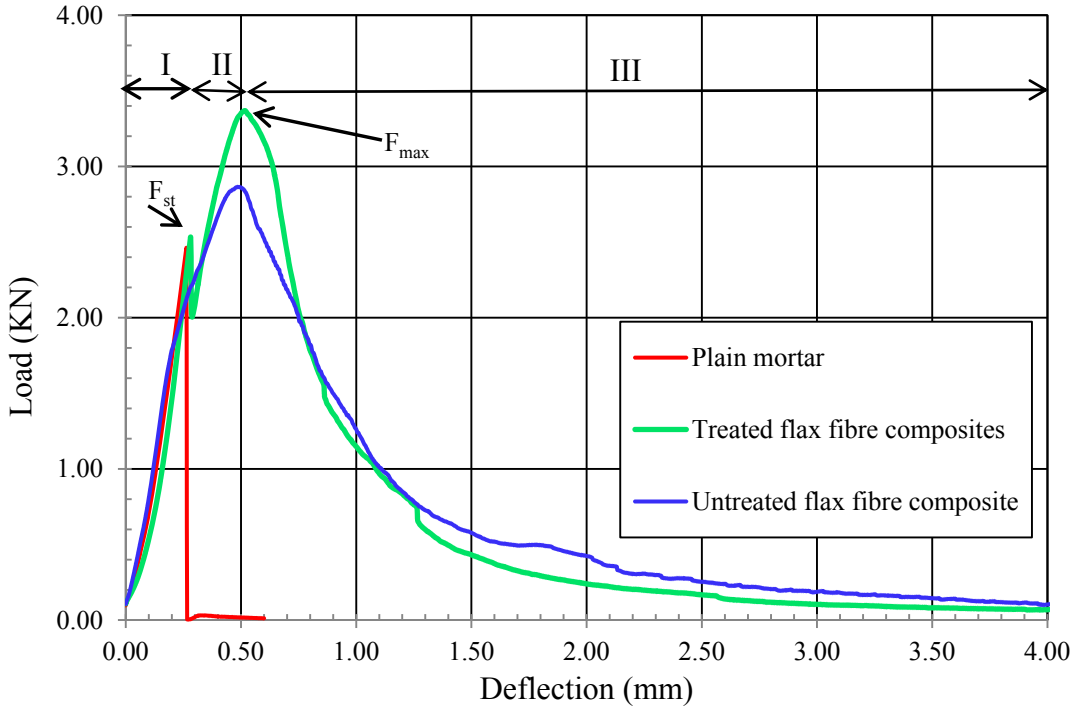

Figure 5.17: Flexural strength–deflection curves for plain mortar, treated and untreated flax fibre composites (n = 3).

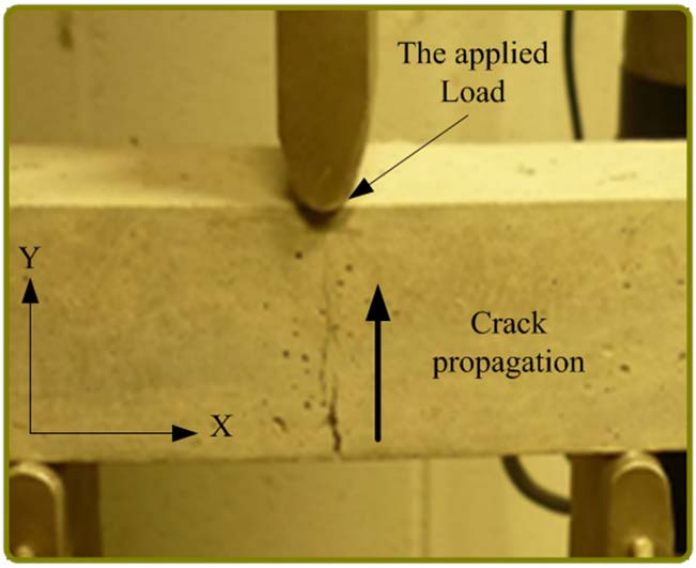

Figure 5.18: Propagation of the crack in the composite during the three point bending test.

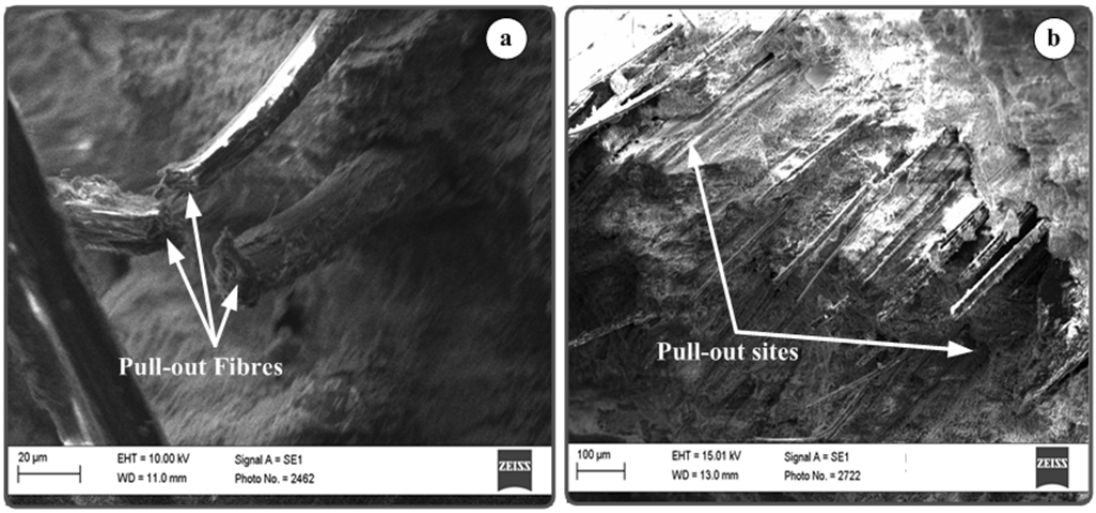

Figure 5.19: SEM micrographs of the composite after three point bending test showing (a) pull-out fibres and (b) pull-out sites.

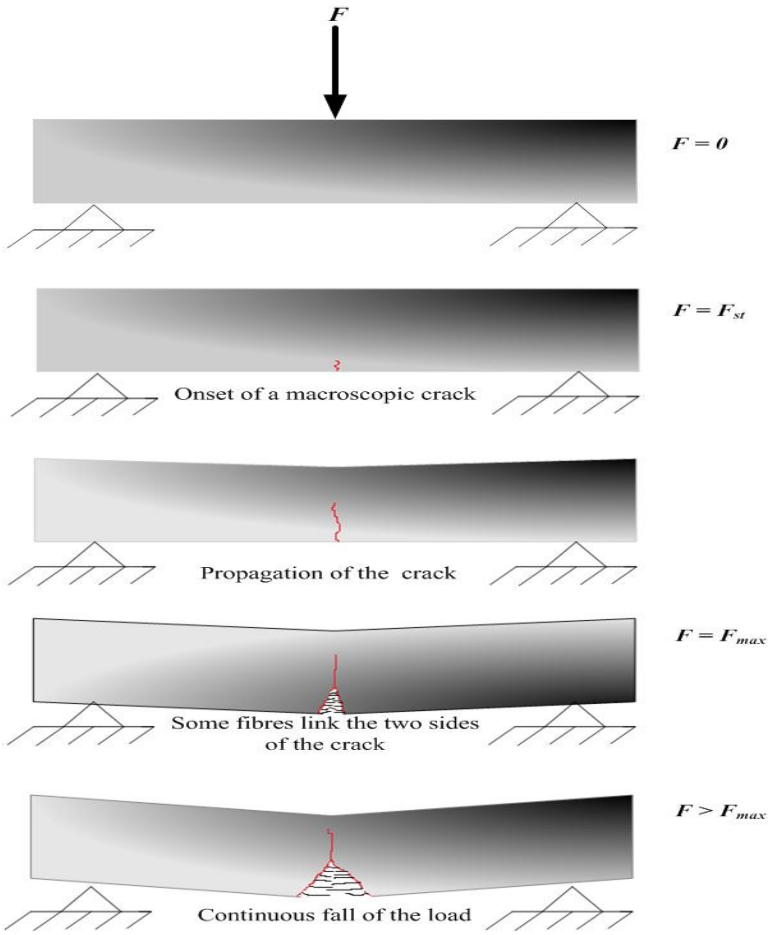

Figure 5.20: Chronology of loading and associated mechanical behaviour of the composite.

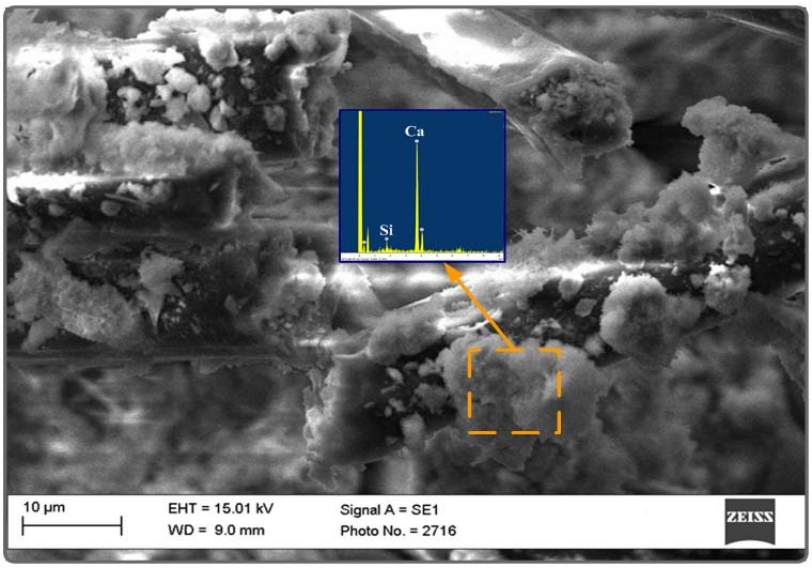

Figure 5.21: SEM micrograph of fracture surface of flax cement composite after three point bending test.

5.4 Effect of Fibre parameters on the Mechanical Properties of Cement Composites

For this study, the experiment was designed based on two variables central composite design. Trial batches of flax fibre cement composites were developed by varying one of the process variables in order to determine the working range of each variable. Increasing fibres by more than 1.5% in volume faction and 50 mm in length creates disruption. The low specific gravity of the flax fibres causes the fibres to float on top of the slurry and creates a lack of homogenous mixture in the composite because the top surface of the composite fills with accumulated fibres. Therefore, making specimens with an excess of 1.5% in volume fraction and more than 50 mm in length was stopped.

Table 5.12 shows the fibre input parameters and experimental design levels that were used for this material. The experiment was carried out according to the design matrix shown in Table 5.13 and in a random order in order to avoid any systematic error. Eight mathematical models were successfully developed to predict the following responses: porosity (P), flexural strength (F_{flex}), fracture energy (G_f), impact strength (F_{imp}), compressive strength (F_{com}) and the toughness indices I_5, I_{10} and I_{20}. The procedures described earlier in Chapter 3 were then followed to determine and record these responses. The averages of at least three measurements for each response are presented in Table 5.14.

Table 5.12: Process variables and experimental design levels used

Variables	Code	Unit	Limits coded/actual		
			-1	0	1
Fibre volume fraction	V	%	0.5	1	1.5
Fibre length	L	mm	10	30	50

Table 5.13: Design matrix in actual values

Exp. No.	Run order	V	L	Exp. No.	Run order	V	L
1	9	0.5	10	10	13	1	30
2	4	1.5	10	11	7	1	30
3	12	0.5	50	12	2	1	30
4	6	1.5	50	13	11	1	30
5	5	0.5	30	-	-	-	-
6	8	1.5	30	-	-	-	-
7	1	1	10	-	-	-	-
8	10	1	50	-	-	-	-
9	3	1	30	-	-	-	-

Table 5.14: Experimental data and results for treated flax fibre cement composites

Run	**P *(%)***	**F_{flex} (Mpa)**	**F_{com} (Mpa)**	**F_{imp} (J/m2)**	**G_f (N.mm)**	**I_5**	**I_{10}**	**I_{20}**
Plain mortar	9.5	5.31	21.98	255	307	1	1	1
1	9.8	5.63	22.41	380	3164	4.46	6.07	7.19
2	10.8	7.10	18.63	499	3996	5.15	7.95	9.90
3	10.5	5.91	22.46	493	3425	5.26	6.84	7.74
4	11.5	7.90	14.58	996	6239	5.47	8.21	12.12
5	10.2	5.40	22.76	473	3718	4.64	6.81	8.02
6	11.0	7.42	18.22	780	4009	4.96	7.87	10.75
7	10.2	6.68	21.92	447	3547	4.47	6.08	6.81
8	10.9	7.00	18.36	760	5155	4.93	6.09	7.62
9	10.6	7.01	21.73	620	3665	4.89	6.42	7.42
10	10.6	7.12	21.73	615	3671	4.99	6.55	7.58
11	10.7	6.98	21.46	622	3663	4.92	6.456	7.47
12	10.6	7.05	21.87	617	3670	4.79	6.28	7.27
13	10.7	6.95	21.33	624	3667	4.77	6.266	7.25

5.4.1 Development of Mathematical Models

As a result of analysing the measured responses by the design expert software, the fit summary output indicated that the linear model was statistically significant for the compressive strength, porosity and toughness index I_5; therefore, it was used for further analysis. For the other responses, the quadratic models are statistically recommended for further analysis as they have the maximum predicted and adjusted R^2 [191]. The test for significance of the regression models, the test for significance on individual model coefficients and the lack of fit test were done using the same statistical package for all responses. By selecting the step-wise regression method, the insignificant model terms can be automatically eliminated. The resulting ANOVA tables (Tables 5.15 to 5.22) for the reduced quadratic models outline the analysis of variance of each response and illustrate the significant model terms. The same tables, also, show the other adequacy measures' R^2, adjusted R^2 and predicted R^2. As it can be seen from Tables 5.15 through 5.22 most of the adequacy measures are close to 1, which is in reasonable agreement and indicates adequate models [187,191]. The adequate precision compares the range of the predicted value at the design points to the average prediction error. In all cases the values of adequate precision are dramatically greater than 4, which indicate adequate model [191].

For the flexural strength model, the Analysis of Variance indicates that the main effects are; of fibre volume fraction (V), fibre length (L), and the second order effect of volume fraction (V^2). The same trend was observed with the toughness index I_{20} model. For the compressive strength model, the ANOVA analysis indicates that there is a linear relationship between the main effects of the two parameters. Also, in the case of the toughness index I_5 and the porosity models, the ANOVA analysis shows a linear relationship between the main effects of the two parameters. In the case of the impact strength model, the main effects of fibre volume fraction (V), fibre length (L), the second order effect of fibre length (L^2) and the two level interactions of volume fraction and fibre length (VL) are significant model terms. Finally, in the case of the fracture energy and toughness index I_{20} models, the ANOVA analysis shows that the main effect of fibre volume fraction (V), fibre length (L), the second order effect of fibre length (V^2) and the two level interactions

of volume and fibre length (VL) are significant model terms. The final empirical models in terms of the actual factors are presented in Eqs. 5.3 to 5.10:

$$F_{flex} = 1.991+7.02V+0.015L - 2.57V^2 \quad (5.3)$$

$$F_{com} = 25.56-3.72V-0.03L \quad (5.4)$$

$$F_{imp} = 311.24-21.67V-1.95L+9.6VL-0.064L^2 \quad (5.5)$$

$$G_f = 1699.62-3364.07V-4.8L+40.55VL-1471.61\ V^2 \quad (5.6)$$

$$I_5 = 4.09-0.41V-0.013L \quad (5.7)$$

$$I_{10} = 8.55-6.44V+0.01L+3.94V^2 \quad (5.8)$$

$$I_{20} = 12.19-13.5\ V-0.012L+0.042VL+7.76\ V^2 \quad (5.9)$$

$$P = 9.16 + 0.93V+ 0.018L \quad (5.10)$$

where:

F_{flex} is flexural strength (MPa)

F_{com} is compressive strength (MPa)

F_{imp} is impact strength (J/m^2)

G_f is fracture energy (N.mm)

I_5, I_{10} and I_{20} are toughness indices

P is porosity (%)

V is fibre volume fraction (%)

L is fibre length (mm)

Table 5.15: ANOVA analysis for the flexural strength model

Source	Sum of Squares	dF	Mean Square	F Value	Prob > F	
Model	8.29	3	2.76	124.07	< 0.0001	Significant
V	6.45	1	6.45	289.58	< 0.0001	
L	0.51	1	0.51	22.92	0.001	
V^2	1.33	1	1.33	59.7	< 0.0001	
Residual	0.2	9	0.022			
Lack of Fit	0.072	5	0.014	0.44	0.801	Not significant
Pure Error	0.13	4	0.032			
Cor Total	8.49	12				
$R^2 = 0.976$			Pred $R^2 = 0.950$			
Adj $R^2 = 0.968$			Adeq Precision = 32.096			

Table 5.16: ANOVA analysis for the compressive strength model

Source	Sum of Squares	dF	Mean Square	F Value	Prob > F	
Model	22.92	2	11.46	24.72	0.0001	Significant
V	20.76	1	20.76	44.78	< 0.0001	
L	2.16	1	2.16	4.66	0.0562	
Residual	4.64	10	0.46			
Lack of Fit	3.76	6	0.63	2.88	0.1625	Not significant
Pure Error	0.87	4	0.22			
Cor Total	27.55	12				
$R^2 = 0.832$			Pred $R^2 = 0.699$			
Adj $R^2 = 0.798$			Adeq Precision = 15.04			

Table 5.17: ANOVA analysis for the impact strength model

Source	Sum of Squares	dF	Mean Square	F Value	Prob > F	
Model	0.003	4	0.007	1463.85	< 0.0001	Significant
V	0.001	1	0.001	2508.79	< 0.0001	
L	0.001	1	0.001	2497.5	< 0.0001	
VL	43056.25	1	43056.25	821.91	< 0.0001	
L^2	1424.77	1	1424.77	27.2	0.0008	
Residual	419.08	8	52.39			
Lack of Fit	365.88	4	91.47	6.88	0.044	Significant
Pure Error	53.2	4	13.3			
Cor Total	0.003	12				
$R^2 = 0.998$			Pred $R^2 = 0.994$			
Adj $R^2 = 0.998$			Adeq Precision = 131.73			

Table 5.18: ANOVA analysis for the fraction energy model

Source	Sum of Squares	dF	Mean Square	F Value	Prob > F	
Model	0.008	4	0.002	58584.23	< 0.0001	Significant
V	0.004	1	0.004	0.001	< 0.0001	
L	0.003	1	0.003	87832.76	< 0.0001	
VL	0.006	1	0.006	18833.67	< 0.0001	
V^2	0.004	1	0.004	12521.89	< 0.0001	
Residual	279.38	8	34.92			
Lack of Fit	234.58	4	58.65	5.24	0.068	Not significant
Pure Error	44.8	4	11.2			
Cor Total	0.008	12				
$R^2 = 0.995$			Pred $R^2 = 0.983$			
Adj $R^2 = 0.991$			Adeq Precision = 836.9			

Table 5.19: ANOVA analysis for the toughness index I_5 model

Source	Sum of Squares	dF	Mean Square	F Value	Prob > F	
Model	0.67	2	0.34	9.84	0.0043	Significant
V	0.25	1	0.25	7.27	0.0224	
L	0.42	1	0.42	12.4	0.0055	
Residual	0.34	10	0.034			
Lack of Fit	0.31	6	0.051	6.04	0.0517	Not significant
Pure Error	0.034	4	0.008			
Cor Total	1.01	12				
$R^2 = 0.663$			Pred $R^2 = 0.595$			
Adj $R^2 = 0.212$			Adeq Precision = 10.569			

Table 5.20: ANOVA analysis for the toughness index I_{10} model

Source	Sum of Squares	dF	Mean Square	F Value	Prob > F	
Model	6.4	3	2.13	42.39	< 0.0001	Significant
V	3.09	1	3.09	61.4	< 0.0001	
L	0. 18	1	0.18	3.58	0.091	
V^2	3.13	1	3.13	62.19	< 0.0001	
Residual	0.45	9	0.05			
Lack of Fit	0.39	5	0.079	5.41	0.0635	Not significant
Pure Error	0.058	4	0.0157			
Cor Total	6.86	12				
$R^2 = 0.933$			Pred $R^2 = 0.834$			
Adj $R^2 = 0.911$			Adeq Precision = 16.462			

Table 5.21: ANOVA analysis for the toughness index I_{20} model

Source	Sum of Squares	dF	Mean Square	F Value	Prob > F	
Model	31.07	4	7.77	127.63	< 0.0001	Significant
V	16.06	1	16.06	263.9	< 0.0001	
L	2.15	1	2.15	35.39	0.0003	
VL	0.7	1	0.7	11.49	0.0095	
V^2	12.15	1	12.15	199.74	< 0.0001	
Residual	0.49	8	0.06			
Lack of Fit	0.41	4	0.1	5.23	0.069	Not significant
Pure Error	0.078	4	0.02			
Cor Total	31.55	12				
$R^2 = 0.984$			Pred $R^2 = 0.915$			
Adj $R^2 = 0.976$			Adeq Precision = 33.936			

Table 5.22: ANOVA analysis for the porosity model

Source	Sum of Squares	dF	Mean Square	F Value	Prob > F	
Model	2.04	2	1.02	246.52	< 0.0001	Significant
V	1.31	1	1.31	315.54	< 0.0001	
L	0.74	1	0.74	177.49	< 0.0001	
Residual	0.041	10	0.0046			
Lack of Fit	0.029	6	0.0049	1.63	0.3303	Not significant
Pure Error	0.012	4	0.003			
Cor Total	2.08	12				
$R^2 = 0.980$			Pred $R^2 = 0.965$			
Adj $R^2 = 0.976$			Adeq Precision = 52.826			

5.4.2 Effect of process parameters on the properties of cement composites

5.4.2.1 Flexure strength

The results indicate that both the volume fraction and fibre length have a positive effect on flexure strength as shown in Figure 5.22 and Figure 5.23. However, the effect of volume fraction on flexure strength is much more significant. As presented in Table 5.14, at a fibre length of 50 mm (aspect ratio of 1428), an increase in the fibre volume fraction from 0 to 1.5% has resulted in an increase in flexure strength of 48%. For fibre lengths of 30 and 10 mm (aspect ratio 856.5 and 285), the increases were 39% and 34% respectively. This increase in flexure strength agrees with the results obtained by Kriker et al.[134], Khorami et al. [202] and Sedan et al. [27].

It can also be observed that for a constant fibre length, there is an increase in the flexural strength as the percentage of fibres is increased. The results show that there is an increase in flexural strength varying from 6% to 48% with the addition of fibres to the cement matrix. Furthermore, it can also be observed from Table 5.14 that the maximum increase in flexural strength taken as an average varied from 6% to 11%, 25% to 28% and 34% to 48% for mixes having 0.5%, 1% and 1.5% volume fraction of fibres, respectively. The maximum increase of 48% was obtained for a matrix with 50 mm of fibre length at a volume fraction of 1.5%.

The reason for this performance can be attributed to the high tensile strength and the high aspect ratio (i.e. length/diameter) of the flax fibres. The high aspect ratio of the fibres leads to an increase in the lateral surface area of the fibres coming into contact with the cement, hence bonding between the cement and the fibres increases. In addition, the high aspect ratio results in increased fibre availability and is thus more efficient in delaying the growth of micro-cracks and improving the ultimate flexural strength of the cement. Also, the high tensile strength of the fibres leads to a change in the rupture mechanism from breaking fibres to pulling up the fibres from the matrix (see Figure 5.19). This means that the bonding strength between the cement and the fibres controls the rupture mechanism. As observed in this investigation, the ultimate load increases with the increase in the aspect ratio of

the fibres in the cement matrix, hence the longer fibres are offering more resistance to the pull out of fibres in the cement matrix due to their better bond characteristics because of their longer length.

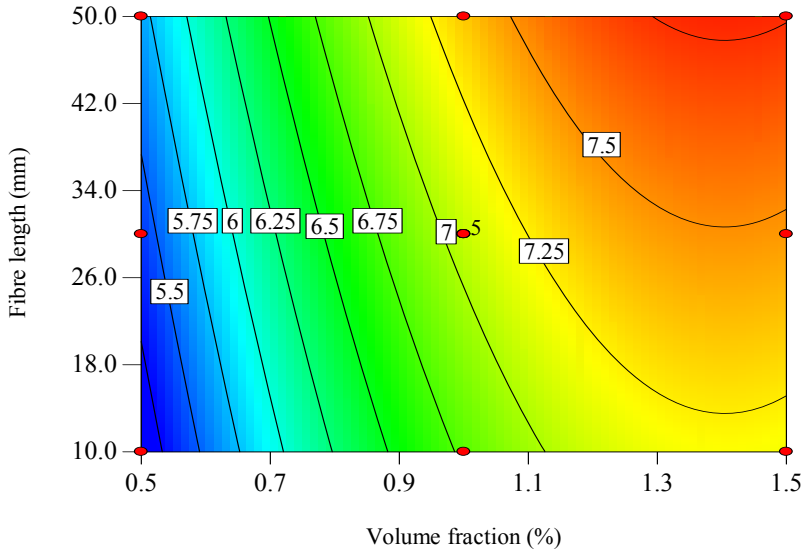

Figure 5.22: Contour plot showing the effect of fibre parameters on flexural strength.

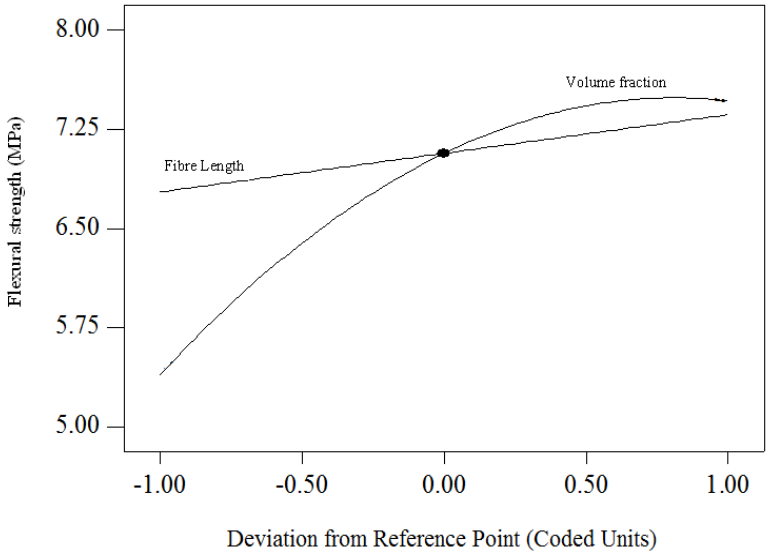

Figure 5.23: Perturbation plot showing the effect of all factors on the flexure strength.

5.4.2.2 Impact strength

The fibres play a very important role in the impact resistance of the composite because they interact with the crack formation in the matrix and act as a

stress transferring medium. These results demonstrate that all of the input parameters have a positive significant effect on the impact strength of the composites as presented in Figure 5.24. It is obvious from the perturbation plot shown in Figure 5.25 and the results listed in Table 5.14 that the incorporation of flax fibres in cement matrix would result in an increase of impact strength by 49-290%, depending on the fibre's length and content. It can be observed from the Table 5.14 and Figure 5.25, that given a constant fibre length, the best impact performance of the flax fibre cement composites is provided by composites having a 1.5% volume fraction of fibres, followed by composites containing a 1% volume fraction and then those with a 0.5% volume fraction. Similarly, for a constant volume fraction of fibres, the best impact performance is provided by composites containing a fibre length of 50 mm, followed by composites with a fibre length of 30 mm and a fibre length of 10 mm. It can be concluded from the above discussion, that as the length of the fibre is decreased, there is a corresponding decrease in the performance of fibrous mortar against impact loading. It seems that short fibres are less effective in arresting the cracks caused by impact loading. This could be due to the fact that because of their small length, they offer less bond resistance and are more easily pulled out of the matrix. Relatively longer fibres are more effective in arresting the cracks due to impact loading because of the interlocking of the fibres in the cement matrix and their superior bond resistance, which would be in agreement with earlier findings made by Ramakrishna and Sundararajan [98].

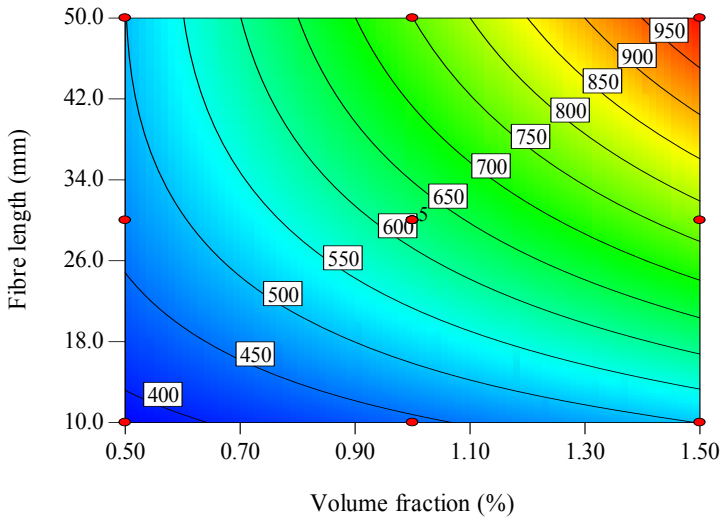

Figure 5.24: Contour plot showing the effect of fibre parameters on impact strength.

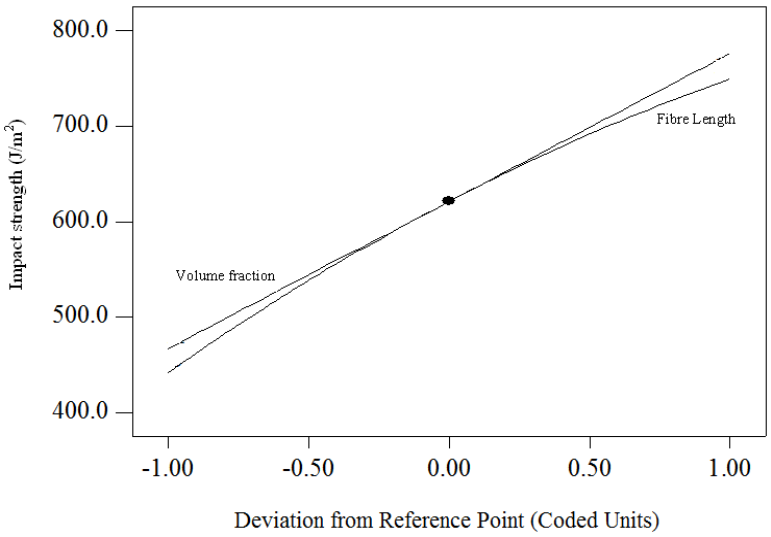

Figure 5.25: Perturbation plot showing the effect of all factors on the impact strength.

5.4.2.3 Compressive strength

In the compression tests, the matrix has greater importance than the fibres so the reinforcement effects are less evident. The test results indicate that both fibre parameters have negative effects on the compressive strength of the composites as shown in Figure 5.26 and Figure 5.27. The higher the fibre content and the length of the fibres, the lower the compressive strength of the cement composites will be. Table 5.14 demonstrates that the compressive strength of the cement composites with fibre volume fraction of 0.5% increases only marginally when compared with that of the plain specimen. The increases in compressive strength were about 2%, 3.5% and 2.1% for flax fibrous composites having fibre length 10, 30, 50 mm (aspect ratio 285, 856.5 and 1428) respectively, which is in agreement with similar results obtained by Dawood and Ramli [203,204]. On the other hand, at a volume fraction of 1.5%, there was a decrease in the compressive strength of 34%, 15% and 16% at fibre lengths of 50, 30, 10 mm respectively, which is in agreement with previously reported results [134].

The incorporation of natural fibres into cement mortar can actually have limited beneficial effects on the compressive strength, but increasing the fibre content would reduce the compressive strength of the composite. This phenomenon may be attributed to the low stiffness and the low specific gravity of these fibres and to the high pore volume induced by the addition of these fibres. Also, it is probably

due to the insufficient dispersion of the fibres in the concrete during mixing. In general, natural fibres are difficult to completely disperse in concrete prepared with a conventional mixing procedure. These fibres tend to form a so called multifilament structure in the concrete during mixing and that increases the local porosity [3,203,204]. It should also be noted that the volume of voids created by the addition of flax fibres is strongly linked to their characteristics (length, and content). The higher the amount of fibres and the longer their lengths, the higher the porosity induced (see section 5.4.3.6) and therefore, the lower the compressive strength of the composites will be.

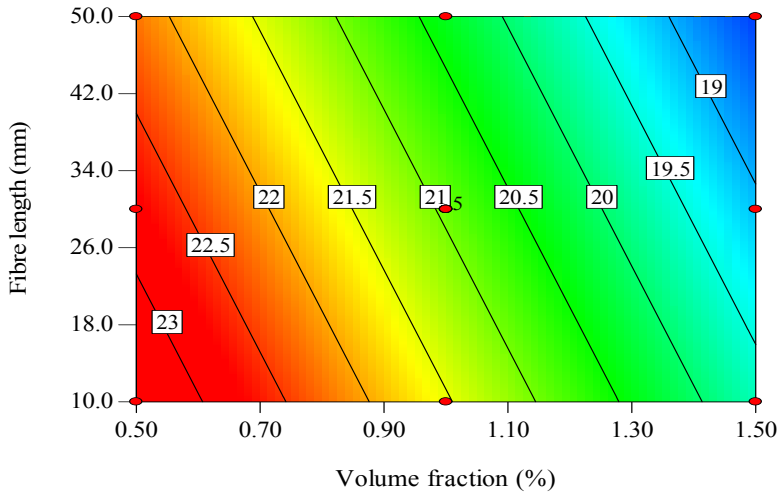

Figure 5.26: Contour plot showing the effect of fibre parameters on compressive strength.

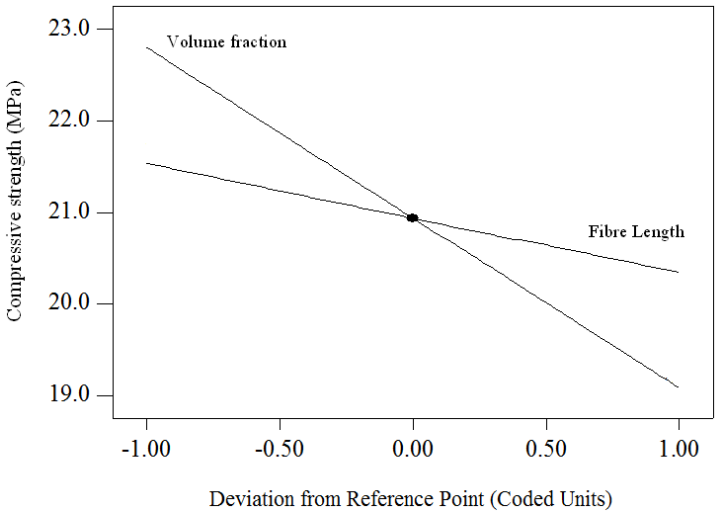

Figure 5.27: Perturbation plot showing the effect of all factors on the compressive strength.

5.4.2.4 Fracture energy

One of the major roles of fibre in cement composites is to improve toughness, where fibres increase the energy needed for fracture by the resultant crack arresting process. Therefore, the incorporation of flax fibres in the cement matrix effectively increases the post cracking behaviour of the matrix as shown in Figures 5.28 and 5.29 and Table 5.14. It can clearly be seen that fracture energy increases as the fibre volume fraction increases. As seen in Figure 5.29 and Table 5.14, these flax fibre composites allow high values of fracture energies to be obtained and as a result of a high ductility; depending on the length and volume fractions of the fibres used. The increase in fracture energy varied from 930% to 1111%, 1055% to 1579% and 1201% to 1932% for composites having a 0.5%, 1% and 1.5% volume fraction of fibres respectively. The maximum increase of 1932% was observed for composites with fibre lengths of 50 mm for composites containing a 1.5% volume fraction of fibres.

The reason for this performance may be attributed to fibre pull-out and fibre debonding during the fracture process. Fibre pull-out seems to be the most significant process in relation to the fracture behaviour of cement based composites. The increase in fracture energy with increasing fibre volume fraction could be attributed to the greater number of fibres, which form a bridge in the crack and lead to a more indirect crack propagation path. Indeed, the presence of the flax fibre did

not result in a compressive strength enhancement, even a slight decrease was observed, but the composite's toughness and ductility were greatly improved.

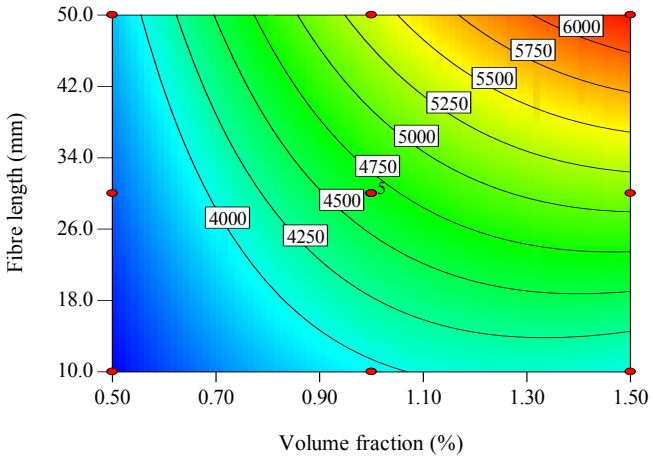

Figure 5.28: Contour plot showing the effect of fibre parameters on fracture energy (N.mm).

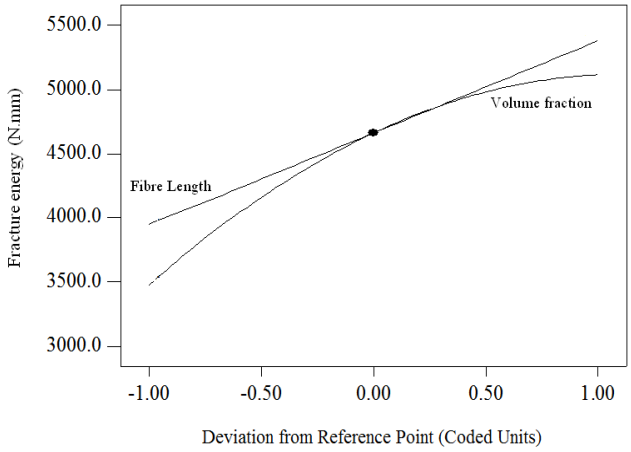

Figure 5.29: Perturbation plot showing the effect of all factors on the fracture energy.

5.4.2.5 Toughness Indices

As explained in chapter 3, the toughness indices were determined according to ASTM C 1018 [170]. Hence, the indices I_5, I_{10} and I_{20} from this test, were calculated where the ratio of the area under the load deflection curves up to 3, 5.5 and 10.5 times the first crack deflection, divided by the area up to the first crack deflection respectively. The results of the toughness indices using the ASTM [170]

method are presented in Table 5.14 and Figures 5.30 to 5.35. The toughness indices for plain mortar are equal to 1.0 in the ASTM [170] method because plain mortar flexural test specimens fail immediately after the formation of first crack (see Figure 5.17).

From a perusal of the test results, it can be seen that the inclusion of flax fibres has significant positive effects on the toughness indices of a cement matrix compared to plain mortar, due to the ability of fibres in arresting cracks at both the micro and macro-levels. It is evident that the indices I_5, I_{10} and I_{20} increase with increasing fibre content and with increasing percentages of long fibres in the concrete mix. Furthermore, a comparison of toughness indices shows that the composites with long fibres (i.e. 30 and 50 mm) have higher values of the indices than those with short fibres (i.e. 10 mm). The toughness indices were also found to be sensitive to the volume fraction and the percentage of the longer fibres in the cement composite. Higher values of the toughness indices were achieved with higher fibre volume fractions and with higher percentages of longer fibres in the cement composite, which agrees with the results obtained by Mohammadi et al. [205] and Meddah and Bencheikh [206].

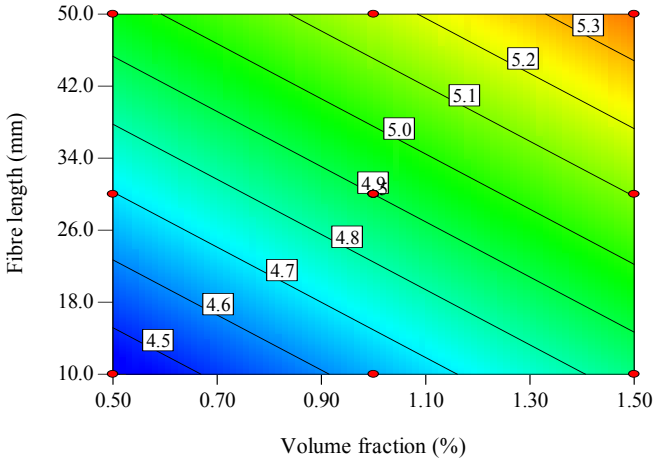

Figure 5.30: Contour plot showing the effect of fibre parameters on I_5.

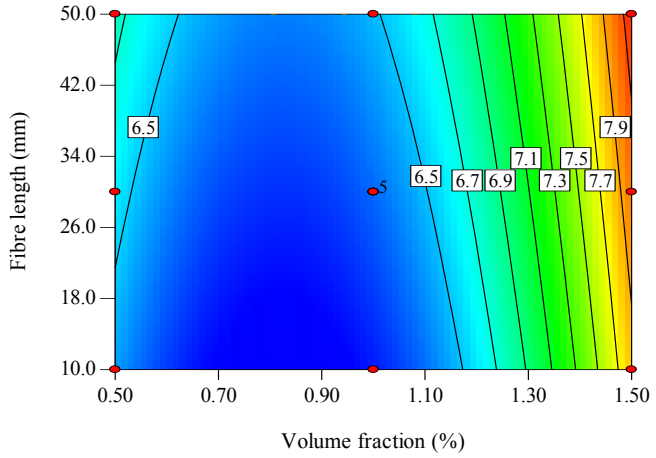

Figure 5.31: Contour plot showing the effect of fibre parameters on I_{10}.

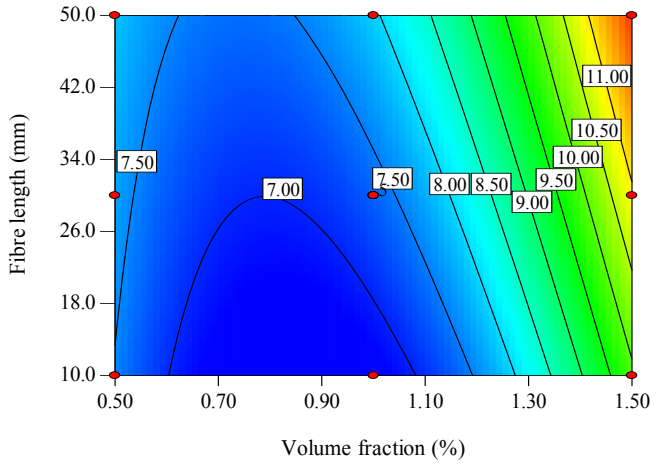

Figure 5.32: Contour plot showing the effect of fibre parameters on I_{20}.

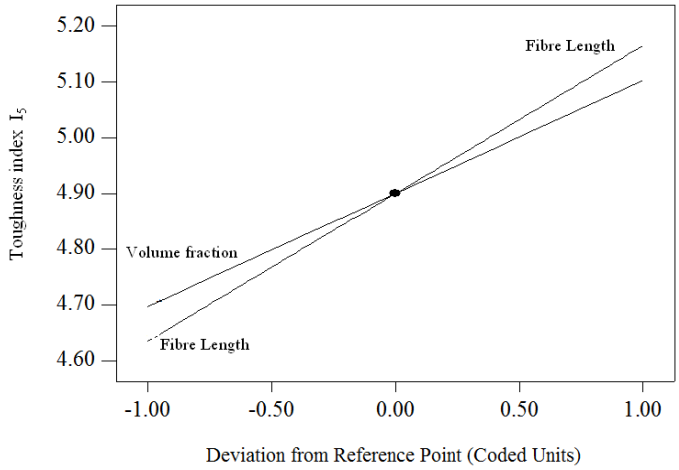

Figure 5.33: Perturbation plot showing the effect of all factors on I_5.

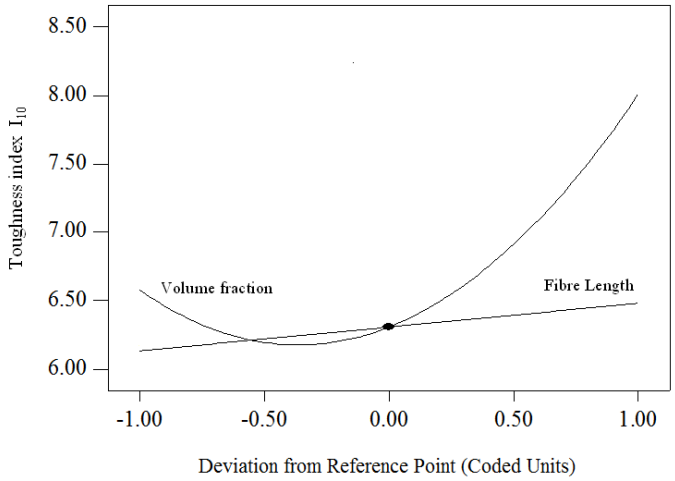

Figure 5.34: Perturbation plot showing the effect of all factors on I_{10}.

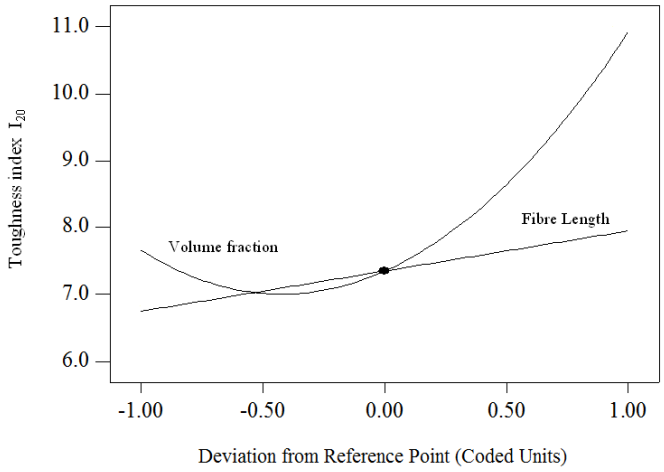

Figure 5.35:Perturbation plot showing the effect of all factors on I_{20}.

5.4.2.6 Porosity of the Cement Composites

Table 5.14 and Figures 5.36 to 5.37 present the results of the porosity of the cement composites after 28 days of hydration. The results indicate that the incorporation of flax fibres in a cement matrix slightly increases the porosity of the hardened composites. This increase is proportional to the fibre's length and content. Hence, the porosity increases by increasing both the length and dosage of fibres. In fact, adding fibres to the cement matrix disturbs the granular skeleton and creates a void space in the composite material.

In general, the addition of the flax fibres has resulted in a slightly increase of porosity when compared to plain mortar, which agrees with the previous findings of Meddah and Bencheikh [206], Neithalath et al. [207] and Neithalath [208]. This could be attributed to the high surface area of flax fibres. A maximum porosity of 11.5 % was induced by the composite containing 50 mm fibre lengths at a 1.5% fibre volume fraction. Therefore, it can be clearly observed that the higher the content and length of the fibres are, the higher the porosity that will be attained in the cement matrix. It may also be due to the tendency of fibres to clump together while mixing, leading to the development of water-filled spaces, which then turn into voids. Therefore, increases in fibre content and fibre length increase the potential for fibre clumping.

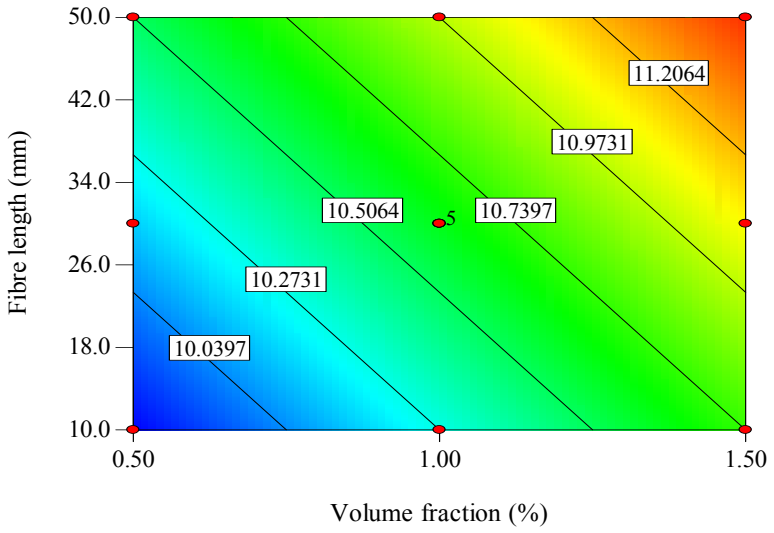

Figure 5.36: Contour plot showing the effect of fibre parameters on the porosity.

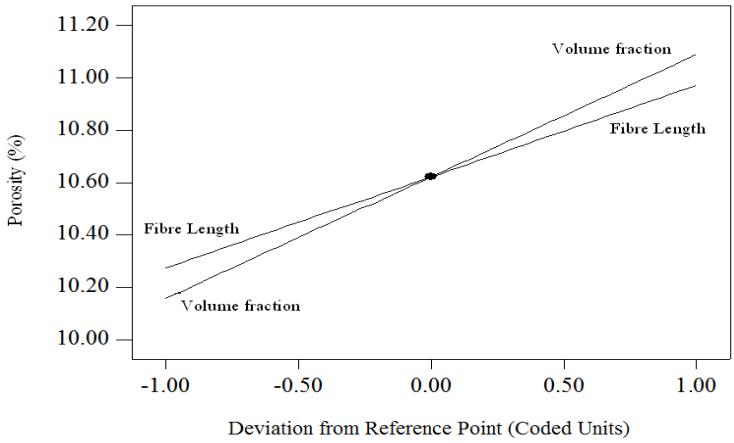

Figure 5.37: Perturbation plot showing the effect of all factors on the porosity.

5.4.3 Optimisation

The issue of links between compressive strength and toughness must be addressed, since any increase in the toughness is usually reflected in a decrease in compressive strength. On balance, it is better to run an optimisation study in order to find out the optimal fibre parameters at which the most desirable mechanical properties of the composite can be achieved. In fact, once the models have been developed and checked for adequacy, the optimisation criteria can then be used to find out the optimum dose. In this work, the optimisation criteria are utilized to maximise fracture energy, flexure, and compressive strength and to minimise porosity, as shown in Table 5.23. Whereas, Table 5.24 summarises the optimal solution obtained by Design-Expert. It is obvious that the graphical optimisation allows for the visual selection of the optimum conditions according to certain criteria. The yellow/shaded area on the overlay plot in Figure 38 is the region that meets the proposed optimisation criteria.

Table 5.23: Optimisation criteria used for fibre parameters

Criterion	Limits		Importance	Goal
	Lower	Upper		
L (mm)	10	50	5	minimise
V (%)	0.5	1.5	5	minimise
F_{flex} (MPa)	5.4	7.9	5	maximise
F_{com} (MPa)	14.58	22.67	5	maximise
G_F (N.mm)	3164	6239	5	maximise
P (%)	9.8	11.5	5	minimise

Table 5.24: Optimal solution as obtained with design-expert software

Number	Volume fraction (%)	Fibre length (mm)	Flexure strength (MPa)	Compressive strength (Mpa)	Fracture energy (N.mm)	Porosity (%)	Desirability
1	1.04	28.46	6.77	21.49	4182	10.37	0.570491
2	1.05	28.43	6.78	21.49	4181	10.36	0.57049
3	1.04	28.47	6.78	21.48	4184	10.36	0.57049
4	1.05	28.42	6.77	21.49	4181	10.37	0.57049

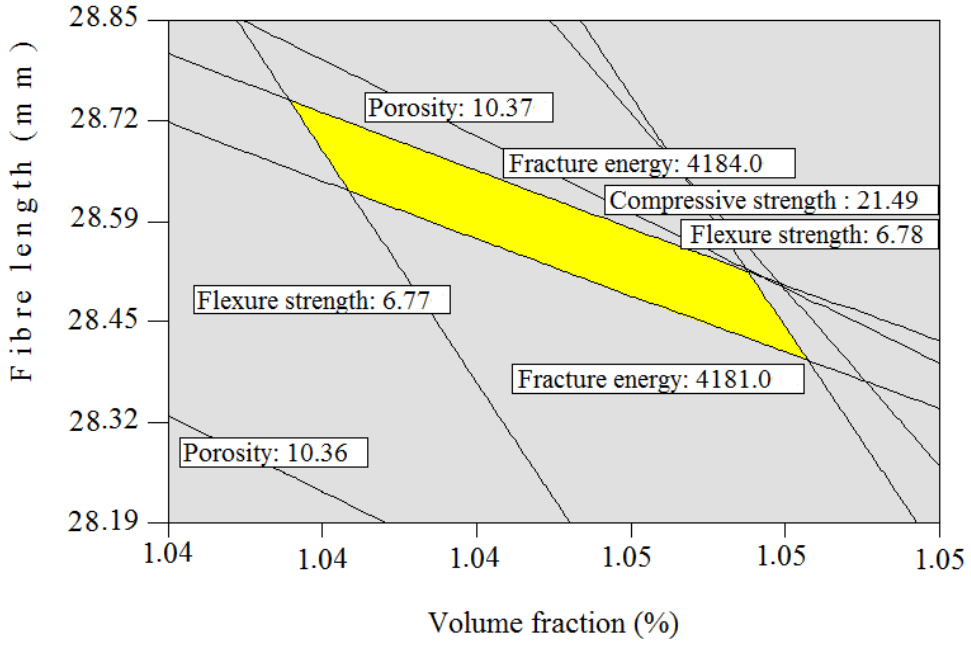

Figure 5.38: Overlay plot shows the region of the optimal fibre parameters condition.

5.4.4 Validation of the Models

Figures 5.39 to 4.46 displays the relationship between the actual and predicted values of the flexural strength (F_{flex}), fracture energy (G_f), impact strength (F_{imp}), compressive strength (F_{com}), toughness indices I_5, I_{10} and I_{20} and porosity (P) respectively. This figure reveals that the developed models are adequate because the residuals in the predictions of each response are small, as the residuals tend to be close to the diagonal line. To verify the adequacy of the developed models further, two confirmation experiments were carried out using new, randomly selected test conditions, each within the experimental range defined earlier. Using the point prediction option in the software, P, F_{flex}, G_f, F_{imp}, F_{com}, I_5, I_{10} and I_{20} of the validation experiments were predicted using the previously developed models and

then compared with the actual measured responses of these confirmation experiments. Table 5.25 shows the experimental conditions, actual experimental values, the predicted values and the percentages of error in the prediction. It is evident that the models can adequately describe the responses within the ranges considered since the maximum error percent in the prediction is -6.8 %, which is in substantial agreement.

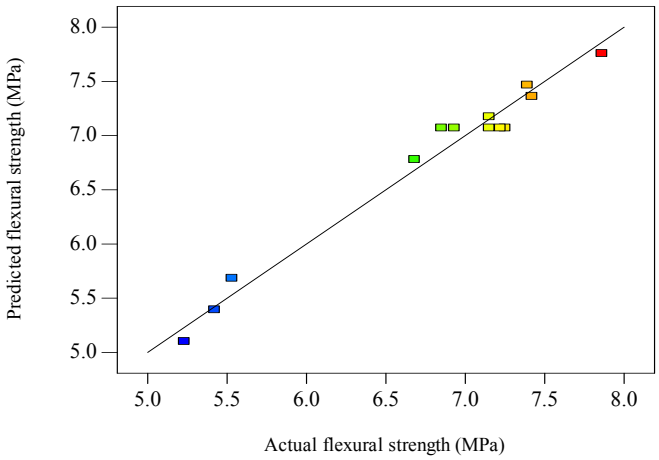

Figure 5.39: Scatter diagram of flexural strength.

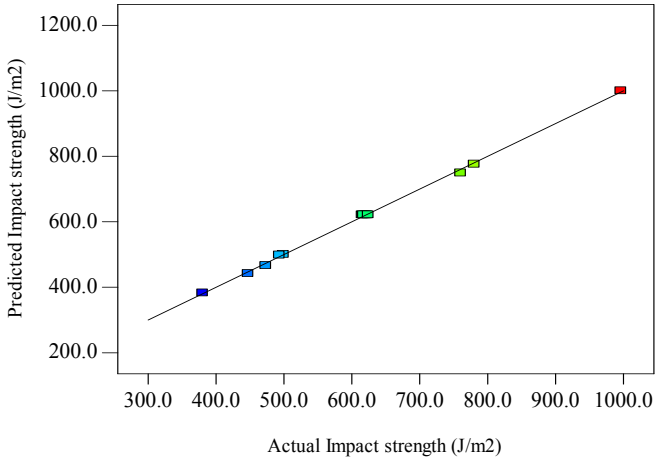

Figure 5.40: Scatter diagram of impact strength.

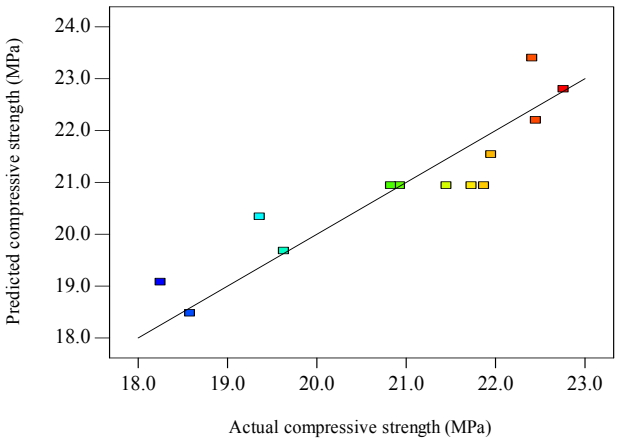

Figure 5.41: Scatter diagram of compressive strength.

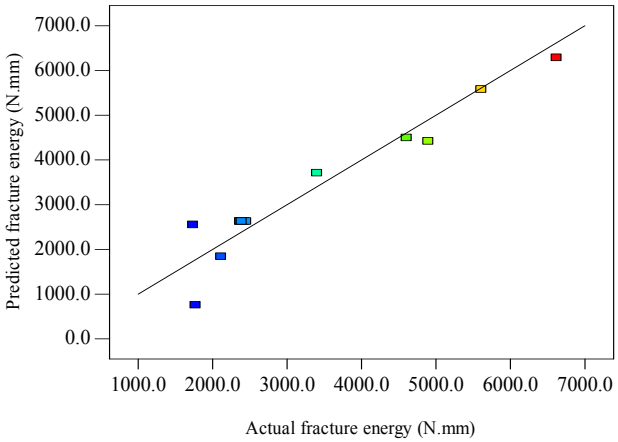

Figure 5.42: Scatter diagram of fracture energy.

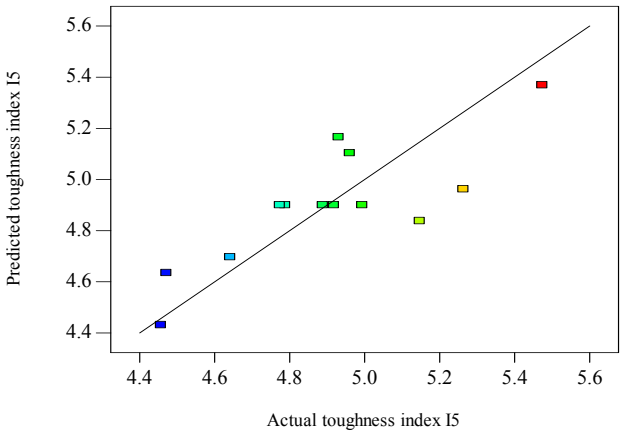

Figure 5.43: Scatter diagram of toughness index I_5.

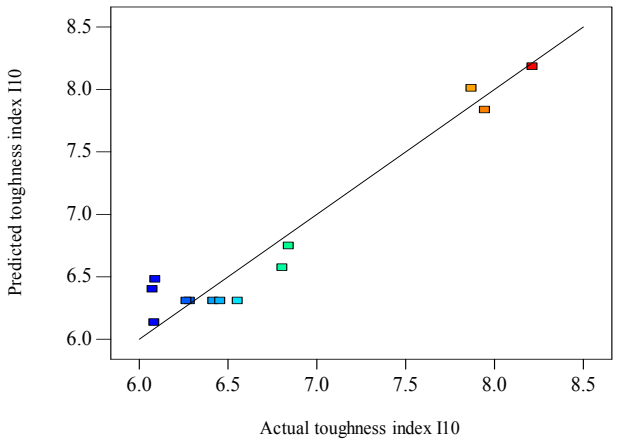

Figure 5.44: Scatter diagram of toughness index I_{10}.

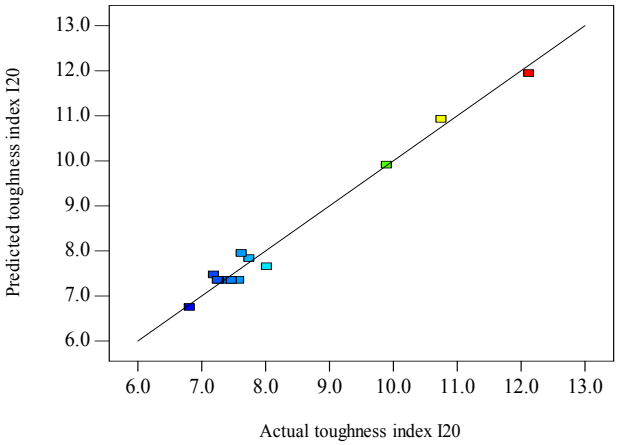

Figure 5.45: Scatter diagram of toughness index I_{20}.

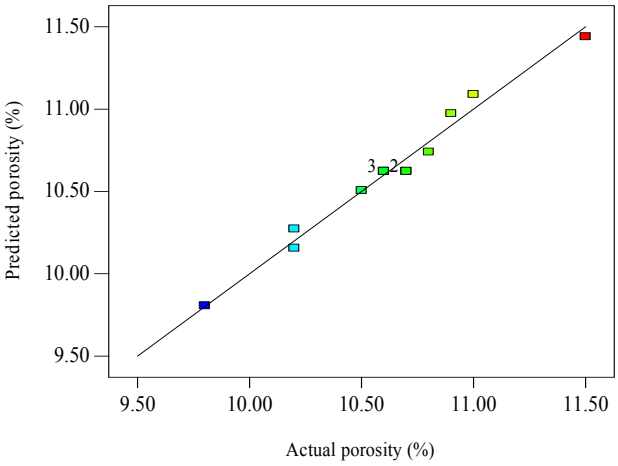

Figure 5.46: Scatter diagram of porosity.

Table 5.25: Confirmation experiments for fibre parameters

Exp. No.	V (%)	L (mm)		F_{flex} (MPa)	F_{imp} (J/m^2)	F_{com} (MPa)	G_F (N.mm)	I_5	I_{10}	I_{20}	P (%)
1	1.25	40	Actual	6.95	710.5	19.86	5043.3	5.12	6.23	7.69	10.82
			Predicted	7.23	692.0	20.63	5022.0	5.03	6.39	7.65	10.79
			Error %	-3.8	2.6	-3.8	1.0	3.3	-2.5	0.5	0.2
1	0.75	25	Actual	7.21	372.0	20.31	4336.0	4.52	6.13	7.35	10.69
			Predicted	6.99	351.5	21.10	4485.8	4.83	6.26	7.2	10.53
			Error %	3.0	5.5	-3.8	-3.4	-6.8	-2.1	2.0	1.5

In this investigation it was found that a fibre length of 30 mm and a fibre volume fraction of 1 % could be used to fabricate cement composites without a reduction in compressive strength. Therefore, these fibre parameters will be utilized for further investigations and this particular cement composite will be considered the control specimen.

5.5 Effect of Nano-clay and Waste Glass Content on the Behaviour of Flax Fibre Cement Composites

5.5.1 Effect of Nano-clay Content

In order to study the effect of NC on the behaviour of flax fibre cement composites, a range of composites were prepared based on the variations of composition that are listed in Table 5.26. For all composites an equal ratio of binder and sand was used for all of the mixes and the fibre parameters chosen were the same as the control specimen (i.e. 30 mm length and 1% volume fraction). The water/binder ratios were tested to reach a flow of 110 ± 5 in order to permit a medium workability to be used for mixing the composites. All of the composites were prepared by the producers described in section 3.3.2.2. The results obtained through this investigation are summarised in the next sections.

Table 5.26: Mixture proportions used to study the effect of NC on the behaviour of the flax fibre cement composites

Batch	Binder material	Water/binder ratio
Control	100% OPC	0.48
NCPC0.5	99.5% OPC+ 0.5% NC	0.482
NCPC1	99% OPC+1% NC	0.495
NCPC1.5	98.5% OPC+1.5% NC	0.51
NCPC2	98% OPC+2% NC	0.515
NCPC2.5	97.5% OPC+ 2.5% NC	0.52
NCPC3	97% OPC+ 3% NC	0.525
NCPC3.5	96.5% OPC+ 3.5% NC	0.527
NCPC4	96% OPC+ 4% NC	0.529
NCPC4.5	95.5% OPC+ 4.5% NC	0.531
NCPC5	95% OPC+ 5% NC	0.535

5.5.1.1 Mechanical Properties

The measured 28-day compressive strength of cement composites reinforced with various doses of NC is shown in Table 5.27 and Figure 5.47, and in all cases, three specimens were measured and then averaged. From the figure, it can be seen that the compressive strength of cement composites increases initially up to a NC dosage of 2.5% and then decreases dramatically after reaching their peak values as the dosage of NC is increased up to 5%. As compared to the 28-day compressive strength of the control composite, the increase of compressive strength of cement mortars reinforced with NC can be up to 9.4% when NC= 0.5%, 17.8% when NC=1% , 23.6% when NC=1.5%, 25.9% when NC= 2% and 37.1% when NC=2.5%. The enhancement of the compressive strength of cement composites due to the addition of NC can be attributed to the packing effect of NC, which acted as filler to fill in the interstitial spaces inside the skeleton of the hardened microstructure of cement mortar which leads to incremental increases in strength [209].

The measured 28-day flexural strengths of cement composites reinforced with various doses of NC are shown in Figure 5.48 and Table 5.27. Again, the flexural strength of the composites increases at the beginning and then drops after

reaching a maximum level as the dosage of NC is increased. From Figure 5.48 and Table 5.27, it can be seen that the flexural strength for cement composites reinforced with 0.5 to 2.5% NC could be up to 20% greater than those of the control specimen.

The experimental results of the measured 28-day impact strengths of cement composites reinforced with different doses of NC are shown in Figure 5.49 and Table 5.27. A perusal of the test results shows that the addition of NC up to a dosage of 2.5% marginally increased the impact strength compared to that of the control specimen. But beyond this dosage (i.e. 2.5%) the impact strength significantly decreased.

Similar to compressive and flexural strength, fracture energy slightly increases up to a NC dosage of 2.5% and then decreases dramatically after reaching a peak value as the dosage of NC is increased up to 5% (see Figure 5.50). As compared to the fracture energy of the control composite, the increases in fracture energy were 16.8%, 17.8%, 21.4%, 24.7% and 27.7% at NC dosage of 0.5, 1, 1.5, 2 and 2.5 % respectively. The same trend was observed for toughness indices $I_{5,}$ I_{10} and I_{20} as shown in Figures 5.51 to 4.53. The tests found that the toughness indices of cement composites reinforced with 0.5 to 2.5% NC could be from 10-31% greater than those of the control specimen. This trend can be explained by the stiffening behaviour of the nano-clay particles as they form bond chains within the binder [210].

Basically, the effects of the addition of NC on the mechanical properties of the cement composites can be divided into two types, one is the filling effect in the porosity of the microstructure of the hydrated cement matrix and the other is the effect of supplementary chemical interactions, such as pozzolanic reaction, of the major oxide compounds of OPC, such as CaO, SiO_2, Al_2O_3 and Fe_2O_3. The increases of compressive strength in this case indicate that although some additional chemical strong bonding due to the addition of NC resulting from the latter effect can be expected, the former filling effect seems to prevail. Microstructural examination of NC cement composites will be discussed in the next section and will be used to assess this behaviour.

Table 5.27: Mechanical properties and porosity of flax fibre cement composites reinforced with various doses of NC

Composite	F_{com} (Mpa)	F_{flex} (Mpa)	F_{imp} (J/m^2)	G_F (N.mm)	I_5	I_{10}	I_{20}	P (%)
Control	21.6	7.02	620	3667	4.37	6.39	7.39	10.7
NCPC0.5	23.65	7.53	627	4285	4.56	6.55	7.66	9.92
NCPC1	25.46	7.82	632	4323	4.89	6.86	7.87	9.86
NCPC1.5	26.71	7.98	635	4454	5.21	7.12	7.98	9.61
NCPC2	27.21	8.11	643	4573	5.61	7.45	8.11	9.42
NCPC2.5	29.63	8.43	646	4685	6.05	7.99	8.45	9.11
NCPC3	25.86	7.56	621	4102	5.16	7.42	8.03	9.39
NCPC3.5	20.54	6.92	610	3322	4.86	7.01	7.12	9.85
NCPC4	17.21	6.03	588	3255	4.23	6.65	6.96	10.5
NCPC4.5	15.32	5.55	570	3180	4.01	6.23	6.25	11.1
NCPC5	14.23	4.49	563	3020	3.86	6.01	5.93	11.96

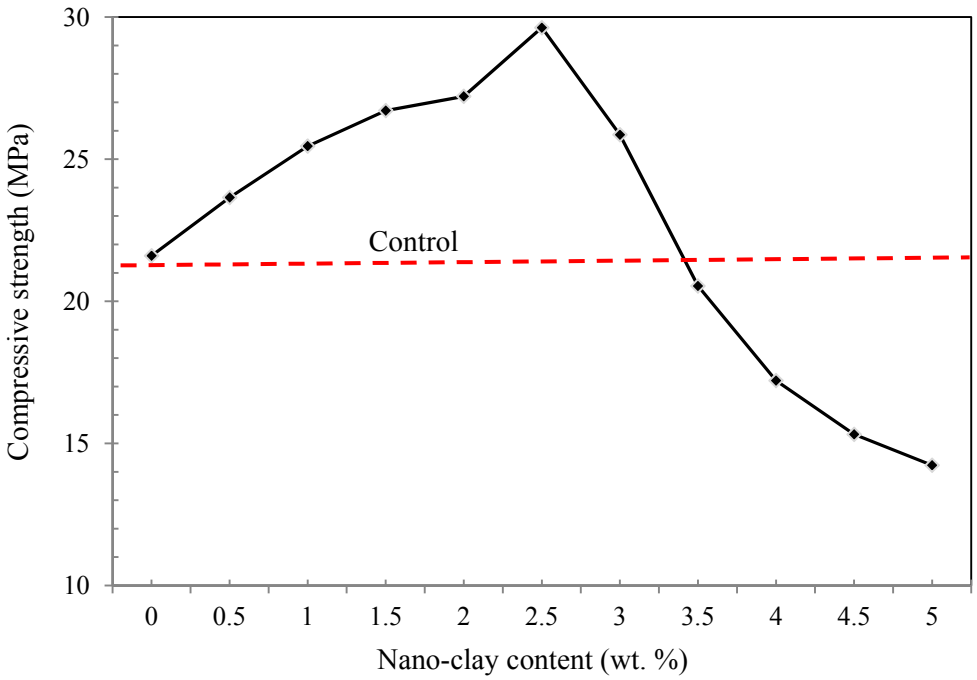

Figure 5.47: Effect of NC content on the compressive strength of cement composites (n = 3).

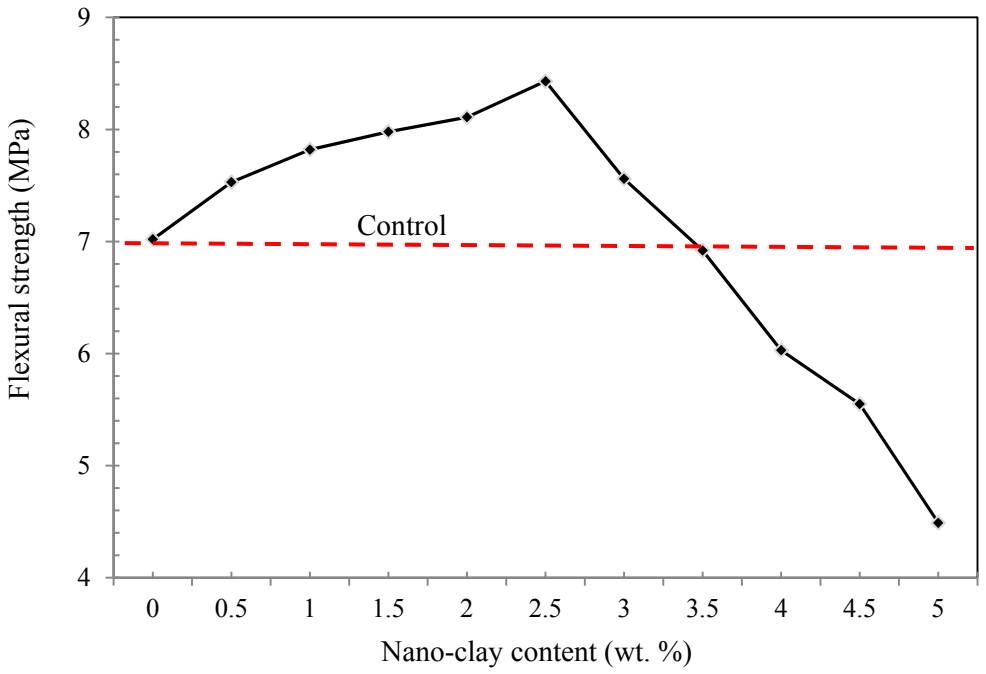

Figure 5.48: Effect of NC content on the flexural strength of cement composites (n = 3).

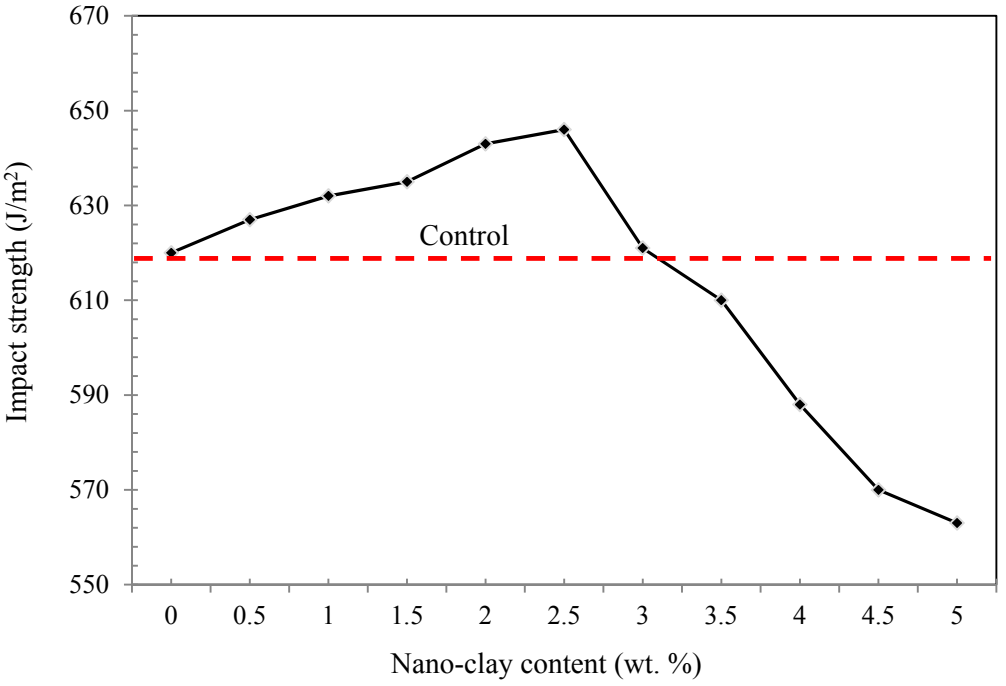

Figure 5.49: Effect of NC content on the impact strength of cement composites (n = 3).

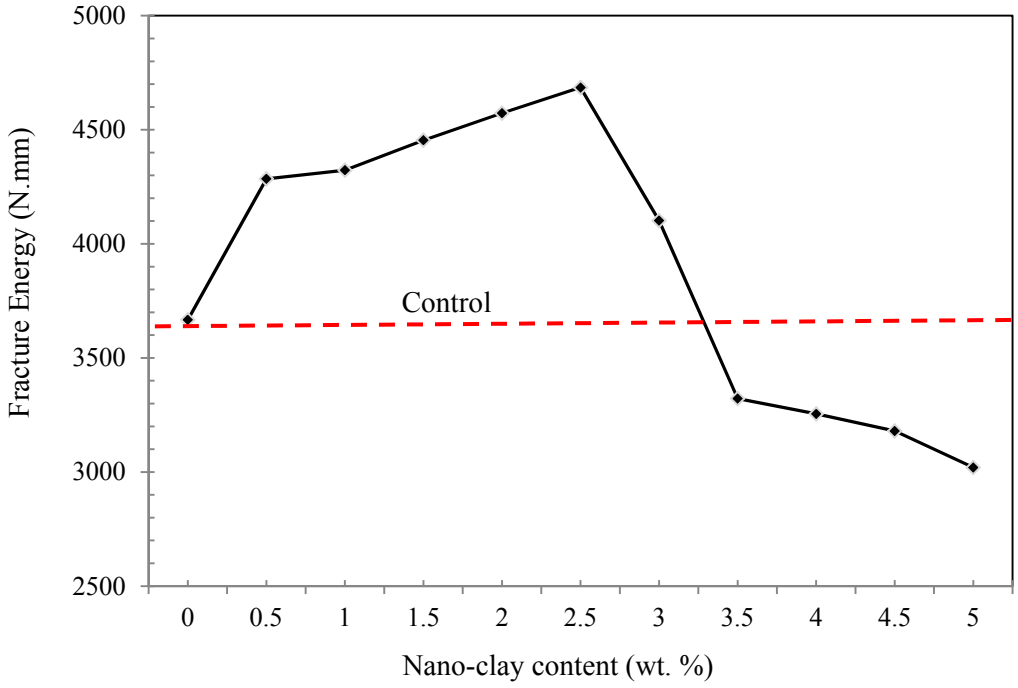

Figure 5.50: Effect of NC content on the fracture energy of cement composites (n = 3).

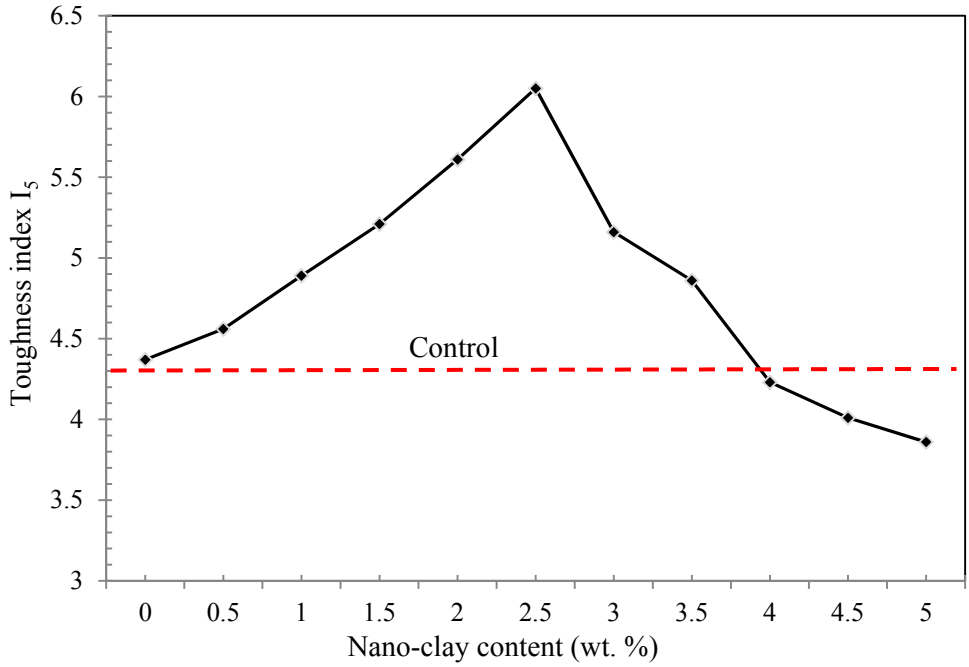

Figure 5.51: Effect of NC content on the toughness index I_5 of cement composites (n = 3).

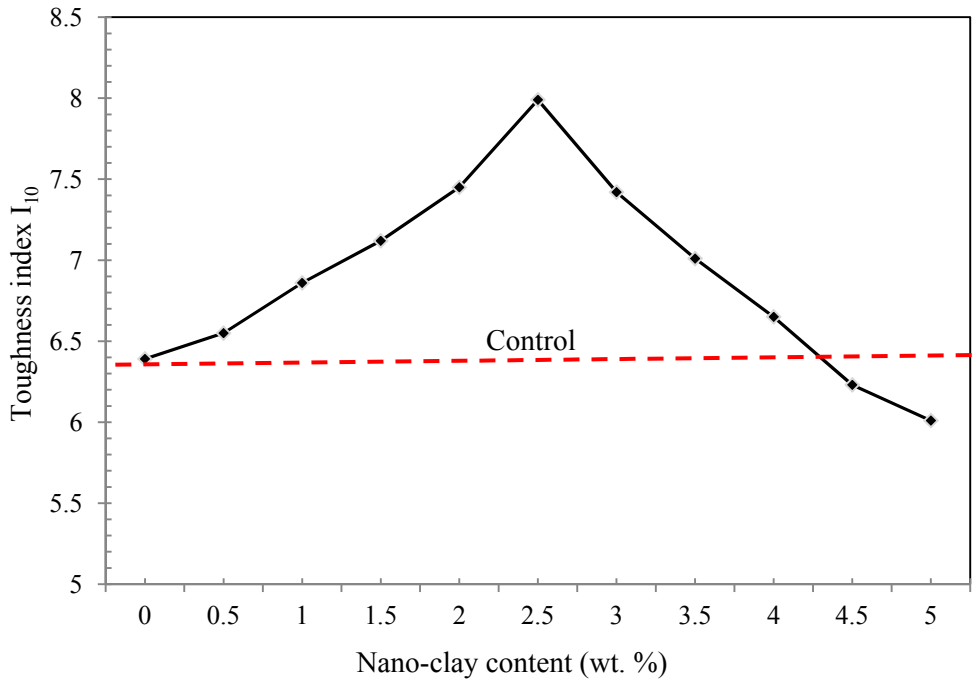

Figure 5.52: Effect of NC content on the toughness index I_{10} of cement composites (n = 3).

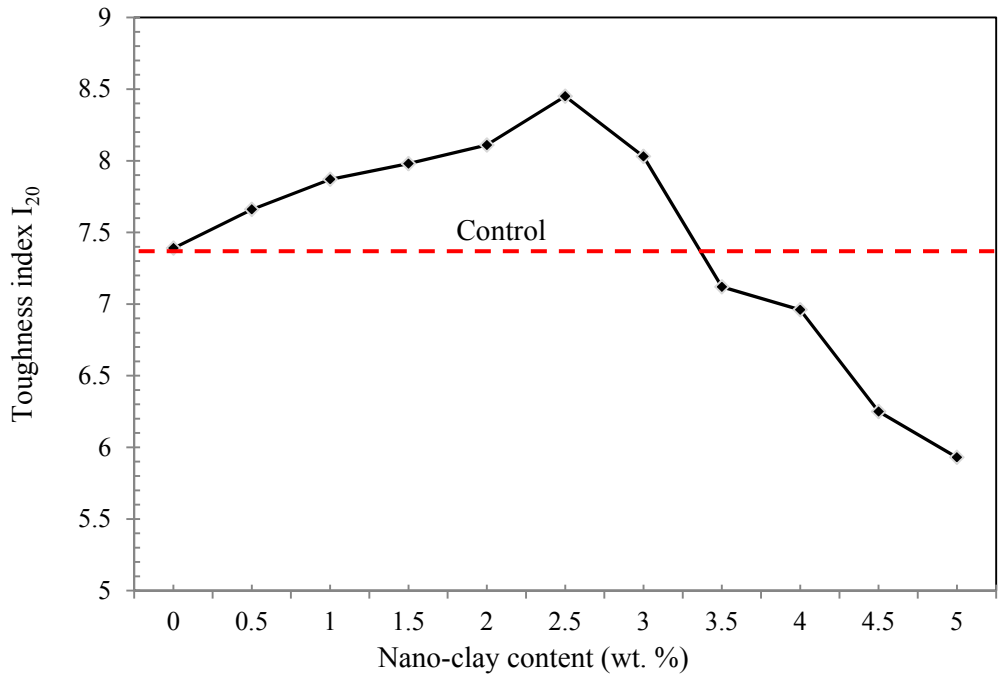

Figure 5.53: Effect of NC content on the toughness index I_{20} of cement composites (n = 3).

5.5.1.2 Microstructural Characterisation

The effect of NC on the microstructure of cement matrices can be observed from their SEM micrographs; for example, the SEM micrographs of cement composites reinforced with 0%, 2.5% and 5% NC are shown in Figure 5.54 (a), (b) and (c), respectively. The locations of NC around the capillary pores in each specimen were identified by using EDX and then marked in the SEM micrographs. The NC around the capillary pores in Figure 5.54 (b) and (c) are identified by EDX analyses from their peak values of carbon, oxygen, aluminium, copper, iron and silicon; a typical EDX result of NC around the capillary pores is shown in Figure 5.55. By comparing the microstructure of Figure 5.54 (b) to that of plain cement mortars in Figure 5.54 (a), it can be seen that NC could act as a diffusion barrier around the capillary pores for cement composites reinforced with a lower dosage of NC. But, the clusters or agglomeration of NC around the capillary pores observed in Figure 5.54 (c) will form for cement composites with a higher dosage of NC. Based on these experimental results, it can be concluded that the agglomeration of NC in cement composites is more likely to occur when the dosage of NC is larger than 2.5%. The NC in its densified state considerably decreases its chemical reactivity with calcium hydroxide. The agglomeration of NC cannot be easily broken up due to the high inter-particle forces, for example, forces due to electrostatic charging, Van der Waal's forces and forces due to moisture. This agglomeration of NC can easily reduce its effectiveness on the properties of cement composites, because of the existence of densified grains of NC, which have a larger diameter, a smaller specific surface area and lower pozzolanic reactivity than unitary grains. In previous papers, some researchers pointed out that these agglomerations were very difficult to disperse, because of their original extremely fine size, by some physical or chemical treatments such as strong mixing, adding a superplasticizer or being treated by a supersonic homogenizer [211,212]. Furthermore, some researchers have proven that pozzolanic reactions can only take place on the surface of the agglomeration [211,212,213,214,215]. It can be deduced from previous research work that the pozzolanic reaction starts from the surface of NC and that the reaction front was penetrated into particles gradually by diffusion-controlled reactions [216]. The coarse NC agglomerations significantly reduces the effective surface area for contacting and reacting with CH, which definitely cuts down the rate of pozzolanic

reactions of NC that in turn leads to a significant reduction in strength and toughness. It is the particle size of NC agglomerations that determines the reactivity of NC rather than the original extreme fine size of the NC.

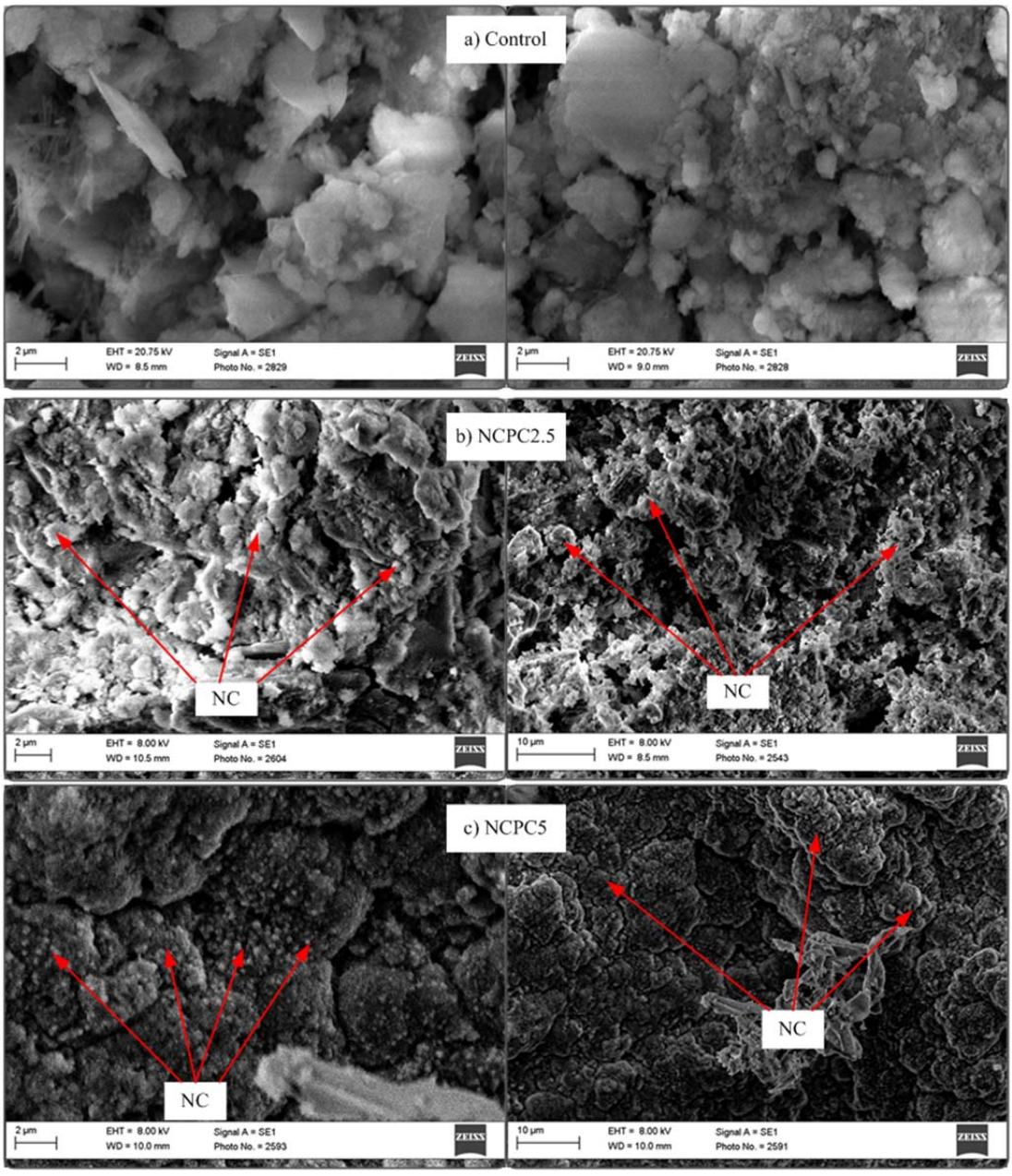

Figure 5.54: SEM micrographs of cement composites reinforced with (a) 0%, (b) 2.5 % and (c) 5 % NC.

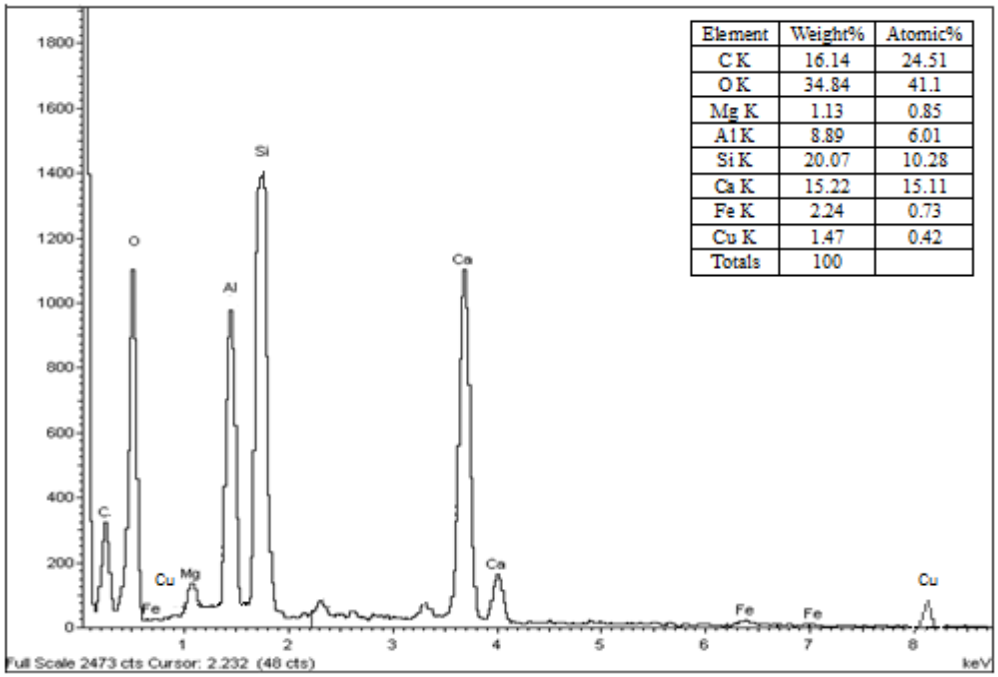

Figure 5.55: A typical EDX result of the NC around capillary pores.

5.5.1.3 Porosity

The porosity of the flax fibre composites reinforced with different doses of NC are shown in Figure 5.56 and also listed in Table 5.27. From a perusal of the test results, it can be seen that the porosity of the composites decreases at first, and then increases rapidly after reaching a minimum value while the dosage of NC is increased. In other words, the porosity of the composites with a dosage of NC less than or equal 2.5% could be dramatically reduced; especially for composites with doses of 0.5, 1, 1.5, 2 and 2.5 % NC, where their porosity become 3–14% lower than that of the control specimen. However, the porosity of composites reinforced with a dosage of NC greater than 2.5% are relatively high when compared to the control specimen. The reason for that, as explained in the previous section, is due to the occurrence of clusters or an agglomeration of NC. When the dosage of NC is larger than 2.5%; a larger total porosity as observed in Figure 5.56 can be expected. Since the effects of NC on enhancing the mechanical properties of cement composites are similar to those reducing their porosity, the porosity of the cement composites is higher than that of the control specimen.

The improvements of strengths for cement composites reinforced with low doses of NC are attributed to the decrease of the capillary porosity. On the contrary,

clusters of NC surrounded by cement grains are more likely to form during the hydration process for cement composites reinforced with higher doses of NC. Consequently, the strengths and durability of cement composites become worse as the dosage of NC is increased. When both strength and durability are sought, the optimal dosage of NC is found to be less than 3% and the NC should be randomly distributed around the capillary pores in cement mortars after mixing has been completed.

In this investigation it was found that a NC dosage of 2.5 % could be used to fabricate cement composites with high strengths and low porosities. Therefore, this dosage level will be used in further investigations.

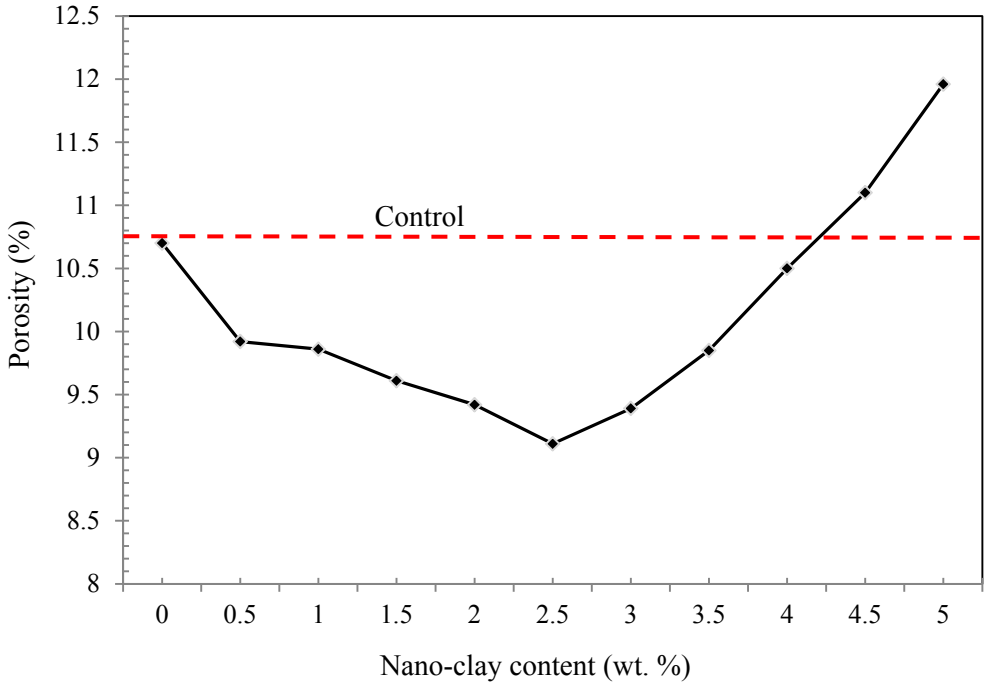

Figure 5.56: Effect of NC content on the porosity of cement composites (n = 3).

5.5.2 Hybrid Effect of Nano-clay and Waste Glass Powder

In order to study the hybrid effect of NC and WG on the behaviour of flax fibre cement composites, a range of composites were prepared based on variations of the composition listed in Table 5.28. For all of the composites an equal ratio of binder and sand was used for all mixes and the same fibre parameters as the control specimen's were used (i.e. 30 mm length and 1% volume fraction). The

water/binder ratios were tested to reach a flow of 110 ± 5 in order to permit a medium workability to be used for mixing the composites. All of the composites were prepared by the producers described in section 3.3.2.3. The results obtained through this investigation of the utilisation of NC/WG as a cement replacement on the behaviour on flax fibre cement composites is summarised in the following sections.

Table 5.28: Mixture proportions used to study the effect of NC/WG on the behaviour of the flax fibre cement composites

Batch	Binder material	Water/binder ratio
WG5	95% OPC+ 5% WG	0.482
WG10	90% OPC+ 10% WG	0.482
WG20	80% OPC+20% WG	0.485
WG30	70% OPC+30% WG	0.487
WG40	60% OPC+ 40% WG	0.489
WG50	50% OPC+50% WG	0.489
NCWG5	92.5% OPC+ 5% WG+2.5% NC	0.51
NCWG10	87.5% OPC+ 10% WG+2.5% NC	0.51
NCWG20	77.5% OPC+ 20% WG+2.5% NC	0.515
NCWG30	67.5% OPC+ 30% WG+2.5% NC	0.52
NCWG40	57.5% OPC+ 40% WG+2.5% NC	0.525
NCWG50	47.5% OPC+ 50% WG+2.5% NC	0.525

5.5.2.1 Mechanical Properties

Table 5.29 and Figure 5.57 compare the compressive strength of WG/NC with WG specimens and apparent improvements in compressive strength when compared to the control specimen is reported. The compressive strength increases by increasing the glass content up to 20%, after which compressive strength slightly decreases, which agrees with the results obtained by Chen et al. [34]. Evidently, incorporating NC particles has a positive effect on the compressive strength of cement composites. Moreover; the increases in compressive strength for NCWG5,

NCWG10, NCWG30, NCWG40 and NCWG50 were 25%, 31%, 40%, 37% and 20% respectively compared to the control specimen's compressive strength. NCWG20 samples show the highest compressive strength, with a 50% increase in compressive strength when compared to the control specimen. This increase indicates that the hybrid incorporation of NC and WG greatly improves the mechanical performance of the cement matrix.

The flexural strength behaves in a similar way to the compressive strength. Figure 5.58 shows that the incorporation of WG improves the flexural strength compared to that of the control specimen, which agrees with the results obtained by Corinaldesi et al. [36]. The addition of NC leads to further improvements in the flexural strength of WG composites. Figure 5.58 exhibits the increase in flexural strengths for mixes NCWG5, NCWG10, NCWG20, NCWG30, NCWG40 and NCWG50 (12%, 25%, 40%, 27%, 15% and 11% respectively); compared to the flexural strength of the control specimen. Mix NCWG20 showed the highest flexural strength followed by mix NCWG30, which confirms the similarity seen between compressive and flexural strength.

Figure 5.59 and Table 5.29 presents the impact strengths of the composites at 28 days of hydration. As it can be seen from Figure 5.59, the partial replacement of OPC by WG slightly increases the impact strength of the composites compared to that of the control specimens. Evidently, the incorporation of 2.5% NC has a further positive effect on the impact strength. The increases in the impact strengths for NCWG5, NCWG10, NCWG20, NCWG30, NCWG40 and NCWG50 were 10%, 14%, 31%, 20%, 14% and 11% respectively as compared to that of the control composites.

Figure 5.60 and Table 5.29 shows the variations of the fracture energy of composites versus waste glass content for different specimens. It can be seen that the incorporation of WG has a remarkable positive effect on fracture energy, which increased with increases in glass content. The increases in the impact strengths for WG5, NCWG10, WG20, WG30, WG40 and WG50 were 39%, 46%, 70%, 68%, 67% and 66% respectively, as compared to the control composites. The incorporation of NC significantly improves the fracture energy of the composites compared to the control specimens. The increases in fracture energy for NCWG5,

NCWG10, NCWG20, NCWG30, NCWG40 and NCWG50 were 50%, 87%, 114%, 105%, 102% and 99% respectively when compared to the control specimens. The same trend was observed for the toughness indices shown in Figures 5.61 to 5.63. This increase indicates that there is greater energy adsorption in NC/WG composites.

Table 5.29: Mechanical properties and porosity of flax fibre cement composites reinforced with various contents of WG at 2.5% NC (n = 3).

Composite	Compressive strength (Mpa)	Flexural strength (Mpa)	Impact strength (J/m^2)	Fracture energy (N.mm)	I_5	I_{10}	I_{20}	Porosity (%)
WG5	22.9	7.33	644	5122	6.11	8.11	8.86	10.23
WG10	25.32	7.55	653	5356	6.33	8.56	9.12	9.85
WG20	27.55	7.64	659	6243	6.45	8.95	9.36	9.72
WG30	26.82	7.25	672	6169	6.43	8.88	9.25	9.74
WG40	25.11	7.11	670	6163	6.37	8.73	9.11	9.86
WG50	23.12	6.96	665	6111	6.28	8.11	9.76	10.02
NCWG5	27.21	7.88	685	5523	6.34	8.44	10.66	9.05
NCWG10	28.31	8.78	710	6869	6.86	9.23	12.96	8.98
NCWG20	32.55	9.88	813	7851	7.14	10.9	14.54	8.74
NCWG30	30.26	8.96	746	7532	6.69	9.36	13.26	8.88
NCWG40	29.63	8.12	712	7412	6.48	9.26	13.12	9.21
NCWG50	26.13	7.82	693	7321	6.33	9.13	12.95	9.69

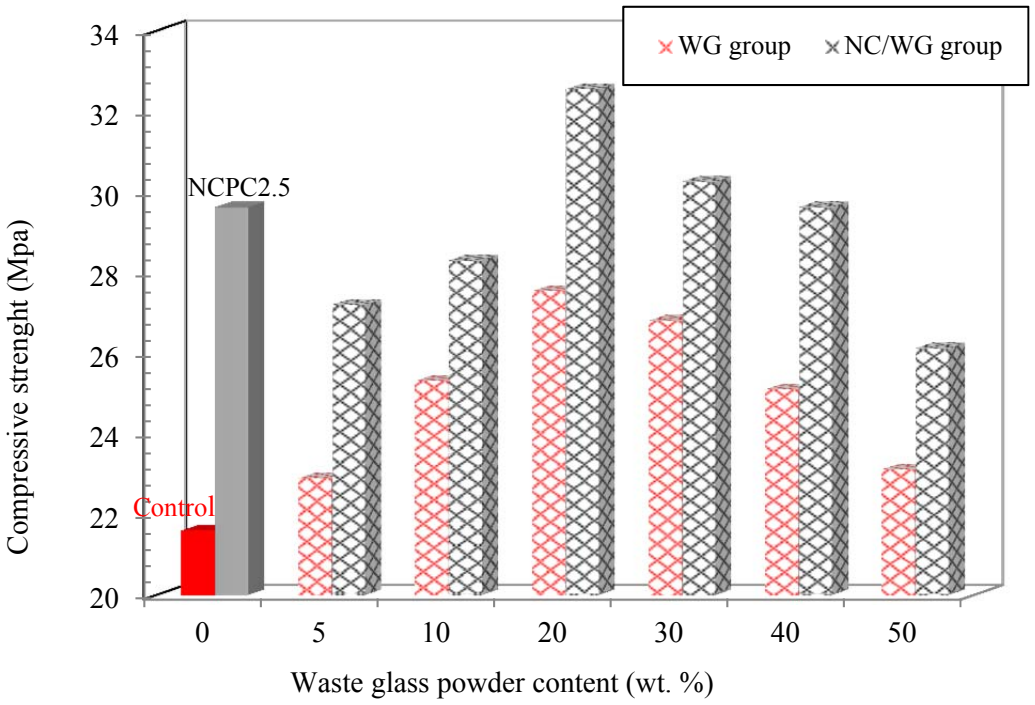

Figure 5.57: Variation of the compressive strengths of cement composites with different contents of WG when NC dosage is 2.5% (n = 3).

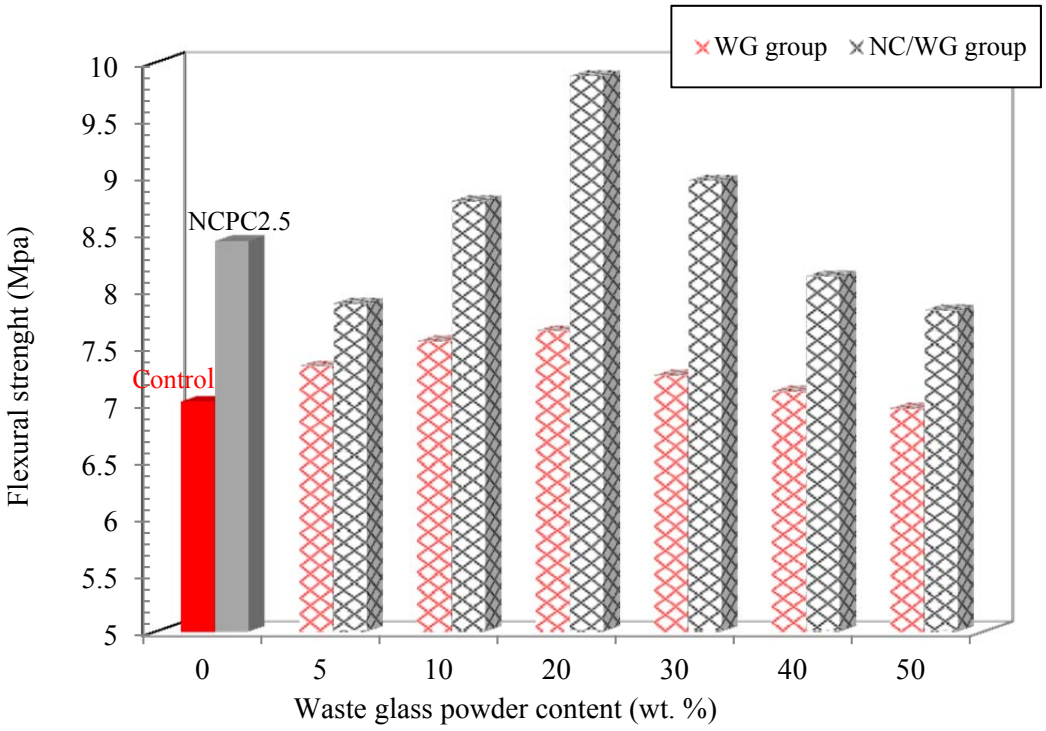

Figure 5.58: Variation of the flexural strengths of cement composites with different contents of WG when NC dosage is 2.5% (n = 3).

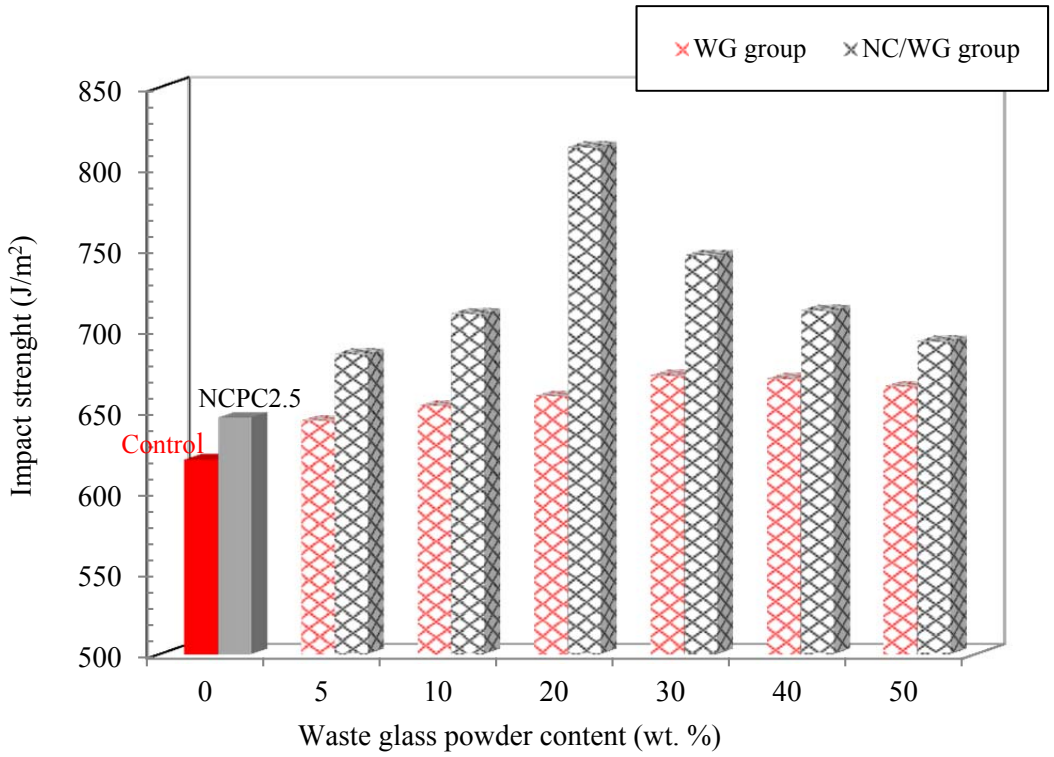

Figure 5.59: Variation of the impact strengths of cement composites with different contents of WG when NC dosage is 2.5% (n = 3).

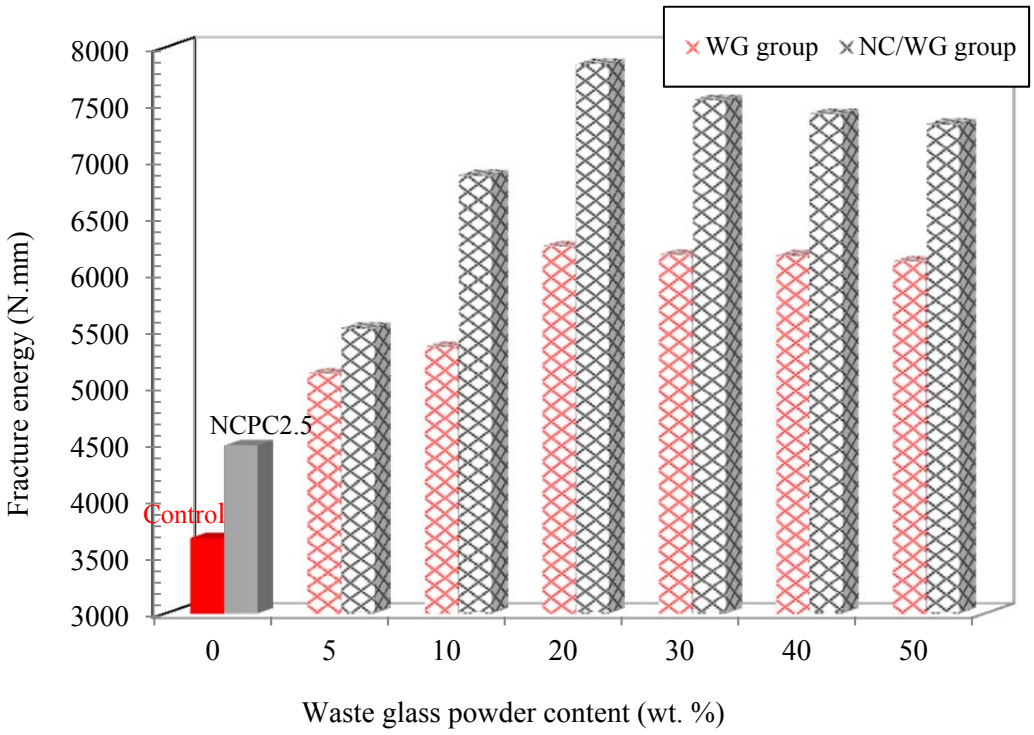

Figure 5.60: Variations of the fracture energy of cement composites with different contents of WG when NC dosage is 2.5% (n = 3).

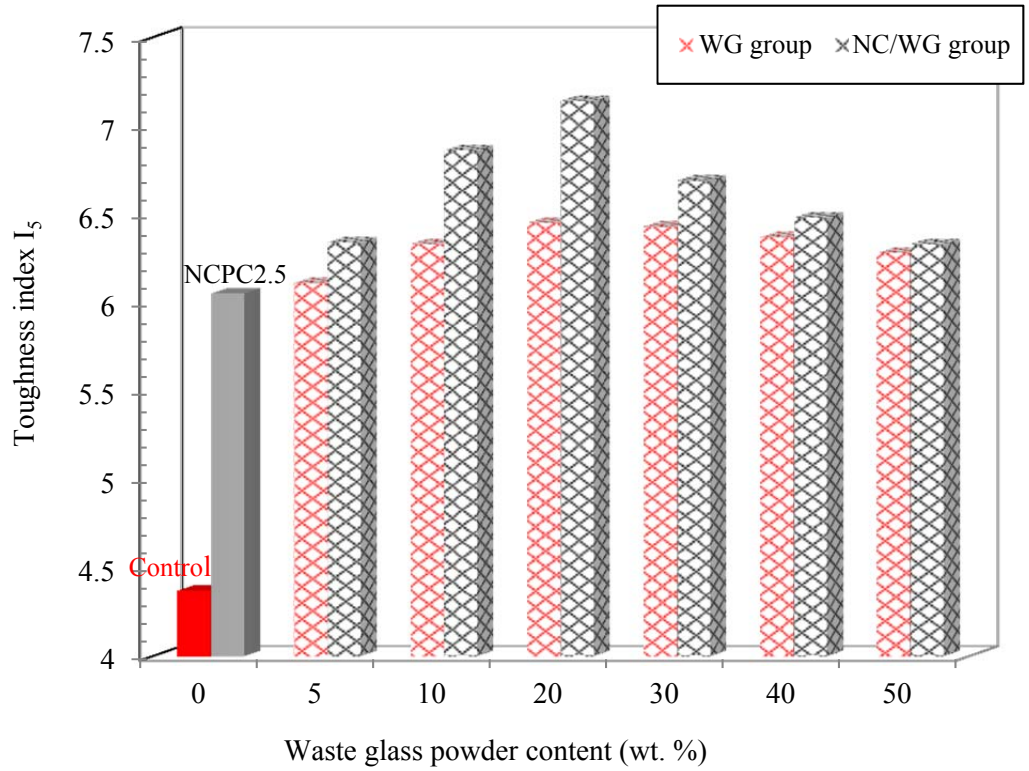

Figure 5.61: Variations of the toughness index I_5 of cement composites with different contents of WG when NC dosage is 2.5% (n = 3).

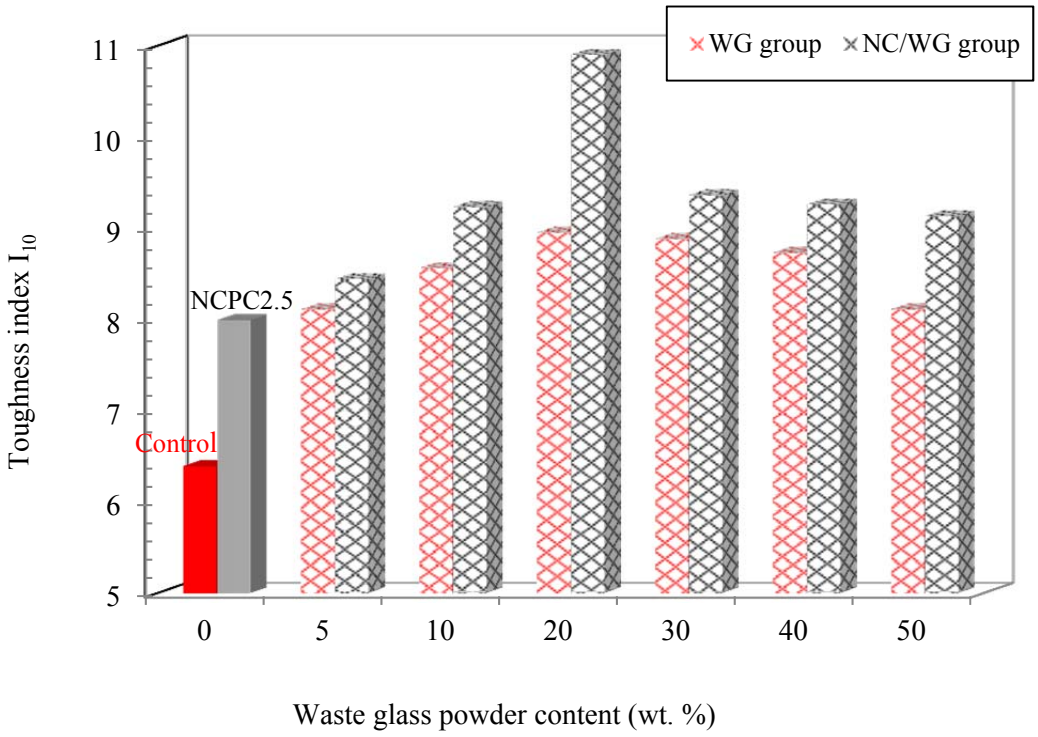

Figure 5.62: Variations of the toughness index I_{10} of cement composites with different contents of WG when NC dosage is 2.5% (n = 3).

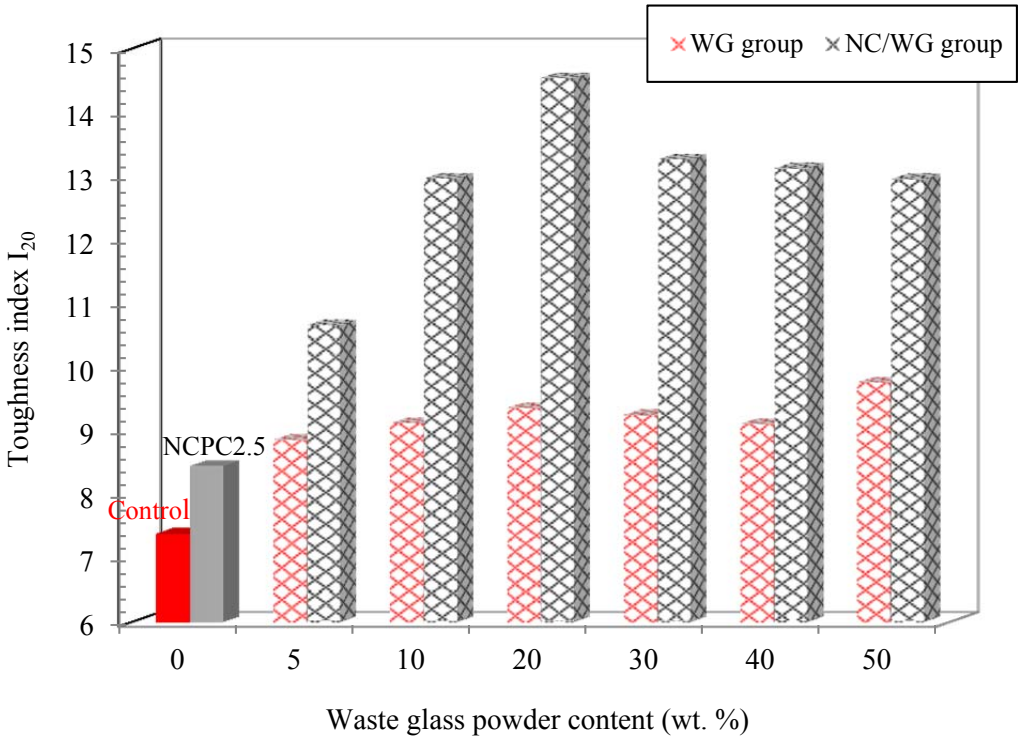

Figure 5.63: Variations of the toughness index I_{20} of cement composites with different contents of WG when NC dosage is 2.5% (n = 3).

5.5.2.2Porosity

Figure 5.64 and Table 5.29 depict the porosity of cement composites. The results show that the porosity decreased as the WG content increased up to 20%, and then it decreased slightly, although it was still lower than the porosity of the control specimen. This result suggests that small particles of ground glass powder can help to fill the voids in the mortar structure, since the porosity of all of the WG composites was 90–95% of that of the control specimen. The composites containing NC+WG had lower porosity than the control specimen, the NCPC3 and the WG specimens with the same percentages of replacement. This indicates that the hybrid combination of NC+WG used in this study is more effective than the single use of WG or NC in the refinement of the pore structure of the blended cement system, although they both reduced the porosity of the cement composites at the studied replacement levels.

The test results provided above show that the hybrid combination of NC+WG can greatly decrease the total porosity of cement composites, thus significantly

improving their mechanical properties. The mechanism for doing this can be summarised as follows:

- As described in chapter 2, a great deal of CH crystal is produced due to the hydration reaction between cement and water. The CH crystal is hexagonal and is arrayed in the interfacial transition zone, which is detrimental to porosity. NC has very high activity due to the galactic specific surface area. Therefore, NC can activate the pozzolanic reaction and react with CH crystals quickly to produce C–S–H gel. The CH crystal can be absorbed and that leads to a remarkable reduction in both the size and the amount of CH crystals. Then the C–S–H gel fills the voids, which improves the density of the interfacial transition zone and the binding paste matrix.

- As pointed out by Ye [217], 70% of the hydration product is C–S–H gel. The average diameter of C–S–H gel is approximately 10 nm. The NC and WG can fill the voids of the C–S–H gel structure, making the binding paste matrix denser and more compact. In the C–S–H gel structure, NC can act as a nucleus to tightly bond with the C–S–H gel particles. As a result, the integration and the stability of the hydration product structure are greatly improved [53].

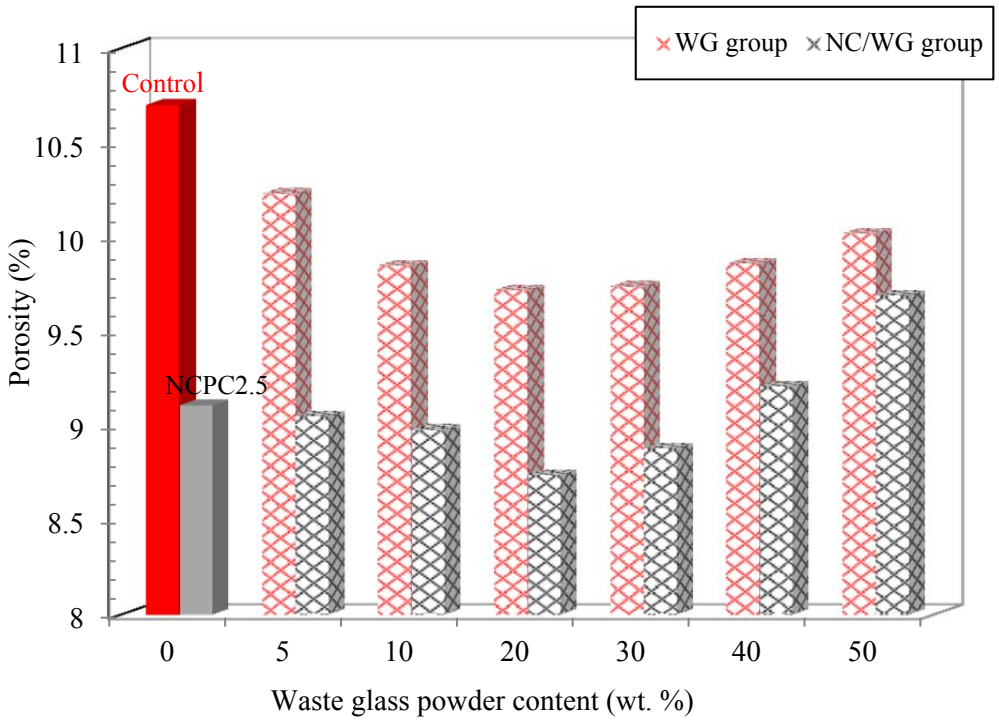

Figure 5.64: Variation of the porosity of cement composites with different contents of WG when NC dosage is 2.5% (n = 3).

5.5.2.3 Alkali Silica Reaction

The percentage expansions in the cement composites are shown in Figure 5.65. Evidently, NCWG20 had less expansion when compared to the control specimen, followed by WG20. But it is clear that all of the specimens had expansions of less than 0.2% and, therefore, according to ASTM C1260 [175], the expansions were all within acceptable limits. From Figure 5.65, it can be seen that the partial replacement of OPC by WG reduces the ASR expansion of the composites, a result that that agrees with the results obtained by Schwarz et al. [35] and Shao et al. [14]. The expansion tests showed that the addition of 20% glass powder (WG20) significantly hindered the expansion of the composites compared to the control specimen, which also confirms the results obtained by Shao et al. [14]. The mechanisms that are normally attributed to the reduction of ASR expansion when supplementary cementing materials are used, the decrease in the alkali hydroxide concentration in the pore solution, alkali dilution, and the consumption of CH through pozzolanic reactions [218,219,220]. For glass powder cement composites, it is unlikely that decreases in alkali hydroxides will be achieved. However, it is also known that expansion is reduced with increases in SiO_2 content and decreases in CaO content [221]. The very high silica content (75.06%) and the absence of CaO content (see Table 3.2) can, therefore, be expected to play a key role in reducing expansion.

As Figure 5.65 clearly shows, the hybrid incorporation of WG and NC also greatly reduced the possible ASR. The role played by NC in reducing ASR expansion is to decrease the amount of CH, which is confirmed by the TGA/DTA analysis and XRD results in sections 5.7.2 and 5.7.3, and thus prevent the formation of a swelling gel [222]. It should also be noted that binary blends containing WG and NC are more effective in reducing ASR expansion than either of these replacement materials are by themselves.

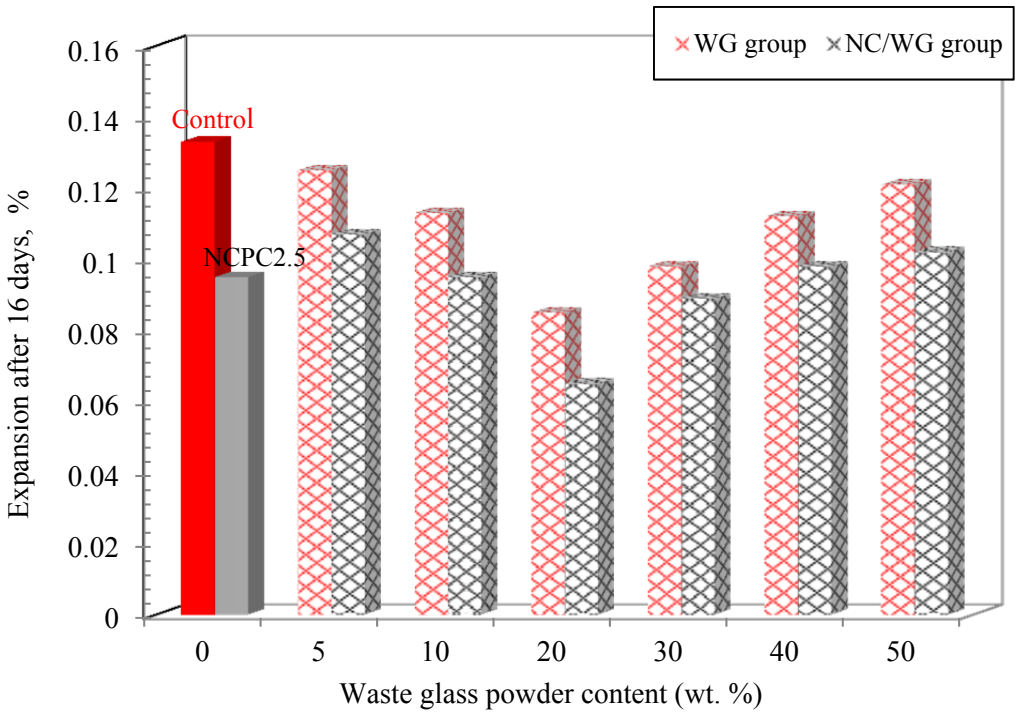

Figure 5.65: ASR test results of cement composites at 2.5 % NC and different contents of WG (n = 3).

5.6 Effect of Nano-silica and Waste Glass content on the Behaviour of Flax Fibre Cement Composites

5.6.1 Effect of Nano-silica Content

In order to study the effect of NS on the behaviour of flax fibre cement composites, a range of composites were prepared based on variations of the composition listed in Table 5.30. For all of these composites an equal ratio of binder and sand was used for all of the mixes and the fibre parameters selected were the same as those of the control specimen (i.e. 30 mm length and 1% volume fraction). The water/binder ratios were tested to reach a flow of 110 ± 5 in order to permit a medium workability to be used for mixing the composites. All of the composites were prepared by the producers described in section 3.3.2.3. The results that were obtained in this investigation are summarised in the next sections.

Table 5.30: Mixture proportions used to study the effect of NS on the behaviour of flax fibre cement composites

Batch	Binder material	Water/binder ratio
NSPC1	99% OPC+1% NS	0.495
NSPC2	98% OPC+2% NS	0.51
NSPC3	97% OPC+3% NS	0.515
NSPC4	96% OPC+ 4% NS	0.52
NSPC5	95% OPC+ 5% NS	0.525
NSPC6	94% OPC+ 6% NS	0.527

5.6.1.1 Mechanical Properties

Figure 5.66 and Table 5.31 show the compressive strength of NS specimens at 28 days of hydration. The results show that the compressive strength increases by adding NS up to 3.0 wt. % replacements and then it decreases, although adding 4.0 wt. % NS produces composites with higher compressive strength compared to specimens with 0.5, 1.0 and 2.0 wt. % NS, a finding that agrees with the results obtained by Nazari and Riahi [21]. The reduced compressive strength, from adding more than 3.0 wt. % NS, may be due to this fact that the quantity of NS used in the mix is higher than the amount required to combine with liberated lime during the process of hydration. This leads to excess silica leaching out which results in a deficiency in strength because it replaces part of the OPC but does not contribute to strength. Furthermore, it can also be attributed to the defects generated in the dispersion of nanoparticles that causes weak zones. Similar to the compressive strength results, the flexural strength, impact strength, fracture energy and toughness indices are increased by adding NS up to 3.0 wt. % but then they decrease after that (see Table 5.31) .

The flexural strength of cement composites reinforced with different doses of NS are shown in Figure 5.67 and listed in Table 5.31. Again, the flexural strength of the cement composites increases up to 3% and then drops with increasing doses of NS. From Figure 5.67 and Table 5.31, it can be seen that the flexural strength for cement composites reinforced with 0.5 to 3% NS could be as much as 26% greater than the flexural strength of the control specimen.

The results of the impact strength tests of cement composites reinforced with different doses of NS are shown in Figure 5.68 and Table 5.31. From a perusal of the test results, it can be seen that specimen NSPC3 showed the highest impact strength reading, recording a 28% increase in impact strength when compared to the control specimen.

As shown in Figure 5.69 and also listed in Table 5.31, the addition of NS up to a dosage of 3% has a positive effect on fracture energy, which increased with increases in NS content. The increases in fracture energy for specimens NSPC0.5, NSPC1 and NSPC2 were 16%, 21% and 25% respectively, compared to that of the control specimen. Mix NSPC3, which contained 3 % NS, showed the highest fracture energy, recording an increase in fracture energy of 32% when compared to the control specimen. The same trend was observed for the toughness indices shown in Figures 5.70 – 5.73.

Table 5.31: Mechanical properties and porosity of flax fibre cement composites reinforced with various doses of NS (n = 3)

Composite	Compressive strength (Mpa)	Flexural strength (Mpa)	Impact strength (J/m^2)	Fracture energy (N.mm)	I_5	I_{10}	I_{20}	Porosity (%)
NSPC1	25.94	7.77	649	4438	4.97	6.87	7.86	9.99
NSPC2	26.87	8.11	710	4598	5.42	7.51	7.9	9.81
NSPC3	30.21	8.86	796	4863	5.83	7.81	8.55	9.12
NSPC4	27.68	7.47	651	4285	5.63	7.13	7.83	9.89
NSPC5	25.21	6.57	532	3322	4.66	6.42	7.03	10.89
NSPC6	18.54	5.41	410	2823	3.86	5.99	6.15	11.32

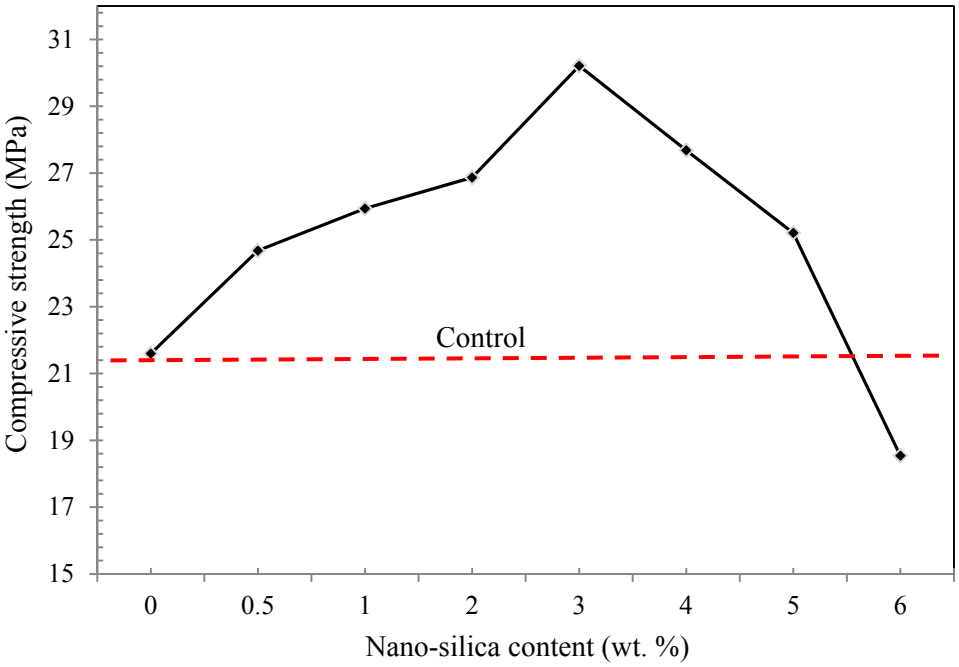

Figure 5.66: Effect of NS content on the compressive strength of cement composites (n = 3).

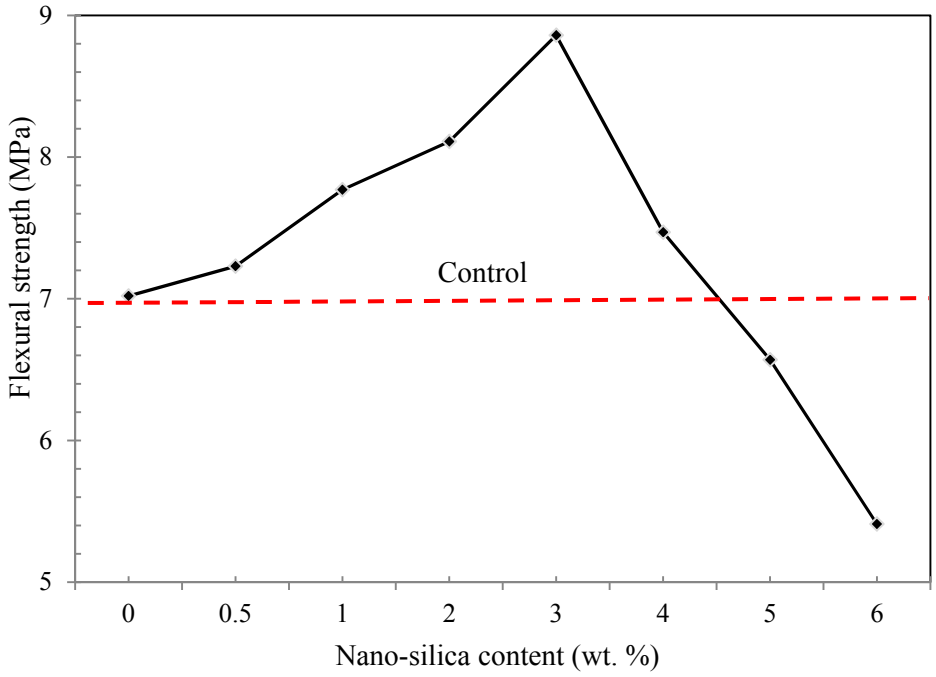

Figure 5.67: Effect of NS content on the flexural strength of cement composites (n = 3).

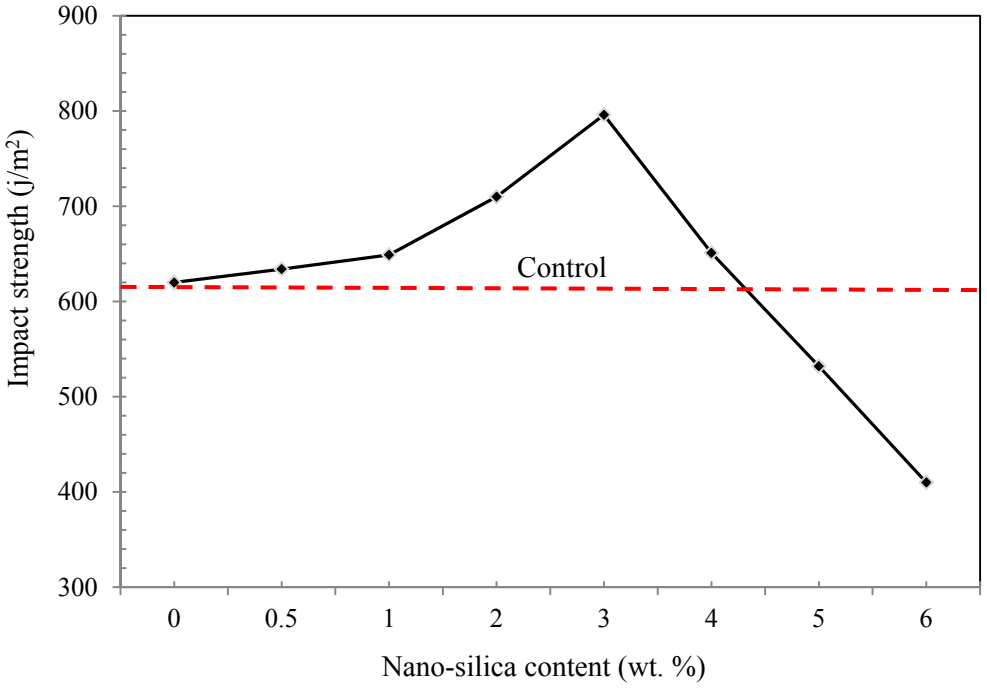

Figure 5.68: Effect of NS content on the impact strength of cement composites (n = 3).

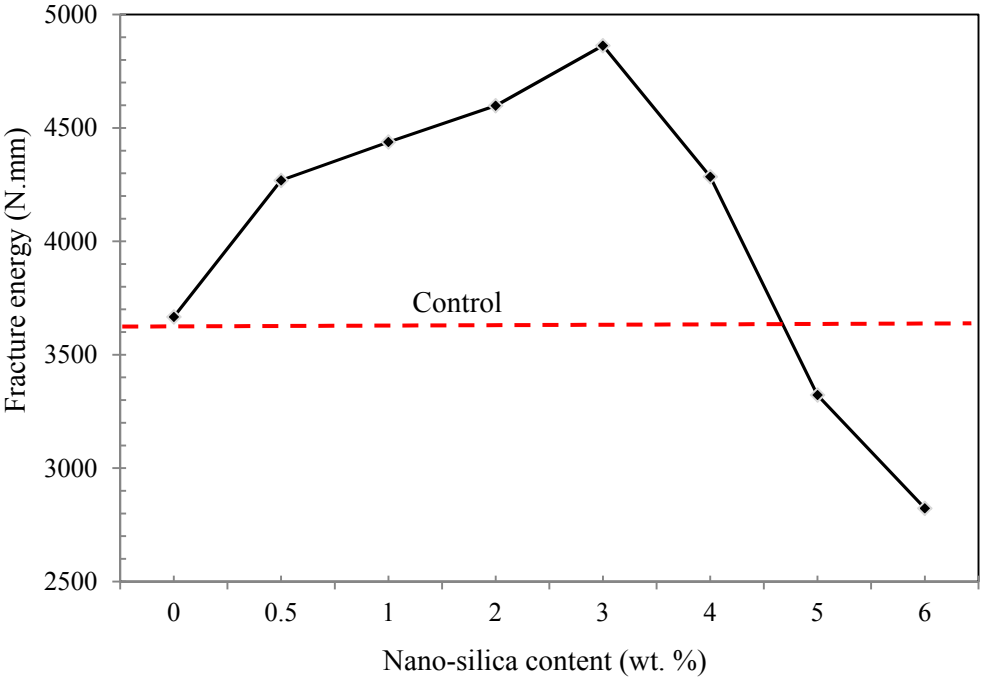

Figure 5.69: Effect of NS content on the fracture energy of cement composites (n = 3).

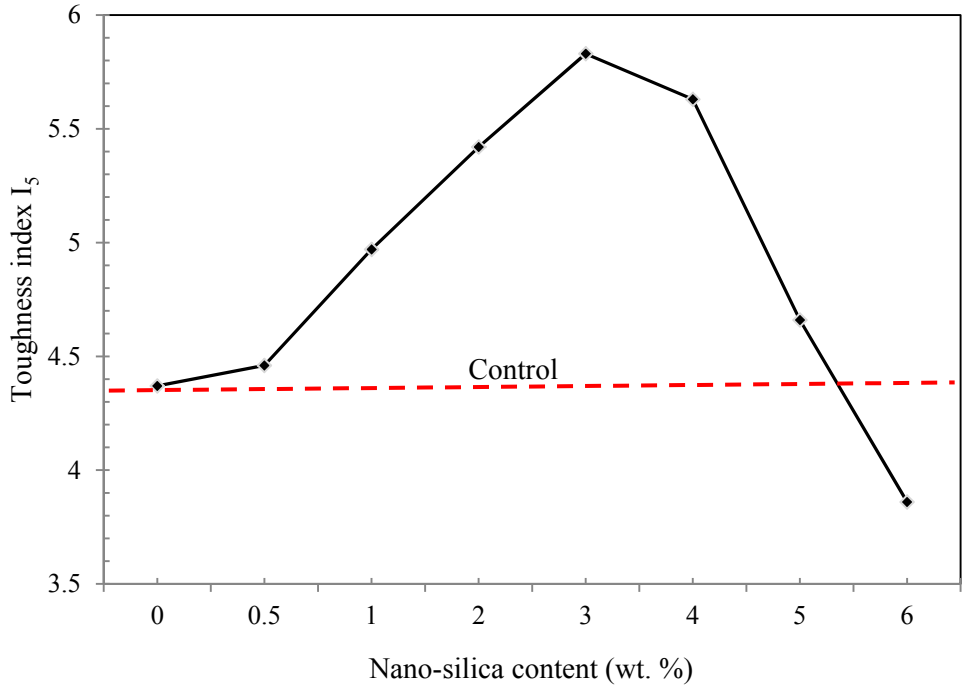

Figure 5.70: Effect of NS content on the toughness index I_5 of cement composites (n = 3).

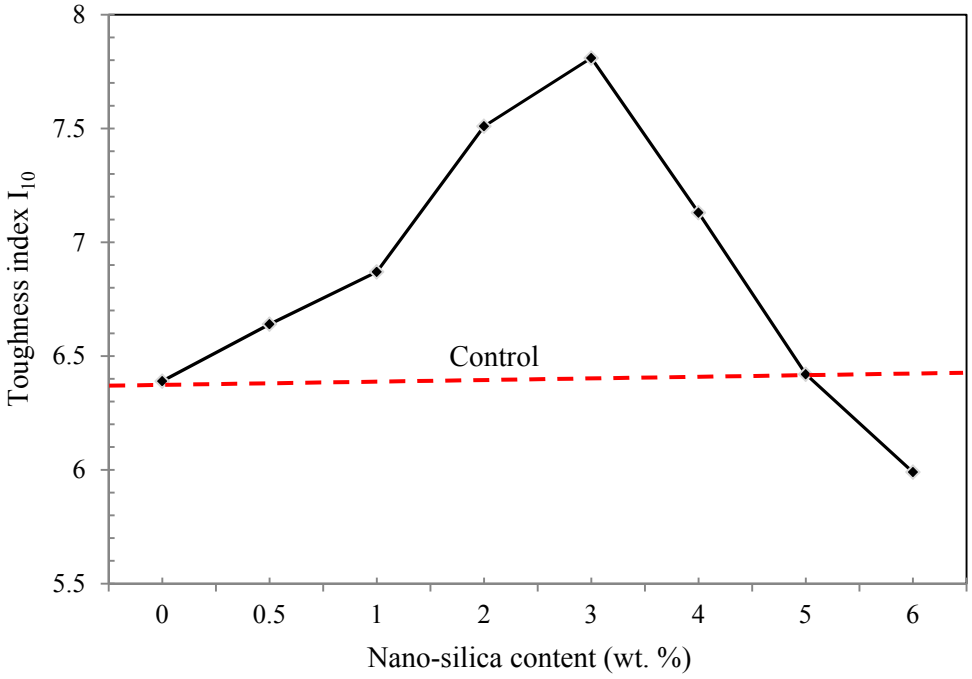

Figure 5.71: Effect of NS content on the toughness index I_{10} of cement composites (n = 3).

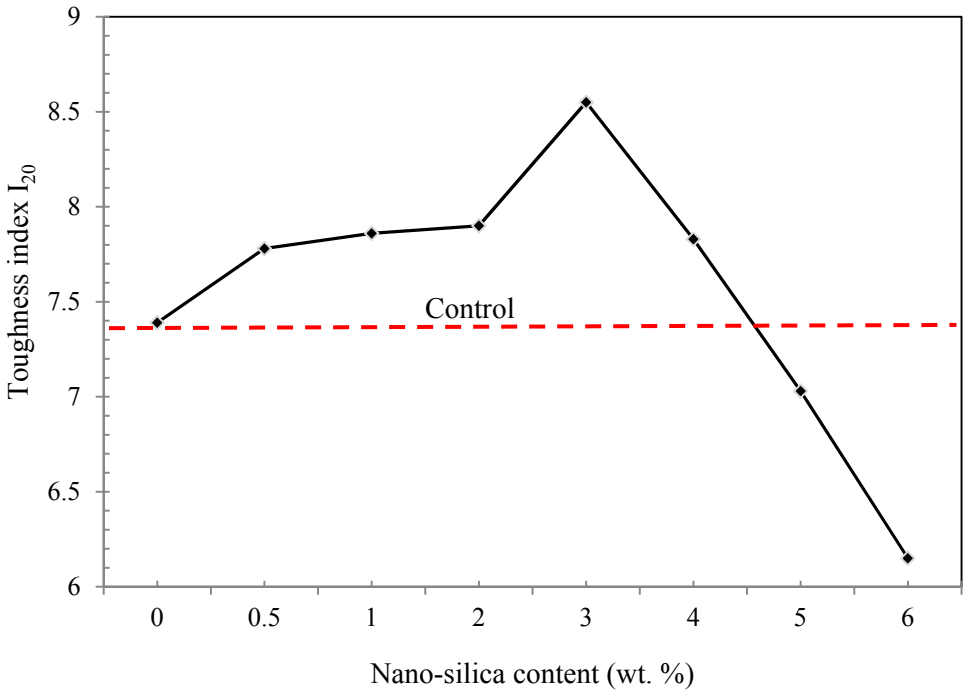

Figure 5.72: Effect of NS content on the toughness index I_{20} of cement composites (n = 3).

5.6.1.2 Porosity

Figure 5.73 and Table 5.31 show that the porosity of NS composites at 28 days of hydration is decreased by increasing the NS content up to 3.0 wt. % and after that point it increases. Once again, these increases could be due to the unsuitable dispersion of nanoparticles in the cement paste, when the content of the nanoparticles exceed 3.0 wt. %. As can be seen in the results above, the addition of NS up to 3% can lead to reductions in porosity. This is due to the high action and filler effects of NS. Another finding of this study is that the interfacial transition zone in cement composites is improved due to high reactivity, as well as the filler effect of the NS. This finding confirms the results of the study by Nazari and Riahi [21].

The mechanism through which nanoparticles improve the pore structure of cement composites can be interpreted as follows [223]: suppose that the nanoparticles are uniformly dispersed in the cement matrix and each particle is contained in a cube pattern, the distance between the nanoparticles can be determined. After hydration starts, hydrate products diffuse and envelop nanoparticles as kernels [223]. If the dosage of nanoparticles and the distance

between them are appropriate, crystallization will be controlled in a suitable state through restrictions on the growth of CH crystals by nanoparticles. Moreover, the nanoparticles located in the cement matrix, as kernels, can further promote cement hydration due to their high activity. This makes the cement matrix more homogeneous and compact. Consequently, porosity is decreased and the pore structure of the cement composite is improved [223].

By increasing the content of nanoparticles more than 3.0 wt. %, in the case of NS or 2.5 wt. % in the case of NC, the improvement of the pore structure of concrete is weakened. This can be attributed to the fact that the distance between nanoparticles decreases with an increasing content of nanoparticles, and CH crystals cannot grow up enough due to limited space and the crystal quantity is decreased. This leads to the ratio of crystal to strengthening gel becoming smaller and increases in the shrinkage and creep of the cement matrix, thus the porosity is increased and the pore structure of the cement matrix becomes relatively looser [21].

The addition of nanoparticles decreases porosity and improves the pore structure of cement composites. Nanoparticles can act as a filler that enhances the density of the cement matrix which significantly reduces the porosity of the cement composites. Nanoparticles cannot only act as an activator that accelerates cement hydration due to their high activity, but they can also act as a kernel in cement paste which makes the size of the CH crystal smaller.

The larger volume of nanoparticles reduces the mechanical performance of the cement composites due to the reduction of hydrated lime, with respect to the nanoparticles content, in addition to the deficiency that occurs during the mixing of nanoparticles in the cement composites.

The above results show that the partial replacement of OPC by 3 wt. % NS could be used to fabricate cement composites with high strengths and low porosities. Therefore, this dosage will also be used in further investigations.

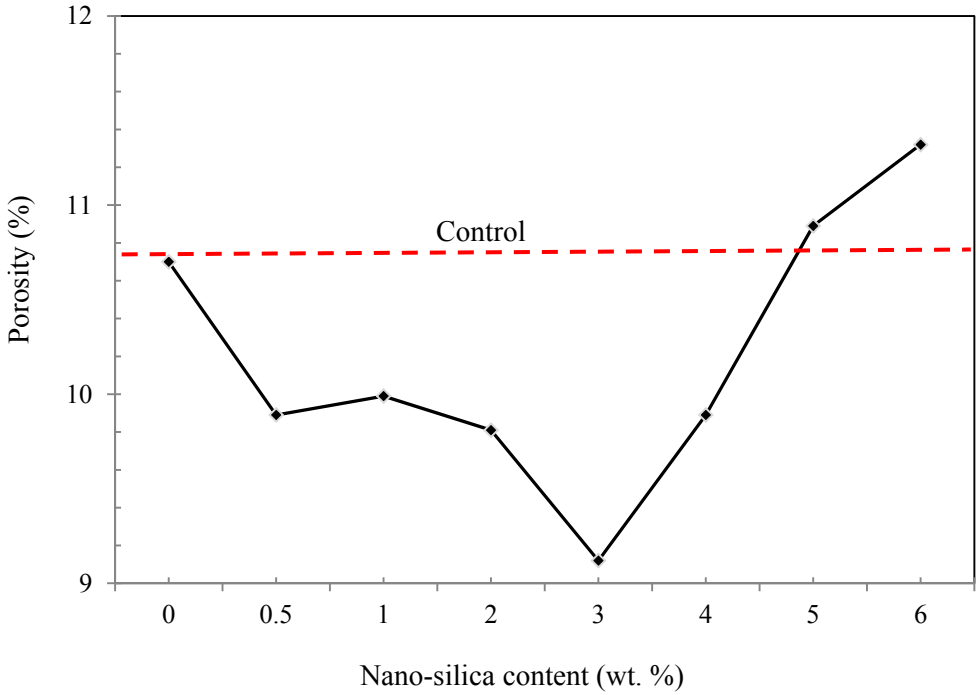

Figure 5.73: Effect of NS content on the porosity of cement composites (n = 3).

5.6.2 Hybrid Effect of Nano-silica and Waste Glass Powder

In order to study the hybrid effect of NS and WG on the behaviour of flax fibre cement composites, a range of composites were prepared based on variations in the composition listed in Table 5.32. For all of the composites an equal ratio of binder and sand was used for all the mixes and the fibre parameters that were selected were the same as the control specimen's (i.e. 30 mm length and 1% volume fraction). The water/binder ratios tested to reach a flow of 110 ± 5 in order to permit a medium workability to be used for mixing the composites. All of the composites were prepared by the producers described in section 3.3.2.3. The results obtained through this investigation of the utilisation of NS/WG as a cement replacement on the behaviour of flax fibre cement composites is summarised in the following sections.

Table 5.32: Mixture proportions used to study the effect of NS/WG on the behaviour of flax fibre cement composites

Batch	Binder material	Water/binder ratio
NSWG5	92% OPC+ 5% WG+3% NS	0.51
NSWG10	87% OPC+ 10% WG+3% NS	0.52
NSWG20	77% OPC+ 20% WG+3% NS	0.52
NSWG200	67% OPC+ 30% WG+3% NS	0.53
NSWG40	57% OPC+ 40% WG+3% NS	0.54
NSWG50	47% OPC+ 50% WG+3% NS	0.54

5.6.2.1 Mechanical Properties

As expected, the hybrid combination of NS+WG greatly improves the mechanical properties of cement composites when compared to the control, NSPC3 and WG composites, as shown Table 5.33 and Figures 5.74 to 5.80. Table 5.33demonstrates that the compressive strength of the NS/WG composites increases between 19% and 46% when compared with the compressive strength of the control composites.

Figures 5.75 and 5.76 show the flexural and impact strengths of NS/WG composites compared to those of the control, NSPC3 and WG composites. It can be seen here that NS/WG composites have about 7% and 38% higher flexural strengths, and about 8% and 32% higher impact strengths, when compared to the control composites. Figure 5.77 shows the fracture energy of NS/WG composites compared to those of the control, NSPC3 and WG composites. From these results it can be seen that the fracture energy of the NS/WG composites was about 45% to 108% higher than that of the control composites.

Figures 5.78 to 5.81 show the toughness indices I_5, I_{10} and I_{20} respectively and the results are listed in Table 5.33. From the results obtained, it can be seen that the toughness indices of the NS/WG composites are relatively higher than those of the WG composites. Although the NS/WG composites have shown a better load-

carrying capacity than the composites with only WG, its toughness indices were in some cases lower than those of the WG composite. Overall, the NS/WG composites have higher toughness indices compared to those of the WG composites. Indeed, the composites with a hybrid combination of NS+WG displayed the highest toughness indices when compared to the mixtures with only WG or NS. Similar to the NC/WG composites, mix NSWG20, which contains 20wt. % WG + 3wt. % NS, showed superior mechanical properties when compared to the control, NSPC3 and WG composites.

The higher mechanical performance of the NS/WG composites compared to WG composites may be as a result of the rapid consumption of crystalline CH which forms quickly during the hydration of OPC, particularly in the early ages as a result of the high reactivity of NS. As a consequence, the hydration of the cement is accelerated and larger volumes of reaction products are formed. Also, NS and WG recover the particle packing density of the blended cement, leading to a reduced volume of larger pores in the cement paste, thus reducing the total porosity (see the next section).

Table 5.33: Mechanical properties and porosity of flax fibre cement composites reinforced with various contents of WG at 3% NS (n = 3)

Composite	Compressive strength (MPa)	Flexural strength (MPa)	Impact strength (J/m^2)	Fracture energy (N.mm)	I_5	I_{10}	I_{20}	Porosity (%)
NSWG5	26.82	7.72	695	5343	6.25	8.41	9.93	9.23
NSWG10	27.63	8.28	704	6532	6.78	9.19	11.94	9.02
NSWG20	31.63	9.74	820	7632	7.03	10.83	13.34	8.82
NSWG30	29.36	8.41	731	7123	6.51	9.14	12.53	8.96
NSWG40	28.63	8.15	695	6984	6.18	9.07	11.82	9.41
NSWG50	25.72	7.52	675	6852	6.03	8.93	11.12	10.31

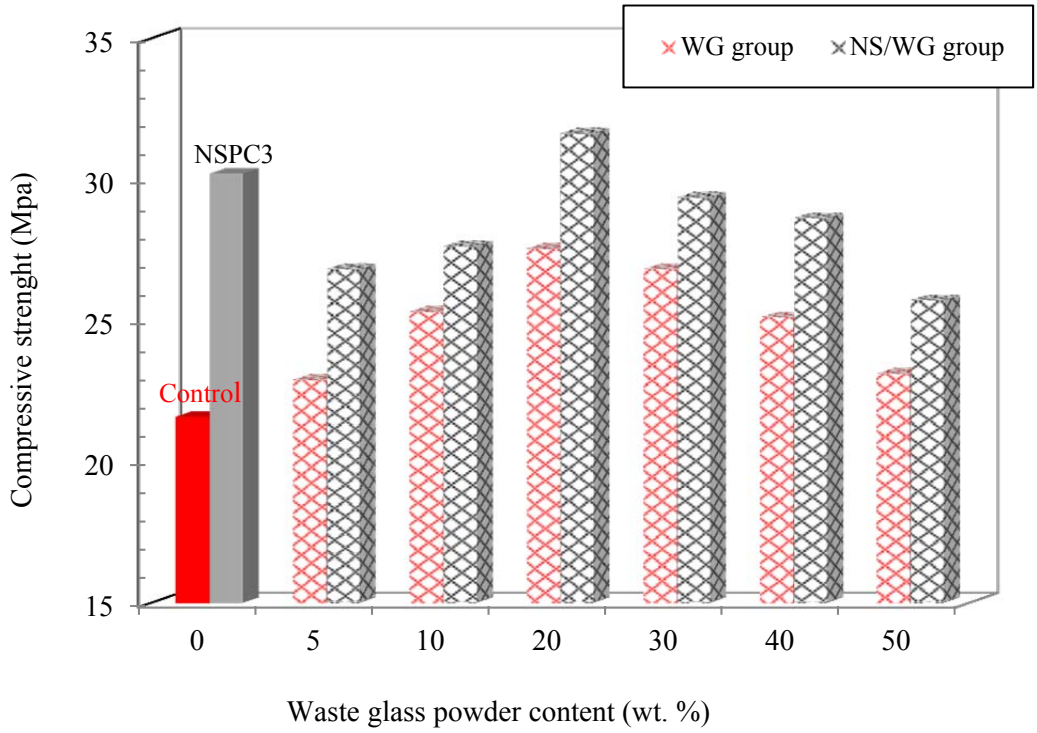

Figure 5.74: Variation of compressive strength of cement composites with different contents of WG when NS dosage is 3% (n = 3).

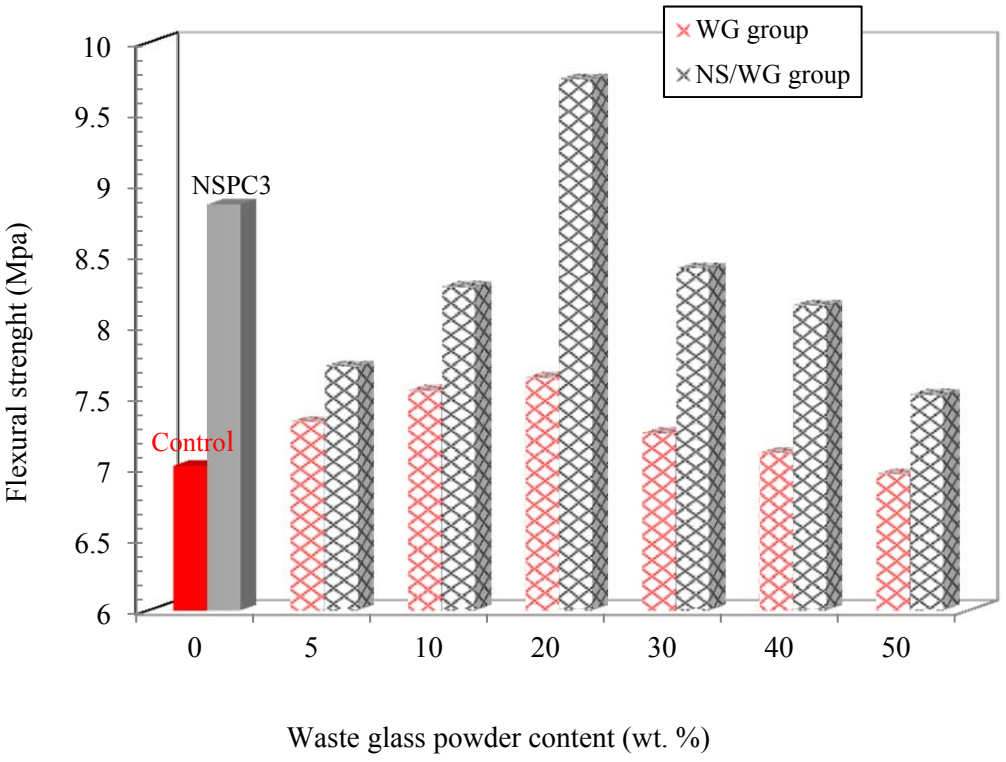

Figure 5.75: Variation of flexural strength of cement composites with different contents of WG when NS dosage is 3% (n = 3).

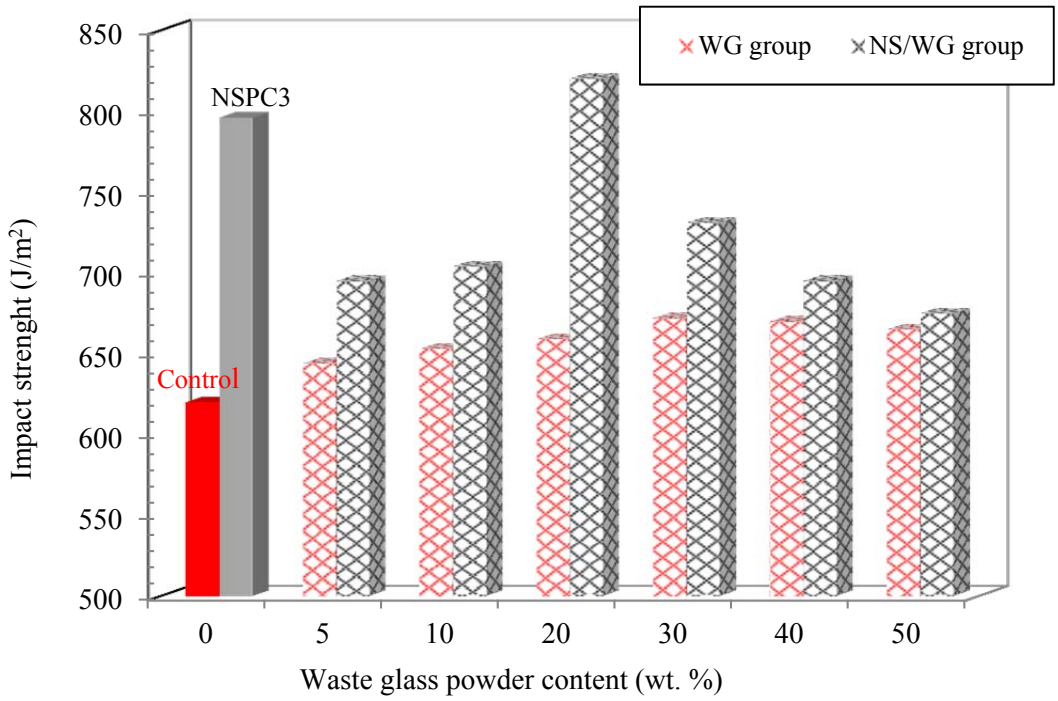

Figure 5.76: Variation of impact strength of cement composites with different contents of WG when NS dosage is 3% (n = 3).

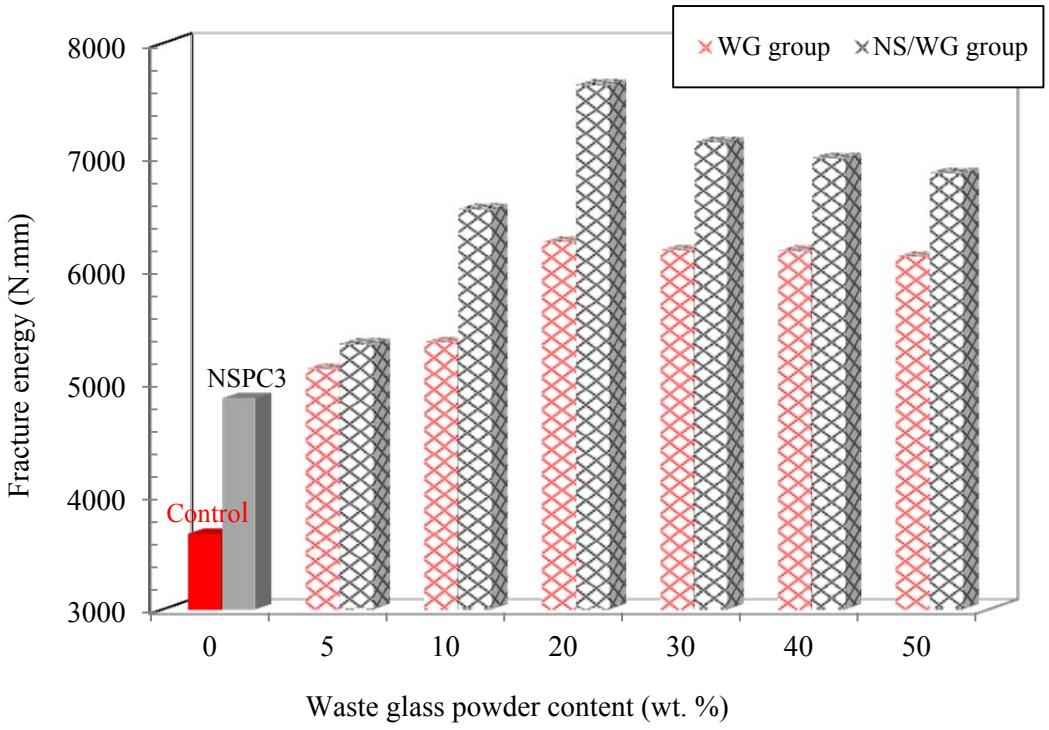

Figure 5.77: Variation of fracture energy of cement composites with different contents of WG when NS dosage is 3% (n = 3).

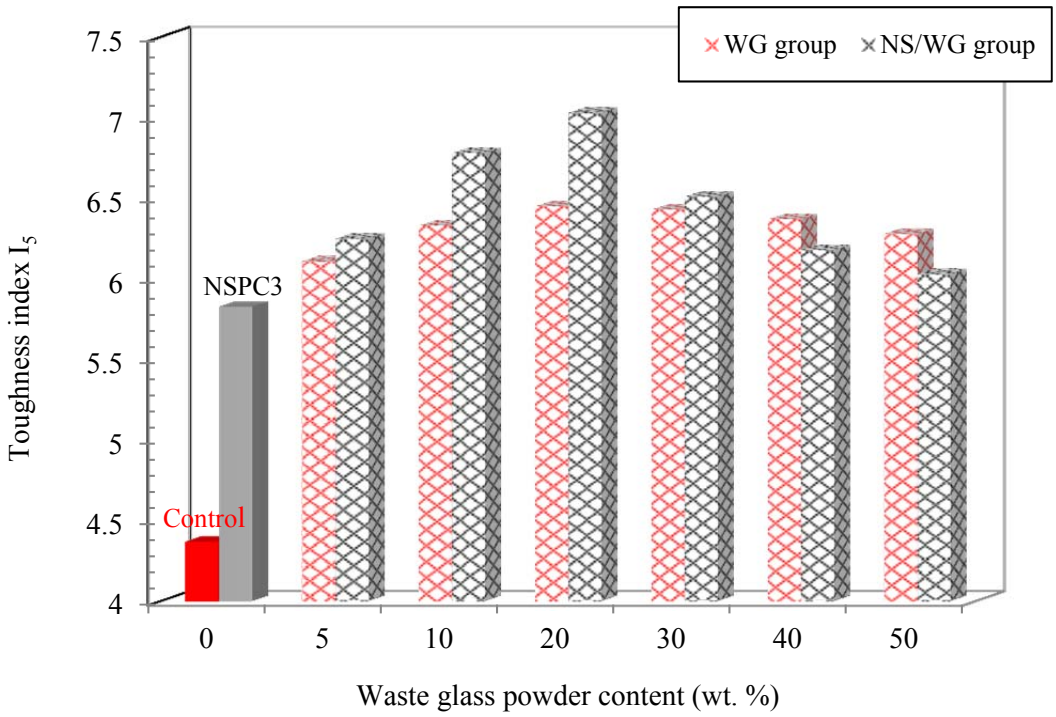

Figure 5.78: Variation of toughness index I_5 of cement composites with different contents of WG when NS dosage is 3% (n = 3).

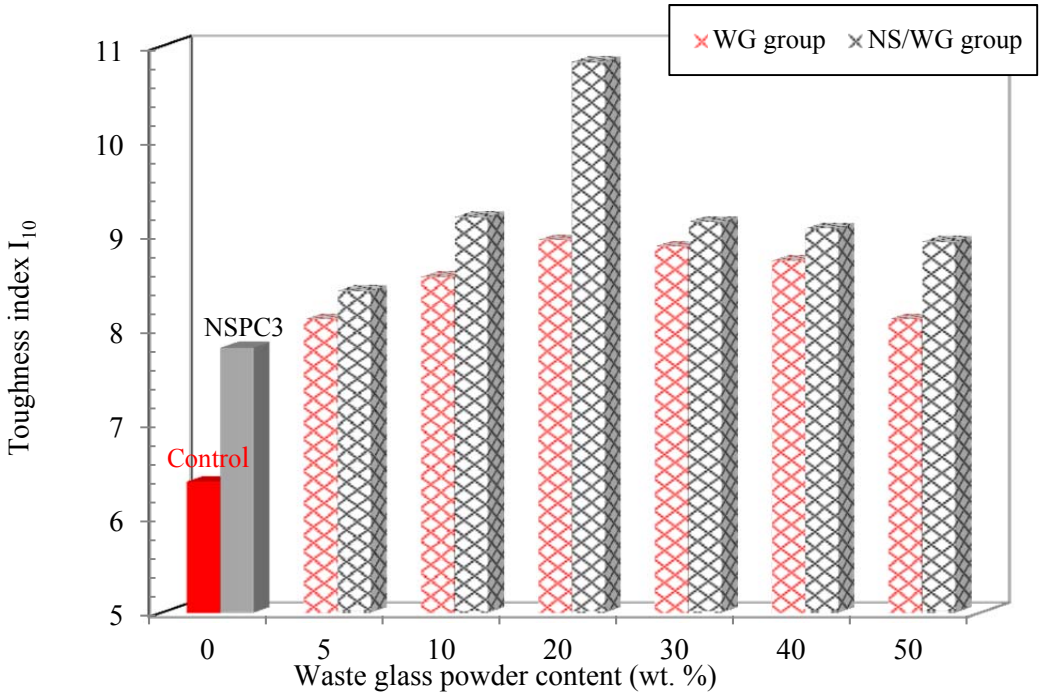

Figure 5.79: Variation of toughness index I_{10} of cement composites with different contents of WG when NS dosage is 3% (n = 3).

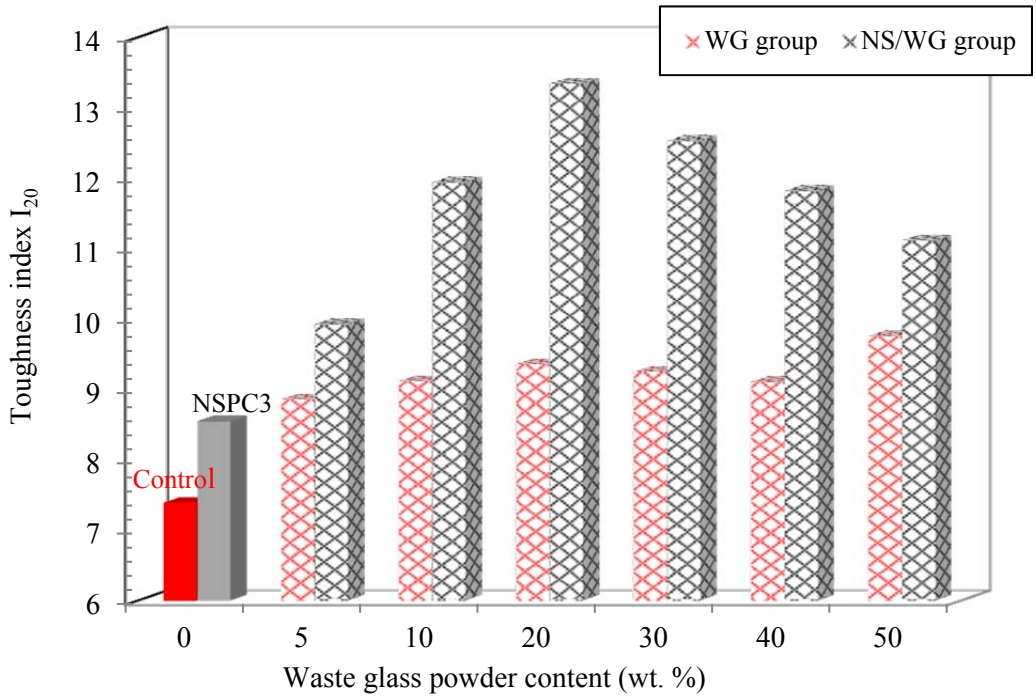

Figure 5.80: Variation of toughness index I_{20} of cement composites with different contents of WG when NS dosage is 3% (n = 3).

5.6.2.2 Porosity

Figure 5.81 and Table 5.33 show the porosity of NS/WG composites compared to those of the control, NSPC3 and WG composites. It is very obvious that the porosity of the NS/WG cement composites is lower than the control, NSPC3 and WG composites. Table 5.33 shows that the porosity of the NS/WG composites is reduced between 3% and 17% when compared with that of the control composites. The mechanism for reducing porosity by using a hybrid combination of NS+WG is the same as the one mentioned above in sections 5.5.2.2 and 5.6.1.2.

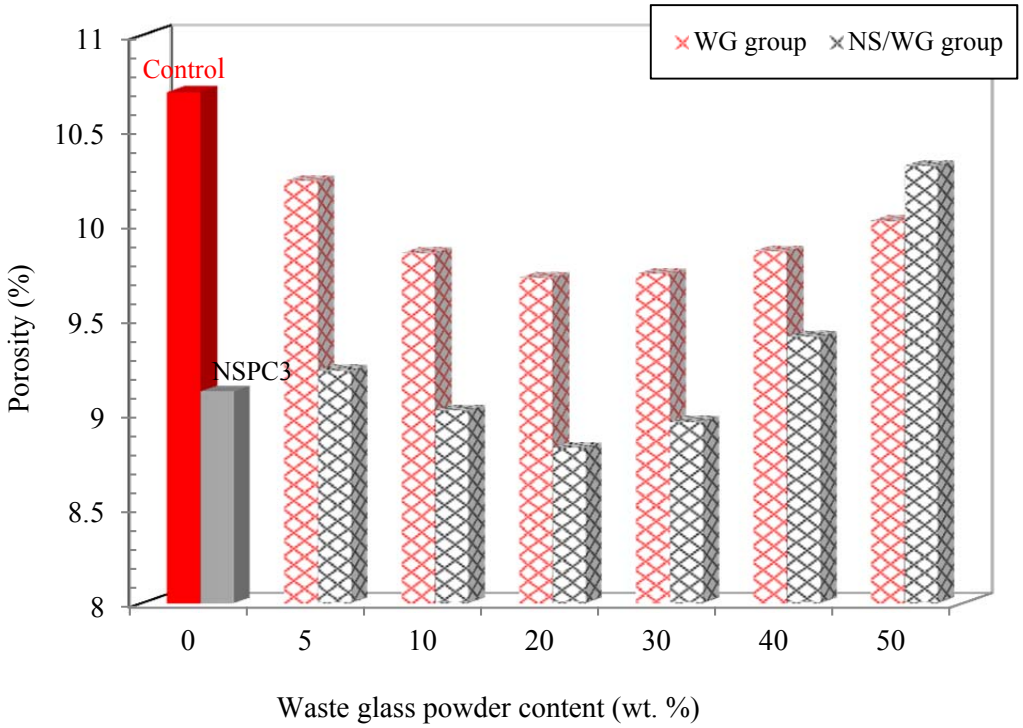

Figure 5.81: Variation of porosity of cement composites with different contents of WG when NS dosage is 3% (n = 3).

5.6.2.3 Alkali Silica Reaction

Figure 5.82 shows the expansions in the mortar bars containing different ratios of WG/NS. Evidently, all of the specimens had expansions of less than 0.2% and, therefore, according to ASTM C1260, the expansions were within accepted limits. Furthermore, the incorporation of NS in WG composites introduces further reductions in expansion. Note that the replacement of OPC with 20% WG + 3% NS (i.e. NSWG20) significantly reduced expansion. One possible explanation is that the pozzolanic reaction between NS and CH results in a remarkable decrease in the total porosity, as explained in the previous section, which leads to a reduction in water penetration [224]. As a result, the gel that formed during ASR does not swell and expansion can be prevented. Also, it should be noted that binary blends containing WG and NS are more effective in reducing ASR expansion than either of the replacement materials separately.

From a perusal of the test results, it can be seen that the replacement of OPC by 20 % WG +2.5% NC or +3 % NS (i.e. NCWG20 and NSWG20) limits the expansion to less than 0.10%. It has been recommended that if the ASR expansions

of mortar bars are less than 0.10% at the end of 14 days when they are evaluated per ASTM C 1260 [175], they are more likely to meet the ASTM C 1293 [225] expansion criteria of 0.04% for concrete prisms after two years [226].

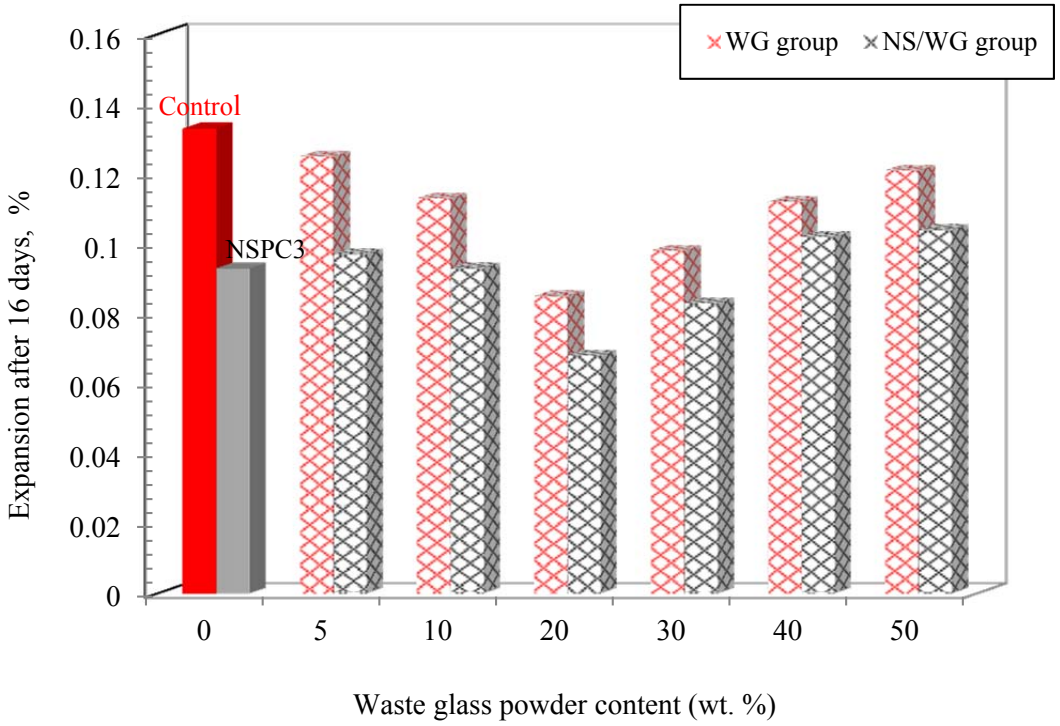

Figure 5.82: ASR test results of cement composites at 3 % NS and different contents of WG (n = 3).

As the above results show, the use of hybrid systems of NC+WG or NS+WG, known as multimodal systems, has led to a significant enhancement of mechanical properties when compared to mono-modal systems (using WG, NS or NC separately). It seems that NC and NS behave not only as a filler to refine the microstructure, but also as an activator that accelerates the pozzolanic reaction and activates WG, due to the large and highly reactive surface of nanoparticles [24,25,227]. These results are further reinforced in sections 5.7.2-4 by DTA/TGA analysis, XRD patterns and SEM micrographs of the cement composites after 28 days of hydration. In fact, the improvements in the mechanical properties of waste glass cement composites due to the addition of nanoparticles can be explained by two mechanisms. The first is the chemical effect, which works on two levels [20]:

- Accelerating the dissolution of C_3S and the rapid formation of the C-S-H phase in the cement paste; and

- The pozzolanic reaction of nanoparticles and glass powder with CH generates additional C-S-H gel in the final stages.

The second mechanism is the physical effect; nanoparticles and glass powder can fill the remaining voids in young and partially hydrated cement paste, which leads to a denser and more compact structure.

5.7 Multimodal and Mono- modal Flax Fibre Composites

A hybrid composite or multimodal composite is defined as two or more different types of materials that are combined to produce a composite which derives benefits from each of the individual materials and exhibits a synergistic response [206,209,228,229]. In order to evaluate the benefits obtained when using a mix of WG/NC or WG/NS, post cracking behaviour analysis, thermal gravimetric analyses (DTA/TGA), thermal behaviour analysis, X-Ray diffraction (XRD) and scanning electron microscopy (SEM) was performed on both the multimodal (i.e. NCWG20and NSWG20) and mono- modal (i.e. WG20, NCPC2.5 and NSPC3) flax fibre composites.

5.7.1 Post Cracking Behaviour

The load–deflection behaviour of the control specimens and the typical behaviour of WG20, NCPC2.5, NSPC3, NSWG20 and NCWG20 are shown in Figure 5.83 In fact, the behaviour of the specimens under flexural loading can be classified into the three categories as seen in Figure 5.83.

Type I behaviour (Figure 5.83, a) is exhibited by the NCPC2.5 and NSPC3 (mono- modal), where the first peak is followed by a drop in load and then a short plateau. As can be seen, the incorporation of nanoparticles has led to an improvement of the post-peak behaviour of the composites when compared to the control composite.

Type II behaviour (Figure 5.83, a) showed by the WG20 (mono- modal), where the first peak is followed by a drop in load and then a long plateau. This type of behaviour confirms, as stated above, the important contribution of the WG to significant improvements in the post-peak behaviour of the cement matrix. Although the flexural strengths of the NCPC2.5 and NSPC3 were higher than WG20, the

fracture energy of WG20 was about 39% and 28% higher than that for the NCPC2.5 and NSPC3. These results can be explained by the filler effect of glass powder, which provides higher ductility for the composites with respect to the NCPC2.5 and NSPC3. Also, the pozzolanic reaction of glass powder has a two-fold benefit. It produces calcium silicate hydrates and calcium aluminate hydrates and it consumes calcium hydroxide, which weakens the matrix-fibre interfaces.

Type III behaviour (Figure 5.83, b) could be considered as a specificity of the multimodal composites containing a mix of WG as well as the nanoparticles (NS and NC) where the post-peak load-carrying capacity and the toughness improvement are more pronounced when compared to that of the mono-modal system. A key feature of the load–deflection curves was a characteristic of strain hardening and multiple cracking (propagation of several cracks). This behaviour may be explained by the densification of the microstructure caused by cement hydration at early ages and at later ages and a subsequent reduction in porosity. The effect of densification in the fibre/matrix interface is an increase in fibre/matrix mechanical interaction, which accounts for the significant increase in strength that was observed in NCWG20 and NSWG20.

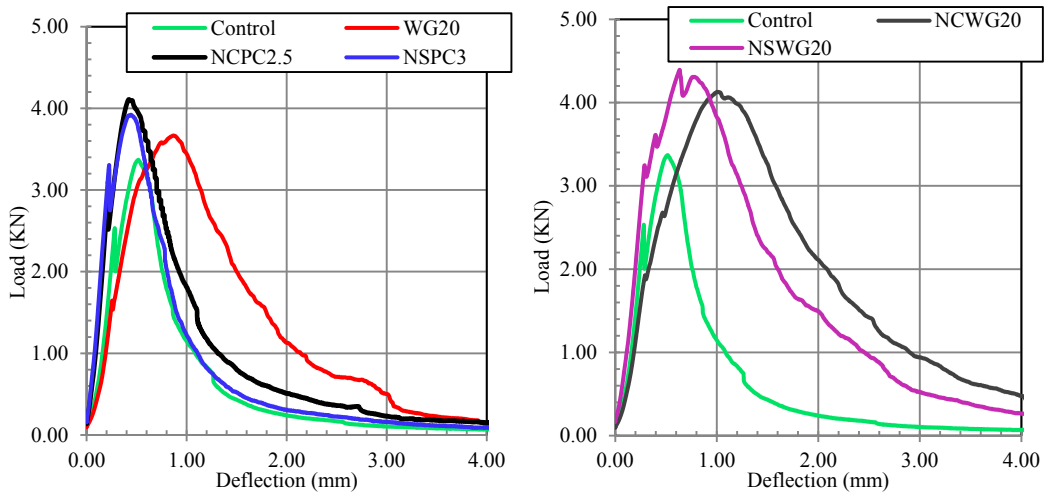

(a) (b)

Figure 5.83: Load-deflection curves of (a) mono-modal and (b) multimodal composites (n = 3).

5.7.2 TGA and DTA

Figure 5.84 shows the DTA/TGA profiles of the control, WG20, NCPC2.5, NSPC3, NCWG20 and NSWG20 specimens. The DTA/TGA curves show the typical reactions occurring in the cement composite when it is subjected to a progressive temperature increase from room temperature up to 1000ºC. The DTA/TGA curves of the specimens show three main endothermic peaks. The first peak was observed between 60-110ºC, corresponding to the mass loss on the TGA curve up to 110, which can be attributed to the gradual departure of the bound water in some hydrates like C-S-H and ettringite [153,154,230,231]. The second endothermic peak was detected at about 475 ºC and represents a new loss in mass starting around 410ºC, which corresponds to the de-hydration of CH. As a result the Portlandite decomposes into free lime (dehydroxylation) at ≈ 450-550ºC [153,154,176,232]. The third peak was observed at ≈ 765–785ºC, which occurs due to the decomposition of calcium carbonate and the escape of CO_2 from the cement matrix [28,152,153,176]. No peak related to the decomposition of the flax fibres was detected, which was probably due to its low content (less than 1.5% of the total weight).

As Figure 5.84 shows, the DTA/TGA profiles of NCWG20 and NSWG20 indicate a strong increase in the first peak, which is related to C-S-H formation, when compared to the control specimen in Figure 5.84. Conversely, the second peak, which is related to the decomposition of CH, appears to be considerably smaller than the same peak of the control specimen. This increase in C-S-H at the cost of CH can be attributed to the consumption of CH by the pozzolanic reaction. This correlates with the remarkable increase in the compressive strength when WG and NC or NS particles were used to replace part of the OPC. Also, it should be mentioned that the DTA/TGA profiles of WG20, NCPC2.5 and NSPC3 show an increase in C-S-H and a decrease in the CH peak in comparison to the control specimen, which confirms the increase in the compressive strength of these specimens when they are compared to control specimens.

Variations between the CH content of the control specimen, WG20, NCPC2.5, NSPC3 NCWG20 and NSWG20 are shown in Figure 5.85. The CH consumed was calculated according to Eq. 3.1. The results indicated that when

WG/NC or WG/NS were used as a partial substitute for OPC, a drop in the average value of CH content was seen from 5.13 % (control) to 1.17% and 1.47 respectively. When WG was only used as a partial substitute for OPC, a lower CH consumption was seen for the same amount of replacement (a reduction of the CH content from 5.13% to 2.15%).

As shown in Figure 5.85, the CH content decreases by adding WG as a cement replacement, which indicates the consumption of CH in the pozzolanic reaction after 28 days of hydration. The reduction of CH content is much greater when NC or NS are loaded in NCWG20 and NSWG20, which indicates more pozzolanic reaction in the WG cement matrix. Also, it can be seen that the CH content of NCPC2.5 and NSPC3 is almost the same as that of WG20. As can be seen in Figure 5.85, a good correlation is found in both the TGA and DTA techniques.

From the earlier discussion it can be inferred that, when a small quantity of the NC or NS is well dispersed in the WG cement matrix, the hydrated products of cement are deposited on the nano-particles due to their greater surface energy, i.e. they act as nucleation sites. Nucleation of hydration products on nano-particles further accelerates the pozzolanic reaction and the hydration process [24,25], which is confirmed by the XRD results and the SEM micrographs.

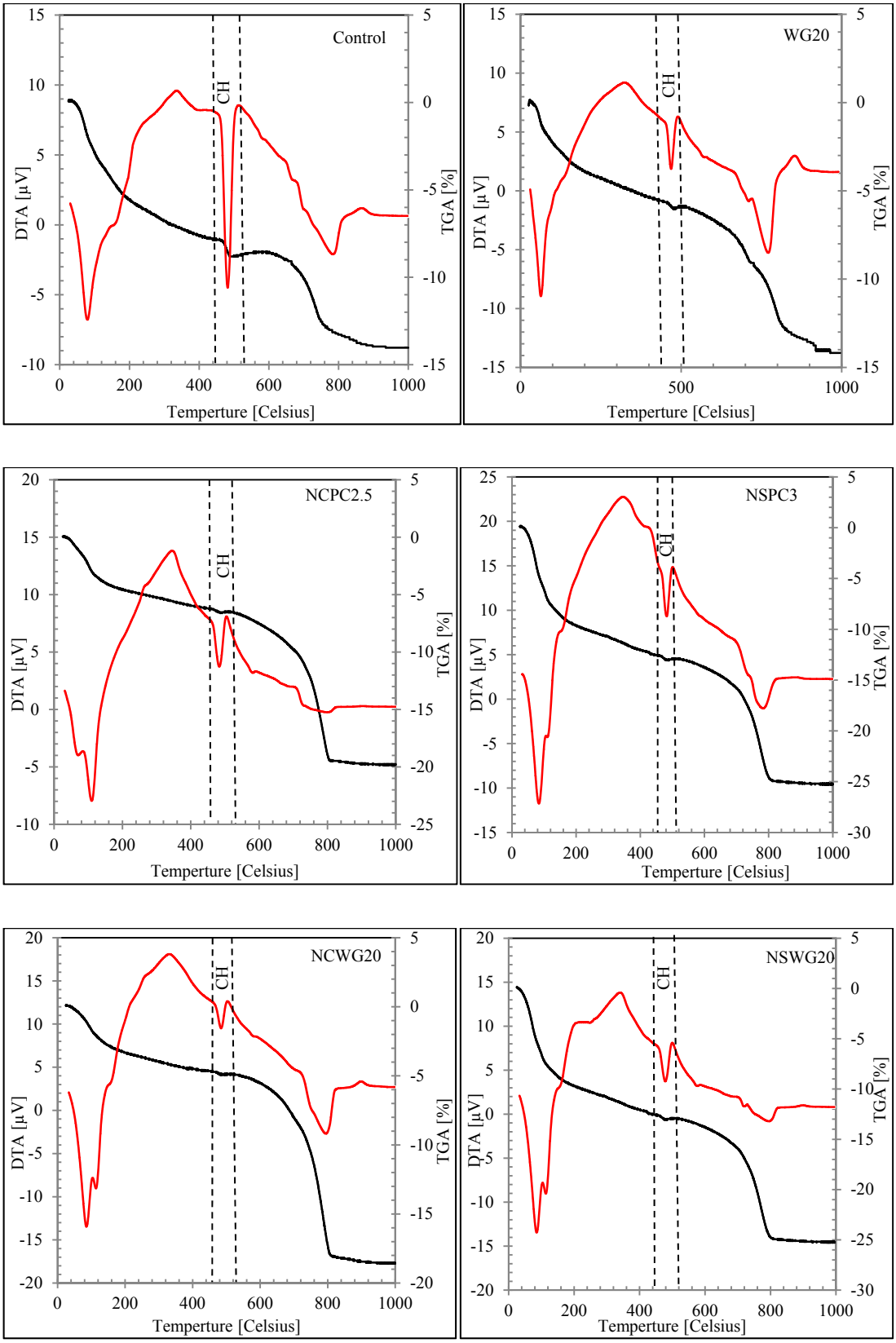

Figure 5.84: DTA/TGA profiles for cement composites after 28 days of hydration.

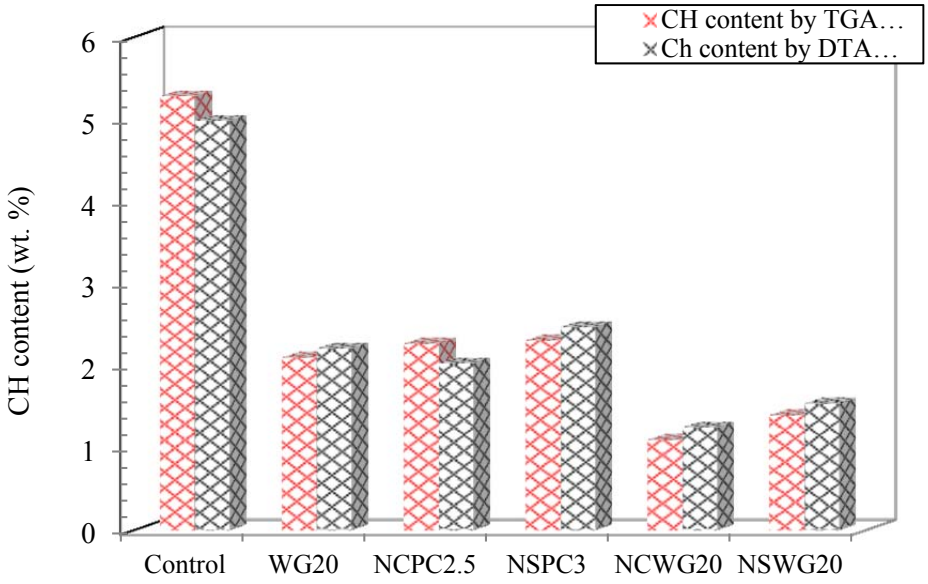

Figure 5.85: CH content for cement composites as measured by TGA and DTA methods.

5.7.3 XRD

XRD analyses were conducted to investigate the mineralogical composition of the cement composites after 28 days of hydration. For comparison, the peak of CH at 18º (2θ) and the peak of C-S-H at 28.6º (2θ) were selected [25,230]. As shown in Figure 5.86, a sharp peak in CH is observed in the control mix which represents the pure hydration product (CH) that is released from the hydration of cement. Evidently, the intensity of the CH peak is decreased in mixes WG20, NCPC2.5 and NSPC3 and is significantly reduced in mixes NCWG20 and NSWG20, which reflects the consumption of CH by pozzolanic reaction. On the other hand, the intensity of the C-S-H peak significantly increased in mixes NCWG20 and NSWG20 when compared to the control mix, which agrees with the DTA/TGA results in the previous section. As a result, the XRD results confirm the improvement in the mechanical properties of mixes NCWG20 and NSWG20 when they are compared to the control mix.

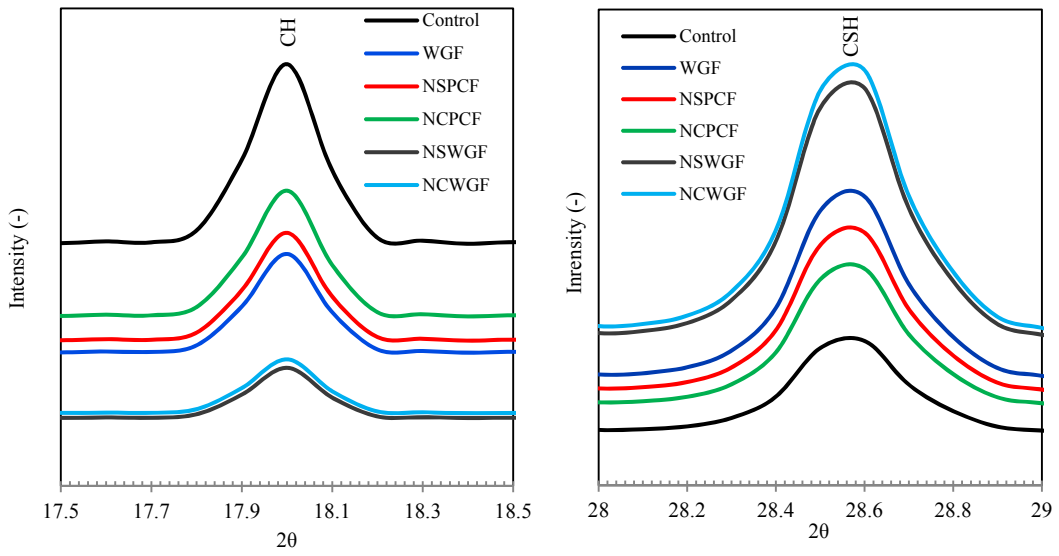

Figure 5.86: XRD pattern for cement composites.

5.7.4 Scanning Electron Microscopy (SEM)

Scanning electron microscopy (SEM) and energy-dispersive X-ray (EDX) analysis were carried out in order to study the influence of WG, NC and NS on the microstructure of the cement matrix. The locations of the EDX analyses are marked on each SEM image. Additions of WG, NC and NS were found to influence the manner of hydration and resulted in differences in the microstructures of hardened cement systems. Figures 5.87 to 5.95 show the microstructure of the cement pastes of the control, WG20, NCPC2.5, NSPC3, NCWG20 and NSWG20 specimens respectively after 28 days of hydration.

Figure 5.87 shows the typical composition of hydrated paste in the control specimen. Evidently, the microstructure of the control specimen showed the existence of C–S–H gel in the form of 'stand-alone' clusters, which were lapped and connected together by many needle hydrates. Also, it can be seen that the calcium hydroxide (CH) crystals and air voids between the hydrated phases were distributed throughout the cement matrix.

The SEM micrographs obtained for the NCPC2.5 and NSPC3 are show in Figures 5.88 and 5.89 respectively. It can be seen that the microstructure of the NCPC2.5 and NSPC3 pastes are shown by the amorphous gel filling the spaces

between the hydrated particles; this gives stability to the structure. Also, the texture of the hydrate products was more dense and compact. Furthermore, big crystals such as CH were absent. Also, the pastes were found to have been slightly enriched with silica. Obviously, the pozzolanic reaction of NC or NS with the CH liberated during hydration produced additional C-S-H gel which leads to an improvement in mechanical properties of blended mortar.

The SEM micrographs of composites containing WG, i.e. WG20, NCWG20 and NSWG20, are shown in Figures 5.90 to 5.95. SEM shows that the glass particles are well dispersed in the paste, resulting in a dense and compact structure, as shown in Figures 5.90 to 5.92. There is a visible densification around the glass grains, possibly due to the partial hydration of glass particles, leading to the formation of additional C-S-H. Also, the glass particles are well connected to the matrix and are coated with a thin layer of the reticulated gel of C-S-H (as illustrated by Figures 5.93 and 5.94). For WG20, the matrix was found to have been enriched with silica (see Figure 5.90). Also, the composition of the paste in NCWG20 showed enrichment in silica, and the assimilation of fine glass particles into the paste was clearly noted (Figure 5.93). This feature was also noted in NSWG20 (Figure 5.95). The enrichment of the paste with Si would greatly increase its capacity to bind K and Na ions, which would not allow the alkali ions to remain in the solution to react with the reactive particles.

Occasional round particles in NSWG20 and NCWG20 appeared to have reacted in the mortar (Figures 5.93, 5.94 (site 1) and 5.95), but the reaction product had small amounts of Na and large amounts of Ca. The compositions mentioned above were different from those of unreacted or partially reacted glass (Figure. 5.94, site 3), and may reflect the composition of the pozzolanic reaction product. The small elongated crystals may be ettringite or some other calcium sulfoaluminate, as indicated by the sulphur peak in the EDX spectrum (Figure 5.94, site 2). Many other sites also showed relics of fine WG particles which were evidently consumed by the paste.

The investigation of the pastes based on NC or NS showed that the glass particles are coated with amorphous reaction rims (Figures 5.93 and 5.95). In the C-S-H phase, the matrix was found to be richer in silica than pastes that only had

WG. The glass grains are partially covered by the thicker and denser reaction rims. A further encapsulation of glass grains into hydration products was also observed.

Needle-shaped crystals were also noted at some sites of the pozzolanic reaction of WG and NC in NCWG20 (Figure 5.94, site 2), where large amounts of alkali were retained. It is possible that the reaction of glass can ultimately lead to the formation of a poorly crystalline Na-bearing phase and this may be another reason why the Na content of glass did not contribute to ASR expansion.

Overall, the SEM/EDX examination showed no deleterious reaction of WG in the mortar mixes due to an insufficient alkali content in the concrete and because WG did not contribute alkali to the pore solution. Evidence for this was noted from features such as those seen in Figures 5.93 to 5.95, in which glass powder particles appear to have been assimilated into the mortar without forming deleterious ASR gel, and also from the observation that larger glass particles were free of alkali attack and ASR gel did not form in the mortar. Moreover, SEM/EDX observations suggested that the alkali originally contained in the glass was bound in the paste and crystalline materials that resulted from the pozzolanic reaction of WG such that it may no longer have been available for reaction with reactive glass particles.

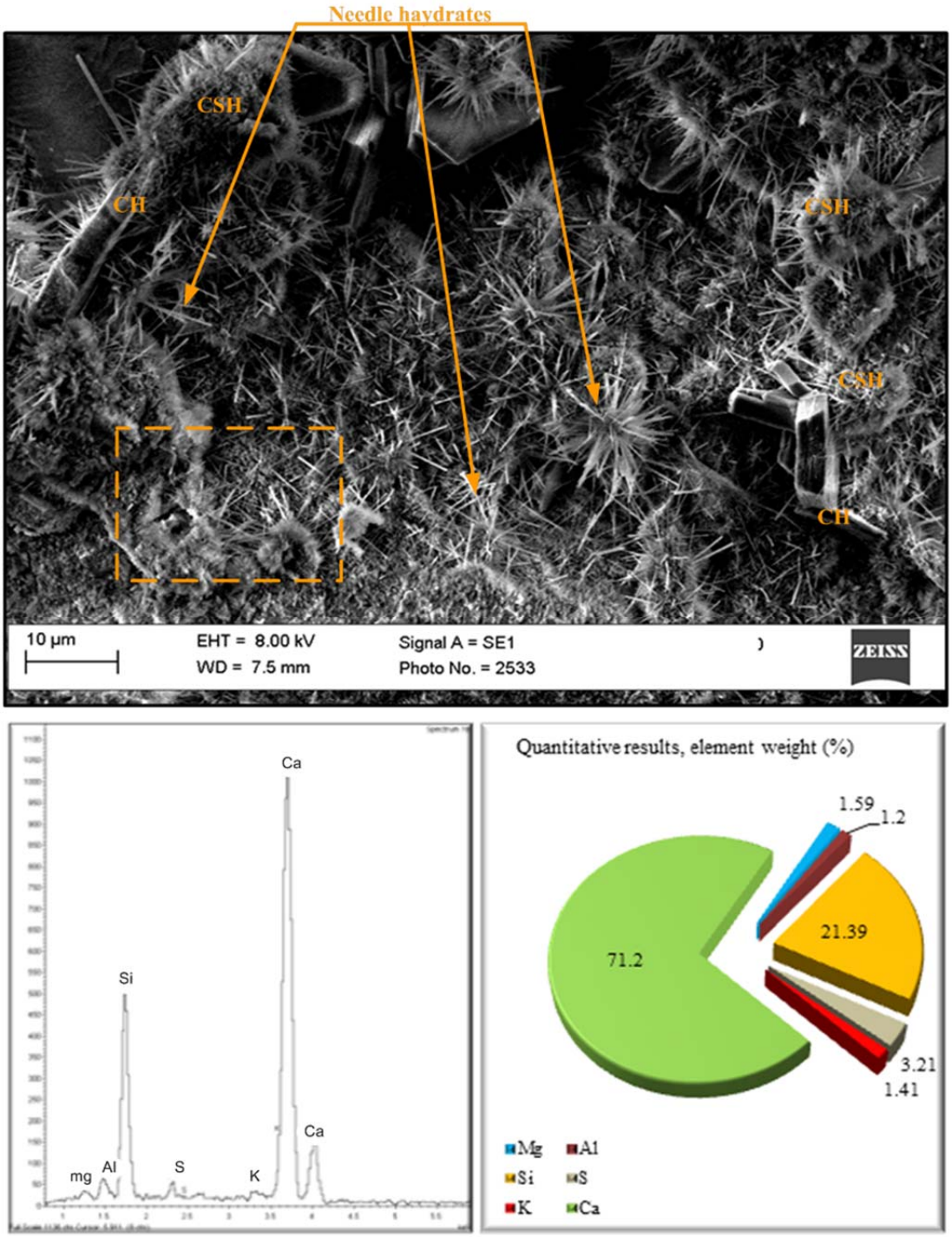

Figure 5.87: Microstructure of control specimen.

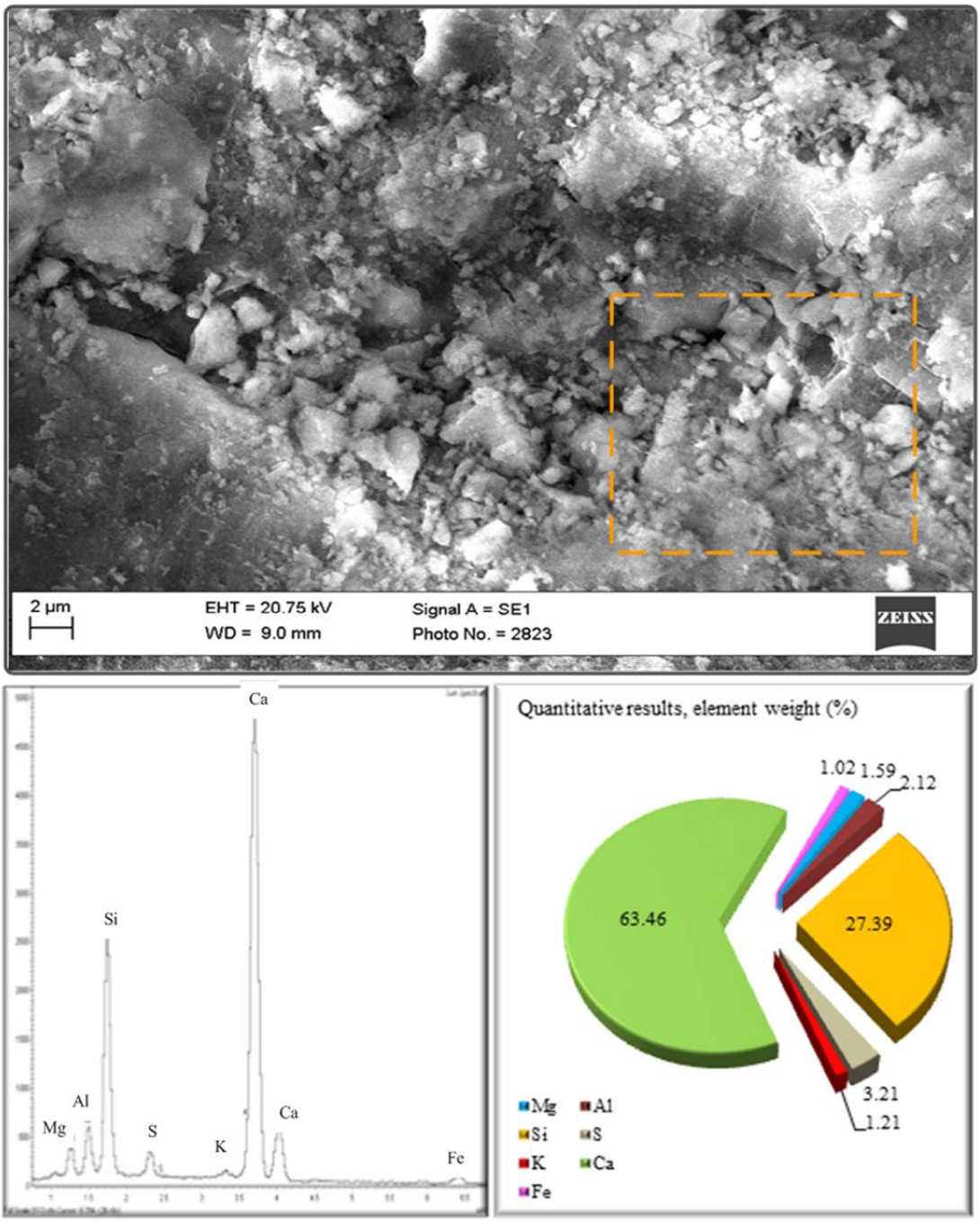

Figure 5.88: Microstructure of NCPC2.5 specimen.

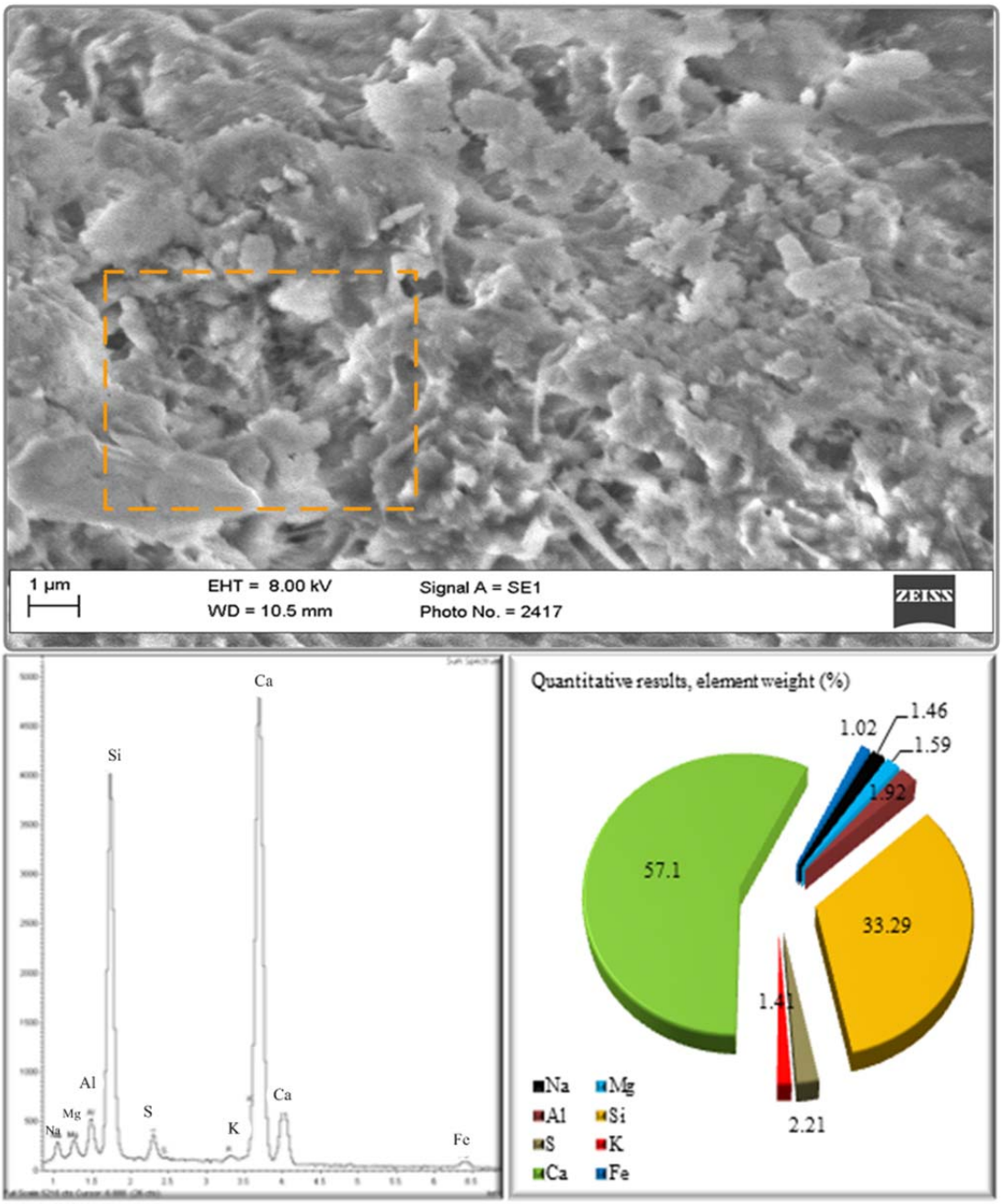

Figure 5.89: Microstructure of NSPC3 specimen.

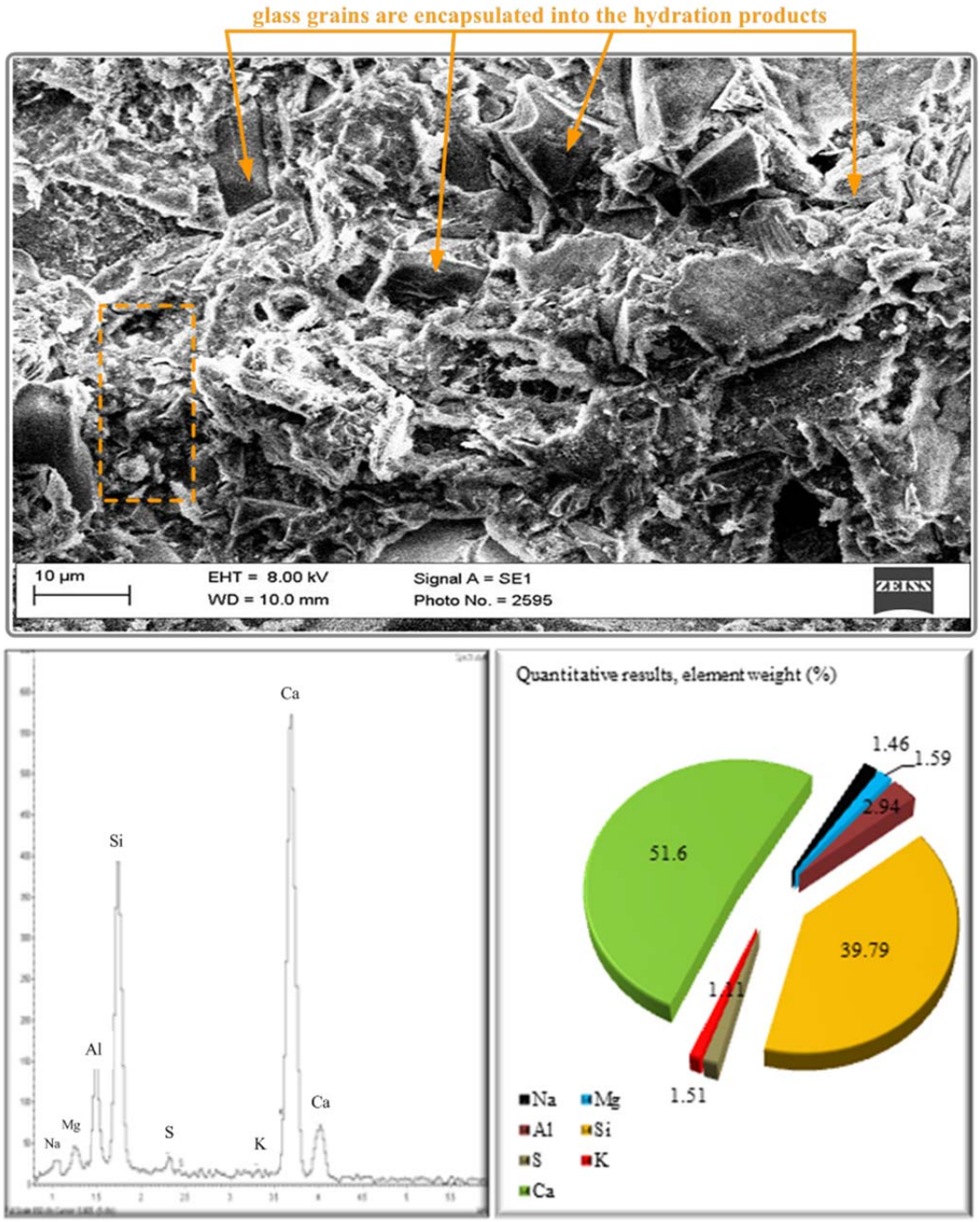

Figure 5.90: Microstructure of WG specimen.

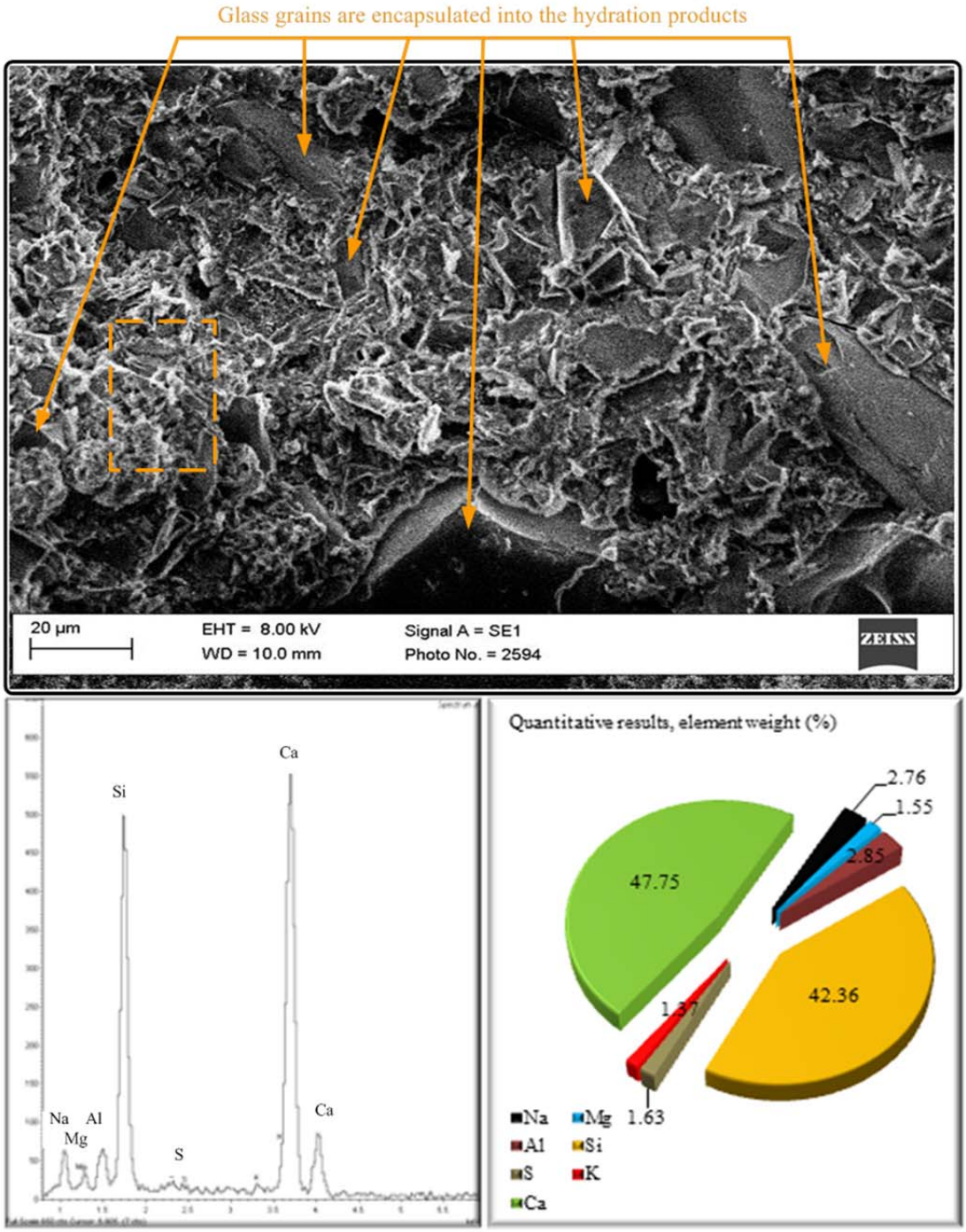

Figure 5.91: Microstructure of NCWG20specimen.

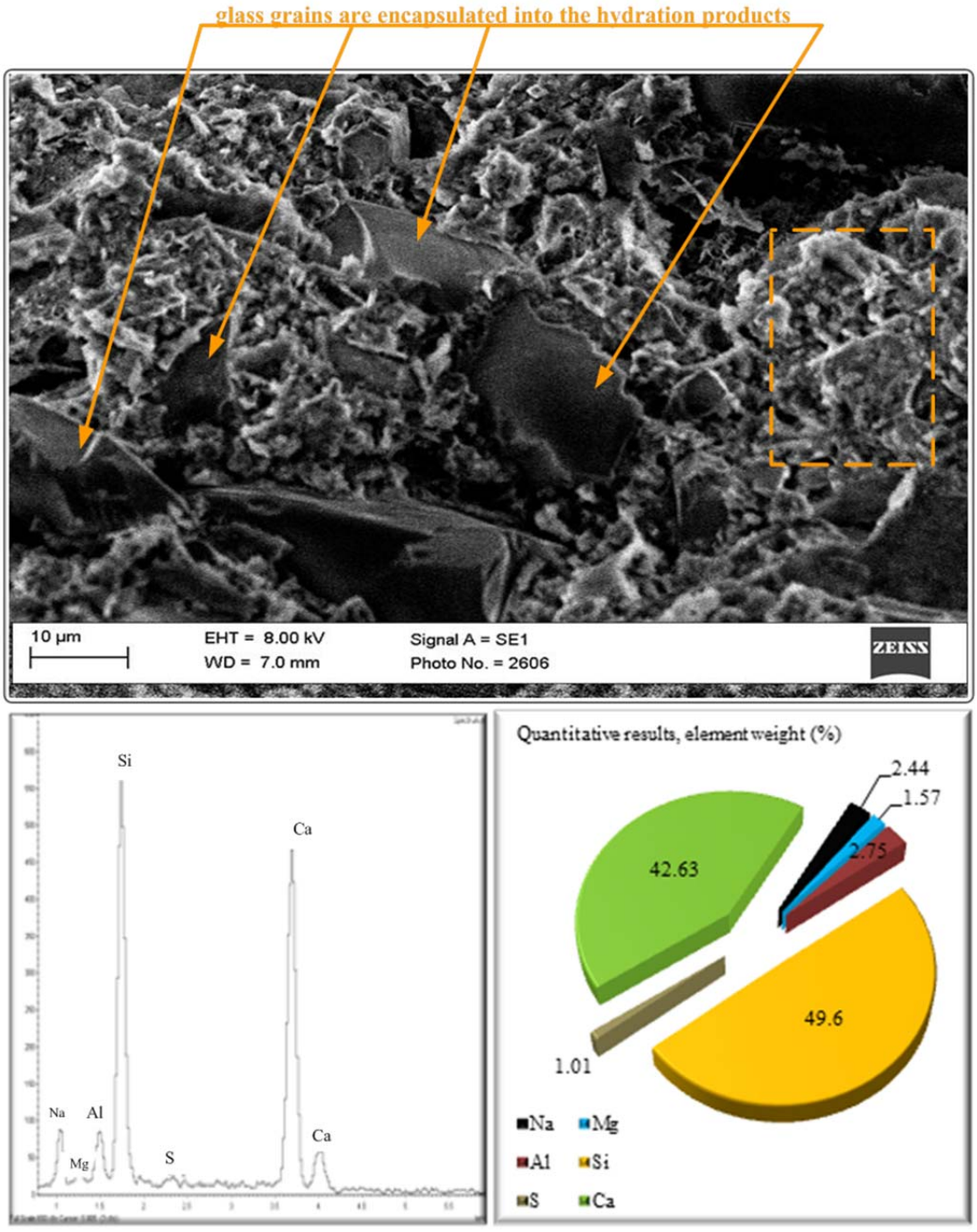

Figure 5.92: SEM micrograph showing the showing the hydration of glass grains in NSWG20.

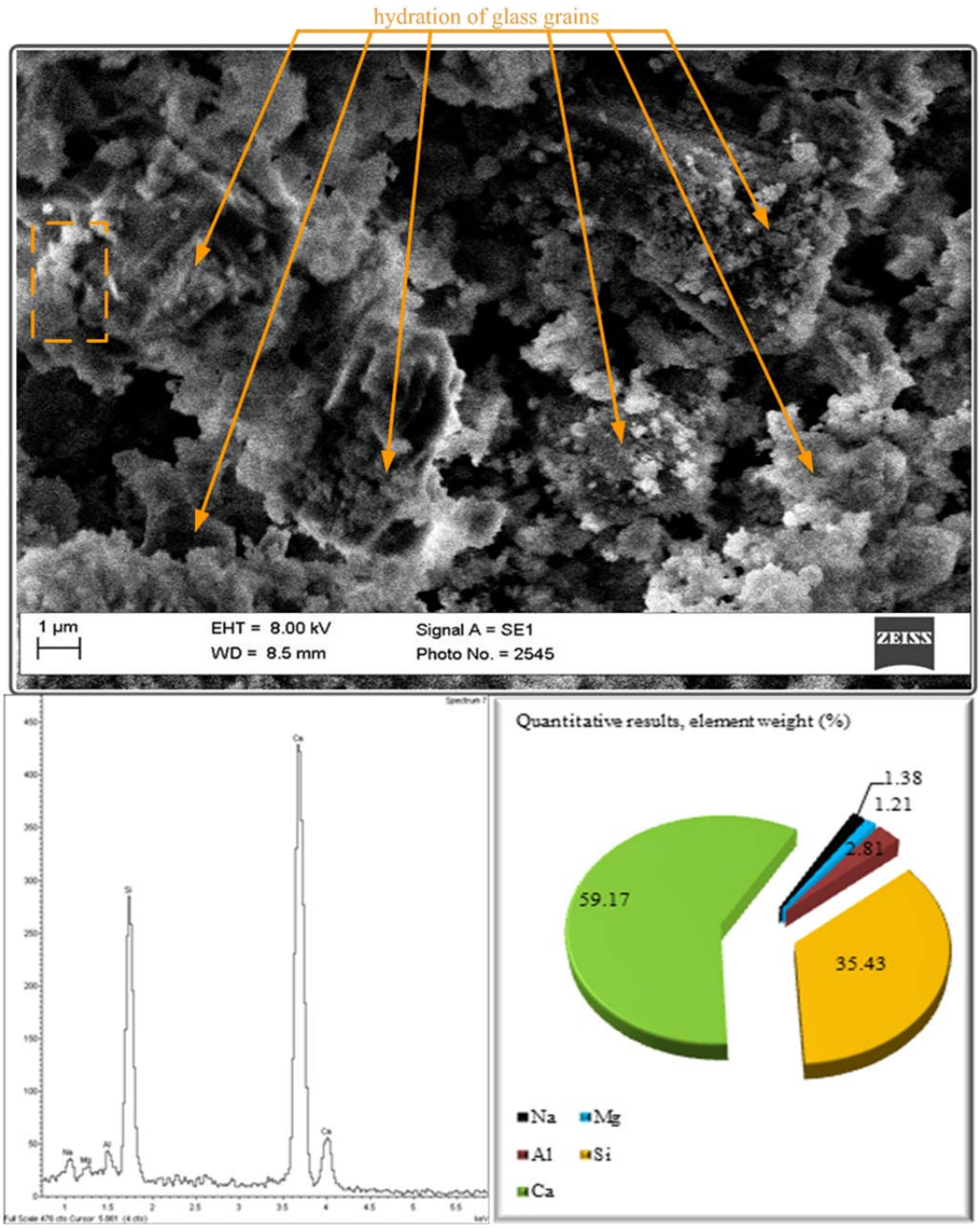

Figure 5.93: SEM micrograph showing the hydration of glass grains in NCWG20.

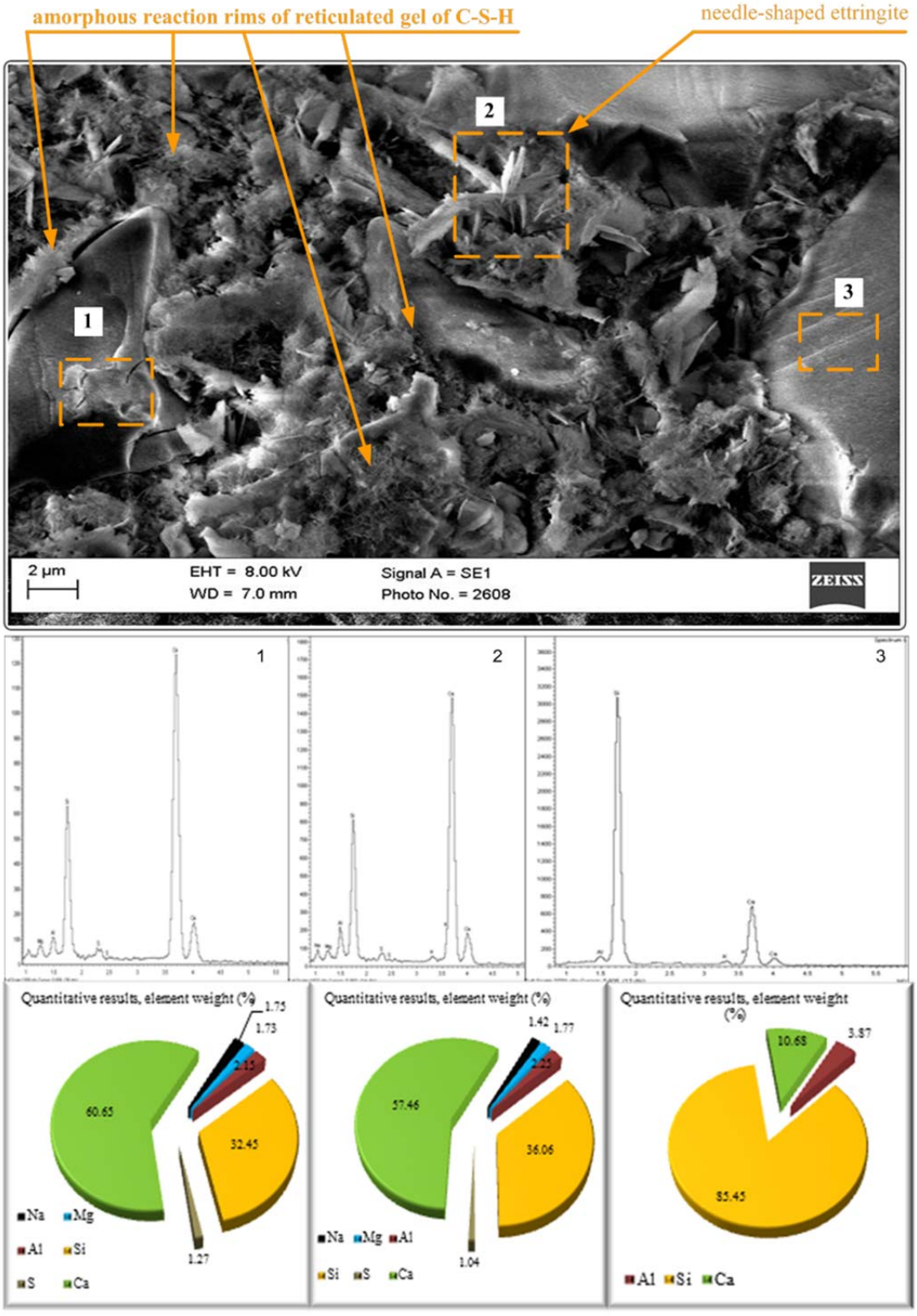

Figure 5.94: SEM micrograph showing the reactions of glass grains in NCWG20.

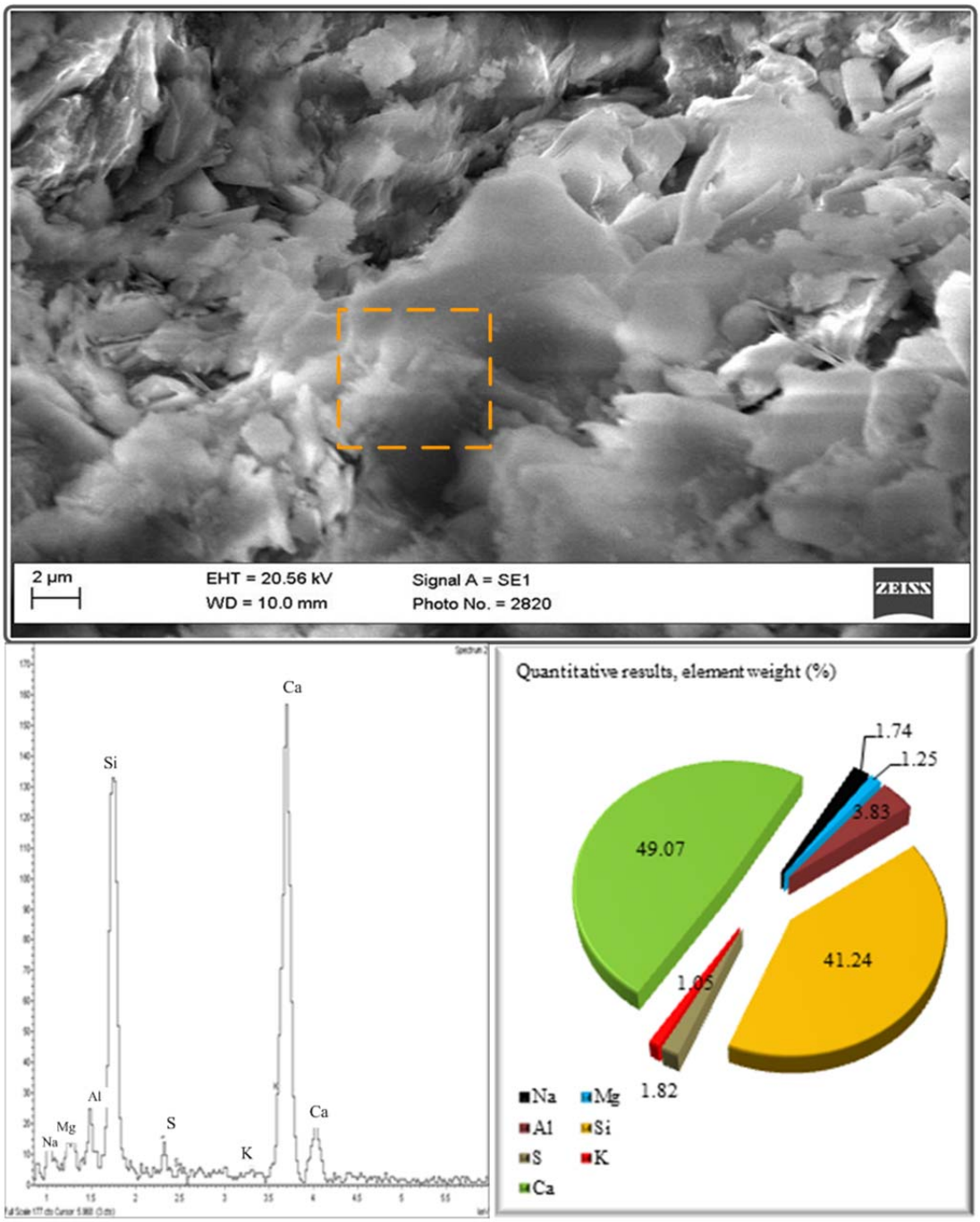

Figure 5.95: SEM micrograph showing the reactions of glass grains in NSWG20.

5.8 Durability of Mono-modal and Multimodal composites

5.8.1 Mechanical Behaviour of the Composites after Ageing

The effects of ageing on the mechanical behaviour of fibre reinforced cement composites are best understood first, from consideration of the mechanisms governing the various slopes of bending load–deflection curves, and secondly, from an analysis of the different stages of load–deflection behaviour of the composite. These mechanisms are related to the matrix and fibre properties.

The several mechanisms that govern the different stages of the bending load–deflection behaviour of fibre reinforced cement composite are: matrix linear bending behaviour at low deflection, development of the first macrocrack which traverses the sample thickness with a subsequent transfer of loading from the matrix to the bridging fibres, propagation and widening of macrocracks up to the peak load, crack localisation, and final failure by fibre rupture.

The slopes of the bending load–deflection curves and their physical significance are: initial slope representing an intact interface; second slope representing microcracking with some fibre debonding and the mobilisation of shearing stresses along the interface; a negative post-peak slope that is manifested after the entire fibre is debonded and the interface has undergone increased damage and cracking; and the final slope, which is asymptotic to the horizontal line representing minimal resistance to fibre pull-out. Mobilisation of the interfacial shear that occurs at the pre-peak phase is associated with microcracking of the fibre/matrix interface, which affects the bond. On the other hand, the slope of the post-peak part of the curve characterises behaviour during the fibre debonding process, and is related to fibre/matrix interface. The post-peak slopes indicate that the more brittle the fibre/matrix interface (which takes place with ageing) the steeper the slope.

Typical examples of bending load–deflection curves obtained from specimens cured for 28 days and specimens subjected to various ageing conditions (aged specimens) are shown in Figures 5.96 to 5.101. It can be seen that the OPC specimens (i.e. control, NSPC3, NSPC3) are seriously embrittled with ageing when compared to the WG specimens (i.e. WG20, NSWG20, and NSWG20). Although the loss of reinforcing capacity has been more significant when the specimens were

subjected to alternately wet and dry conditions, some embrittlement was also observed when the specimens were exposed to natural weathering or when specimens were stored in water. One of the main reasons for this is that the migration of OH^- ions or Ca^{2+} ions from the cement matrix to the fibres rises gradually when the environment is kept constant (i.e. stored in water). When the composites are subjected to alternating wet and dry conditioning this migration increases as follows [127,142]:

- In the first dry cycle, the dimensions of the flax fibres are reduced due to the loss of water, which leads to a loss of adherence with the matrix and the appearance of void spaces at the fibre–matrix interface;
- In the following wet cycle, the water dissolves the hydration compounds of the cement (calcium hydroxides), which is absorbed by the flax fibres and hence swells;
- In the second dry cycle, water is evaporated and the calcium hydroxide precipitates on the surface and in the lumen of the fibres. This movement increases during the subsequent wet–dry cycles, which causes a ‘‘pump-like’’ effect with the resulting densification of the surface and lumen of the fibres with products that have high alkalinity.

The control composites (composites at 28 days) showed a ductile behaviour which was drastically decreased by the aging process (see Table 5.34 and Figure 5.96). For the cases where the control composites were aged outdoors and submitted to 50 cycles of wetting and drying, the drop in the G_F is more significant and it retains only 40% and 18%, respectively, of its value before ageing. The same trend was observed for the toughness indices I_{10}, I_{20} and I_{30}, hence they retain about 24%, 17% and 15%, respectively, of their value before ageing.

This tendency is less intense when a part of the OPC was replaced by 20 wt. % waste glass powder (i.e. WG20). As can be seen in Table 5.34, when the WG20 specimens were aged outdoors or submitted to wetting and drying cycles they maintained about 60%, 72, 81% and 85% of the initial values of G_F, I_5, I_{10} and I_{20} respectively. Table 5.34 also shows a minor reduction in the F_{flex} values after WG20 specimens were aged outdoors or exposed to wetting and drying cycles. This minor reduction could be attributed to competing mechanisms: a wetting cycle at

ambient temperatures with readily available moisture would have been conducive to greater hydration and an increase in fibre/matrix bonding. On the other hand, the drying cycle induced microcracks in the matrix, which leads to a reduction in the peak loads. The load–deflection curves, as shown in Figure 5.97, of the WG20 specimens weathered outside, submitted to wetting and drying cycles or stored in water, indicate that the post-cracking ductility behaviour was retained.

Figures 5.98 and 5.99 show typical examples of the flexural load-deflection curves obtained from the NCPC2.5 and NSPC3 specimens. As can be seen from Figures 5.98 and 5.99, a ductile behaviour was observed when the NCPC2.5 and NSPC3 were stored in water or aged outdoors. This trend was not seen when the same specimens were exposed to wetting and drying cycles. In this situation, the specimens submitted to wet/dry environments showed a significant reduction in the final gradients relative to the non-aged specimens. Conversely, a denser matrix in the NCWG20 and NSWG20 specimens compensated for the effects of fibre damage, and therefore, an increase in the final slope before failure was observed for NCWG20 and NSWG20.

Figures 5.100 and 5.101 shows typical examples of the load–deflection curves obtained from the NCWG20 and NSWG20 specimens. A ductile behaviour is observed not only for the specimens before ageing, but also after ageing. The area under the load–deflection curve is a measure of energy absorption or toughness during the fraction process. As illustrated in Table 5.34, the hybrid combinations of WG/NC or WG/NS improves the durability of flax fibre cement composites when compared to specimens containing only WG, NC or NS (i.e. WG20, NCPC2.5 and NSPC3). This was attributed to matrix densification and improved fibre/matrix bonding. Also, Table 5.34 indicates that ageing in wet/dry environments or outdoors did not lead to significant changes in the toughness of the fibre pull-out mechanism for NCWG20 and NSWG20.

Furthermore, Table 5.34 shows that no significant change was observed in the peak loads (F_{flex}) after either outdoor exposure or wet/dry environments, but that there was a marked increase of approximately 4% and 12% for NCWG20 and NSWG20 after they were stored in water. This behaviour may be related to a twofold action that combines the degradation of the flax fibres in the OPC mixtures with the aging process and the late pozzolanic reaction in the NC/WG/NS mixtures. It is well

known that the mineralisation of flax fibres leads to a reduction in its strength and strain capacity [4–9]. It can, therefore, be assumed that a reduction in the homogenised session of the OPC composites occurs after submitting the specimens to wetting and drying cycles. Pozzolanic reactions can also contribute, to some extent, to the increase of the F_{flex} value when the hydration reactions of the OPC continue to progress at later ages and the CH produced is consumed by the pozzolan during the evolution of these reactions. This is confirmed by the XRD results in the next section.

For the NCWG20 and NSWG20 specimens, the results show that the specimens stored in water, aged outdoors or submitted to wetting and drying cycles revealed nearly the same properties as those observed for the non-aged specimens. The load-deflection curves of the NCWG20 and NSWG20 clearly indicate the deflection hardening behaviour of the non-aged and aged composites. At the same time, these composites also exhibited post-peak ductility prior to failure (as opposed to brittle behaviour). This behaviour was credited to favourable hydration conditions and a fibre/matrix interface that sufficiently mobilised crack propagation and extension prior to final failure by fibre rupture.

The use of pozzolanic fillers such as waste glass powder can greatly reduce the alkalinity of the matrix as well as the content of calcium hydroxide, thus significantly slowing down the processes which lead to degradation in the properties of natural fibre cement composites. The results obtained indicate that the hybrid combination of NC/WG or NS/WG was found to be a very effective means of slowing down the strength loss and embrittlement of the flax fibre cement composites. When WG and nanoparticles (i.e. NC or NS) were uniformly dispersed throughout the cement matrix, the high pozzolanic activity that combines silicon and alumina elements in WG, and nanoparticles with the lime elements of calcium oxide and hydroxide in cement, leads to a significant reduction in the content of calcium hydroxide and mitigates fibre–cement composite degradation. Furthermore, the packing effect of waste glass powder and nanoparticles, due to their great surface area, fills the interstitial spaces inside the skeleton of cement mortar which leads to increases in toughness and durability. In other words, the WG and nano-particles provide more micro/nano-filler and nucleation sites for cement hydration at early ages and at later ages, which leads to a densification of the microstructure.

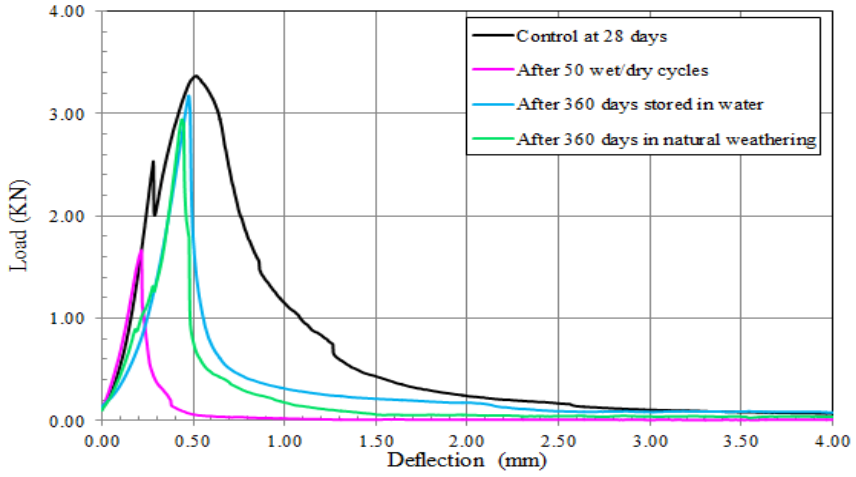

Figure 5.96: Load-deflection curves of control specimens after ageing (n = 3).

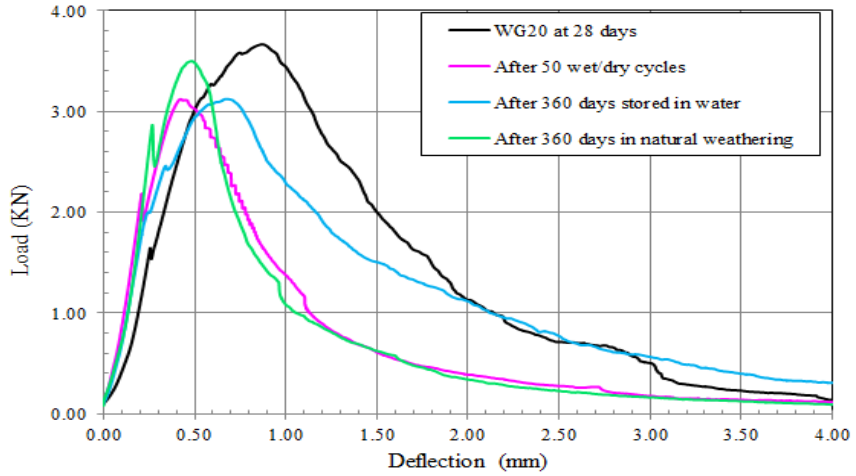

Figure 5.97: Load-deflection curves of WG specimens after ageing (n = 3).

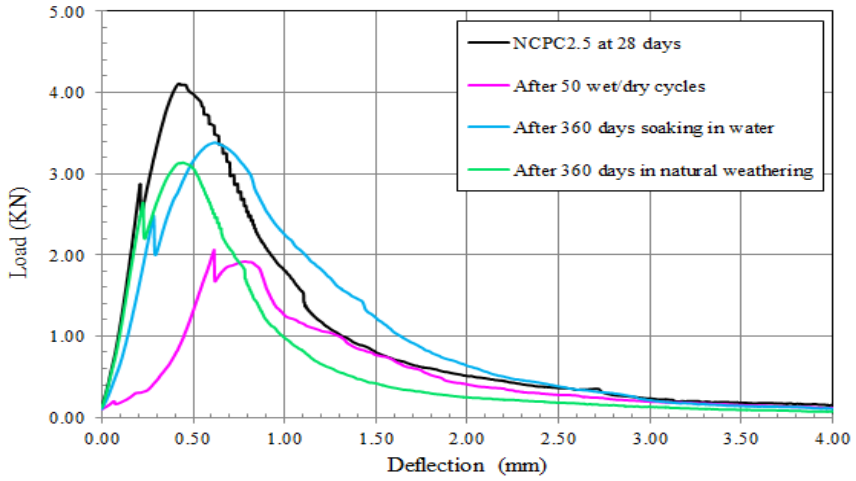

Figure 5.98: Load-deflection curves of NCPC2.5 specimens after ageing (n = 3).

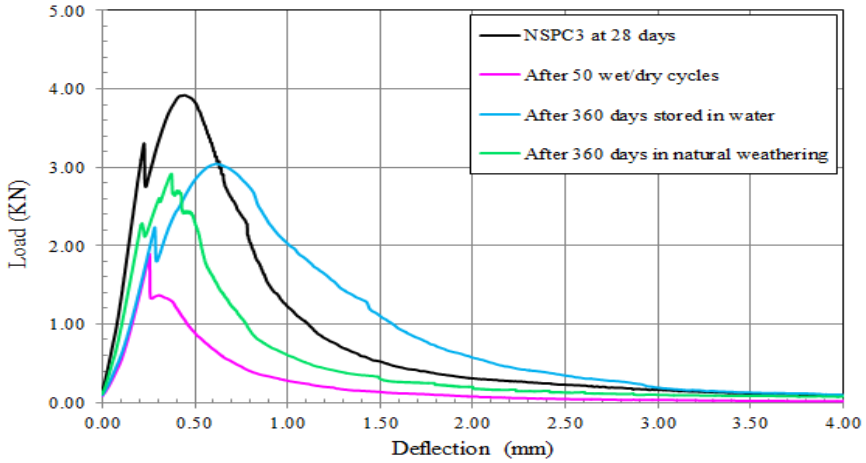

Figure 5.99: Load-deflection curves of NSPC3 specimens after ageing (n = 3).

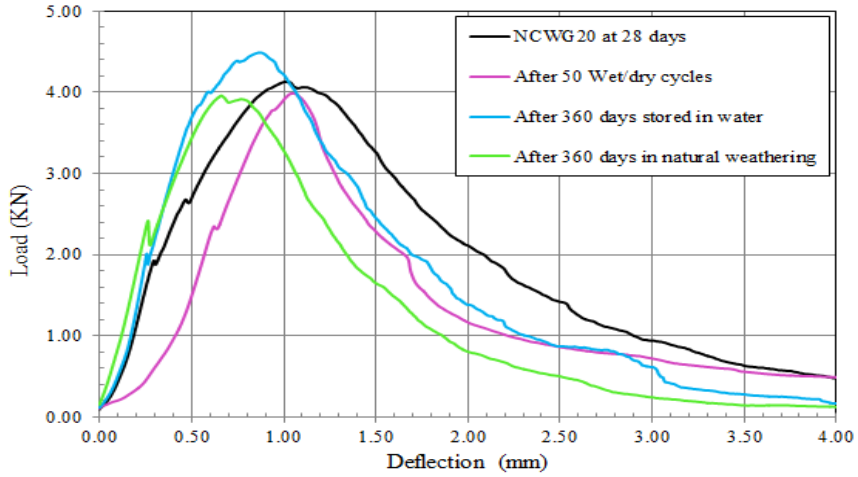

Figure 5.100: Load-deflection curves of NCWG20 specimens after ageing (n = 3).

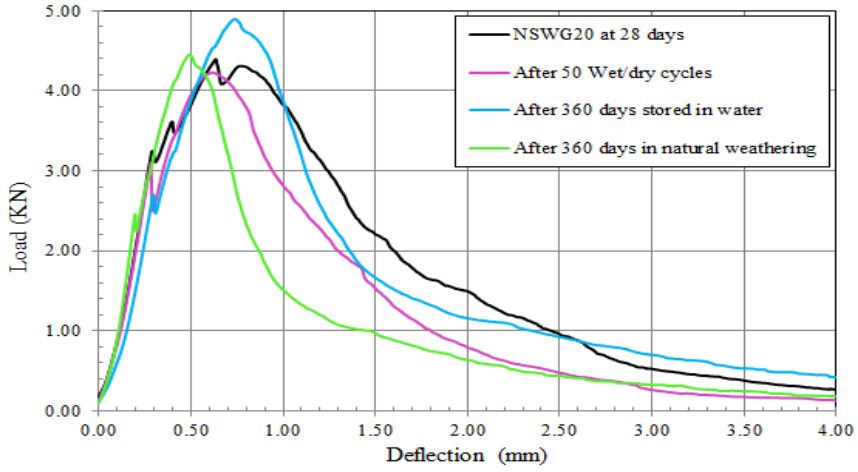

Figure 5.101: Load-deflection curves of NSWG20 specimens after ageing (n = 3).

Table 5.34: Toughness properties of cement composites after ageing (n = 3)

Composite	Ageing condition	Ageing time	Flexural strength (MPa)	Fracture energy (N.mm)	I_5	I_{10}	I_{20}
Control	Non	28	7.02	3667	4.37	6.39	7.39
	Water	360	6.75	1466	3.56	5.41	6.32
	Out doors	360	6.11	1401	3.21	4.98	5.63
	Wet/dry	50 cycle	3.37	653	1.13	1.15	1.15
WG20	Non	28	7.74	6243	6.45	8.95	9.36
	Water	360	6.81	4995	5.96	8.03	8.86
	Out doors	360	6.23	3775	4.96	7.63	8.03
	Wet/dry	50 cycle	6.21	3321	4.69	7.06	7.96
NCPC2.5	Non	28	8.43	4685	6.05	7.99	8.45
	Water	360	6.82	3541	5.55	6.62	7.82
	Out doors	360	6.25	2956	4.63	5.65	6.93
	Wet/dry	50 cycle	3.8	1103	2.11	2.85	3.01
NSPC3	Non	28	8.86	4863	5.83	7.81	8.55
	Water	360	6.2	3654	5.23	7.11	7.96
	Out doors	360	5.52	2963	4.56	6.25	6.69
	Wet/dry	50 cycle	7.53	827	2.25	2.63	2.89
NCWG20	Non	28	9.88	7851	7.14	10.9	14.54
	Water	360	10.32	7781	6.98	10.23	14.26
	Out doors	360	9.23	7023	6.86	9.63	13.87
	Wet/dry	50 cycle	9.59	6853	6.52	9.15	13.66
NSWG20	Non	28	9.74	7632	7.03	10.83	13.34
	Water	360	10.96	7235	6.86	10.23	13.06
	Out doors	360	9.85	5962	6.13	9.86	12.63
	Wet/dry	50 cycle	9.24	6965	6.63	8.96	12.79

5.8.2 Analysis of the SEM Images

Visual observations of the failure surface of the control composite after wetting and drying cycles indicated that the pull-out length of the fibres from the aged specimen was considerably smaller than that observed from non-aged specimens and that the fibres in the aged specimens could be easily broken off at their anchorage in the mortar. The fibres also indicate that the flexibility of the fibres was reduced to such an extent that the fibres could be pulled apart fairly easily by finger force. Scanning electron micrographs of the flax fibres showing the surface changing with ageing are shown in Figure 5.102. As can be seen from Figure 5.102, the surface of the fibres extracted from the control specimen does reveal signs of degradation. This can be attributed mainly to the migration of hydration products, especially calcium hydroxide, in the lumen, walls and voids in the fibre. The extent of alkaline attack was smaller when part of the OPC was replaced by 20wt. % waste glass powder in WG20 and it almost disappears in the combination of WG and nanoparticles in NCWG20 and NSWG20.

Visual observation of the fibres extracted from aged NCPC2.5 and NSPC3 specimens indicates a loss of flexibility, since they were easily broken off at their anchorage in the mortar. Scanning electron micrographs shown in Figure 5.102 do not reveal a considerable deterioration of the fibre surface after ageing, although the surface of the fibre extracted from the specimen exposed to wetting and drying cycles does indicate some alteration.

Visual observation of the fibres extracted from aged NCWG20and NSWG20 specimens indicates that they kept their original flexibility. SEM show that the surface of the fibres extracted from NCWG20 and NSWG20 does not show signs of significant damage, which reflects the fact that the less CH matrix was capable of maintaining the flax fibres integrity during the aging process.

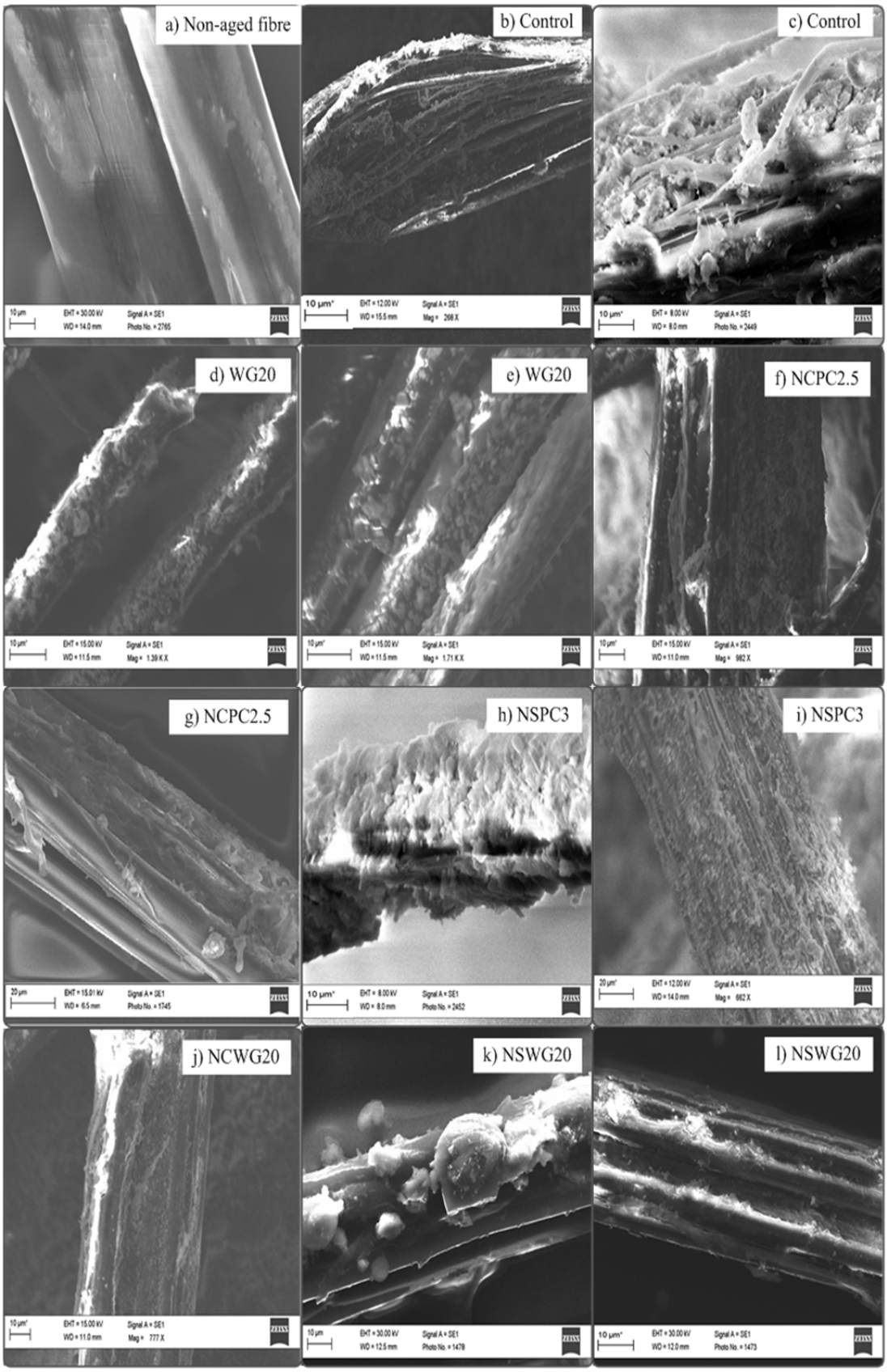

Figure 5.102: SEM micrographs of flax fibre surfaces (a) Before ageing, (b-g) fibre extracted from specimens after ageing (b) control, (c) WG20, (d) NCPC2.5, (e) NSPC3, (f) NCWG20 and (g) NSWG20.

5.8.3 Changes in the Mineral Composition of the Composites

Figures 5.103 to 5.108 show the main cementitious phases (detected by X-ray diffraction) present in the composites at 28 days of hydration (non-aged) and after ageing. Calcite peaks and vaterite vestiges were identified in all of the composites before and after ageing. Further hydration products were identified in the composites after ageing, which can be attributed to the continued hydration process at later ages [6]. Diffuse peaks at 48.6°, 47.6° and 47.3° in the non-aged composites, similar to those reported by Cole and Kroone [233] and Dias et al. [234], confirmed the presence of poorly crystallized calcite. Anhydrous calcium silicate (alite and belite) peaks were only found in the non-aged composites, demonstrating that the matrices of these composites had not yet completely hydrated.

Calcium hydroxide (CH) was not identified in the WG20, NCWG20 and NSWG20 aged specimens (Figs. 5.104, 5.107 and 5.108), since 5% by mass is the limit of the sensitivity of the apparatus. After ageing, the main peak of C–S–H at 28.6° is coincident with the main peak of calcite at 29.5° for all of the composites, however, the halos between 25° and 40° are characteristic of the C–S–H phase [234]. The C–S–H halo in the control specimen is less intense than the halos of other samples. This relates to a decrease in the amount of C–S–H during the ageing process. No other differences were perceptible between the XRD pattern of the control specimen and the other composites.

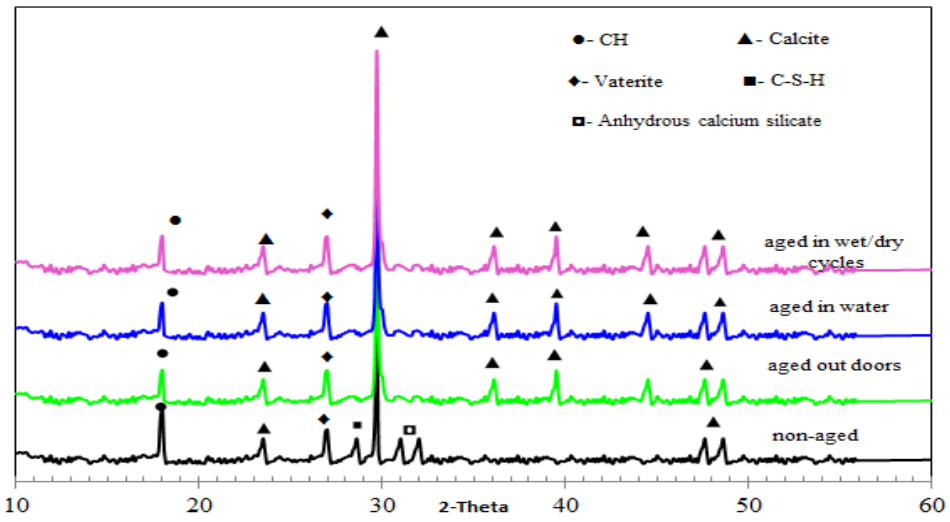

Figure 5.103: XRD patterns of control specimens after ageing.

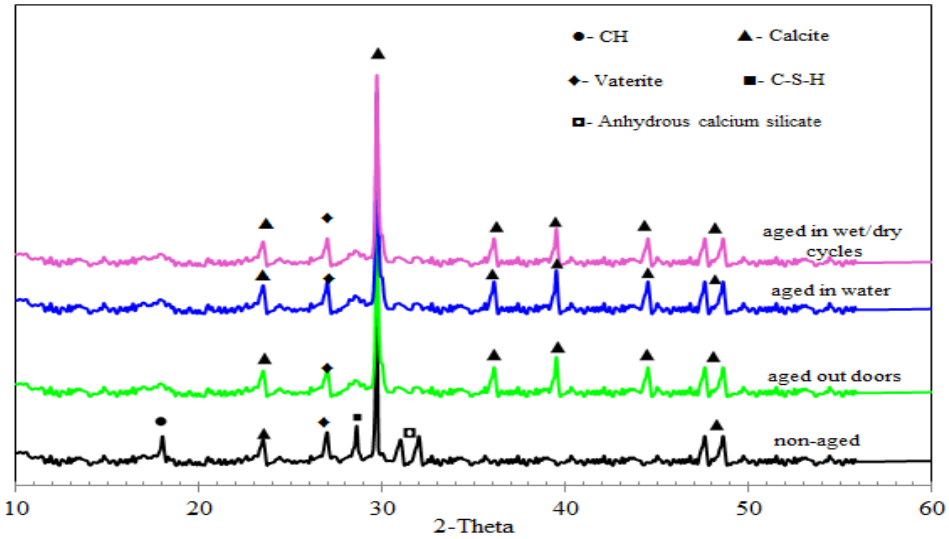

Figure 5.104: XRD patterns of WG specimens after ageing.

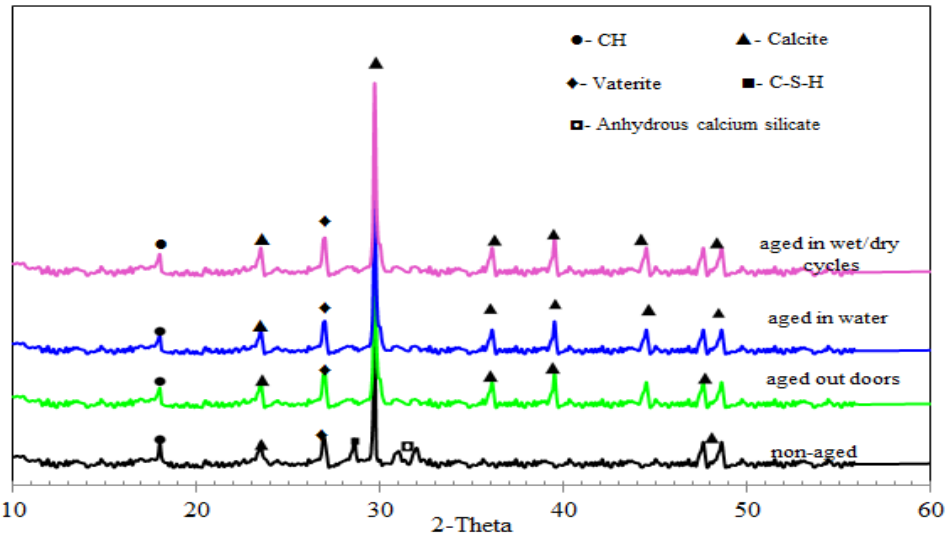

Figure 5.105: XRD patterns of NCPC2.5 specimens after ageing.

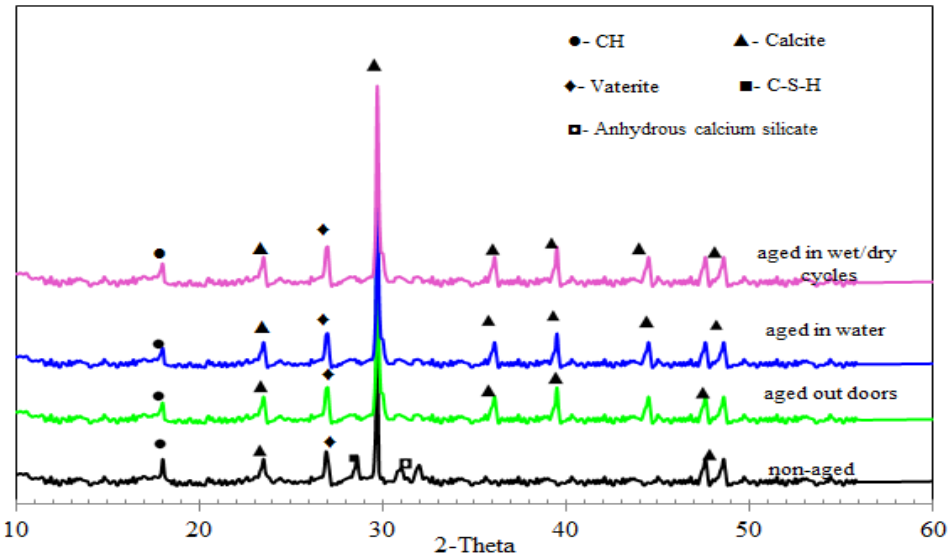

Figure 5.106: XRD patterns of NSPC3 specimens after ageing.

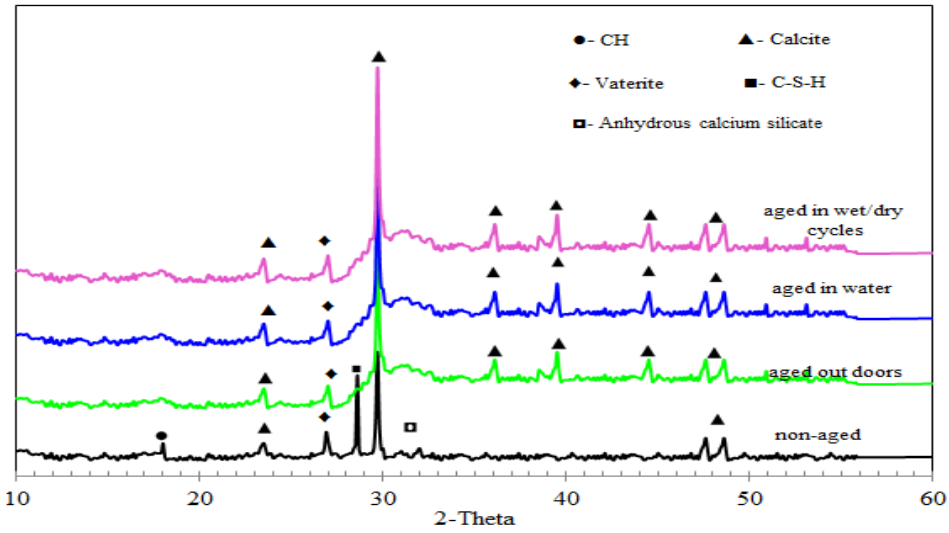

Figure 5.107: XRD patterns of NCWG20specimens after ageing.

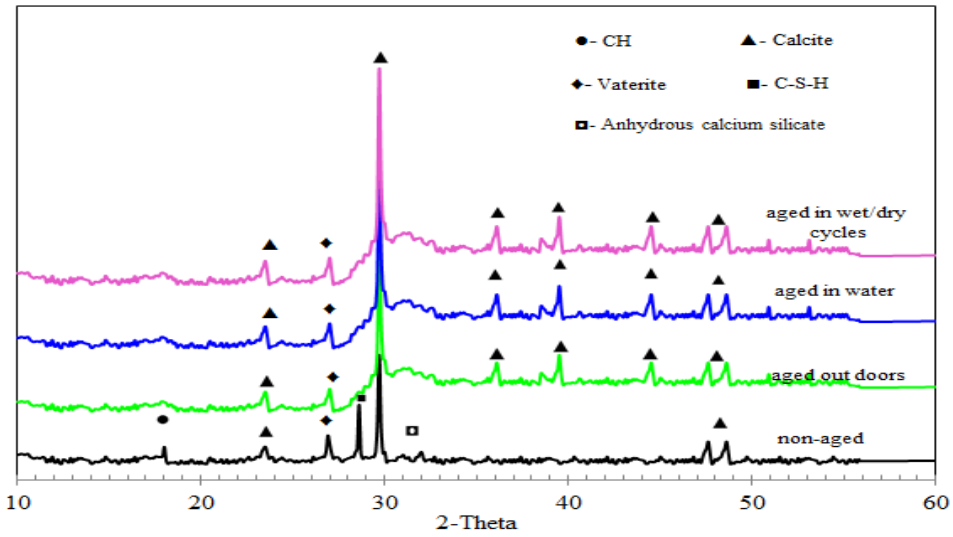

Figure 5.108: XRD patterns of NSWG20 specimens after ageing.

Chapter 6 : Conclusions

6.1 Overview

This work reports a comprehensive study of the behaviour of waste glass flax fibre cement composites. The main objective of this study is to use flax fibres as secondary reinforcement and to re-use waste glass as a replacement of the currently used Portland cement; which is not only costly but also environmentally unfriendly component in concrete. Chapters 3 and 4 described the experiments performed on fibre modification, characterisations for composite applications and the design of experiments used in this work. Chapter 5 presented the results of the studies done to fabricate eco-friendly cement composites by using alkali treated flax fibre, waste glass powder (WG), nano-clay particles (NC) and colloidal nano-silica (NS). The results in chapter 5 were divided into main four sections. The first section presented the effect of alkali treatment on mechanical and physical behaviour of flax fibre and its cement composites. The second section showed the effect of fibre parameters (i.e. fibre length and fibre volume fraction) on porosity, flexural, impact, compressive and toughness properties of cement composites. The third part described the effect of WG, NC and NS on the mechanical, physical and thermal properties of flax fibre cement composites. The last section presented the durability and long term performance of the composites. Individual conclusions have been presented for the results described in each section. Inclusive conclusions are presented in the following section expressing the inter-relationship between results and relating to objective of the thesis.

6.2 Conclusions

6.2.1 Treatment of flax fibres

Untreated flax fibres were subjected to 9 different alkali treatments by varying three different treatment parameters (concentration of NaOH, treatment temperature, and digestion time). A decrease in average fibre diameter was detected for all alkali treatments which appeared to increase with the harshness of the alkali treatment. The parameters that most significantly influenced fibre tensile strength

(TS) and Young`s Modulus (YM) were the NaOH concentration and treatment temperature. The decrease in TS with increased NaOH concentration and treatment temperature appeared to be due to increased degradation of structural cellulose in the fibres. The decrease in YM is believed to be due to the removal of lignin and other intra-fibrillar binders resulting in degradation of cellulose and molecular relaxation of the cellulose fibre components. Upon analysis of the alkali fibre treatments by TS, SEM, DTA/TGA and XRD, the alkali treatment with 5 wt. % NaOH, 55 °C treatment temperature, and 10 minutes soaking time was found to give the best combination of:

- Fibre tensile strength.
- Increased fibre roughness, fibre separation from fibre bundles, and removal of noncellulosic fibre component (as revealed by SEM).
- Increased thermal stability (as revealed by DTA/TGA analysis).
- Increased crystalline cellulose by better packing of cellulose chains (recorded by XRD analysis).

The mathematical models for the TS and YM of alkali treated fibres were obtained by using Box-Behnken design using three different alkali treatment parameters as mentioned above. The TS and YM of the alkali treated flax fibres could be predicted using the models within the range of experimental conditions under investigation which was verified experimentally in this study. The accuracy of the prediction of TS and YM using the mathematical models was quite satisfactory as the experimental TS and YM of alkali treated fibre obtained was almost within the range of tolerance limit of the models.

6.2.2 Flax Fibre Cement Composites

The fibres obtained from the optimised alkali treatment were used to fabricate all cement composites. Alkali treated flax fibres are a satisfactory fibre for incorporation into a cement matrix. Mechanical and physical properties of both untreated and treated flax fibres were studied. Treated flax fibre cement composites revealed some improvement in mechanical and thermal performance compared to untreated composites. These improvements appeared to be due to the changes in morphology and in chemical composition of the fibres, which leads to increase the

contact area and to improve the fibre surface adhesive, hence giving rise to additional sites for mechanical interlocking.

Fibre volume fraction plays a significant role in determining the composite mechanical properties. The mechanical properties of composites are highly influenced by the fibre content. This study was carried out by fabricating cement composites with three different fibre volume fractions (i.e. 0.5, 1 and 1.5%). The results showed that the increase in fibre content has significant positive effects on the fracture energy, toughness indices, flexural and impact strength; however, these improvements are always associated with a decrease in compressive strength.

Fibre length plays an important role in the mechanical performance of fibre cement composites. If the fibre is long enough (length ≥ 30 mm), a greater amount of fracture energy is needed to pull the fibre through the matrix and the composite can be tougher and stronger. This work was carried out by fabricating cement composites with three different lengths (i.e. 10, 30, 50 mm). The results showed that when short fibres (10 mm) were used as reinforcement and compared with longer fibres (30, 50 mm), a reduction in composite fracture toughness and flexural and impact strength was observed. For example, at 1% by volume fraction the short fibre composites showed around 10-15% decrease in fracture energy and impact strength and around 20-22% decrease in flexural strength compared to composites containing the same amount of the longer fibre.

The mathematical models for the fracture energy, toughness indices, porosity, flexural, impact and compressive strength of flax fibre cement composites were obtained by using central composite design using two fibre parameters (fibre length and volume fraction). The results indicate that within the limits of fibre parameters used in this study the proposed models predict the above properties adequately.

6.2.3 Partial Replacement of Ordinary Portland Cement by Glass Powder and Nanoparticles

In this work, waste glass powder (up to 50% by cement weight) was tested for potential employment as a cement replacement in cementitious materials. The following conclusions can be drawn:

- Based on the ASR test results, no damaging effect can be detected at a macroscopic level due to the reaction between glass powder (up to 50%) and cement paste with particle size up to 75 μm. Inversely, the incorporation of WG into the cement matrix helps to control ASR.
- Fracture energy greatly increased with increasing WG content.
- Based on toughness, flexural and compressive strength, the ASR test and the CH content of the WG cement composites, it was observed that the replacement of cement by 20 wt. % glass powder is feasible in a cementitious system.

Partial replacement of OPC by NC (up to 2.5%) improved compressive strength and toughness of composites at 28 days of hydration compared to those prepared using only OPC. However, clusters of NC are more likely to occur and can be observed from SEM micrographs when the dosage of NC is larger than 2.5%. Consequently, the strengths and toughness become worse as the dosage of NC is increased.

As the content of NS is increased up to 3.0 wt. %, the compressive strength, flexural strength and toughness of the composites is increased. This is due to more formation of hydrated products in presence of NS at 28 days of hydration. Also the incorporation of NS (up to 3%) reduced porosity, which leads to more compact and dens matrices compared to OPC matrix. However at higher dosage (up to 6%) the composites undergo significant reductions in strength and toughness due to defects generated in dispersion of NS. Also it could be due to the content of silica, which is higher than the amount required to combine with the liberated lime during the process of hydration thus leading to excess silica leaching out and causing a deficiency in strength and toughness.

The addition of nanoparticles has great potential to accelerate the pozzolanic reaction of WG. It seems that their nano size allows them to react more readily with the CH, thereby increasing C-S-H conversion at 28 days of hydration. The hybrid combination of nanoparticles and WG was found to be a very effective method to use WG as a high-volume cement replacement, to achieve good performance and as an economic way to use nanoparticles. Furthermore, the replacement of OPC by 20 wt. % WG and nanoparticles (2.5 wt. % NC or 3 wt. % NS) is found to limit the

ASR expansion to less than 0.10% at end of 14 days when evaluated as per ASTM C 1260. Therefore, they are more likely to meet the ASTM C 1293 expansion criterion of concrete prisms of 0.04% after two years.

Based on the results of this study, it can be concluded that hybrid combinations of WG and nanoparticles can improve the strength of mortars more than WG, NC or NS alone. It seems that NC and NS behaves not only as a filler to refine microstructure, but also as an activator to accelerate the pozzolanic reaction and activate WG; this is due to the large and highly reactive surface of nanoparticles. Moreover, these hybrid combinations are more effective in reducing ASR expansion, than either of the replacement materials alone.

6.2.4 Durability of Flax Fibre Cement Composites

Composites manufactured with flax fibres and OPC mortar matrix presented a significant reduction in toughness after submitted to cycles of wetting and drying. Some embrittlement was also observed in specimens aged in water or aged outdoors. The embrittlement is mainly associated with the mineralisation of the fibres due to migration of hydration products, especially calcium hydroxide, to the fibre lumen, walls and voids.

Partial replacement of OPC by 20 wt. % WG improved the durability of flax fibre cement composites compared to the control specimen. The WG aged specimens presented a smaller reduction in the values of fracture energy and flexure strength when compared with those measured at 28 days.

Partial replacement of OPC by NC or NS did not lead to reduced embrittlement with ageing under conditions of cyclic wetting and drying. However, the specimens subjected to natural weathering or stored in water revealed a better behaviour.

Partial replacement of OPC by hybrid combination of NC+WG and NS+WG is a promising alternative for increasing the durability of the material with ageing. The use of these combinations can be greatly reduce the alkalinity of the matrix as well as the content of calcium hydroxide, which confirmed by TGA/DTA, SEM and XRD analyses, and hence significantly slow down the processes which lead to

degradation in the properties of natural fibre cement composites. It is believed that high pozzolanic activity that combines silicon and alumina elements in WG and nanoparticles with the lime elements of calcium oxide and hydroxide in cement, leads to a significant reduction in the content of calcium hydroxide and greatly mitigate fibre–cement composite degradation. Moreover, the WG and nanoparticles could provide more micro/nano-filler effect and nucleation sites for cement hydration at early ages and at later ages, which leads to densification of the microstructure and improve durability.

6.3 Recommendations for Future Work

The results obtained during the course of this research have laid an important platform from which to further improve the properties of the developed composites. Some recommendations for future work have been proposed:

- In the grinding of waste glass, a great amount of the total electric energy consumption is consumed in this process. Because of the diminishing available sources of energy and the attendant rise in energy costs, it is important to pay particular attention to this major cost item and develop grinding aids in order to reduce the energy cost and grinding time.
- More research is required to enhance the dispersion of natural fibre in the cement matrix.
- Also more research is needed to modify the production methods of nanoparticles in order to avoid the formation of agglomerates, and to achieve better dispersion in the cement matrix.
- More research is required to study the fatigue of waste glass/natural fibre cement composites
- Nanotechnology becomes a double-edge sword to the construction industry. Production of nano materials requires high energy. The engineered materials should be sustainable as well as cost-and-energy effective. Use of nanotechnology creates an environmental challenge to the construction industry.

References

[1] R.R. Franck, Bast and Other Plant Fibres, Woodhead Publishing Limited, Cambridge, England, 2005.

[2] B. Wang, Pre-treatment of flax fibers for use in rotationally molded biocomposites Department of Agricultural and Bioresource Engineering, University of Saskatchewan, Saskatoon,Saskatchewan, 2004.

[3] A. Bentur, S. S.Mindess, Fibre Reinforced Cementitious Composites, 2nd edition ed., Taylor & Francis, London &New York, 2007.

[4] S.J. Pickering, Recycling technologies for thermoset composite materials-current status, Composites: Part A 20 (2005) 1-10.

[5] F. Pacheco-Torgal, S. Jalali, Cementitious building materials reinforced with vegetable fibres: A review, Construction and Building Materials 25 (2011) 575-581.

[6] G.H.D. Tonoli, S.F. Santos, H. Savastano Jr, S. Delvasto, R. Mejía de Gutiérrez, M.d.M. Lopez de Murphy, Effects of natural weathering on microstructure and mineral composition of cementitious roofing tiles reinforced with fique fibre, Cement and Concrete Composites 33 (2011) 225-232.

[7] J. Claramunt, M. Ardanuy, J.A. García-Hortal, R.D.T. Filho, The hornification of vegetable fibers to improve the durability of cement mortar composites, Cement and Concrete Composites 33 (2011) 586-595.

[8] M.S. Islam, The influence of fibre processing and treatments on hemp Fibre/Epoxy and hemp Fibre/PLA composites, University of Waikato, Hamilton, New Zealand, 2008.

[9] F.A. Silva, R.D.T. Filho, J.A.M. Filho, E.M.R. Fairbairn, Physical and mechanical properties of durable sisal fiber–cement composites, Construction and Building Materials 24 (2010) 777-785.

[10] R.D. Tolêdo Filho, M.A. Sanjuán, Effect of low modulus sisal and polypropylene fibre on the free and restrained shrinkage of mortars at early age, Cement and Concrete Research 29 (1999) 1597–1604.

[11] R. Toledo Filho, Ghavami K., England GL., S. K., Development of vegetable fibre–mortar composites of improved durability, Cement and Concrete Composites 25 (2003) 185-196.

[12] R.D. Toledo Filho, F.d.A. Silva, E.M.R. Fairbairn, J.d.A.M. Filho, Durability of compression molded sisal fiber reinforced mortar laminates, Construction and Building Materials 23 (2009) 2409-2420.

[13] C. Shi, Y. Wu, C. Riefler, H. Wang, Characteristics and pozzolanic reactivity of glass powders, Cement and Concrete Research 35 (2005) 987-993.

[14] Y. Shao, T. Lefort, S. Moras, D. Rodriguez, Studies on concrete containing ground waste glass, Cement and Concrete Research 30 (2000) 91- 100.

[15] C. Shi, K. Zheng, A review on the use of waste glasses in the production of cement and concrete, Resources, Conservation and Recycling 52 (2007) 234-247.

[16] R. Idir, M. Cyr, A. Tagnit-Hamou, Pozzolanic properties of fine and coarse color-mixed glass cullet, Cement and Concrete Composites 33 (2011) 19-29.

[17] A. Shayan, A. Xu, Performance of glass powder as a pozzolanic material in concrete: A field trial on concrete slabs, Cement and Concrete Research 36 (2006) 457-468.

[18] ASTM C 618, Specification for coal fly ash and raw or calcined natural pozzolan for use in concrete, Annual Book of ASTM Standards, 2005.

[19] L.M. Federico, S.E. Chidiac, Waste glass as a supplementary cementitious material in concrete – Critical review of treatment methods, Cement and Concrete Composites 31 (2009) 606-610.

[20] K. Gopalakrishnan, B. Birgisson, P. Taylor, N. Attoh-Okine, Nanotechnology in Civil Infrastructure, Springer, Berlin Heidelberg, 2011.

[21] A. Nazari, S. Riahi, The role of SiO2 nanoparticles and ground granulated blast furnace slag admixtures on physical, thermal and mechanical properties of self compacting concrete, Materials Science and Engineering: A 528 (2011) 2149-2157.
[22] A. Nazari, S. Riahi, Improvement compressive strength of concrete in different curing media by Al2O3 nanoparticles, Materials Science and Engineering: A 528 (2011) 1183-1191.
[23] A. Nazari, S. Riahi, Splitting tensile strength of concrete using ground granulated blast furnace slag and SiO2 nanoparticles as binder, Energy and Buildings 43 (2011) 864-872.
[24] J. Björnström, A. Martinelli, A. Matic, L. Börjesson, I. Panas, Accelerating effects of colloidal nano-silica for beneficial calcium–silicate–hydrate formation in cement, Chemical Physics Letters 392 (2004) 242-248.
[25] K.L. Lin, W.C. Chang, D.F. Lin, H.L. Luo, M.C. Tsai, Effects of nano-SiO(2) and different ash particle sizes on sludge ash-cement mortar, Journal of environmental management 88 (2008) 708-714.
[26] W. Kuo, J. Huang, C. Lin, Effects of organo-modified montmorillonite on strengths and permeability of cement mortars, Cement and Concrete Research 36 (2006) 886-895.
[27] D. Sedan, C. Pagnoux, A. Smith, T. Chotard, Mechanical properties of hemp fibre reinforced cement: Influence of the fibre/matrix interaction, Journal of the European Ceramic Society 28 (2008) 183-192.
[28] V. Ramachandran, J.J. Beaudoin, Handbook of analytical technique in concrete science and technology, Noyes Publications USA, New Jersey, 2002.
[29] S.S. Shebl, L. Allie, M.S. Morsy, H.A. Aglan, Mechanical behavior of activated nano silicate filled cement binders, Journal of Materials Science 44 (2009) 1600-1606.
[30] J.J. Beaudoin, L. Raki, R. Alizadeh, L. Mitchell, Dimensional change and elastic behavior of layered silicates and Portland cement paste, Cement and Concrete Composites 32 (2010) 25-33.
[31] V.M. Malhotra, P.K. Mehta, Pozzolanic and cementitious materials, Gordon and Breach Publishers, New York, 1996.
[32] L.M. Federico, S.E. Chidiac, L. Raki, Reactivity of cement mixtures containing waste glass using thermal analysis, Journal of Thermal Analysis and Calorimetry 104 (2011) 849-858.
[33] O. Ozkan, I. Yuksel, Studies on mortars containing waste bottle glass and industrial by-products, Construction and Building Materials 22 (2008) 1288-1298.
[34] C.H. Chen, R. Huang, J.K. Wu, C.C. Yang, Waste E-glass particles used in cementitious mixtures, Cement and Concrete Research 36 (2006) 449-456.
[35] N. Schwarz, H. Cam, N. Neithalath, Influence of a fine glass powder on the durability characteristics of concrete and its comparison to fly ash, Cement and Concrete Composites 30 (2008) 486-496.
[36] V. Corinaldesi, G. Gnappi, G. Moriconi, A. Montenero, Reuse of ground waste glass as aggregate for mortars, Waste management 25 (2005) 197-201.
[37] A. Karamberi, A. Moutsatsou, Participation of coloured glass cullet in cementitious materials, Cement and Concrete Composites 27 (2005) 319-327.
[38] S. Park, B. Lee, J. Kim, Studies on mechanical properties of concrete containing waste glass aggregate, Cement and Concrete Research (2004).
[39] K. Sobolev, P. Turker, S. Soboleva, G. Iscioglu, Utilization of waste glass in ECO-cement: strength properties and microstructural observations, Waste management 27 (2007) 971-976.
[40] A. Buchwald, C. Kaps, M. Hohmann, Alkali-activated binders and pozzolan cement binders-compete binder reaction or two sides of the same story? , Proceedings of the 11th international congress on the chemistry of cement (ICCC), Durban, 2003, pp. 1238–1246.
[41] S. Urhan, Alkali silica and pozzolanic reactions in concrete. Part 1: Interpretation of published results and an hypothesis concerning the mechanism, Cement and Concrete Research 17 (1987) 141–152.

[42] H. Wang, J.E.C.n.o.a.s.f.a.a. Gillott, a.s.r.M.C.R. 1992;44(161):235–9., Competitive nature of alkali–silica fume and alkali–aggregate (silica) reaction, Magazine of Concrete Research 44 (1992) 235-239.
[43] G. Chen, H. Lee, K.L. Young, P.L. Yue, A. Wong, T. Tao, K.K. Choi, Glass recycling in cement production—an innovative approach, Waste Management 22 (2002) 747–753.
[44] M. Liu, Incorporating ground glass in self-compacting concrete, Construction and Building Materials 25 (2011) 919-925.
[45] K. Ganesh Babu, D. Saradhi Babu, Behaviour of lightweight expanded polystyrene concrete containing silica fume, Cement and Concrete Research 33 (2003) 755–762.
[46] P. Mahieux, J. Aubert, G. Escadeillas, Utilization of weathered basic oxygen furnace slag in the production of hydraulic road binders, Construction and Building Materials 23 (2009) 742-747.
[47] S.A. Barbhuiya, J.K. Gbagbo, M.I. Russell, P.A.M. Basheer, Properties of fly ash concrete modified with hydrated lime and silica fume, Construction and Building Materials 23 (2009) 3233-3239.
[48] R.L. Reis, S. Weiner, Learning from Nature How to Design New Implantable Biomaterials: From Biomineralization Fundamentals to Biomimetic Materials and Processing Routes, KLUWER ACADEMIC PUBLISHERS Dordrecht 2004.
[49] F. Sanchez, K. Sobolev, Nanotechnology in concrete – A review, Construction and Building Materials 24 (2010) 2060-2071.
[50] K.E. Drexler, C. Peterson, G. Pergamit, Unbounding the future: the nanotechnology revolution, William Morrow, New York, 1991.
[51] H. Li, Microstructure of cement mortar with nano-particles, Composites Part B: Engineering 35 (2004) 185-189.
[52] K. Sobolev, I. Flores, L.M. Torres-Martinez, P.L. Valdez, E. Zarazua, E.L. Cuellar, Engineering of SiO2 nanoparticles for optimal performance in nano cement-based materials, Nanotechnology in construction: Proceedings of the NICOM3, 3rd International Symposium on Nanotechnology in Construction, Prague, Czech Republic, 2009, pp. 139–148.
[53] T. Ji, Preliminary study on the water permeability and microstructure of concrete incorporating nano-SiO, Cement and Concrete Research 35 (2005) 1943-1947.
[54] M.H. Zhang, H. Li, Pore structure and chloride permeability of concrete containing nano-particles for pavement, Construction and Building Materials 25 (2011) 608-616.
[55] G. Li, Properties of high-volume fly ash concrete incorporating nano-SiO2, Cement and Concrete Research 34 (2004) 1043-1049.
[56] P. Mondal, S.P. Shah, L.D. Marks, J.J. Gaitero, Comparative study of the effects of microsilica and nanosilica in concrete, Journal of Transportation Research Record: Journal of the Transportation Research Board 2141 (2010) 6-9.
[57] J. Gaitero, I. Campillo, A. Guerrero, Reduction of the calcium leaching rate of cement paste by addition of silica nanoparticles, Cement and Concrete Research 38 (2008) 1112-1118.
[58] D.F. Lin, K.L. Lin, W.C. Chang, H.L. Luo, M.Q. Cai, Improvements of nano-SiO2 on sludge/fly ash mortar, Waste management 28 (2008) 1081-1087.
[59] J. Shih, T. Chang, T. Hsiao, Effect of nanosilica on characterisation of Portland cement composite, Materials Science and Engineering: A 424 (2006) 266-274.
[60] J.J. Gaitero, L.D. Marks, S.P. Shah, P. Mondal, Comparative Study of the Effects of Microsilica and Nanosilica in Concrete, Transportation Research Record: Journal of the Transportation Research Board 2141 (2010) 6-9.
[61] F. Uddin, Clays, Nanoclays, and Montmorillonite Minerals, Metallurgical and Materials Transactions A 39 (2008) 2804-2814.
[62] M.A. Siddiqui, Z. Ahmed, Mineralogy of the swat kaolin deposits, Pakistan Arabian Journal for Science and Engineering 2005, vol. 30 (2A), p. 196 30 (2005) 195-218.
[63] K.K. Maniar, A literature survey on nano composites, 2002.

[64] T.-P. Chang, J.-Y. Shih, K.-M. Yang, T.-C. Hsiao, Material properties of portland cement paste with nano-montmorillonite, Journal of Materials Science 42 (2007) 7478-7487.
[65] Y.W. Mai, Z.Z. Yu, Polymer nanocomposites, CRC Press, New York 2006.
[66] M.S.G. Zhou, Preparation, structure, and properties of advanced polymer composites with long fibers and nanoparticles The Ohio State University, 2007.
[67] S. Sinha Ray, M. Okamoto, New Polylactide/Layered Silicate Nanocomposites, 6, Macromolecular Materials and Engineering 288 (2003) 936-944.
[68] J.H. Koo, Polymer Nanocomposites – Processing, Characterisation, and Applications, McGraw-Hill, New York/Chicago/San Francisco, 2006.
[69] M. Morsy, H. Aglan, M. Abdelrazek, Nanostructured zonolite–cementitious surface compounds for thermal insulation, Construction and Building Materials 23 (2009) 515-521.
[70] X. He, X. Shi, Chloride permeability and microstructure of Portland cement mortars incorporating nanomaterials, Transportation Research Board Record: Journal of the Transportation Research Board (2008) 13-21.
[71] H. Lindgreen, M. Geiker, H. Kroyer, N. Springer, J. Skibsted, Microstructure engineering of Portland cement pastes and mortars through addition of ultrafine layer silicates, Cement and Concrete Composites 30 (2008) 686-699.
[72] F. Annabi-Bergaya, Layered clay minerals. Basic research and innovative composite applications, Microporous and Mesoporous Materials 107 (2008) 141-148.
[73] T.R.D. Filho, M.A. Sanjuán, Effect of low modulus sisal and polypropylene fibre on the free and restrained shrinkage of mortars at early age, Cement and Concrete Research 29 (1999) 1597–1604.
[74] G. Beckermann, Performance of Hemp-Fibre Reinforced Polypropylene Composite Materials, Materials and Process Engineering, University of Waikato, Hamilton, New Zealand, 2007.
[75] M.S. Islam, K.L. Pickering, N.J. Foreman, Influence of alkali treatment on the interfacial and physico-mechanical properties of industrial hemp fibre reinforced polylactic acid composites, Composites Part A: Applied Science and Manufacturing 41 (2010) 596-603.
[76] H.E. Gram, Durability of natural fibres in concrete, Swedish Cement and Concrete Research Institute, Research Fo., Stockholm (1983).
[77] J.B. Buick, T.R.A. Magee, Microbial contamination of flax dust, Resources, Conservation and Recycling 27 (1999) 99-104.
[78] J. George, J. Ivens, I. Verpoest, Mechanical properties of flax fibre reinforced epoxy composites, Die Angewandte Makromolekulare Chemie 272 (1999) 41-45.
[79] C. Baley, F. Busnel, Y. Grohens, O. Sire, Influence of chemical treatments on surface properties and adhesion of flax fibre–polyester resin, Composites Part A: Applied Science and Manufacturing 37 (2006) 1626-1637.
[80] A.K. Bledzki, J. Gassan, Composites reinforced with cellulose based fibres, Progress in Polymer Science 24 (1999) 221–274.
[81] V.D.M.J.A. Oever, H.L. Bos, Flax physical fibre structure and its effect on composite properties, 2nd International Wood and Natural Fibre Composites Symposium, Kassel/Germany, June 28-29, (1999).
[82] C. Baley, Analysis of the flax fibres tensile behaviour and analysis of the tensile stiffness increase, Composites Part: A 33 (2002) 939-948.
[83] L.Y. Mwaikambo, M.P. Ansell, Chemical modification of hemp, sisal, jute, and kapok fibers by alkalization, Journal of Applied Polymer Science 84 (2002) 2222-2234.
[84] M. John, S. Thomas, Biofibres and biocomposites, Carbohydrate Polymers 71 (2008) 343-364.
[85] C. Qin, N. Soykeabkaew, N. Xiuyuan, T. Peijs, The effect of fibre volume fraction and mercerization on the properties of all-cellulose composites, Carbohydrate Polymers 71 (2008) 458-467.

[86] J.C.F. Walker, Wood chemistry and cell wall ultrastructure, in Primary Wood Processing., Chapman and Hall London, 1993.
[87] E. Sjöström, . Wood Chemistry: Fundamentals and Applications, Academic Press, 1981.
[88] B. Madsen, Properties of plant fibre yarn polymer composites - an experimental study, Department of civil Engineering, Technical University of Denmark, 2004.
[89] A. Sakakibara, N. Shiraishi, Wood and Cellulose Chemistry, Marcel Dekker, New York, 1991.
[90] S.J. Eichhorn, C.A. Baillie, N. Zafeiropoulos, L.Y. Mwaikambo, M.P. Ansell, A. Dufresne, K.M. Entwistle, P.J. Herrera-Franco, G.C. Escamilla, L.H. Groom, M. Hughes, C. Hill, Rials, Timothy G., P.M. Wild, Current international research into cellulosic fibres and composites, Journal of Materials Science 36 (2001) 2107-2131.
[91] R.M. owell, A new generation of composite materials from agro-based fiber, The 3rd International Conference on Frontiers of Polymers and Advanced Materials, Plenum Press, Kuata Lumpur, Malaysia, 1995.
[92] A. Thygesena, A.B. Thomsen, G. Daniel, H. Lilholt, Comparison of composites made from fungal defibrated hemp with composites of traditional hemp yarn, Industrial Crops and Products 25 (2007) 147-159.
[93] P.V. Josepha, K. Josepha, S. Thomas, C.K.S. Pillaic, V.S. Prasadc, G. Groeninckxd, M. Sarkissova, The thermal and crystallisation studies of short sisal fibre reinforced polypropylene composites, Composites Part A: Applied Science and Manufacturing 34 (2003) 253-266.
[94] P.V. Joseph, M.S. Rabello, L.H.C. Mattoso, K. Joseph, S. Thomas, Environmental effects on the degradation behaviour of sisal fibre reinforced polypropylene composites, Composites Science and Technology 62 (2002) 1357-1372.
[95] X. Yuan, K. Jayaraman, D. Bhattacharyya, , Plasma treatment of sisal fibers and its effects on tensile strength and interfacial bonding, In Proceedings theThird International Symposium on Polymer Surface Modification:Relevance to Adhesion, Newark, NJ: MST Conferences, LLC, 2002, pp. 1-25.
[96] Y. NI, Natural fibre reinforced cement composites, Deparment of mechanical engineering, Victoria University of TechnologyI, Australia, 1995.
[97] L.Y. Mwaikambo, M.P. Ansell, The effect of chemical treatment on the properties of hemp, sisal, jute and kapok fibres for composite reinforcement, Journal of Applied Polymer Science 84 (2002) 2222–2234.
[98] G. Ramakrishna, T. Sundararajan, Impact strength of a few natural fibre reinforced cement mortar slabs: a comparative study, Cement and Concrete Composites 27 (2005) 547-553.
[99] G. Ramakrishna, T. Sundararajan, Studies on the durability of natural fibres and the effect of corroded fibres on the strength of mortar, Cement and Concrete Composites 27 (2005) 575-582.
[100] T.R.D. Filho, Ghavami K., England GL., S. K., Development of vegetable fibre–mortar composites of improved durability, Cement and Concrete Composites 25 (2003) 185-196.
[101] X. Li, L.G. Tabil, S. Panigrahi, Chemical Treatments of Natural Fiber for Use in Natural Fiber-Reinforced Composites: A Review, Journal of Polymers and the Environment 15 (2007) 25-33.
[102] A.K. Mohanty, M.A. Khan, G. Hinrichsen, Influence of chemical surface modification on the properties of biodegradable jute fabrics—polyester amide composites, Composites: Part A 31 (2000) 143–150.
[103] M. Di Candilo, P. Ranalli, C. Bozzi, B. Focher, G. Mastromei, Preliminary results of tests facing with the controlled retting of hemp, Industrial Crops and Products 11 (2000) 197-203.
[104] D.G. Hepworth, D.M. Bruce, J.F.V. Vincent, G. Jeronimidis, The manufacture and mechanical testing of thermosetting natural fibre composites, Journal of Materials Science 35 (2000) 293-298.

[105] D.G. Hepworth, R.N. Hobson, D.M. Bruce, J.W. Farrent, The use of unretted hemp fibre in composite manufacture, Composites Part A:Applied Science and Manufacturing 31 (2000) 1279-1283.
[106] J. Dorado, G. Almendros, J.A. Field, R. Sierra-Alvarez, Infrared spectroscopy analysis of hemp (Cannabis sativa) after selective delignification by Bjerkandera sp. at different nitrogen levels, Enzyme and Microbial Technology 28 (2001) 550-559.
[107] M.A. Arsène, A. Okwo, K. Bilba, A.B.O. Soboyejo, W.O. Soboyejo, Chemically and Thermally Treated Vegetable Fibers for Reinforcement of Cement-Based Composites, Materials and Manufacturing Processes 22 (2007) 214-227.
[108] D. Ray, B.K. Sarkar, Characterisation of alkali-treated jute fibers for physical and mechanical properties, Journal of Applied Polymer Science 80 (2001) 1013-1020.
[109] M.F. Rosa, B.S. Chiou, E.S. Medeiros, D.F. Wood, T.G. Williams, L.H. Mattoso, W.J. Orts, S.H. Imam, Effect of fiber treatments on tensile and thermal properties of starch/ethylene vinyl alcohol copolymers/coir biocomposites, Bioresource Technology 100 (2009) 5196-5202.
[110] T.H. Nam, S. Ogihara, N.H. Tung, S. Kobayashi, Effect of alkali treatment on interfacial and mechanical properties of coir fiber reinforced poly(butylene succinate) biodegradable composites, Composites Part B: Engineering (2011).
[111] K. Mylsamy, I. Rajendran, Influence of alkali treatment and fibre length on Mechanical properties of short Agave fibre reinforced epoxy composites, Materials & Design (2011).
[112] H.M. Wang, R. Postle, R.W. Kessler, W. Kessler, Removing pectin and lignin during chemical processing of hemp for textile applications, Textile Research Journal 73 (2003) 664-669.
[113] A. Jähn, M.W. Schröder, M. Füting, K. Schenzel, W. Diepenbrock, Characterisation of alkali treated flax fibres by means of FT raman spectroscopy and environmental scanning electron microscopy, Spectrochimica Acta Part A: Molecular and Biomolecular Spectroscopy 58 (2002) 2271-2279.
[114] M. Le Troedec, D. Sedan, C. Peyratout, J. Bonnet, A. Smith, R. Guinebretiere, V. Gloaguen, P. Krausz, Influence of various chemical treatments on the composition and structure of hemp fibres, Composites Part A: Applied Science and Manufacturing 39 (2007) 514-522.
[115] M.S. Sreekala, M.G. Kumaran, S. Joseph, M. Jacob, S. Thomas, Oil palm fiber reinforced phenol formaldehyde composites: influence of fiber surface modifications on the mechanical performance, Applied Composite Materials 7 (2000) 295-329.
[116] S. Mishra, M. Misra, S.S. Tripathy, S.K. Nayak, A.K. Mohanty, The influence of chemical surface modification on the performance of sisal-polyester biocomposites, Polymer Composites 23 (2002) 164-170.
[117] P. Saha, S. Manna, S.R. Chowdhury, R. Sen, D. Roy, B. Adhikari, Enhancement of tensile strength of lignocellulosic jute fibers by alkali-steam treatment, Bioresource Technology 101 (2010) 3182-3187.
[118] M.A. Sawpan, K.L. Pickering, A. Fernyhough, Effect of various chemical treatments on the fibre structure and tensile properties of industrial hemp fibres, Composites Part A: Applied Science and Manufacturing 42 (2011) 888-895.
[119] K. Pickering, G. Beckermann, S. Alam, N. Foreman, Optimising industrial hemp fibre for composites, Composites Part A: Applied Science and Manufacturing 38 (2007) 461-468.
[120] I. Van de Weyenberg, T. Chi Truong, B. Vangrimde, I. Verpoest, Improving the properties of UD flax fibre reinforced composites by applying an alkaline fibre treatment, Composites Part A: Applied Science and Manufacturing 37 (2005) 1366–1376.
[121] I. Van de Weyenberg, Influence of processing and chemical treatment of flax fibres on their composites, Composites Science and Technology 63 (2003) 1241-1246.

[122] P.V. Joseph, J. Kuruvilla, S. Thomas, Effect of processing variables on the mechanical properties of sisal-fiber-reinforced polypropylene composites, 59 (1999) 1625-1640.
[123] T. Nishino, K. Hirao, M. Kotera, X-ray diffraction studies on stress transfer of kenaf reinforced poly(l-lactic acid) composite, Composites Part A: Applied Science and Manufacturing 37 (2006) 2269-2273.
[124] E. Boghossian, L. Wegner, Use of flax fibres to reduce plastic shrinkage cracking in concrete, Cement and Concrete Composites 30 (2008) 929-937.
[125] R.D.T. Filho, K. Ghavami, M. Sanjuan, G. England, Free, restrained and drying shrinkage of cement mortar composites reinforced with vegetable fibres, Cement and Concrete Composites 27 (2005) 537-546.
[126] Z. Li, X. Wang, L. Wang, Properties of hemp fibre reinforced concrete composites, Composites Part A: Applied Science and Manufacturing 37 (2006) 497-505.
[127] R. Filho, K. Scrivener, G. England, K. Ghavami, Durability of alkali-sensitive sisal and coconut fibres in cement mortar composites, Cement & Concrete Composites 22 (2000) 127-143.
[128] F. Silva, N. Chawla, R. Filho, Tensile behavior of high performance natural (sisal) fibers, Composites Science and Technology 68 (2008) 3438-3443.
[129] F.A. Silva, B. Mobasher, R.D.T. Filho, Cracking mechanisms in durable sisal fiber reinforced cement composites, Cement and Concrete Composites 31 (2009) 721-730.
[130] G.H.D. Tonoli, U.P. Rodrigues Filho, H. Savastano Jr, J. Bras, M.N. Belgacem, F.A. Rocco Lahr, Cellulose modified fibres in cement based composites, Composites Part A: Applied Science and Manufacturing 40 (2009) 2046-2053.
[131] G.H.D. Tonoli, H. Savastano Jr, E. Fuente, C. Negro, A. Blanco, F.A. Rocco Lahr, Eucalyptus pulp fibres as alternative reinforcement to engineered cement-based composites, Industrial Crops and Products 31 (2010) 225-232.
[132] S. Al-Oraimi, A. Seibi, Mechanical characterisation and impact behavior of concrete reinforced with natural fibres, Composite Structures 32 (1995) 165–171.
[133] Z. Li, L. Wang, X. Wang, Compressive and flexural properties of hemp fiber reinforced concrete, Fibers and Polymers 5 (2004) 187–197.
[134] A. Kriker, G. Debicki, A. Bali, M. Khenfer, M. Chabannet, Mechanical properties of date palm fibres and concrete reinforced with date palm fibres in hot-dry climate, Cement and Concrete Composites 27 (2005) 554-564.
[135] A. Razak, T. Ferdiansyah, Toughness characteristics of Arenga pinnata fibre concrete, Natural Fibers 2 (2005) 89–103.
[136] A. Elsaid, M. Dawood, R. Seracino, C. Bobko, Mechanical properties of kenaf fiber reinforced concrete, Construction and Building Materials 25 (2011) 1991-2001.
[137] K. Bilba, M. Arsene, Silane treatment of bagasse fiber for reinforcement of cementitious composites, Composites Part A: Applied Science and Manufacturing 39 (2008) 1488-1495.
[138] L.C.J. Roma, L.S. Martello, H.J. Savastano, Evaluation of mechanical, physical and thermal performance of cement-based tiles reinforced with vegetable fibers, Construction and Building Materials 22 (2008) 668–674.
[139] G. Tonoli, A. Joaquim, M. Arsne, Bilba. K, H. Savastano, Performance and durability of cement based composites reinforced with refined sisal pulp, Materials and Manufacturing Processes 22 (2007) 149–156.
[140] K. Ghavami, Bamboo as reinforcement in structure concrete elements, Cement and Concrete Composites 27 (2005) 637–649.
[141] J. Claramunt, M. Ardanuy, J.A. García-Hortal, Effect of drying and rewetting cycles on the structure and physicochemical characteristics of softwood fibres for reinforcement of cementitious composites, Carbohydrate Polymers 79 (2010) 200-205.

[142] M. Ardanuy, J. Claramunt, J.A. García-Hortal, M. Barra, Fiber-matrix interactions in cement mortar composites reinforced with cellulosic fibers, Cellulose 18 (2011) 281-289.
[143] B. Mohr, H. Nanko, K. Kurtis, Durability of kraft pulp fiber?cement composites to wet/dry cycling, Cement and Concrete Composites 27 (2005) 435-448.
[144] S.K. Canovas, N.H. Selva, G.M. Kawiche, New economical solutionsor improvement of durability of Portland cement mortarsreinforced with sisal fibres, Materials and Structures 25 (1992) 417–422.
[145] R.D.T. Filho, F.d.A. Silva, E.M.R. Fairbairn, J.d.A.M. Filho, Durability of compression molded sisal fiber reinforced mortar laminates, Construction and Building Materials 23 (2009) 2409-2420.
[146] Z. Berhane, Performance of natural fibre reinforced mortar roofing tiles, Materials and Structures 27 (1999) 347–352.
[147] D. Asprone, M. Durante, A. Prota, G. Manfredi, Potential of structural pozzolanic matrix–hemp fiber grid composites, Construction and Building Materials 25 (2011) 2867-2874.
[148] M. Truong, W. Zhong, S. Boyko, M. Alcock, A comparative study on natural fibre density measurement, Journal of the Textile Institute 100 (2009) 525-529.
[149] V.S. Ramachandran, R.F. Feldman, P.J. Sereda, Application of Differential Thermal Analysis in Cement Research, Highway Research Board, Washington, DC, USA (1964) 40-61.
[150] G.L. Kalousek, C.W. Davis, Jr., W.E. Schmertz, An Investigation of Hydrating Cements and Related Hydrous Solids by Differential Thermal Analysis, Proceedings of the American Concrete Institute 45 (1949) 693-712.
[151] I. Pane, W. Hansen, Investigation of blended cement hydration by isothermal calorimetry and thermal analysis, Cement and Concrete Research 35 (2005) 1155-1164.
[152] R. Vedalakshmi, Quantification of hydrated cement products of blended cements in low and medium strength concrete using TG and DTA technique, Thermochimica Acta 407 (2003) 49-60.
[153] L.P. Esteves, On the hydration of water-entrained cement–silica systems: Combined SEM, XRD and thermal analysis in cement pastes, Thermochimica Acta 518 (2011) 27-35.
[154] M. Frias, J. Cabrera, Influence of MK on the reaction kinetics in MK/lime and MK-blended cement systems at 20 degree C, Cement and Concrete Research 31 (2001) 519 - 527.
[155] N. Mostafa, S. El-Hemaly, E. Al-Wakeel, S. El-Korashy, P. Brown, Characterisation and evaluation of the pozzolanic activity of Egyptian industrial by-products: I. Silica fume and dealuminated kaolin. , Cement and Concrete Research 31 (2001) 467 – 474.
[156] C. Shi, R. Day, Pozzolanic reaction in the presence of chemical activators: Part I. Reaction kinetic, Cement and Concrete Research 30 (2000) 51- 58.
[157] Q. Yu, K. Sawayama, S. Sugita, M. Shoya, Y. Isojima, Reaction between rice husk ash and Ca(OH)2 solution and the nature of its product, Cement and Concrete Research 29 (1999) 37 – 43.
[158] H.S. Sharifah, M.P. Ansell, The effect of alkalization and fibre alignment on the mechanical and thermal properties of kenaf and hemp bast fibre composites: Part 1 – polyester resin matrix, Composites Science and Technology 64 (2004) 1219-1230.
[159] S. Ouajai, Biopolymer composite based on natural and derived hemp cellulose fibres RMIT University, Melbourne, Australia, 2005.
[160] T. Nishino, K. Takano, K. Nakamae, Elastic modulus of the crystalline regions of cellulose polymorphs, Journal of Polymer Science Part B: Polymer Physics 33 (1995) 1647–1651.

[161] S. Stutzman, Development of an ASTM standard test method on X-ray powder diffraction analysis of hydraulic cement International Centre for Diffraction Data, Advances in X-ray Analysis 47 (2004) 206-211.
[162] J. Roncero, S. Valls, R. Gettu, Study of the influence of superplasticizers on the hydration of cement paste using nuclear magnetic resonance and X-ray diffraction techniques, Cement and Concrete Research 32 (2002) 103 – 108.
[163] P. Gupta, S. Chatterji, J.W. Jeffery, Studies on the Effect of Various Additives on the Hydration Reaction of Tricalcium Aluminate, Part I, Cement Technology 1 (1970) 3-10.
[164] S. Diamond, Cement Paste Microstructure—An Overview at Several Levels, Hydraulic Cement Pastes: Their Structure and Properties, Cement and Concrete Association, Sheffield, 1976, pp. 2–30.
[165] ASTM D3379, Standard Test Method for Tensile Strength and Young's Modulus for High-Modulus Single-Filament Materials, ASTM Annual Book, 1989.
[166] ASTM C348, Standard test method for flexural strength of hydraulic-cement mortars, Annual Book of ASTM Standards, 2002.
[167] ASTM C109, Standard test method for compressive strength of hydraulic-cement mortars, Annual Book of ASTM Standards, 2002.
[168] F. Bayramov, Optimisation of steel fibre reinforced concretes by means of statistical response surface method, Cement and Concrete Composites 26 (2004) 665-675.
[169] M.C. Nataraja, N. Dhang, A.P. Gupta, Toughness characterisation of steel fiber-reinforced concrete by JSCE approach, Cement and Concrete Research 30 (2000) 593- 597.
[170] ASTM C 1018, Standard test method for flexural toughness and first crack strength of steel fibre reinforced concrete (using beam with third-point loading), ASTM Annual Book, 1997.
[171] SCE-SF4, Method of tests for flexural strength and flexural toughness of steel fibre reinforced concrete, Japan Society of Civil Engineers 3 (1984) 8-61.
[172] A. Hillerborg, M. Modeer, P.E. Peterson, Analysis of crack formation and crack growths in concrete by means of fracture mechanics and finite elements, Cement and Concrete Research 6 (1976) 773–782.
[173] R. 50-FMC, Committee of fracture mechanics of concrete. Determination of fracture energy of mortar and concrete by means of three-point bend tests on notched beams, Material and Structures 18 (1985) 285 - 290.
[174] ASTM C593, Standard Specification for Fly Ash and Other Pozzolans for Use With Lime for Soil Stabilization, Annual Book of ASTM Standards, 2006.
[175] ASTM C1260, Standard Test Method for Potential Alkali Reactivity of Aggregates (Mortar-Bar Method), Annual Book of ASTM Standards, 2007.
[176] Z.-h. Shui, R. Zhang, W. Chen, D.-x. Xuan, Effects of mineral admixtures on the thermal expansion properties of hardened cement paste, Construction and Building Materials 24 (2010) 1761-1767.
[177] J. Antony, Design of Experiments for Engineers and Scientists, Elsevier Science and Technology Books, 2003.
[178] K.Y. Benyounis, Prediction and Optimization of Residual Stresses, Weld-Bead Profile and Mechanical Properties of Laser Welded Components, Dublin City University, Dublin, Ireland, 2006.
[179] E.M. Hassan, Feasibility and Optimization of Dissimilar Laser Welding Components, Dublin City University, Dublin, Ireland, 2008.
[180] M.A. Sanjuán, A. Moragues, Polypropylene-fibre-reinforced mortar mixes:optimization to control plastic shrinkage, Composites Science and Technology 51 (1997) 655-660.
[181] İ. Türkmen, R. Gül, C. Çelik, A Taguchi approach for investigation of some physical properties of concrete produced from mineral admixtures, Building and Environment 43 (2008) 1127-1137.

[182] S.L. Correia, F.L. Souza, G. Dienstmann, A.M. Segadaes, Assessment of the recycling potential of fresh concrete waste using a factorial design of experiments, Waste Management 29 (2009) 2886-2891.
[183] S.L. Correia, T. Partala, F.C. Loch, A.M. Segadães, Factorial design used to model the compressive strength of mortars containing recycled rubber, Composite Structures 92 (2010) 2047-2051.
[184] G.H.D. Tonolia, J.H. Savastano, E. Fuente, C. Negro, A. Blanco, F.A. Rocco Lahr, Eucalptus pulp fibres as alternative reinforcement to engineered cement-based composites, Industrial Crops and Products 31 (2010) 225-232.
[185] V.K. Mathur, Composite materials from local resources Construction and Building Material 20 (2006) 470-477.
[186] S. Robert, A. Coutts, Review of Australian research into natural fibre cement composites, Cement and Concrete Composites 27 (2005) 518-526.
[187] D.C. Montgomery, Design and Analysis of Experiments, 5th Edition ed., John Wiley & Sons, New York, 2002.
[188] A.I. Khuri, J.A. Cornell, Response surfaces design and analysis, 2nd edition ed., Marcel Dekker, New York, 1996.
[189] X. Zhang, R. Wang, X. Yang, J. Yu, Central composite experimental design applied to the catalytic aromatization of isophorone to 3,5-xylenol, Chemometrics and Intelligent Laboratory Systems 89 (2007) 45-50.
[190] NIST, SEMATECH e-Handbook of Statistical Methods, http://www.itl.nist.gov/div898/handbook/pri/section3/pri3361.htm.
[191] Design-Expert software, V6, user's guide, technical manual, Stat-Ease Inc., Minneapolis, MN., (2005).
[192] R. Myers, D. Montgomery, Response surface methodology — process and product optimization using designed experiment Wiley, 1995.
[193] A. Edeerozey, H.M. Akil, A. Azhar, M. Ariffin, Chemical modification of kenaf fibers, Materials Letters 61 (2007) 2023-2025.
[194] A.K. Bledzki, H.P. Fink, K. Specht, Unidirectional hemp and flax EP- and PP-composites: Influence of defined fiber treatments, Journal of Applied Polymer Science 93 (2004) 2150-2156.
[195] K. Oksman, M.L. Wallstro, L.A. Berglund, R.D.T. FILHO, Morphology and mechanical properties of unidirectional sisal–epoxy composites, Journal of Applied Polymer Science 84 (2001) 2358-2365.
[196] D. Ray, B.K. Sarkar, R.K. Basak, A.K. Rana, Study of the thermal behavior of alkali-treated jute fibers, Journal of Applied Polymer Science 85 (2002) 2594-2599.
[197] V. Tserki, N.E. Zafeiropoulos, F. Simon, C. Panayiotou, A study of the effect of acetylation and propionylation surface treatments on natural fibres, Composites: Part A 36 (2005) 1110-1118.
[198] H. Fares, S. Remond, A. Noumowe, A. Cousture, High temperature behaviour of self-consolidating concreteMicrostructure and physicochemical properties, Cement and Concrete Research 40 (2010) 488-496.
[199] T. Uygunoğlu, İ.B. Topçu, Thermal expansion of self-consolidating normal and lightweight aggregate concrete at elevated temperature, Construction and Building Materials 23 (2009) 3063-3069.
[200] P.E.G. Bellew, Microstructural investigation of deteriorated Portland cement concretes, Construction and Building Materials 10 (1996) 3-16.
[201] B. Chen, Effect of fibers on expansion of concrete with a large amount of high f-CaO fly ash, Cement and Concrete Research 33 (2003) 1549-1552.
[202] M. Khorami, E. Ganjian, Comparing flexural behaviour of fibre–cement composites reinforced bagasse: Wheat and eucalyptus, Construction and Building Materials 25 (2011) 3661-3667.
[203] E.T. Dawood, M. Ramli, Mechanical properties of high strength flowing concrete with hybrid fibers, Construction and Building Materials 28 (2012) 193-200.

[204] E.T. Dawood, M. Ramli, High strength characteristics of cement mortar reinforced with hybrid fibres, Construction and Building Materials 25 (2011) 2240–2247.
[205] Y. Mohammadi, S.P. Singh, S.K. Kaushik, Properties of steel fibrous concrete containing mixed fibres in fresh and hardened state, Construction and Building Materials 22 (2008) 956–965.
[206] M.S. Meddaha, M. Bencheikh, Properties of concrete reinforced with different kinds of industrial waste fibre materials, Construction and Building Materials 23 (2009) 3196-3205.
[207] N. Neithalath, J. Weiss, J. Olek, Acoustic performance and damping behavior of cellulose–cement composites, Cement & Concrete Composites 26 (2004) 359–370.
[208] N. Neithalath, Damage assessment in cellulose–cement composites using dynamic mechanical characteristics, Cement & Concrete Composites 28 (2006) 658–667.
[209] M.S. Morsy, S.H. Alsayed, M. Aqel, Hybrid effect of carbon nanotube and nano-clay on physico-mechanical properties of cement mortar, Construction and Building Materials 25 (2011) 145-149.
[210] Z. You, J. Mills-Beale, J.M. Foley, S. Roy, G.M. Odegard, Q. Dai, S.W. Goh, Nanoclay-modified asphalt materials: Preparation and characterisation, Construction and Building Materials 25 (2011) 1072-1078.
[211] D.R.G. Mitchell, I. Hinczak, R.A. Day, Interaction of silica fume with calcium hydroxide solutions and hydrated cement pastes, Cement and Concrete Research 28 (1998) 1571–1584.
[212] J. Yajun, J.H. Cahyadi, Effects of densified silica fume on microstructure and compressive strength of blended cement pastes, Cement and Concrete Research 33 (2003) 1543–1548.
[213] D. Bonen, S. Diamond, Occurrence of large silica fume-derived particles in hydrated cement paste, Cement and Concrete Research 22 (1992) 1059– 1066.
[214] v. Sánchez de Rojas, J. Rivera, M. Frías, Influence of the microsilica state on pozzolanic reaction rate, Cement and Concrete Research 29 (1999) 945– 949.
[215] V. Mostafa , Q. Mohsen, S.A.S. El-Hemaly, S.A. El-Korashy, P.W. Brown, High replacements of reactive pozzolan in blended cements: Microstructure and mechanical properties, Cement & Concrete Composites 32 (2010) 386–391.
[216] S. Wild, B.B. Sabir, J.M. Khatib, Factors influencing strength development of concrete containing silica fume, Cement and Concrete Research 27 (1995) 1567–1580.
[217] Q. Ye, Study and development of nanocomposite cement-based material, Gypsum and Cement for Building 11 (2001) 4-6.
[218] G.J.Z. Xu, D.F. Watt, P.P. Hudec, Effectiveness of mineral admixtures in reducing ASR expansion Cement and Concrete Research 25 (1995) 1125–1236.
[219] R.F. Bleszynski, M.D.A. Thomas, Microstructural studies of alkali– silica reaction in fly ash concrete immersed in alkaline solutions. Advn Cem Based Mater 1998;7:66–78., Advanced Cement Based Materials 7 (1998) 66–78.
[220] M.H. Shehata, M.D.A. Thomas, Use of ternary blends containing silica fume and fly ash to suppress expansion due to alkali–silica reaction in concrete, Cement and Concrete Research 32 (2002) 341–349.
[221] M.H. Shehata, M.D.A. Thomas, The effect of fly ash composition on the expansion of concrete due to alkali–silica reaction, Cement and Concrete Research 30 (2000) 1063–1072.
[222] B. Sabir, S. Wild, J. Bai, Metakaolinand calcined clays as pozzolans for concrete: a review, Cement and Concrete Composites 23 (2001) 441 - 454.
[223] H. Li , M.-h. Zhang, J.-p. Ou, Flexural fatigue performance of concrete containing nano-particles for pavement, International Journal of Fatigue 29 (2007) 1292–1301.
[224] I.B. Topcu, A.R. Boga, T. Bilir, Alkali-silica reactions of mortars produced by using waste glass as fine aggregate and admixtures such as fly ash and Li2CO3, Waste management 28 (2008) 878-884.

[225] A.C.-. 08b, Standard Test Method for Determination of Length Change of Concrete Due to Alkali-Silica Reaction, (2008).
[226] M.A. Bérubé, J. Duchesne, D. Chouinard, Why the accelerated mortar bar test method ASTM C1260 is reliable for evaluating the effectiveness of supplementary cement, Cement & Concrete Aggregates 17 (1995) 26-34.
[227] B. Jo, C. Kim, G. Tae, J. Park, Characteristics of cement mortar with nano-SiO2 particles, Construction and Building Materials 21 (2007) 1351-1355.
[228] N. Banthia, N. Nandakumar, Crack growth resistance of hybrid fiber reinforced cement composites, Cement & Concrete Composites 25 (2003) 3-9.
[229] P. Rossi, High performance multimodal fiber reinforced cement composites (HPMFRCC): the LCPC experience, ACI Materials Journal 94 (1997) 478–483.
[230] W. Wongkeo, A. Chaipanich, Compressive strength, microstructure and thermal analysis of autoclaved and air cured structural lightweight concrete made with coal bottom ash and silica fume, Materials Science and Engineering: A 527 (2010) 3676-3684.
[231] M. Ashraf, A. Naeem Khan, Q. Ali, J. Mirza, A. Goyal, A.M. Anwar, Physico-chemical, morphological and thermal analysis for the combined pozzolanic activities of minerals additives, Construction and Building Materials 23 (2009) 2207-2213.
[232] W. Sha, E. O'Neill, Z. Guo, Differential scanning calorimetry study of ordinary Portland cement, cement and Concrete Research 29 (1999) 1487 - 1489.
[233] W.F. Cole, B. Kroone, Carbon dioxide in hydrated Portland cement, Journal of American Concrete Institute 31 (1960) 1275–1295.
[234] C. Dias, M. Cincotto, H. Savastanojr, V. John, Long-term aging of fiber-cement corrugated sheets – The effect of carbonation, leaching and acid rain, Cement and Concrete Composites 30 (2008) 255-265.

Appendix I: List of Publications

Paper Published in Peer reviewed Journal

M. Aly, M.S.J. Hashmi, A.G. Olabi, M. Messeiry, A. I. Hussain, E.F.Abadir. Effect of colloidal nano-silica on the mechanical and physical behaviour of waste-glass cement mortar. Materials and Design. 2012;33:127-35.

M. Aly, M.S.J. Hashmi, A.G. Olabi, M. Messeiry, A. I. Hussain. Effect of nano-clay particles on mechanical, thermal and physical behaviours of waste-glass cement mortars. Materials Science and Engineering A. 2011; 528:7991– 7998.

M. Aly, M.S.J. Hashmi, A.G. Olabi, M. Messeiry, A. I. Hussain, E.F.Abadir. Effect of nano-clay and waste glass powder on the properties of flax fibre reinforced mortar. ARPN Journal of Engineering and Applied Sciences. 2011; 6(10): 19-28.

Paper Submitted to Peer reviewed Journal

M. Aly, M.S.J. Hashmi, A.G. Olabi, K. Y. Benyounis**,** M. Messeiry, A. I. Hussain, E.F.Abadir, Optimization of alkaline treatment conditions of flax fibre, Industrial Crops and Products, March 2011, Under reviewing.

M. Aly, M.S.J. Hashmi, A.G. Olabi, K. Y. Benyounis, M. Messeiry, A. I. Hussain, E.F.Abadir, Mechanical and thermal behaviour of flax fibre reinforced mortar, Cement and Concrete Research, February 2011, Under reviewing.

M. Aly, M.S.J. Hashmi, A.G. Olabi, M. Messeiry, A. I. Hussain, E.F.Abadir, Durability of waste glass cement composites, Cement and Concrete Composites, January 2011, Under reviewing.

Conference Paper

M. Aly, M.S.J. Hashmi, A.G. Olabi, M. Messeiry, A. I. Hussain, E.F.Abadir. Effect of Alkaline treatment on behaviour of flax fibre reinforced cement mortar. Published in the Proceedings of 4th International Conference on sustainable energy and environmental protection (SEEP 2010), 29 June-2 July 2010, Bari, Italy.

M. Aly, M. S. J. Hashmi, A. G. Olabi, M. Messeiry. Durability of waste glass flax fibre reinforced Mortar. International conference on advances in materials and processing technologies (AMPT 2010) AIP Conf. Proc. January 17, 2011, vol. 1315, pp. 241-246; doi: 10.1063/1.3552448.

Poster

M. Aly, M.S.J. Hashmi, A.G. Olabi, M. Messeiry. Mechanical properties of flax fibre reinforced mortar. Faculty of engineering and computing research day, May 2010, Dublin City University, Dublin, Ireland.

Appendix II: Cost Analysis

Table 1.II: Approximated cost of glass fibre cement mix

Element of cost	**Cost**	**Cost per m^3 of mix (€)**
Portland Cement	60 €/ton	37.8
Sand	4.2 €/m^3	1.99
Water	0.5 €/m^3	0.157
E-Glass fibre	1585 €/ton	31.7
Total approximated cost per m^3 of mix		**73.06 €**

Table 2.II: Approximated cost of waste glass/flax fibre cement mix

Element of cost	**Cost**	**Cost per m^3 of mix (€)**
Waste glass powder	10 €/ton	1.62
Portland Cement	60 €/ton	32.1
Sand	4.2 €/m^3	2.06
Water	0.5 €/m^3	0.163
Bleached flax fibre	189 €/ton	2.46
Total approximated cost per m^3 of mix		**38.04€**

$$\textbf{Total cost saving/m}^3 = \frac{73.06-38.04}{73.06}\ x\ 100 = \ 47\%$$